A Thesis, entitled

"THERMODYNAMIC PROPERTIES OF LOW-MELTING INORGANIC SALTS",

presented for the Degree of Doctor of Philosophy in the Faculty of Science at the University of London,

by

Brian Cleaver, B.A. (Oxford),

July, 1963.

ABSTRACT.

The opening Chapters summarise the previous work on electrical conductivity, density and ultra-violet spectroscopy in fused salt systems, and on the melting process for ionic substances. The aim of the present work is defined in relation to this previous knowledge.

The electrical conductivities and densities of fused KNO_3 - $Ba(NO_3)_2$ mixtures were measured. The conductivity of KNO_3 is depressed when $Ba(NO_3)_2$ is added, so the divalent ions restrict ionic migration. Consistently with this interpretation, the equivalent volumes of the molten mixtures decreased with rising barium concentration, and the fraction of the volume actually occupied by the ions also decreased. These results contrast sharply with corresponding results for ionic crystals, which points to limitations in the applicability of the 'quasi-crystalline' model to ionic melts.

The near ultra-violet absorption spectra of the alkali metal nitrates, silver, thallous and ammonium nitrates, nitric acid and iso-propyl nitrate were measured at temperatures up to and beyond their melting-points. The weak band at 33 kcm^{-1} is due to an internal transition

($n \longrightarrow \pi^*$) in the nitrate ion; its maximum frequency, E(2), depends on the identity of the cation, on the temperature and on crystal structure. E(2) is determined largely by the first shell of cations around each nitrate ion; for a given salt an increase in E(2) corresponds to a decrease in the nearest cation - oxygen distance, and vice versa. This leads to the important conclusion that the nearest-neighbour cation - oxygen separation decreases on fusion, in spite of the macroscopic increase in volume.

Similar conclusions were reached about the melting process in sodium and potassium nitrites.

The temperature dependence of the % transmission of a thin film of salt at fixed frequency provided a means for determining transition temperatures and for studying hysteresis in phase transformations.

* * * * * * * * * * * *

ACKNOWLEDGEMENTS.

It is a pleasure to thank Professor A.R. Ubbelohde, F.R.S., for supervising this work. He has been a constant source of stimulating ideas, and his interest and enthusiasm have on many occasions provided an effective counter to the despondency and disappointments which are a part of research.

Sincere thanks are also offered to Dr. Elizabeth Rhodes, for much sound advice and for innumerable discussions throughout the course of the work.

A maintenance grant from the Ministry of Aviation, and funds for apparatus from the Ministry and from the Royal Society, are gratefully acknowledged.

INDEX.

page

Chapter 1. The physical chemistry of fused salts; a brief historical introduction. - - - - 13

Chapter 2. Evidence for the ionic nature of fused metallic nitrates and nitrites. - - - - 16

2.1. X-ray diffraction - - - - - - - - - - - - 16
2.2. Raman Spectroscopy - - - - - - - - - - - - 17
2.3. Ultra-violet spectroscopy - - - - - - - - 19
2.4. Self-diffusion coefficients - - - - - - - 21
2.5. Cryoscopy - - - - - - - - - - - - - - - - 22
2.6. Electrical conductivity - - - - - - - - - 23
2.7. Summary - - - - - - - - - - - - - - - - - 24

Chapter 3. Previous work on the electrical conductivities of ionic melts and solids. - - - 27

3.1. Conductivity cells for ionic melts - - - 27
3.2. Polarisation effects - - - - - - - - - - - 28
3.3. Calibration of conductivity cells - - - 29
3.4. Treatment of electrode surfaces - - - - 30
3.5. Theoretical treatment of the conductivity of melts - - - - - - - - - - - - - - - - 30
3.6. Results of earlier investigations - - - 32
3.7. Conductivity in ionic solids, and the Wagner effect - - - - - - - - - - - - - - - 36
3.8. Aim of the present work on electrical conductivities of melts - - - - - - - - - 38

Chapter 4. Previous work on the densities of fused salt systems. - - - - - - - - - - - - - - - 44

4.1. Experimental techniques - - - - - - - - - 44

page

4.2. Results obtained by previous workers - - 46
4.3. Aim of the present work on fused salt densities - - - - - - - - - - - - - - - - - 47

Chapter 5. The ultra-violet spectroscopy of fused-salt systems.- - - - - - - - - - - - - - - 50

5.1. Developments in experimental technique - 50
5.2. An outline of previous experimental studies in the field of fused-salt spectroscopy - - - - - - - - - - - - - - - 53
5.3. Aim of the present work on ultra-violet spectroscopy of salts - - - - - - - - - 56

Chapter 6. The absorption of light by ionic substances (with particular reference to nitrates and nitrites). - - - - - - - - - 60

6.1. Introduction - - - - - - - - - - - - - - - - 60
6.2. Charge-transfer spectra - - - - - - - - - 60
6.3. Absorption due to 'internal' transitions 64
6.4. Possibility of transitions having characteristics intermediate between 'charge-transfer' and 'internal' - - - - 65
6.5. Previous knowledge on the absorption spectra of nitrates in the region 50 - 20 kcm^{-1}- - - - - - - - - - - - - - - - 67
6.6. Previous knowledge on the absorption spectra of nitrites in the range 50 - 20 kcm^{-1}- - - - - - - - - - - - - - - - 75

Chapter 7. Previous studies on the melting process in ionic crystals. - - - - - - - - - - - - - 82

7.1. Diffraction techniques - - - - - - - - - - 82

		page
7.2.	Changes in electrical conductivity on melting - - - - - - - - - - - - - - - - -	85
7.3.	Volume changes on fusion - - - - - - - -	86
7.4.	Heat and entropy changes on fusion - -	91
7.5.	Spectroscopic methods - - - - - - - - - -	93
Chapter 8.	Experimental techniques - general.- - -	97
8.1.	Materials - - - - - - - - - - - - - - - -	97
8.2.	Purification techniques - - - - - - - - -	99
8.3.	The melt bath - - - - - - - - - - - - - -	104
8.4.	Temperature measurement - - - - - - - - -	107
Chapter 9.	The measurement of the electrical conductivity of fused potassium nitrate barium nitrate mixtures.- - - - - - - -	113
9.1.	Apparatus - - - - - - - - - - - - - - - -	113
9.2.	Measurement of the cell constant - - -	115
9.3.	Preliminary fused-salt conductivity measurements - - - - - - - - - - - - - -	118
9.4.	Definitive conductivity measurements -	121
Chapter 10.	Measurement of the densities of fused potassium nitrate - barium nitrate mixtures. - - - - - - - - - - - - - - - - -	125
10.1.	Apparatus - - - - - - - - - - - - - - - -	125
10.2.	Principle of the method - - - - - - - - -	128
10.3.	Assessment of the error in ρ produced by errors in the measurement of M, V_o, ρ_o and h - - - - - - - - - - - - - - - - -	130
10.4.	Calibration of the densitometer - - - -	132
10.5.	Measurement of the density of di-n-butyl phthalate - - - - - - - - - - - - - - - -	137

page

10.6. Experimental procedure for the measurement of the density of a liquid mixture of KNO_3 and $Ba(NO_3)_2$ - - - - - - - - - - - - 138

Chapter 11. Ultra-violet spectroscopy of nitrates and nitrites. - - - - - - - - - - - - - - - - 145

11.1. The spectrophotometer - - - - - - - - - - - 148
11.2. Checking the calibration of the frequency scale - 154
11.3. The sample and reference thermostat units 160
11.4. Measurement of temperature gradients in the original thermostat unit - - - - - - - - 168
11.5. Improvement of thermostat design - - - - - 175
11.6. Measurement of thermal gradients in the improved thermostat unit - - - - - - - - - - 176
11.7. Summary of temperature gradients in the original and in the modified thermostat unit - 177
11.8. Influence of temperature gradients on the accuracy of the spectroscopic measurements on salt films - - - - - - - - - - - - 179
11.9. Calibration of the Pallador thermocouples used in the sample and reference thermostats - - - - - - - - - - - - - - - - - - - 182
11.10. Preparation of salt samples for spectroscopy - - - - - - - - - - - - - - - - - - - 184
11.11. Procedure for obtaining absorption spectra of salt films - - - - - - - - - - - - - - - 185
11.12. Measurement of the true transmission in the range 54,000 - 50,000 cm^{-1} - - - - - - - 194
11.13. Spectroscopic observations at constant frequency - - - - - - - - - - - - - - - - - 199

page

Chapter 12. Results: electrical conductivities of fused KNO_3 - $Ba(NO_3)_2$ mixtures. - - - - - 202

12.1. Tabulation of results - - - - - - - - - - - 202

12.2. Accuracy of the conductivity results - - 206

12.3. Comparison of the results with those of earlier workers - - - - - - - - - - - - - - 210

Chapter 13. Results: densities, equivalent volumes and partial equivalent volumes in liquid KNO_3 - $Ba(NO_3)_2$ mixtures. - - - - - - - - - 212

13.1. Densities and equivalent volumes - - - - 212

13.2. Densities and equivalent volumes as functions of temperature - - - - - - - - - 215

13.3. Equivalent volume isotherms, and partial equivalent volumes - - - - - - - - - - - - 217

13.4. Errors in the measured densities - - - - 221

13.5. Comparison of the present results with those of earlier workers - - - - - - - - - 221

Chapter 14. Results: ultra-violet absorption spectra of nitrates and nitrites. - - - - - - - - - 225

14.1. Introduction - - - - - - - - - - - - - - - - 225

14.2. Changes in % absorption with rising temperature - - - - - - - - - - - - - - - - - 226

14.3. Estimation of sample thicknesses and molar extinction coefficients - - - - - - - 228

14.4. Errors in the recorded values of E(2) - - 229

14.5. Temperature measurements - - - - - - - - 230

14.6. The nitrates - - - - - - - - - - - - - - - 231

14.7. The nitrites - - - - - - - - - - - - - - - 281

		page
Chapter 15.	The study of phase-changes by measurement of % transmission at constant frequency. - - - - - - - - - - - - - - - - -	297
15.1.	Introduction - - - - - - - - - - - - - - - -	297
15.2.	Transitions in crystalline nitrates - -	300
15.3.	Summary of results for the nitrates - -	307
15.4.	The transition in potassium nitrite at 40 - 50°C - - - - - - - - - - - - - - - -	311
15.5.	Potentialities of the technique - - - -	318
Chapter 16.	Discussion: The electrical conductivity of KNO_3 - $Ba(NO_3)_2$ mixtures. - - - - - - -	321
Chapter 17.	Discussion: equivalent volumes of fused KNO_3 - $Ba(NO_3)_2$ mixtures. - - - - - - - -	326
17.1.	Volume change on mixing fused KNO_3 and $Ba(NO_3)_2$ - - - - - - - - - - - - - - - - -	326
17.2.	Heat of mixing of fused KNO_3 and $Ba(NO_3)_2$ - - - - - - - - - - - - - - - - -	334
17.3.	The structure of KNO_3 - $Ba(NO_3)_2$ melts	338
Chapter 18.	Discussion: the ultra-violet absorption spectra of crystalline and fused nitrates and nitrites - - - - - - - - - -	342
18.1.	The strong absorption bands of the nitrates and nitrites - - - - - - - - - -	342
18.2.	The weak absorption band of the nitrates at 33 kcm^{-1} - - - - - - - - - -	344
18.3.	The weak absorption band of the nitrites at 27 - 28 kcm^{-1} - - - - - - -	368
18.4.	Possibilities for future work - - - - -	370

page

Appendix A Details of experimental procedure used for calibrating a Pallador thermocouple at the steam, naphthalene and sulphur points - - - - - - - - - - - - - - - - - - 375

Appendix B Preliminary conductivity results for fused KNO_3 - $Ba(NO_3)_2$ mixtures - - - - 381

Appendix C Details of spectroscopic observations made on thin films of nitrates and nitrites - - - - - - - - - - - - - - - - 386

- - - - -

INTRODUCTORY

SECTION

CHAPTER I.

THE PHYSICAL CHEMISTRY OF FUSED SALTS : A BRIEF HISTORICAL INTRODUCTION.

The terms 'fused salt' and 'ionic melt' are used in this thesis to mean liquids whose structural units are ions. Fused sodium chloride may be taken as a typical example. The ionic liquids are thereby differentiated from the molecular liquids, which are composed of (uncharged) molecules; carbon tetrachloride is a typical member of the second group.

This definition of an ionic melt suffers from the same shortcomings as the corresponding definition of an ionic solid, in that certain substances defy classification because their physical properties are intermediate between those of sodium chloride and carbon tetrachloride. This intermediate category includes the halides of the less electropositive metals Be, Al, Sc, Y, Zr, Hf, Nb, Ta, Mo, W, U, Hg, In, Tl, Sn, Pb, and Bi. The fused halides of these metals probably consist largely of molecules but contain a small proportion of ions; some of the experimental evidence for this will be reviewed in subsequent sections, when the different experimental techniques are described.

The first systematic study of fused salts was carried out by Michael Faraday, from 1831 onwards. Between this date and about 1950 a steady interest in the subject was maintained, and papers appeared in the literature describing experimental work on phase diagrams, density, cryoscopy, electromotive

force, refractive index, surface tension, electrical conductivity, viscosity and specific heats of pure fused salts and their mixtures. Since 1950 there has been a marked increase in activity in the field; new experimental techniques have been devised and used, and much effort has been devoted to the theoretical aspects of the subject. This upsurge of interest was stimulated by the appearance of new possibilities for the use of fused salts in technology, where the need was soon felt for a better understanding of the basic physical chemistry of these systems. Some of the more recent applications are in the field of reactor technology, where melts are being used as heat-exchange fluids and in the processes of extraction and purification of radioactive metals. Ionic melts are also being used as electrolytes in batteries and fuel cells, where, in some circumstances, they have advantages over the more conventional aqueous electrolytes.

Fused salts are involved in some of the older technologies. Glasses, and the slags formed during the chemical reduction of some metal ores, contain a complex mixture of polysilicate ions as well as some simple ions M^{n+} and SiO_3^{--}. They are not typical ionic liquids according to the above definition, and the changes which take place in them often involve the breaking or formation of covalent Si - O bonds, followed by changes in the proportions of the ions and polymers in the mixture. Attainment of the equilibrium distribution is often very slow, and equilibrium may never be reached during an actual smelting process. For these reasons the study of slags and glasses is regarded as a special branch of chemical technology.

The preparation of electropositive metals by electrolysis of melts was first carried out (on an experimental scale) by Sir Humphrey Davy, and is now used for the commercial

production of some metals, notably aluminium.

The increase in activity in the field of fused salt chemistry since 1950 has occurred partly by intensified use of the older experimental techniques mentioned above and partly by the introduction of new techniques. These 'new' techniques have nearly all been used for many years for the study of conventional liquids; some modifications have been necessary before they could be used to study fused salts, owing to the corrosive nature of the latter and the high temperatures involved. Some of the techniques introduced recently are Raman, infra-red and ultra-violet spectroscopy, X-ray and neutron diffraction, measurement of thermal conductivity, transport numbers, diffusion coefficients (by tracer techniques), vapour pressure, compressibility, gas solubility, heats of mixing and heats of reaction in fused salt media.

The experimental work carried out by the author involved measurement of electrical conductivities, densities and ultra-violet spectra of fused salt systems, the salts examined being alkali-metal nitrates, barium, ammonium, silver and thallous nitrates and sodium and potassium nitrites. The next chapter describes some of the evidence for supposing that these melts are ionic in nature. In subsequent chapters a summary is given of the experimental techniques developed by previous workers, and the results obtained, in the fields of conductivity measurement, density measurement and ultra-violet spectroscopy of ionic melts.

CHAPTER 2.

EVIDENCE FOR THE IONIC NATURE OF FUSED METALLIC NITRATES AND NITRITES.

There is considerable support for the hypothesis that the fused salts studied in the author's experimental work (listed in the last paragraph of Chapter 1) are made up of ions. Some of the main contributions are now described, under the headings of the physical techniques employed.

2.1. X-ray diffraction.

X-ray diffraction experiments have been carried out on fused sodium nitrate (Refs.1 and 2), potassium nitrate (Ref.2) and sodium nitrite (Ref.1), just above their respective melting-points. The experimental observations were converted into radial distribution curves, with the nitrogen atom as centre.

For the two nitrates, the first maximum in the distribution curve appeared at $r = 1.2 \pm 0.1$A, and must correspond to the N-O distance. This is in good agreement with the value $r(N-O) = 1.218 \pm 0.008$A obtained by Sass et al (Ref.3) from their study of crystalline sodium nitrate at room temperature. The equality of these bond-lengths strongly suggests that the nitrate ion is present in the melt as well as in the crystal.

The areas under the first peak in the radial distribution curves of the melts showed that the coordination number of

oxygen around nitrogen was three in the nitrates (Refs.1 and 2) and two in sodium nitrite (Ref.1). There was no evidence for supposing that one N-O distance in each nitrate group was longer than the other two (as it would be if covalent molecules $MO.NO_2$ were present).

2.2. Raman spectroscopy.

The Raman spectrum of 23.4N nitric acid consists of eight lines, at 3386, 1680, 1538, 1301, 926, 675, 607 and 480 cm^{-1} (Ref.4). When the acid is diluted with water, the intensities of these lines diminish progressively and they are replaced by three lines at 1390, 1050 and 720 cm^{-1}. All eleven lines can be observed in the spectrum of a solution of intermediate concentration (15N; Ref.5). The Raman spectra of dilute aqueous solutions of metallic nitrates also consist of the three lines at 1390, 1050 and 720 cm^{-1}. It is clear that these frequencies are characteristic of the (hydrated) nitrate ion, while the eight lines in the spectrum of the concentrated acid are due to the undissociated molecule $HO.NO_2$.

This evidence shows that the Raman spectrum of the nitrate ion is profoundly changed if covalent bond formation occurs between one of its oxygen atoms and another atom or group. The point is confirmed by the work of Woodward et al, who have recorded the Raman spectrum of the covalent molecule $H_3C.Hg.ONO_2$ in benzene solution (Ref.6). The Raman technique therefore enables us to find whether the fused metallic nitrates contain only metal ions and nitrate ions or whether there is any formation of covalent molecules $MO.NO_2$.

Janz and James (Ref.7) have recorded the Raman spectra of

the nitrates of the alkali metals in the solid and fused states. The spectra of the solid salts contained only the three lines characteristic of the nitrate ion; for caesium nitrate the frequencies were 1346, 1050 and 715 cm^{-1}. The frequencies were higher for the salts of the smaller cations, the corresponding values for lithium nitrate being 1391, 1086 and 728 cm^{-1}. In potassium nitrate the line at $\sim$1350 cm^{-1} was split into a doublet.

On fusion of the salts, the lines underwent small shifts (up to 20 cm^{-1}), and for lithium nitrate the line at $\sim$1390 cm^{-1} was resolved into two peaks. For all the melts, a new line appeared at $\sim$1650 cm^{-1}. This was assigned as the first overtone ($2\omega_2$) of the mode A_2'', in which the vibration is perpendicular to the plane of the nitrate ion (see Ref.8). Excitation of this mode in the Raman spectrum of an isolated nitrate ion is forbidden by selection rules, but the transition is allowed in the infra-red spectrum and the frequency of the vibration is therefore known (Ref.9). The presence of the line at 1650 cm^{-1} in the Raman spectrum of the fused nitrates must be attributed to an increase in the perturbation of the anions by the cations on melting.

The line at 1390 cm^{-1} represents two asymmetric, in-plane vibrations (E'), which are degenerate in the free nitrate ion (Ref.7). The splitting of this line on fusion of lithium nitrate can be ascribed to the abrupt loss of symmetry in the electrostatic field exerted by the cations on the anions. This interpretation is supported by the observation that the line is also split in the room-temperature Raman spectrum of crystalline potassium nitrate, in which symmetry at the site of each nitrate ion, C_s, is already low. (The remaining alkali-nitrate crystals all have three-fold symmetry at the nitrate ion sites).

Thus, although the Raman spectra of the alkali-metal nitrates change on fusion, the changes can be related to the corresponding reduction in the symmetry of the electrostatic field exerted by the cations on each nitrate ion. The lines at 1050 and 720 cm^{-1} undergo only small shifts, and no new lines appear which require the postulation of covalently-bonded molecules $MO.NO_2$.

In fused silver nitrate the Raman spectrum has lines at 1596, 1035 and 733 cm^{-1}, and a doublet at (1272, 1407) cm^{-1}. The separation between the peaks of the doublet was even greater for this melt than for lithium nitrate melt (135 cm^{-1} as against 90 cm^{-1}), which suggests that the anion-cation interaction in fused silver nitrate is more marked than in any of the fused alkali-metal nitrates.

2.3. Ultra-violet spectroscopy.

In the ultra-violet absorption spectra of covalent nitrates such as concentrated nitric acid ($HO.NO_2$) or alkyl nitrates ($RO.NO_2$), the lowest-energy absorption occurs as a shoulder at 38 - 39,000 cm^{-1} on the low-frequency edge of a much stronger absorption band. Spectra of conc. nitric acid and of iso-propyl nitrate are illustrated on pages 279 and 282, respectively. When nitric acid is diluted with water, the lowest-energy absorption band moves progressively from 38 - 39,000 to 33,000 cm^{-1} (see page 279), and the spectrum of the dilute acid is identical with that of a dilute aqueous solution of an alkali-metal nitrate. It seems reasonable to conclude that the shoulder at 38 - 39,000 cm^{-1} is characteristic of the covalently-bonded nitrate group, while the peak at 33,000 cm^{-1} is characteristic of the (hydrated) nitrate ion.

Crystalline alkali-metal and ammonium nitrates have absorption spectra which are very similar in appearance to those of dilute aqueous solutions of nitric acid or metallic nitrates. The lowest-energy peak occurs at 32 - 34,000 cm^{-1}, the frequency depending on the size of the cation. On fusion of the salts, the maximum of the peak is displaced to higher frequency by not more than 350 cm^{-1}, but the general features of the spectrum remain unchanged (see, for example, pages 232 and 259).

These observations lead to the conclusion that crystalline and fused alkali-metal and ammonium nitrates consist of cations and nitrate ions rather than of covalent molecules $MO.NO_2$. Nevertheless, the variations in the position of the 33,000 cm^{-1} band show that there is some interaction between the nitrate ions and the cations, and that this undergoes some abrupt change on fusion. The nature of this change is discussed more fully in Chapter 18.

The ultra-violet absorption spectra of silver and thallous nitrates at room temperature resemble those of the alkali-metal nitrates rather than those of the covalent nitrates. However, the behaviour of the weak band on heating and fusion of these two salts indicates that the anion-cation interactions in the melts are of a different nature to those of the alkali-nitrate melts (see page 350).

Aqueous solutions of alkali-metal nitrites have a prominent absorption band at 28,000 cm^{-1} (Ref.10). The same band is observed in the spectra of crystalline sodium and potassium nitrites (see pages 283 and 289), and undergoes only a small displacement when the salts are fused (280 cm^{-1} for sodium nitrite, 70 cm^{-1} for potassium nitrite).

The work of Vassian and Eberhardt (Ref.11) has shown that the band is displaced to 31,200 cm^{-1} if covalent bond formation occurs between a metal ion and the nitrogen atom of the nitrite ion to give a molecule $M.NO_2$. This evidence strongly suggests that no such bond formation takes place when sodium and potassium nitries are fused.

Since the spectra of alkyl nitrites, R.ONO, also have a band at 28,000 cm^{-1}, (Ref12), the possiblity of the formation of molecules M.ONO in alkali-nitrite melts cannot be excluded on the evidence of ultra-violet spectroscopy alone.

2.4. Self-diffusion coefficients.

Van Artsdalen et al (Ref.13) used the radioactive isotopes N^{15} and O^{18} to label the nitrate group in alkali-metal nitrates. They then made separate measurements of the rate of diffusion of the two radioactive materials through melts of the corresponding normal salts. For a given salt, the two tracers gave the same value for the diffusion coefficient. This indicates that nitrogen and oxygen move together through the melts in a common structural unit, and that oxygen cannot be exchanged between neighbouring units (since this could lead to an enhancement of the diffusion coefficient of oxygen relative to that of nitrogen).

This evidence relates to the stablity of the nitrate ion in melts, and has, of course, no bearing on the question of association of the ions into molecules MNO_3.

2.5. Cryoscopy.

Measurement of the depression of the freezing-point of a salt by a solute (in the concentration range 0 - 2 mole%) can yield information about the state of dissociation of the solute.

Suppose that the solute is a salt of formula M_aX_b, and that it is potentially capable of dissociating into cations M and anions X:

$$M_aX_b \rightleftharpoons a.M + b.X.$$

If the solute is present in the solution as undissociated molecules M_aX_b, the freezing-point depression of the solvent is

$$(x_2.RT^2)/(L_f),$$

where x_2 is the mole fraction of the solute and L_f the molar heat of fusion of the solvent. If, however, the solute is fully dissociated, the depression is

$$(a + b).(x_2.RT^2)/(L_f),$$

provided that the solvent does not contain either of the ions M or X as a product of its own dissociation; if the solute and solvent do have ions in common, only the 'foreign' ions of the solute are active in depressing the freezing point. For example, when potassium nitrate (KNO_3), potassium perchlorate ($KClO_4$) and lead chloride ($PbCl_2$) are dissolved in silver nitrate, the freezing-point depression corresponds to the formation of one, two and three foreign particles, respectively, per molecule of added salt (Ref.14).

There is ample evidence of this kind to show that alkali-metal and alkaline-earth halides, sulphates, carbonates, perchlorates and dichromates are completely dissociated in solution in alkali nitrates (Refs.14,15,16), silver nitrate (Ref.14) and thallous nitrate (Ref.17). Far fewer results are available to demonstrate that the nitrates and nitrites are fully dissociated when they are themselves dissolved in other melts. This is because nitrates and nitrites are thermally unstable above 450°C, and only relatively few salts have sufficiently low melting-points to be usable as solvents below this temperature. However, the existing evidence supports the hypothesis that complete dissociation occurs; for example, Foote and Levy have shown that potassium nitrate gives a twofold freezing-point depression when dissolved in fused sodium chlorate (Ref.18).

2.6. Electrical conductivity.

The equivalent conductivities of fused alkali-metal nitrates and nitrites, at a temperature 1.10 times the melting temperature in °K, lie in the range 37 - 60 $ohm^{-1}cm^{2}equiv^{-1}$ (see page 34 for a table of results). These values are of the same order of magnitude as the equivalent conductivities of dilute aqueous solutions of alkali halides and nitrates (which are about 100 $ohm^{-1}cm^{2}equiv^{-1}$ at room temperature), which indicates that the melts are at least largely ionised.

There is no doubt that the nitrate melts conduct by ion migration (as opposed to electron migration), and that both ions contribute to the conductivity; for example, the cation transport numbers in pure lithium nitrate, sodium nitrate, potassium nitrate and silver nitrate melts have been found to be 0.84, 0.71, 0.60 and 0.75 respectively (Refs 19, 20, 21).

For silver and thallous nitrates at $1.1 T_m$, the equivalent conductivities are 38 and 26 $ohm^{-1}cm^2equiv^{-1}$. Although these values are still high enough to indicate that the melts are ionic rather than covalent, they do suggest that the anion-cation interactions may be more specific than in the alkali nitrate melts (particularly in the case of thallous nitrate).

Structural influences on the electrical conductivities of melts are discussed more fully in the next chapter.

2.7. Summary.

The evidence provided by all six of the physical techniques mentioned in the foregoing sections shows that it is legitimate to regard fused alkali-metal nitrates and nitrites as being made up of cations M^+ and anions NO_3^- or NO_2^-.

In melts of silver and thallous nitrates the anion-cation interactions may be more specific than those in the alkali metal salts, but these two melts may still be described as ionic to a good first approximation.

REFERENCES TO CHAPTER 2.

1. K. Furukawa, Sci. Reps. Res. Inst., Tokohu Univ., (1960), A12, 150; Discuss. Farad. Soc., (1961), 32, 53.

2. V.I. Danilov and S.Ya. Krasnitskii, Dokl. Akad. Nauk. S.S.S.R., (1955), 101, 661.

3. R.L. Sass, R. Vidale and J. Donohue, Acta Cryst., (1957), 10, 567.

4. O. Redlich and L.E. Nielsen, J. Amer. Chem. Soc., (1943), 65, 654.

5. T.F. Young, L.F. Maranville and H.M. Smith, "Structure of Electrolytic Solutions", ed. Hamer, John Wiley, New York, 1959.

6. P.L. Goggin and L.A. Woodward, Trans. Farad. Soc.,(1962), 58, 1495.

7. D.W. James, Ph.D. Thesis, Rensselaer Polytechnic Institute, Troy, New York,(1960).

8. E.V. Sayre, J. Chem. Phys., (1959), 31, 73.

9. J.C. Decius, J. Chem. Phys., (1955), 23, 1290.

10. S.F. Mason, Quart. Revs. Chem. Soc., (1961), 15, 287.

11. E.G. Vassian and W.H. Eberhardt, J. Phys. Chem., (1958), 62, 84.

12. H.E. Ungnade and R.A. Smiley, J. Org. Chem., (1956), 21, 993.

13. E.R. Van Artsdalen, D. Brown, A.S. Dworkin and J. Miller, J. Amer. Chem. Soc., (1956), 78, 1772.

14. E. Kordes, W. Borgman and W. Vogel, Z, Elektrochem., (1951), 55, 600.

15. E.R. Van Artsdalen, J. Phys. Chem., (1956), 60, 172.

16. P.H.J. Hoenen, Z. phys. Chem., (1913), 83, 513.

17. M. Rolla, P. Franzosini and R. Riccardi, Discuss. Farad. Soc., (1961), 32, 84.

18. Foote and Levy, Amer. Chem. Journal, (1907), 37, 494.

19. R.W. Laity, Discuss. Farad. Soc., (1961), 32, 172.

20. F.R. Duke, R.W. Laity and B. Owen, J. Electrochem. Soc., (1957), 104, 299.

21. H. Bloom and D.W. James, J. Phys. Chem., (1959), 63, 757.

CHAPTER 3.

PREVIOUS WORK ON THE ELECTRICAL CONDUCTIVITIES OF IONIC MELTS AND SOLIDS.

The development of experimental techniques for the measurement of the conductivities of ionic melts is described in the opening sections of this chapter. This is followed by a brief dicussion of theoretical treatments of the problem of ionic conduction in melts. A review is then given of some of the results obtained, and the allied subject of conductivity in ionic solids is introduced. The chapter is concluded with a statement of the aim of the author's experimental work on electrical conductivity.

3.1. Conductivity cells for ionic melts.

Two types of cell have been used for the measurement of the electrical conductivity of fused salts. In the more commonly used design, the flow of electricity between the electrodes is restricted by a capillary, so that the cell constant is of the order 200 cm^{-1} (Refs.1 and 2). Since ionic melts usually have specific conductivities of the order 1 $ohm^{-1}cm^{-1}$, the resistance of a capillary-type cell filled with melt is about 200 ohms; this is sufficiently high to be conveniently measurable with a resistance bridge (Ref.3).

The second type of cell, less often used, consists of a crucible made from platinum or some other conducting material. The crucible is filled with melt, and forms one of the electrodes; the second electrode is a metal rod or hemisphere which is lowered into the melt to a pre-set position (Ref.4).

Crucible-type cells have cell constants of the order 0.1 cm^{-1} (Ref.5), and therefore have resistances of about 0.1 ohm when filled with a melt such as sodium chloride. The measurement of such a small resistance is not easy, and lead resistances have to be taken into account. However, suitable apparatus has been devised (Ref.5). The cell is useful for making measurements on poorly-conducting melts (when resistance is higher), and for measuring the conductivities of melts which contain some solid material in suspension or from which gas bubbles are constantly evolved. If a capillary cell were used in the latter cases, the solid particles or gas bubbles could cause large errors by entering the capillary and restricting the flow of electricity between the electrodes.

3.2. Polarisation effects.

Whichever kind of cell is used, alternating current must be employed in order to minimise errors due to electrode polarisation. In the most accurate work, the resistance of the cell is measured at a series of frequencies in the range 500 - 20,000 c/s. The measured resistance (R_ω) is plotted against the reciprocal of the square root of the frequency ($\omega^{-\frac{1}{2}}$), when a straight line is obtained. This is extrapolated, and the resistance corresponding to infinite frequency (R_∞) is assumed to be free from error due to polarisation (Ref.1). The difference between $R_{1,000\ c/s}$ and R_∞ depends on the current density at the surface of the electrodes; if the current density is low, the correction is small. In the measurements on potassium nitrate made by Krüger and Weisgerber (Ref.6), $R_\infty - R_{1,000}$ was as much as 5% of R_∞. However, Jaeger and Kampa (Ref.4), using a platinum crucible cell, applied no correction and yet obtained results for potassium nitrate which were almost identical with the

corrected results of Kröger and Weisgerber. In this case the large area of the electrodes of the crucible cell caused the polarisation error to be negligible. Janz and Lorenz (Ref.7) measured the conductivities of alkali-metal carbonate melts, using a capillary cell; they found that $R_{\infty} - R_{1,000}$ was about 0.2%.

3.3. Calibration of conductivity cells.

The specific conductivity of the melt (σ) is calculated from the (corrected) cell conductivity ($1/R_{\infty}$) by multiplication by the cell constant c. The cell constant is found by filling the cell with a standard aqueous solution of potassium chloride, and measuring its resistance at 25.0°C. If R is the measured resistance and σ_s is the specific conductivity of the standard solution, c at 25.0°C is given by

$$c = R_{\circ} \sigma_s . \qquad (3.1)$$

Values of σ_s for solutions of different concentration are given in the literature.(Ref.8) The cell constant at higher temperatures is calculated from that at 25°C by allowing for the thermal expansion of the cell (see page 117). The correction is usually very small for capillary-type cells made from glass or silica; in the work described below it was 0.05% per 100°C. It may be larger for crucible cells, since these are made from metal and have a relatively high coefficient of thermal expansion.

When calibrating a conductivity cell in the way described above, it is best to use a standard solution whose specific conductance is as close as possible to that of the melt examined.

3.4. Treatment of electrode surfaces.

Cowen and Axon investigated the effect of platinising the electrodes of a fused salt conductivity cell. They found that platinisation had little effect on the results (at 200 - 400°C) (Ref.2).

3.5. Theoretical treatment of the conductivity of melts.

The equivalent conductivity of a melt, Λ, is calculated from the specific conductivity Λ by the expression

$$\Lambda = \sigma . V_e , \qquad (3.2)$$

where V_e is the equivalent volume of the melt. For a pure salt,

$$V_e = M/\rho , \qquad (3.3)$$

M being the equivalent weight of the salt and ρ the density of the melt. For a mixture,

$$V_e = \sum_i (M_i . x_i)/\rho , \qquad (3.4)$$

where M_i and x_i are the equivalent weight and equivalent fraction of the i'th component of the mixture.

The variations of σ and Λ with temperature are usually expressed by the equations

$$\sigma = \sigma_0 . \exp(-E_\sigma/RT) \qquad (3.5)$$

and

$$\Lambda = \Lambda_0 . \exp(-E_\Lambda/RT) . \qquad (3.6)$$

E_σ and E_Λ are known as the activation energies for

conduction (although comparison of (3.5) and (3.6) with the equations given below for the conductivity of solid salts indicates that the term 'activation energy' is used rather loosely here. For the solids, the exponential term in the conductivity expression contains the sum of two energies; one of these is the energy of activation for ion migration and the other is related to the energy of formation of a lattice defect).

E_Λ is always greater than E_σ ; they are related by the expression

$$E_\Lambda = E_\sigma + \alpha . RT^2 \qquad (3.7)$$

where α is the coefficient of cubic expansion of the melt. (Ref.9)

Absolute reaction-rate theory has been applied to the problem of ion migration in melts (Ref.10), and an expression for Λ has been derived which, after some simplification (Ref.1), reduces to

$$\Lambda = 5.18 \times 10^{18} . (D + 2) . z d_i^2 . \exp(\Delta S^*/R) . \exp(-\Delta H^*/RT) \qquad (3.8)$$

where D is the microscopic dielectric constant of the melt, z the valency of the migrating ions, $2d_i$ the distance (in ~~Angstrom units~~ cms.) moved by an ion when it migrates from one equilibrium position to the next and ΔS^* and ΔH^* are the entropy and enthalpy of activation for the migration process. The equation (3.8) gives the conductivity due to migration of a single ionic species. In practice, both anions and cations make significant contributions to the conductivity of melts. (see, for example, Refs.11 - 14).

3.6. Results of earlier investigations.

The results of conductivity measurements provide important evidence on the nature of the structural units in melts. It has been shown in many cases that Faraday's laws of electrolysis apply to molten salts (see, for example, Ref.15 (silver and thallous halides) and Refs. 16 and 17 (potassium chloride)). This indicates that the conduction of electricity by these melts occurs by ion migration as opposed to electron transfer.

The value of the equivalent conductivity σ gives an indication of the degree of ionisation of a melt. When the equivalent conductivities of different substances are to be compared, σ is usually calculated at a temperature 1.10 T_m, where T_m is the melting-point of the salt in ^{o}K. For the alkali halide melts, σ at 1.10 T_m is of the order 80 - 200 $ohm^{-1}cm^{2}.\ equiv.^{-1}$. This is of the same order of magnitude as the equivalent conductivity of a dilute aqueous solution of an alkali halide, which suggests that these melts are composed of ions.

The literature contains several collections of fused-salt conductivity data (Refs.18 - 22).

Table 3.1. shows some selected values for chloride melts. The figures given in the Table have been chosen to show that there is no sharp demarcation between highly-conducting and poorly-conducting substances. The weakly conducting melts are supposed to consist mainly of undissociated molecules; this has been confirmed by Raman spectroscopy in some cases (see, for example, Ref.23, which describes the Raman spectrum of zinc chloride).

TABLE 3.1. Equivalent conductivities (Λ) of some chloride melts at temperature 1.10 T_m (^oK) (From Janz et al., Ref.19).

Salt	($ohm^{-1}cm^2$ $equiv.^{-1}$)
LiCl	183
CsCl	86
$BaCl_2$	77
$CaCl_2$	64
$MgCl_2$	35
$LaCl_3$	29
$InCl_3$	14.7
YCl_3	9.5
$ZrCl_4$	0.85
$BeCl_2$	8.8×10^{-2}
$HgCl_2$	3×10^{-2}
$ZnCl_2$	2×10^{-2}
$TlCl_3$	3×10^{-3}
$PbCl_4$	2×10^{-5}
WCl_6	2×10^{-6}
$NbCl_5$	2×10^{-7}

Table 3.2 gives values of σ and Λ for the nitrate and nitrite melts dealt with in the experimental section of this thesis. It is seen that the conductivities of these melts (at 1.10 T_m ^oK) are lower than those of the fused alkali halides (also at 1.10 T_m) by a factor of two or three. However, the difference between the two groups is much smaller if the results obtained for the nitrates and nitrites are extrapolated to above the melting-point of the halides (say to 1000°C), and comparison is made at this temperature.

These facts are consistent with the hypothesis that the melts listed in Table 3.2. are ionic in nature.

TABLE 3.2. Specific and equivalent conductivities of nitrate and nitrite melts at 1.10 T_m (^oK).

Salt	Melting point (^oC)	Specific conductivity ($ohm^{-1}cm^{-1}$)	Equivalent conductivity (ohm^{-1} cm^2 $equiv^{-1}$)
$NaNO_3$	308	1.21 (b)	55.05
KNO_3	334	0.794(c)	45.02
$RbNO_3$	310	0.550(b)	37.51
$CsNO_3$	409	0.639(b)	45.47
NH_4NO_3	169	0.447(b)	(a)
$AgNO_3$	206	0.87 (b)	37.75
$TlNO_3$	207	0.475(d)	26.4
$NaNO_2$	281	1.545(d)	59.80
KNO_2	420	1.37 (d)	(a)

(a) The equivalent volumes of ammonium nitrate and potassium nitrite have not been measured.

(b) International Critical Tables.

(c) Present work.

(d) Ref.20.

For most pure fused salts, $\log(\sigma)$ is a straight-line function of I/T (^{o}K); this is so for the alkali halides and alkaline-earth halides, silver chloride, thallous chloride, cadmium chloride and lead bromide (Ref.24), and also for some mixtures of alkali halides with one ion in common, e.g. NaBr + NaCl, NaBr + KBr, NaI +KI (Ref.25).

Very slight curvature is observed in the plots of $\log(\sigma)$ against I/T for some pure fused salts and mixtures which are believed to be fully dissociated, for example NaCl + CsCl, KCl + LiCl, NaCl + $CaCl_2$ (Refs.26,27). For the mixtures, the change in slope is most marked in the temperature range between the lower of the two melting-points and the eutectic point; in every case, the plot becomes steeper as the temperature is lowered.

However, similar plots for lanthanum chloride, zinc chloride and beryllium chloride show marked curvature; as the melts are heated from their melting-points through a temperature interval of $50^{o}C$, the slope of the $\log(\sigma)$ - $1/T$ plot falls by a factor of 3 for $BeCl_2$ and by a factor of 2 for $ZnCl_2$ (see Refs.28,29). These changes in slope are almost certainly due to constitutional changes which occur when the melts are heated (i.e. changes in the degree of polymerisation and degree of ionisation of the simple molecules MCl_2).

Plots of $\log\Lambda$ against $1/T$ have slight curvature even for pure alkali halide melts (Ref.30). This indicates that the enthalpy of activation for ion migration varies with temperature; the linearity of plots of $\log\sigma$ against $1/T$ for some substances mentioned above is probably due to fortuitous cancelling of opposing factors.

The variation of equivalent conductivity with composition has been investigated for a large number of binary fused salt systems. In only one system ($NaNO_3$ - $NaNO_2$; Ref.31) were the conductivity isotherms found to be straight lines; in most cases a negative deviation is observed. If the maximum deviation from linearity is less than 15%, it is usually ascribed to non-specific ionic interaction. Examples of systems in this category are $NaNO_3$ - KNO_3 (Ref.32), $NaNO_3$ - $AgNO_3$ (Ref.33) and KCl - $CaCl_2$ (Ref.34); many others are listed by Bloom (Ref.35).

In some systems much larger negative deviations are recorded. The maximum deviation often occurs at a composition corresponding to the formula of a compound formed between the two components in the solid phase (as indicated by a maximum in the freezing-point diagram), and the activation energy E_A also has a maximum at this composition. These larger deviations are ascribed to specific ionic interactions in the mixtures, with formation of complex ions. Systems showing this behaviour include KCl - $CdCl_2$ (Ref.24), KCl - $ZnCl_2$ (Ref.36) and KCl - $MnCl_2$ (Ref.32). In the last example, the maximum deviation in the equivalent conductivity isotherms was -35% at 850°C.

3.7. Conductivity in ionic solids, and the Wagner effect.

A brief discussion of this subject must be given here, since it has a bearing on the experimental work presented later.

Consider a sodium chloride crystal in which all the lattice sites are occupied. Suppose that an equal number of anion and cations are removed from their sites and transferred to vacant positions on the surface of the crystal. This

rearrangement must be accompanied by an increase in the enthalpy of the system, but the entropy will also increase because the vacancies can be positioned anywhere in the lattice. The introduction of defects of this type into a perfect crystal therefore results in a lowering of its free energy, which reaches a minimum when the concentration of 'holes' attains a certain value. This equilibrium concentration is given by

$$n = N.\gamma.B \exp-(\tfrac{1}{2}W_0/kT), \qquad (3.9)$$

where n/N is the fraction of lattice sites vacant, γ is a factor (~ 100) allowing for the effect of the 'holes' on the vibrational entropy of the crystal, W_0 is the energy required to form one vacancy of each sign at $0^\circ K$ and B is a constant (~ 100) which accounts for the fact that the thermal expansion of the crystal is accompanied by a reduction in the energy of hole formation (Ref.37).

If an electric field is applied to a crystal containing defects of this kind, (Schottky defects), conduction can occur by migration of ions into neighbouring vacancies. If U_0 is the energy of activation for this process at $0^\circ K$, it can be shown that the specific conductivity σ of the crystal is

$$\sigma = (\sigma_0/kT).\exp -(\tfrac{1}{2}W_0 + U_0)/kT \qquad (3.10)$$

where σ_0 is a constant for a given substance and W_0 is the energy of formation of a pair of Schottky defects at $0^\circ K$. (Ref.37).

The expression (3.10) gives the conductivity due to migration of one species of ion only. In principle, both anions and cations can contribute to the flow of current, each having its own value of U_0. However, transport

experiments have shown that, in practice, one ion carries nearly all the current, which implies that the two values of U_o differ by much more than kT. For example, only the negative ions are mobile in solid $BaCl_2$, $BaBr_2$, $PbCl_2$, and $PbBr_2$, while the positive ions carry all the current in the alkali halides below 500°C and in silver and cuprous halides (Ref.38). In the case of the last two examples, conduction occurs by movement of interstitial cations (Frenkel defects).

Suppose that some cadmium chloride is made to enter solid solution in sodium chloride. Since the cadmium ions are divalent, a cation site must remain vacant for each cadmium ion introduced, in order that the overall electrical neutrality of the lattice may be maintained. The sodium ions can migrate into these new vacancies, which therefore cause the electrical conductivity of the crystal to increase. The enhancement is very large if the concentration of cadmium ions is high compared with the concentration of Schottky defects which were originally present in thermal equilibrium. The phenomenon is known as the Wagner effect, after its discoverer (Ref.39), and has been observed in several halide systems (for example, KCl + Ba^{++}, (Ref.40)). The Wagner effect has also been observed in a solid nitrate system (KNO_3 + Ca^{++} ; Ref. 44).

3.8. Aim of the present work on electrical conductivities of melts.

Attempts have been made to interpret the behaviour of ionic melts by regarding them as 'quasi-crystalline'; that is, the melt is considered as a crystal containing various defects such as Schottky holes, Frenkel defects and paired vacancies (Refs.45,46,47).

The Wagner effect, described in the previous Section, is a characteristic property of ionic crystals; it has been observed in many halide systems, and recent work has shown that it also takes place in solid nitrates (Ref.44). In order to investigate the extent to which the term 'quasi-crystalline' could be applied to melts, it was thought interesting to carry out Wagner's experiment on an ionic melt system, and to find whether the electrical conductivity of a melt of formula M'X could be enhanced by addition of one of formula $M''X_2$ (where M' and M'' are monovalent and divalent cations, respectively).

The salts chosen for the investigation were potassium nitrate (as M'X) and barium nitrate (as M''X). The freezing-point diagram for binary mixtures of these melts (see page 140) shows that no intermediate solid compounds are formed, so the situation is not complicated by the possibility of complex ion formation. Both salts are readily obtainable in a high state of purity (see page 97), and neither is hygroscopic. The anions K^+ and Ba^{++} have almost equal ionic radii (1.33 and 1.35A respectively; Ref.48), so the replacement of one by the other in any crystalline structure should take place with minimum distortion of the lattice.

Since the object of the investigation was to find the change in the electrical conductivity of potassium nitrate brought about by the addition of barium nitrate, the relative accuracy of the measurements on different mixtures was of more significance than the absolute accuracy of the individual results. For this reason, the conductivities of the melts were all measured in the same cell, using an a.c. bridge operating at a single frequency. It was considered unnecessary to correct the results for polarisation effects by measuring conductivities at different frequencies and making an extrapolation to infinite frequency. This

correction would have no effect on the relative accuracy of the conductivities of the mixtures, since the polarisation effects were the same for all.

The experimental details of this work are described in Chapter 9, and the results are given in Chapter 12.

REFERENCES TO CHAPTER 3.

1. E.R. Van Artsdalen and I.S. Yaffe, J. Phys. Chem., (1955), 59, 118.

2. H.C. Cowen and H.J. Axon, Trans.Farad.Soc., (1956), 52, 242.

3. G. Jones and R.C. Josephs, J. Amer. Chem. Soc., (1928), 50, 1049.

4. F.M. Jaeger and B. Kampa, Z. anorg. u. allg. Chem., (1920), 113, 27.

5. J.D. Edwards, C.S. Taylor, A.S. Russell and L.F. Maranville, J. Electrochem. Soc., (1952), 99, 527.

6. C. Kröger and P. Weisgerber, Z. phys. Chem., (neue Folge), (1955), 5, 192.

7. G.J. Janz and M.R. Lorenz, Fuel Cell Symposium, Electrochemical Society National Meeting, Indianapolis, May,1961.

8. G. Jones and B.C. Bradshaw, J. Amer. Chem. Soc., (1933), 55, 1780.

9. R.L. Martin, J. Chem. Soc., (1954), 3246.

10. J.O'M. Bockris, J.A. Kitchener, S. Ignatowicz and J. Tomlinson, Trans. Farad. Soc., (1952), 48, 76.

11. Laity and Duke, J. Electrochem. Soc., (1958), 105, 97.

12. A. Klemm, Discussions Farad. Soc., (1961), 32, 203.

13. F.R. Duke and A.L. Bowman, J. Electrochem. Soc., (1959), 106, 626.

14. F.R. Duke and B. Owens, J. Electrochem. Soc., (1958), 105, 477.

15. C. Tubandt and E. Lorenz, Z. phys. Chem., (1914), 87, 513.

16. R.Lorenz, "Die Elektrolyse geschmolzener Salze", Halle, (1905).

17. P. Drossbach, "Elektrochemie geschmolzener Salze" Berlin, (1938).

18. J. O'M. Bockris, "Modern Aspects of Electrochemistry", Butterworths, London, (1959).

19. G.J. Janz, C. Solomons and H.J. Gardner, Chemical Reviews, (1958), 58, 461.

20. J.P. Frame, E. Rhodes and A.R. Ubbelohde, Trans. Farad. Soc., (1959), 55, 2039.

21. Iu.K. Delimarskii and B.F. Markov, "Electrochemistry of Fused Salts", Sigma Press, Washington, (1961), Chapter 1.

22. A.I. Belyaev, E.A. Zhemchiuzhina and L.A. Firsanova, "Fizicheskaya Khimiya Rasplavlennikh Soley", Moscow, (1957), Chapter IV.

23. W. Bues, Z. anorg. Chem., (1955), 279, 104; Z. phys. Chem., (neue Folge), (1957), 10, 1.

24. H. Bloom and E. Heymann, Proc. Roy. Soc., (1947), A188, 392.

25. Delimarskii and Markov, loc. cit., page 27.

26. Delimarskii and Markov, loc. cit., page 30.

27. B.F. Markov, Doklady Akad. Nauk. S.S.S.R., (1955), 102, 1163.

28. Delimarskii and Markov, loc.cit., page 18.

29. J.D. Mackenzie and W.K. Murphy, J. Chem. Phys., (1960) 33, 366.

30. I.S. Yaffe and E.R. Van Artsdalen, J. Chem. Phys., (1956), 60, 1125.

31. H. Bloom, I.W. Knaggs, J.J. Molloy and D. Welch, Trans. Farad. Soc., (1953), 49, 1458.

32. I.G. Murgulescu and St. Zuca, Revue de Chemie, Acad. R.P.R., (1959), 4, 227.

33. J. Byrne, H. Fleming and F.E.W. Wetmore, Canad. J. Chem., (1952), 30, 922.

34. R.W. Huber, E.V. Potter and H.W. St.Clair, U.S. Bur. Mines., Repts. Invest., (1952), 4858, 1.

35. H. Bloom, Revs. of Pure and Applied Chem., (1959),9,139.

36. F.R. Duke and R.A. Fleming, J. Electrochem. Soc., (1957), 104, 251.

37. N.F. Mott and R.W. Gurney, "Electronic Processes in Ionic Crystals", Oxford, (1940).

38. W. Jost, "Diffusion und chemische Reaktion in festen Stoffen", Dresden, (1937), page 80.

39. Koch and Wagner, Z. phys. Chem., B, (1937), 38, 295.

40. H. Kelting and H. Witt, Z. Physik, (1949), 126, 697.

41. H.W. Etzel and R.J. Maurer, J. Chem. Phys., (1950), 18, 1003.

42. S. Tetlow, Z. phys. Chem., (1950), 195, 197 and 213.

43. H. Pick and H. Weber, Z. Phizik, (1950), 128, 409.

44. B. Cleaver, E. Rhodes and A.R. Ubbelohde, Discuss. Farad. Soc., (1961), 32, 210.

45. Frenkel, "Kinetic Theory of Liquids", Clarendon Press, Oxford, (1946) (Second edition).

46. A.R. Ubbelohde, Quart. Revs. Chem. Soc., (1950), 4, 380.

47. M. Blander, J. Phys. Chem., (1959), 63, 1262.

48. L. Pauling, "The Nature of the Chemical Bond", Oxford, (1940), (Second edition).

CHAPTER 4.

PREVIOUS WORK ON THE DENSITIES OF FUSED SALT SYSTEMS.

4.1. Experimental techniques.

The most widely used method for the measurement of density involves weighing a bob of precious metal which is suspended in the melt (Refs. 1 and 2). Several practical difficulties limit the accuracy of this method:

(a). The bob may be buoyed up by gas bubbles formed in the melt.

(b). Some salt may freeze onto the suspension wire at the point where it passes through the surface of the melt. The weight of the bob must be corrected by subtracting the weight of this salt.

(c). The apparent weight of the bob is sensitive to convection currents in the melt sample. The furnace containing the melt must have a very even temperature distribution if this source of error is to be avoided.

(d). Surface tension effects cause a small downward pull on the suspension wire.

(e). The weighing-balance must be protected from warm air currents rising from the region of the furnace.

(f). A correction must be made for the thermal expansion of the bob; for a platinum bob at 1000°C, the correction is

as much as 3%. Care must be taken to avoid the use of metals which have transitions between room temperature and the temperature of measurement.

Because of these difficulties, some workers have preferred to use a dilatometer, i.e. a Pyrex or silica bulb with a graduated capillary emerging from it (Refs. 3 and 4). The volume of the bulb and the area of cross-section of the capillary are both determined at room temperature. The dilatometer is filled with melt and placed in a thermostat, and the density is found by observing the position of the meniscus in the capillary. Measurements can be made on the same sample over a range of temperatures, which requires that the whole of the capillary should be visible to the experimenter. This is inconvenient because the presence of a large observation window in the thermostat makes accurate temperature control more difficult.

A modification of the dilatometric method has recently been introduced in which these difficulties are avoided (Ref.5). The measuring cell consists of a U-tube whose two limbs are capillaries (see diagram on page 126). The cell is filled with melt, and a pressure is applied above the liquid in one limb until the meniscus is brought to a fiducial mark (which is observed through a small window). The gas pressure required to hold the meniscus in this position is then measured with a manometer. The density of the melt can be calculated from this pressure if the volume of the bulb, the cross-sectional area of the capillaries and the mass of the melt are known.

This method has the following advantages over the simple dilatometric technique:

(a). Only the fiducial mark has to be observed. The

thermostat need have only a small window, and heat losses are thereby minimised.

(b). The manometric fluid can be chosen to have a density of ~ 1, whereas salt densities are commonly in the range 2 - 4. When a measurement is being made, the vertical height between the menisci in the manometer is 2 - 4 times the corresponding height in the densitometer. The error in the determination of the latter is therefore less by a factor of 2 - 4 times than the error which would be involved in a direct measurement.

Since the introduction of the method in 1958, only Pyrex densitometers have been used (at temperatures below 500°C). Metal cells could be used at higher temperatures if some means could be devised for observing the positions of the menisci (e.g. the use of electrical contacts).

The manometric method was used to make the density measurements on fused mixtures of potassium nitrate and barium nitrate which are presented in this thesis. A full description of the technique is given on page 125.

4.2. Results obtained by previous workers.

When the density of a melt is measured over a range of temperature, the results are usually summarised by an equation of the type

$$\rho_t = \rho_o \cdot \left[1 + A(t - t_o) + B(t - t_o)^2 \right], \quad (4.1)$$

where ρ_t is the density at $t^\circ C$, ρ_o is the density at $t_o^\circ C$ and A and B are constants. The first two terms are often sufficient if the temperature range covered is less than 100°C.

The equivalent volume of a melt is calculated by dividing the equivalent weight by the measured density. For a mixture, the mean equivalent weight $\bar{E}$ must be used ; it is given by

$$\bar{E} = \sum_i \left(E_i . x_i \right), \qquad (4.2)$$

where E_i and x_i are the equivalent weight and equivalent fraction of the i'th component of the mixture.

The equivalent volume isotherms of binary salt systems sometimes provide evidence for the formation of complex ions. When no complexes are present, the isotherms are nearly straight lines (the maximum deviation from ideality being of the order 0.5%). The deviation is particularly small if the components of the mixture have an ion in common; examples are KNO_3 - $NaNO_3$, and $NaNO_2$ - $NaNO_3$ (Ref.2).

If complex ions are formed in the mixture, the equivalent volume isotherms are curved; the maximum deviation occurs at a composition corresponding to the formula of the complex, and may be up to 5%. The excess volume is usually positive.

The diagram on page 329 shows the excess volume plotted against composition for several binary melt systems, two of which contain complex ions, ($MnCl_2$ - KCl and CdI_2 - KI).

4.3. Aim of the present research on fused salt densities.

In suitable cases, the study of equivalent volume isotherms can yield information about the structure of binary melt mixtures in which no complex ions are formed.

If in a solid salt of formula M'X some of the monovalent cations M' are replaced by divalent cations M", an equivalent

number of cation vacancies are produced (provided that the structure of the anion lattice remains that of the pure salt M'X). Density measurements have shown that this occurs when calcium ions enter solid solution in potassium chloride (Ref.6).

The properties of melts have sometimes been discussed in terms of theories of disordered solids (Refs.7,8,9), and it is therefore pertinent to enquire whether the same observation would be made if the above experiment were performed with two melts.

Potassium nitrate and barium nitrate are a convenient pair of salts on which to carry out an investigation of this kind; the cations K^+ and Ba^{++} have very similar ionic radii (1.33 and 1.35 A respectively; Ref.10), so simple replacement of 2n K^+ions by n Ba^{++} ions and n cation vacancies should leave the equivalent volume practically unchanged.

Measurement of the electrical conductivity of fused potassium nitrate with small additions of barium nitrate had shown that the Wagner effect did not occur in this salt system; in fact the conductivity of the potassium nitrate was reduced slightly when barium nitrate was added. This implies that replacement of potassium ions by barium ions in the melt is not accompanied by an increase in the number of cation vacancies. If this is so, the equivalent volume of the mixture should not remain constant when barium replaces potassium, but should be reduced progressively.

In order to confirm this interpretation of the conductivity results, the densities of fused potassium nitrate - barium nitrate mixtures were measured over the composition range 0 - 50 equivalent % barium nitrate, and the equivalent volume isotherms were derived.

The experimental technique used gave results of very high relative precision (see page 221), and this allowed accurate determination of the equivalent volume changes accompanying the composition changes.

The work is described in Chapter 10, and the results are given in Chapter 13.

REFERENCES TO CHAPTER 4.

1. E.R. Van Artsdalen and I.S. Yaffe, J. Phys. Chem.,(1955), 59, 118; ibid., (1956), 60, 1125.

2. H. Bloom, I.W. Knaggs, J.J. Molloy and D. Welch, Trans. Farad. Soc., (1953), 49, 1458.

3. N.K. Boardman, F.H. Dorman and E. Heymann, J. Phys. Chem., (1949), 53, 375.

4. K. Laybourn and W.M. Madgin, J. Chem. Soc., (1934), 1.

5. L.J.B. Husband, J.Sci.Instrum., (1958), 35, 300.

6. H.Pick and H. Weber, Z. Physik, (1950), 128, 409.

7. Frenkel, "Kinetic Theory of Liquids", Clarendon Press, Oxford (1946) (Second edition).

8. A.R. Ubbelohde, Quart. Revs. Chem. Soc., (1950), 4, 380.

9. M. Blander, J. Phys. Chem., (1959), 63, 1262.

10. L. Pauling, "The Nature of the Chemical Bond", Oxford (1940), (Second edition).

CHAPTER 5.

THE ULTRA-VIOLET SPECTROSCOPY OF FUSED-SALT SYSTEMS.

The first part of the Chapter contains an account of the developments in technique which have enabled ultra-violet spectroscopy to be carried out on fused-salt systems. An outline is then given of the types of study so far made in the field, and of the way in which progress has been made from qualitative work to the accurate measurement of molar extinction coefficients and frequencies of maximum absorption. The Chapter is concluded with a statement of the aims of the author's experimental study of the absorption spectra of nitrates and nitrites in the near ultra-violet region.

5.1. Developments in experimental technique.

The main practical problems which have to be overcome in order to obtain absorption spectra of fused salts are the following;

(a) A suitable container must be found which is transparent to the radiation used and which is not attacked by the melt. When pure melts are studied, a cell with a path-length of a few microns is sometimes required, because of the high extinction coefficients encountered.

(b) The sample must be maintained at a high temperature (up to 800°C) while the examination is carried out, using a thermostat having entry and exit ports for transmission of the light beam. The heat generated by the thermostat must not be allowed to reach the surrounding structure of the spectrophotometer.

(c) At temperatures above 500°C, the radiation emitted by the sample is sufficiently intense to be detected by the photomultiplier, and could give rise to serious errors in a spectrophotometer having the conventional optical arrangement (as illustrated on page 150).

Solutions have been found to all these problems, and will be described in turn.

5.1.1. Choice of material for absorption cells.

Quartz cells of 1-cm path-length have been used as containers for solutions of transition-metal salts in chloride or bromide eutectics (Refs.1 and 2), and in sulphate eutectics (Ref.3). The concentration of the solution is adjusted until the optical density reaches a suitable value; by this means, absorption maxima can be plotted even if the molar extinction coefficient of the solute is greater than 10,000 litres/mole. cm.

In order to record the maxima in the absorption spectra of pure salts, much shorter path-lengths must often be used (100μ - less than 3μ). Two methods have been devised for preparing samples of this thickness; they are both described in detail on pages 55-56.

Melts containing fluoride ions or lithium ions present special difficulties because they etch silica. They have been studied successfully in cells made from magnesium oxide (Ref.4), and have also been examined as drops held on loops of platinum wire (Ref.4). This 'pendant drop' technique has been used to obtain the spectra of very viscous melts and glasses (Ref.5).

Solutions of alkali metals in fused alkali halides attack all the materials mentioned above. They are being examined in cells made from artificial sapphire (Al_2O_3); even this is etched slowly by such solutions, and the use of a diamond cell has been suggested by Sundheim.

5.1.2. Thermostats.

Several thermostats have been described which are suitable for maintaining fused salt samples at temperatures up to 800°C (Refs.1,2,4,6,7). The design used by the author was based on that of Rhodes and Ubbelohde (Ref.7).

Most workers have used a water-jacket to cool the outside of the thermostat unit, and so prevent heat from reaching the surrounding parts of the spectrophotometer.

The thermostat must have entry and exit windows to allow passage of the ultra-violet beam, and the loss of heat through these windows causes temperature gradients to be set up in the sample. In the present work these gradients were measured and steps were taken to minimise them (see page 168). No previous worker seems to have paid any attention to this factor.

5.1.3. Elimination of black-body radiation.

The difficulties arising from the emission of black-body radiation by a hot sample have been elegantly overcome by Gruen and by Sundheim (Refs.1,2). They reversed the normal positions of the detector and light-source units, so that light from the lamp passed first through the sample, then through the chopper and monochromator and finally to the detector. The radiation emitted by the sample was of much

lower frequency than the measuring beam, and was effectively filtered out by the monochromator.

This problem did not arise in the work carried out by the author, because samples were not heated above 450°C.

5.2. An outline of previous experimental studies in the field of fused salt spectroscopy.

5.2.1. Semi-quantitative work.

The first measurement of the ultra-violet absorption spectrum of a fused salt was made as long ago as 1916 by K. Schaefer, who studied pure potassium nitrate (Ref.8). He plotted the weak absorption band of this melt at 33 kcm^{-1}, and noticed that the frequency at the absorption maximum was very near to that of a dilute aqueous solution of the salt. This was a remarkable achievement at the time, but by modern standards the spectra obtained by Schaefer are of poor quality.

The next report of work on pure melts did not appear until 1957, when Sakai recorded the spectra of thin films (0.5 μ) of rubidium, caesium and ammonium nitrates (Ref.9). He found that these salts all had an absorption edge in the region 35 - 40 kcm^{-1}, and showed that, when the samples were heated from room temperature through their respective melting-points, the band edge moved towards the visible. In the case of ammonium nitrate the band-edge frequency changed abruptly at the transition-point at 125°C and at the melting-point, but no such abrupt changes were detected for the other two salts either at transitions or on melting.

The absorption edge referred to by Sakai can now be identified as the low-energy edge of the strong absorption

band whose maximum is at 50 kcm^{-1} in aqueous solutions of nitrates (see page 73).

In 1958, Sundheim and Greenberg measured the absorption spectra of twenty pure fused salts (nitrates, halides, potassium dichromate and potassium thiocyanate) at temperatures about 20°C above their melting-points. They used thicker samples than Sakai (0.02 mm to 2 mm), and for every salt they recorded only an absorption edge. In the case of the nitrates this edge can now be identified as the low-energy edge of the weak absorption band whose maximum is at 33 kcm^{-1} (see page 67). In some cases measurements were made over a range of temperatures, and it was shown that the band-edge moved to lower frequency as the melts were heated (Ref.10).

5.2.2. Quantitative measurements; development of cells with short path-length.

The work described above must be regarded as semi-quantitative, because the spectra were characterised only by arbitrarily-defined band-edge parameters whose value depended on sample thickness. Parameters with more precise meaning, such as frequencies of absorption maxima and molar extinction coefficients, were first measured not for pure melts but for dilute solutions of absorbing ions in a transparent fused-salt solvent. The solute was usually a transition-metal salt, and its concentration was adjusted until the optical density of the solution reached a value suitable for the recording of absorption maxima. Ions whose spectra have been examined in this way include Mn(2) and Co(2) dissolved in chloride and in bromide eutectics (Ref.11), Co(2) and Ni(2) in a sulphate eutectic (Ref.3), and Ni(2), Co(2), Cr(3) and U(4) in a fluoride eutectic (Ref.4). These ions all have absorption in the visible region which can be attributed to

electronic transitions between the d-levels. The results have been interpreted in terms of the ligand-field theory, and it has often been possible to deduce the type of coördination of the anions around each transition-metal ion; for example, Gruen and McBeth (Ref.12) showed that Ni(2) has tetrahedral coördination of chloride ions when dissolved in fused caesium chloride.

The first accurate measurement of extinction coefficients and frequencies of band maxima for anions in fused-salt media were made by Smith and Boston (Ref.13), who recorded the absorption spectra of NO_3^-, NO_2^- and $CrO_4^=$ in dilute solution in a halide eutectic.

Corresponding data for <u>pure</u> fused salts containing these anions were more difficult to obtain, because the extinction coefficients are too high to permit the absorption maxima to be plotted using a cell of path-length about 1 mm. Further progress awaited the introduction of cell having much shorter path lengths (3μ to 100μ).

Two types of cell have been designed to meet this requirement. G.P. Smith (Ref.6) used a conventional 2mm. silica cell with a precision-ground, solid silica insert of thickness slightly less than 2 mm. The melt was displaced by the insert to form two thin films between it and the inner walls of the cell. Different path-lengths were obtained by using inserts of slightly different thickness; the shortest attainable was 20μ. Path-lengths were measured to $\pm$ 1% by use of a micrometer device, or by filling the cell with aqueous potassium chromate solution and measuring its optical density with the insert in position.

Using this type of cell, Smith measured the molar extinction coefficients of pure alkali nitrate melts at the maximum of

the weak band at 33 kcm^{-1}, with an absolute precision of ± 5%. He also recorded the frequencies of the band maxima to ± 20 cm^{-1} (but see page 240).

The 'silica insert' cell suffers from one serious defect; it is very likely to be broken if its contents are frozen and then remelted. It is therefore unsuitable for measuring the spectra of solid and liquid salt films in the region of the melting-point.

In order to make measurements of this kind, Rhodes and Ubbelohde introduced a different type of cell (Ref.7). The salt sample was held as a thin film between two silica plates, which were mounted in a stainless-steel holder. Films as thin as 3μ could be obtained in this way; thicker samples could be prepared by using spacers of platinum foil. The salt could be melted and frozen any number of times without risk of breaking the plates. Film thicknesses were estimated by weighing, but could not be measured to better than ± 10% because of edge effects. This cell is therefore less good than Smith's for the measurement of the extinction coefficients of the melts, but it is entirely satisfactory for comparing frequencies of absorption maxima for solid and fused salt samples. It was used by the author for the work described in this thesis; an illustration appears on page 165, and the method of preparing samples for spectroscopy is described on page 184.

5.3. Aim of the present work on ultra-violet spectroscopy of salts.

The work of Rhodes and Ubbelohde has shown that the two absorption bands of nitrates in the near ultra-violet have

variations with temperature which are related to corresponding structural changes. Their research was carried out mainly with reference to the stronger of these bands, and, because a hand operated instrument was used, the number of spectra obtained for each salt ($\sim$10) was the minimum necessary to map out the trends.

The spectrophotometer available for the present work scanned and recorded spectra automatically, and this greatly increased the ease and speed with which spectra could be obtained. A detailed and systematic survey of the effect of temperature on the spectra of nitrates and nitrites was undertaken, particular care being taken to measure the changes in the positions of the absorption bands which occured at melting-points and transition-points. Fifty or more scans were carried out on each salt studied. It was originally hoped that the survey would include measurements of the frequencies of the maxima of both bands, but the extinction coefficient in the region of the strong band was so high that only its low-frequency edge could be recorded. Attention was therefore focussed on the weaker band of the nitrate and nitrite absorption spectra, at 33 kcm^{-1} and 27 kcm^{-1} respectively.

The nature of the electronic transitions causing these bands is fairly well understood (see Chapter 6), and some knowledge has been gained on the influence of environment on the frequencies of the absorption maxima. The aim of the present research was:

(i) To add to the understanding of this environmental influence by measuring the frequency of the maximum of the weak band for nitrates and nitrites and observing the changes in this frequency which accompany known structural changes (i.e. those due to thermal expansion and to solid-solid transitions).

(ii) To measure the changes in the frequency of maximum absorption on fusion of the salts, and to use the previously-gained knowledge on environmental influence to elucidate the nature of the structural changes which occur on melting.

As a preliminary to the investigation of the spectra of solid nitrates and nitrites, some work was carried out to measure the polymorphic transition temperatures of the crystalline salts, using a simple spectroscopic technique. Prior knowledge of these temperatures simplified measurement of the abrupt changes in absorption frequency associated with the transitions.

To facilitate discussion of the results of this work, a summary of the present knowledge on the absorption of light by ionic substances is given in the next chapter. Particular attention is paid to the previous work (both practical and theoretical) on those absorption bands of the nitrates and nitrites which were the subject of the author's experimental study.

REFERENCES TO CHAPTER 5.

1. D.M. Gruen, J. Inorg. Nucl. Chem., (1957), 4. 74.

2. B.R. Sundheim and J. Greenberg, Revs. Sci. Instr., (1956), 27, 703.

3. K.E. Johnson and T.S. Piper, Discuss. Farad. Soc., (1961), 32, 32.

4. J.P. Young and J.C. White, Anal. Chem., (1959), 31, 1892.

5. J.D. Mackensie, R.S. McDonald and W.K.Murphy, Revs. Sci. Instr., (1961), 32, 118.

6. C.R. Boston and G.P. Smith, J. Phys. Chem., (1958),62,409.

7. E. Rhodes and A.R. Ubbelohde, Proc. Roy. Soc., (1959), A251,156.

8. K. Schaefer, Z. anorg. u. allgem. Chem., (1916), 97, 285.

9. K. Sakai, J. Phys. Chem., (1957), 61, 1131.

10. B.R. Sundheim and J. Greenberg, J. Phys. Chem., (1958), 28, 439.

11. B.R. Sundheim and M. Kukk, Discuss. Farad. Soc., (1961), 32, 49.

12. D.M. Gruen and R.L. McBeth, J. Phys. Chem., (1959), 63, 393.

13. G.P. Smith and C.R. Boston, Ann. N. Y. Acad. Sci., (1960), 79, 930.

CHAPTER 6.

THE ABSORPTION OF LIGHT BY IONIC SUBSTANCES (WITH PARTICULAR REFERENCE TO NITRATES AND NITRITES).

6.1. Introduction.

Electronic transitions accompanying light absorption in ionic media can be divided into two groups:

(i) 'Charge transfer' processes, in which an electron is transferred from one ion to an orbital centred on another ion (or group of ions).

(ii) 'Internal' transitions, in which an electron is excited from an occupied orbital to an empty orbital on the same ion.

The two types of transition represent extremes of possible behaviour; cases met with in practice often approximate to one or to the other, but sometimes have intermediate properties. Characteristic examples of the two main types of transition are given in the following sections.

6.2. Charge-transfer spectra.

Most of the features of charge-transfer absorption can be illustrated by reference to the spectra of the alkali halides.

In the vapour phase, these halides have particularly simple absorption spectra. In the frequency range between 50 kcm^{-1}

and the visible, sodium chloride vapour has a single absorption maximum and sodium bromide and iodide have two maxima (Ref.1). The frequency of the lowest-energy peak decreases in the order NaCl, NaBr, NaI, and the intervals between the pairs of peaks in the spectra of the bromide and the iodide are equal to the differences in energy between the $^2P_{3/2}$ and $^2P_{1/2}$ states of the respective halogen atoms. At higher frequencies further peaks are observed, at intervals corresponding to the separations between the lowest unoccupied energy levels in the sodium atom. If the alkali halide vapour is irradiated with light of frequency greater than that of the second absorption maximum, the atomic spectra of the alkali and halogen atoms are observed in emission.

The above evidence indicates that the absorption of light by a single alkali halide molecule causes the transfer of an electron from the halide ion to the metal ion:

$$Na^+Cl^- \xrightarrow{h\nu} Na\ Cl.$$

The lowest-frequency peak in the absorption spectrum corresponds to the production of atoms in their ground state, and the other peaks involve production of excited atoms. The fluorescence spectrum is emitted when these atoms return to their ground states (Ref.2)

The energy ($h\nu$) of the photon corresponding to the lowest-energy peak in the absorption spectrum is given by

$$h\nu = E - I + \Delta \quad , \qquad (6.1)$$

where E is the electron affinity of the halogen atom, I is the ionisation energy of the alkali atom and Δ is the difference between the dissociation energies of the ion-pair and the atom-pair. (Ref.3).

The absorption spectra of crystalline alkali halides are similar to those of the vapours, except that the maxima occur at higher frequencies (Ref.4); for example, the lowest-energy peak in the spectrum of sodium bromide vapour is at 36.4 kcm^{-1}, while that for the crystalline salt is at 52.6 kcm^{-1}. Broad bands are again observed at room temperature, and the extinction coefficients at the band maxima are of the order 10^3 - 10^4 litres/mole.cm. (Ref.5). Excitation is supposed to correspond to transfer of an electron from the halide ion to the shell of cations immediately surrounding it in the crystal. The frequency of the first absorption peak is again given by an expression of the type (6.1). Δ is now the difference in energy between a normal crystal and one in which atoms are substituted for a pair of adjacent ions; it is approximately equal to the energy of the Coulomb interaction of these adjacent ions with each other and with the remainder of the crystal (although detailed calculations have shown that the interaction energy between the atoms and the remainder of the crystal is not negligible; Refs.6,7).

For a series of alkali halides containing the same cation, the frequency of the lowest-energy absorption peak decreases in the sequence MF, MCl, MBr, MI, corresponding to the progressive decrease in the electron affinity E of the halogen atom. However, the frequency varies irregularly in the series NaI, KI, RbI, CsI, as Table 6.1. shows.

This irregularity must be ascribed to changes in the value of the interaction parameter Δ.

TABLE 6.1. Energy of the first ultra-violet absorption peak for alkali iodides, at 20°K. (Ref.5).

Salt	Frequency of first peak (kcm^{-1})
NaI	45.0
KI	47.0
RbI	46.1
CsI	46.8

Changes in the positions of the absorption maxima which occur when a given alkali halide is heated are also due to changes in Δ. This interaction term is smaller for an ion-pair in the vapour than for the same ion-pair in a crystal, and this explains why the peaks in the spectra of the vapours are at lower frequencies than those for the corresponding crystals (Ref.3). For the melts, Δ would be expected to have intermediate values; this has been shown to be true for lithium iodide, which is the only alkali halide melt for which the frequency of the first absorption maximum has been measured (Ref.8).

All ionic crystals are capable of showing charge-transfer absorption at sufficiently high frequency, although other processes can contribute to the spectrum. These are discussed in the next section.

6.3. Absorption due to 'internal' transitions.

The transitions between d-levels in the penultimate electronic shell of cations such as Ni^{++} and Co^{++} are examples of internal transitions which can occur in ionic media. They give rise to weak absorption in the visible and near ultraviolet region (molar extinction coefficients up to 500 litres/mole. cm). The energies of the d-orbitals (and therefore the frequencies of absorption) are influenced by the electrostatic field set up by the medium surrounding the absorbing ion, and it is sometimes possible to deduce from the spectrum the positions of the atoms or ions forming the first coordination shell around each transition-metal cation. Some examples are referred to on page 54.

In a medium containing polyatomic ions, another type of internal transition can occur. Consider the formation of a cation such as $(NO_3)^-$ from its constituent atoms, which can be visualised in the following way. The atomic orbitals of the outermost quantum shells of the atoms are combined to form molecular orbitals of σ and π symmetry, some of which are bonding, some non-bonding and some anti-bonding. The available electrons are then placed in the molecular orbitals, those of lowest energy being filled first. The order of filling is:

(i) σ-bonding (σ)
(ii) π-bonding (π)
(iii) non-bonding (n)
(iv) π-antibonding (π^*)
(v) σ-antibonding (σ^*)

The σ and π bonding orbitals are always equal in number to the σ^* and π^* antibonding orbitals, so if a stable ion is

to be formed some of the latter must remain unoccupied when all the electrons have been allocated. It is therefore possible for an electronic transition to occur between the filled orbitals and these empty antibonding orbitals. Since the π^* orbitals usually have lower energy than the σ^* ones, and the most weakly-bound electrons in the ion are usually in non-bonding orbitals, the transition of lowest energy involves excitation from n to π^* ($n \rightarrow \pi^*$ transition). $\pi \rightarrow \pi^*$, $n \rightarrow \sigma^*$ and $\sigma \rightarrow \sigma^*$ transitions can also occur, at progressively higher energies (Ref.9). If the energy of any of these processes is smaller than that for 'charge transfer' absorption, the spectrum will show additional bands on the low-frequency side of the charge-transfer bands.

There is evidence that the lowest-energy absorption bands of nitrates and nitrites are due to internal transitions of the kind described here. This evidence is presented in sections 6.5 and 6.6.

Absorption bands due to internal transitions have been observed in the spectra of many organic molecules (in the vapour phase, or dissolved in hydrocarbon solvents). It is found that the molar extinction coefficient is 10 - 100 litres /mole. cm for a forbidden $n \rightarrow \pi^*$ transition, 100 - 1,000 for an allowed $n \rightarrow \pi^*$ transition and about 10,000 for an allowed $\pi \rightarrow \pi^*$ transition. (Ref.10). The low intensity ($\epsilon \leqslant 20$) of the bands in the nitrate and nitrite spectra at 33 and 27 kcm^{-1} respectively therefore supports their assignment to 'internal' transitions.

6.4. Possibility of transitions having characteristics intermediate between 'charge-transfer' and 'internal'.

For an absorption band due to an internal transition in a

poly-atomic anion, the frequency of the maximum may be influenced by the neighbouring cations. These cations may affect the energies of the orbitals corresponding to the ground state and the excited state. The excited-state orbital is usually antibonding, and is situated at the periphery of the ion; it may therefore overlap with the cations. If the lowest unoccupied orbitals of the latter can combine with this anion orbital to produce an orbital having lower energy than either, this new orbital will receive the electron on excitation and the band will thereby acquire some charge-transfer character. This amplifies the statement made on page 60: the distinction between 'charge-transfer' and 'internal' transitions in a condensed medium is not a sharp one, and some absorption bands may have intermediate properties.

The formal definition of a charge-transfer process given on page 61 is also oversimplified. In an ion-pair molecule such as Na^+Cl^- in the vapour phase, the wave-function ψ of the ground state contains contributions both from the fully-ionised structure and from the structure in which a covalent bond is formed between the two atoms. The total wave-function may be written

$$\psi = a.\phi_{Na^+Cl^-} + b.\phi_{Na-Cl} ,$$

where $a > b$ in the ground state. If the molecule now absorbs light in the charge-transfer band, the wave-function of the excited state, ψ', is given by

$$\psi' = a'.\phi_{Na^+Cl^-} + b'.\phi_{Na-Cl} ,$$

where $b' > a'$.

It is a conclusion of wave-mechanical theory that light

absorption cannot occur unless b and a' are non-zero, i.e. the ground state must contain a contribution from the covalent structure and the excited state must have a partial ionic character (Ref.11). The formal definition of a charge-transfer process given at the beginning of this chapter therefore represents a limit which can never be achieved in practice.

6.5. Previous knowledge on the absorption spectra of nitrates in the region 50 - 20 kcm^{-1}.

Solid and fused metallic nitrates, and aqueous solutions containing nitrate ions, have a weak absorption band in the near ultra-violet with a maximum in the range 30 - 34 kcm^{-1}. The frequency of the maximum depends on temperature, the identity of the cation and, in the case of solids, on the crystal structure. For pure alkali nitrate melts, the molar extinction coefficient at the maximum of this band increases with the polarising power of the cation, and lies in the range 5 - 20 litres/mole cm. (Ref.12).

The weak band is overlapped on its high-frequency side by a stronger band which has a steeply rising edge at 39 - 41 kcm^{-1} and which reaches a maximum at 50 kcm^{-1} in aqueous solution ($\epsilon \sim$ 10,000 litres/mole cm; Ref.13).

The two bands are now discussed in detail. Particular attention is devoted to the weak band, because it formed the main subject of the author's experimental work in this field.

6.5.1. The weak band at 33 kcm^{-1}.

Experiments with single crystals of sodium nitrate and

potassium nitrate have shown that absorption in the region of the weak band occurs most strongly when the electric vector of the light is in the plane of the nitrate ion (Refs.14,15).

When nitrate crystals are cooled, the weak band is resolved into a series of peaks. These have been recorded at 20°K by Rodloff and by Schaumann (Refs.16,17), and in greater detail at 4°K by Sayre (Ref.15). Sayre studied single crystals of sodium and potassium nitrates, and recorded lines between 28 and 31 kcm^{-1}. The lines were sharp in the lower part of this frequency range, but became diffuse above 30.3 kcm^{-1}, which therefore represents a pre-dissociation limit. This frequency corresponds roughly to the energy required for the process

$$NO_3^- \longrightarrow NO_2^- + O\ (^3P).$$

The intensity of the lines increased with frequency. Sayre was able to analyse the spectrum in terms of two vibrational frequencies of 700 and 260 cm^{-1}, which he identified with the two asymmetric, in-plane vibrations of the excited ion. The spectrum arose by excitation from the lowest vibrational level of the ground-state ion to higher vibrational levels of the electronically excited ion; the observed lines corresponded to transitions $0 \rightarrow 1$, $0 \rightarrow 2$, ... $0 \rightarrow 5$, in terms of the vibration of frequency 700 cm^{-1}. The $0 \rightarrow 0$ line, (the band origin), was not recorded, and this may be taken as evidence for the assignment of the band to a 'forbidden' electronic transition. The maximum of the weak band corresponds to changes of vibrational quantum number in the range $0 \rightarrow 10$ to $0 \rightarrow 12$ (referring to the 700 cm^{-1} vibration).

From the results of his analysis, Sayre showed that the excited ion is equilateral and planar in its vibrational ground state. The stretching force-constants for the N-O

bonds are reduced to about 80% of the ground-state values, and the N-O bond-length is 1.7A in the equilibrium configuration (compared with 1.22A for the ground-state ion; Ref.18).

Application of the Franck-Condon principle shows that the excited ion is formed in a 'compressed' state over the entire frequency range in which absorption has been observed, i.e. transitions at $4^{o}K$ always occur from the v = 0 level of the ground state to the repulsive side of the potential energy surface of the excited state.

Calculation of the energies of the molecular orbitals in the nitrate ion show that the bonding and non-bonding (or weakly anti-bonding) orbitals in the second quantum shell are all filled in the ground state, the remaining empty orbitals in this shell being anti-bonding (σ^* and π^*). The relative energies of the highest occupied and lowest unoccupied levels, and diagrams of the molecular orbitals corresponding to them, are shown in Figure 6.1.

Opinions differ as to the exact nature of the electronic transition responsible for the weak band. Three possibilities have been suggested:

(i) $A_1' \not\rightarrow A_1''$ $(n \rightarrow \pi^*)$ (Refs.10,12,19,20)

(ii) $A_1' \longrightarrow E'$ $(\pi \rightarrow \pi^*)$ (Ref.15)

(iii) $A_1' \not\rightarrow A_2'$ $(n \rightarrow \sigma^*)$ (Ref.20)

The three transitions are marked on the energy-level diagram. Although the others cannot be eliminated conclusively, the first possibility seems the most likely, for the following reasons:

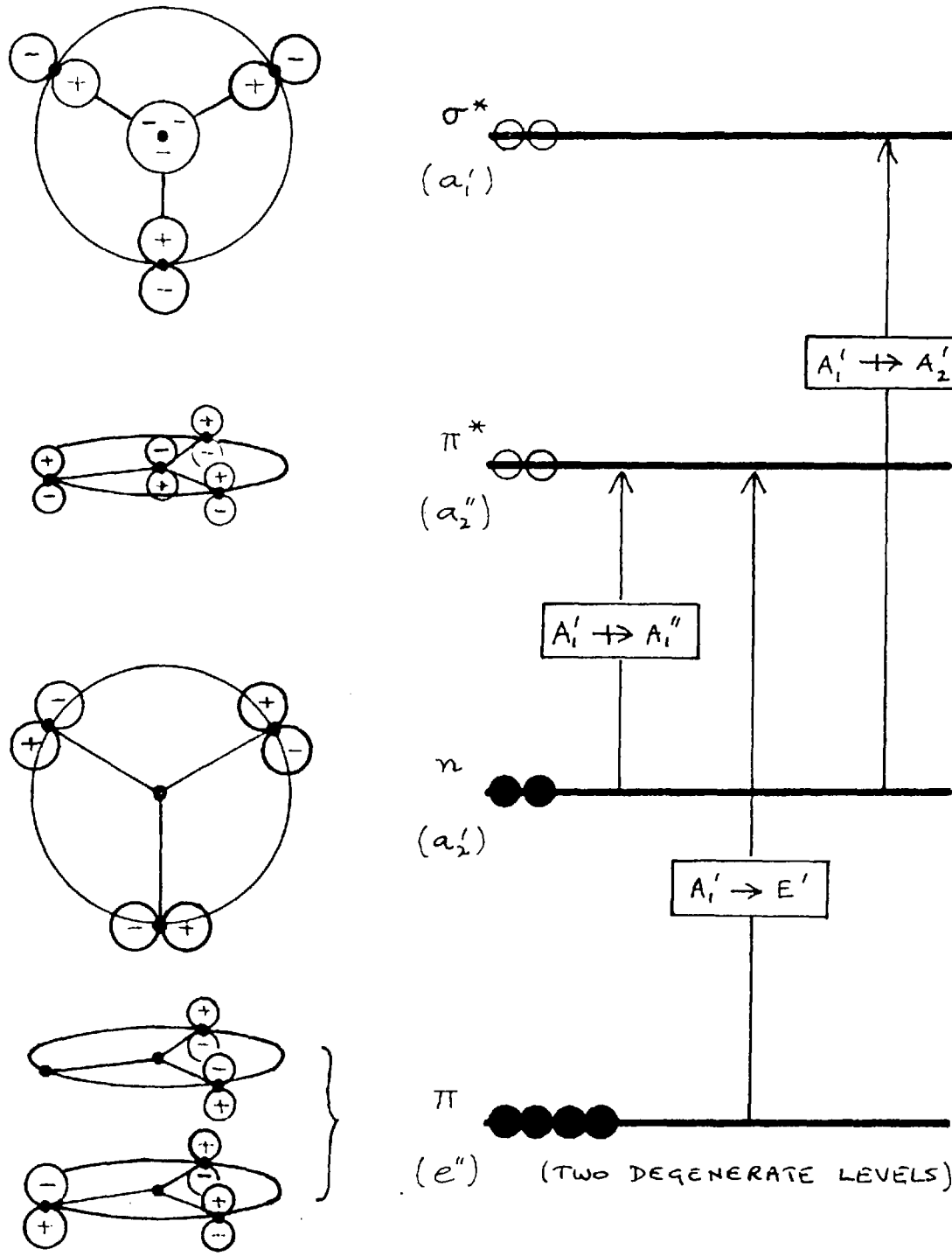


FIGURE 6.1. ENERGY LEVELS AND MOLECULAR ORBITALS IN THE NITRATE ION.

(a) The origin of the band is absent, which suggests that the transition is forbidden by selection rules. This eliminates (ii), which is an 'allowed' transition (although Sayre, in defence of mechanism (ii), suggests that the absence of the band origin is due to the large disparity between the N-O bond lengths of the ground and excited states. This causes the transition probability for the $0 \rightarrow 0$ transition to be very small, by the Franck-Condon principle).

(b) Wave-mechanical calculations suggest that the π^* orbital in the diagram has a lower energy than the σ^* orbital. The $n \rightarrow \pi^*$ transition energy should therefore be less than the $n \rightarrow \sigma^*$ energy, so the former should correspond to the lowest-frequency band in the absorption spectrum.

Assuming that the $n \rightarrow \pi^*$ assignment is correct, the transition can be described qualitatively in the following terms: the electron is excited from a non-bonding (or weakly anti-bonding) orbital centred on oxygen to an anti-bonding molecular π orbital. This antibonding orbital is relatively diffuse, and although the transition involves displacement of charge from the oxygen atoms towards the nitrogen atom (Ref.12) an overall expansion of the ion is involved.

Smith has measured the frequency of the absorption maximum of the weak band for pure alkali nitrate melts (Ref.12), and for mixtures of alkali nitrate melts with nitrates containing polyvalent cations (Ref.21). He was able to show that, for nitrate melts containing cations of rare-gas electronic configuration, the frequency E(2) of the maximum is given (at $365^{\circ}C$) by

$$E(2) = 3.81 + 0.34 \sum_i (X_i . z_i / r_i) \qquad (6.2)$$

where X_i, z_i and r_i are the electrical equivalent fraction, the valency and the radius (in Å) of the i'th cation species. The equation gives E(2) in electron-volts. This relationship is valid provided z_i/r_i does not exceed 3 $Å^{-1}$ for any cation species. If z/r exceeds this value (as it does for Mg^{++} and Y^{+++}), the band maximum occurs at a lower frequency than that calculated from the equation.

Smith points out that the neighbours of a nitrate ion can influence the value of E(2) in two ways:

(i) In a fused nitrate, the cations can assume positions around the nitrate ions which tend to stabilise the non-bonding electrons on the oxygen atoms. In this way the energy of these non-bonding electrons is lowered relative to their energy in a free nitrate ion. When optical excitation occurs, the non-bonding oxygen electrons are displaced, but the cations do not move during the time of the transition. Since their positions at this stage are not the most suitable ones for stabilisation of the excited ion, the stabilisation energy is reduced when the transition occurs and E(2) increases by a corresponding amount (relative to its value for an isolated nitrate ion). Since the stabilising influence is greatest when the electrostatic field set up by the cations is greatest, this effect contributes to the movement of the band maximum to higher frequencies which occurs when the cationic charge/radius ratio is increased.

This mechanism is analagous to the stabilisation of non-bonding electrons in organic molecules by hydrogen bonding, which gives rise to the well-known 'blue shift' of $n \rightarrow \pi^*$ bands when the solvent is changed in the sequence hydrocarbon,

alcohol, water (Ref 10).

Smith has used the following expression for the frequency ν_{max} of the maximum of the weak band in a nitrate melt:

$$h\nu_{max} = h\nu_o + e.\int_o^\infty (|\psi_{ex}|^2 - |\psi_{gr}|^2).V\ dv.$$

In the equation, ν_o is a constant, e is the electronic charge, ψ_{ex} and ψ_{gr} are the wave-functions of the excited and ground-state ion respectively and v is the volume. V is the potential at the site of a nitrate ion due to the surrounding cations, and it can be replaced by a multipole expansion. If the assignment of the weak band as $A_1' \nrightarrow A_1''$ is correct, the symmetry of the transition is such that the first two terms of this multipole expansion of V have no effect on the transition energy; the first significant term is the quadrupole term (Ref.21) This term can be attributed almost entirely to the first shell of cations surrounding the nitrate ion, the contribution from more distant ions being relatively slight.

(ii) The π^* orbital which receives the electron upon excitation is diffuse, and may overlap with the nearest-neighbour cations. In the case of alkali or alkaline-earth cations this overlap would be expected to be repulsive; it would raise the energy of the excited nitrate ion, and so increase the transition energy relative to its value for a free nitrate ion. The effect would be greatest for cations with the highest surface-potential z/r.

6.5.2. The strong band at 50 kcm^{-1}.

Since the experimental work carried out by the author did

not include measurements of the maximum of this band, the account given here will be very brief.

The band has been ascribed to a $\pi \rightarrow \pi^*$ transition (Refs.20, 22). This assignment is supported by observations on the effect of solvent polarity on the frequency of the maximum (Ref.13). Some earlier workers had assumed that the band is due to charge transfer (Ref.23, and others quoted in Ref.13).

Rhodes and Ubbelohde measured the frequency of the maximum of this strong band, $E_{max}(I)$, for pure lithium, sodium and potassium nitrates, over temperature ranges which included the melting-points. For the solids, $E_{max}(I)$ fell linearly with rising temperature for individual crystalline phases. It changed abruptly at transition-points, and increased abruptly when the salts were fused (Ref.8).

The results were interpreted in terms of a model for the excitation process in which the excited electron was assumed to be confined in a spherical potential well of radius r_o. The boundary of the well was formed by the cations surrounding the nitrate ion, so the radius r_o is approximately equal to the anion-cation distance minus the cation radius.

If the excited electron is assumed to move in a potential which is zero inside the cavity but infinite outside it, application of Schrödinger's equation gives the following expression for the transition energy:

$$E_{max}(I) = E_o + h^2/8mr_o^2 \qquad (6.3)$$

where E_o is the energy required to remove an electron from an isolated nitrate ion in vacuo, h is Planck's constant and m is the mass of an electron.

Differentiating the above expression,

$$dE_{max}/dT = - (h^2/4mr_o^3).(dr_o/dT) \qquad (6.4)$$

If dE_{max}/dT is measured for the crystalline nitrates, dr_o/dT can be calculated by use of equation (6.4), assuming that r_o is equal to the anion-cation distance minus the cation radius. Rhodes and Ubbelohde carried out this calculation for lithium, sodium and potassium nitrates, and showed that $1/r_o.dr_o/dT$ for each salt was approximately equal to the coefficient of linear expansion of the crystal.

The abrupt increase in $E_{max}(I)$ which was recorded at the melting-point of each of these salts was ascribed to a reduction in r_o, i.e. the cation-anion distance decreased abruptly on fusion.

6.6. Previous knowledge on the absorption spectra of nitrites in the range 50 - 20 kcm^{-1}.

Crystalline and fused sodium and potassium nitrites, and aqueous solutions containing nitrite ions, have an absorption band in the near ultra-violet with a maximum at 27 - 28 kcm^{-1} at room temperature (ϵ = 23 litres/mole.cm in aqueous solution; Ref.9).

There is a shoulder on the high frequency side of this weak band; it would have a maximum at about 33.5 kcm^{-1} ($\epsilon \sim 8$ in aqueous solution; Ref.9).

The weak band and its shoulder are separated by a region of relatively low absorption from a stronger band which has a steeply-rising edge at $\sim$40 kcm^{-1} and reaches a maximum at $\sim$47.4 kcm^{-1} (ϵ = 6,000 in aqueous solution; Ref.9).

6.6.1. The weak band at 27 kcm^{-1}.

Experiments with single crystals of sodium nitrite have shown that, in the region of this band, absorption occurs most strongly if the electric vector of the light is perpendicular to the plane of the nitrite ion (Refs.24,25).

Sidman (Ref.25) has recorded the absorption spectra of single crystals of $NaNO_2$ and $NaN^{15}O_2$ at 4°K. He found that the band at 27 kcm^{-1} was resolved into a series of lines at this temperature, and was able to analyse the spectrum in terms of two vibrational frequencies (632 and 1018 cm^{-1}). These were shown to correspond respectively to the bending and symmetric stretching modes of the electronically excited ion. The lowest-frequency line in the spectrum (25,977 cm^{-1}) was identified as the band origin (i.e. the line arising from transition between the vibrational ground states of the two electronic levels). The transition is therefore 'allowed' by selection rules. At 4°K, the maximum of the weak band corresponds to excitation from the lowest vibrational level of the lower electronic state to higher vibrational levels of the upper state.

In the normal nitrite ion, the N-O bond-length is 1.23A and the ONO angle is 116°C. Sidman, from his analysis of the ultra-violet and infra-red spectra of sodium nitrite, has shown that the bond-length in the excited ion (in its equilibrium configuration) is "not very different" from that in the ground state, but the ONO angle differs from the ground-state value by 9°. The sign of this difference could not be established unambiguously, but the angle was probably greater in the excited ion. Application of the Franck-Condon principle shows that, when absorption occurs from the $v = 0$ level of the ground-state ion, the excited ion is produced in

a 'flexed' condition over the entire frequency range in which absorption is observed (Refs.25,26).

Figure 6.2. shows a diagram of the highest occupied and lowest unoccupied energy levels in the nitrite ion, and illustrates the molecular orbitals associated with each level. π_1 is a bonding π-orbital, π_2, n_{O2}, and n_{O1} are non-bonding orbitals centred on oxygen and n_N is a non-bonding π-orbital centred on nitrogen. π_3 is the lowest unoccupied orbital, and is anti-bonding in character.

The band at 27 kcm^{-1} is associated with the transition $n_N \rightarrow \pi_3$ ($^1A_1 \longrightarrow {}^1B_2$), i.e. it involves excitation of an electron from the nitrogen 'lone pair' to a molecular anti-bonding π-orbital.

Several pieces of empirical evidence support this hypothesis that the nitrogen lone pair electrons are concerned in the transition giving rise to the 27 kcm^{-1} band:

(i) The band is present in the spectra of all solutions containing nitrite ions, nitrous acid (H.ONO) or alkyl nitrites (R.ONO) (Refs.24,27), but is absent from the spectra of nitro-paraffins ($R.NO_2$) and nitryl chloride ($Cl.NO_2$) (Ref.24). The nitrogen 'lone pair' is present in the first group of molecules, but all the nitrogen electrons are contained in bonding orbitals in the second group.

(ii) If an aqueous solution of cadmium perchlorate is added to one of potassium nitrite, the absorption band at 27 kcm^{-1} decreases in intensity and is replaced by another band at 31.2 kcm^{-1}. The new band is ascribed to the complex ion $(CdNO_2)^+$, in which the nitrogen lone pair is involved in a donor bond (Ref.28).

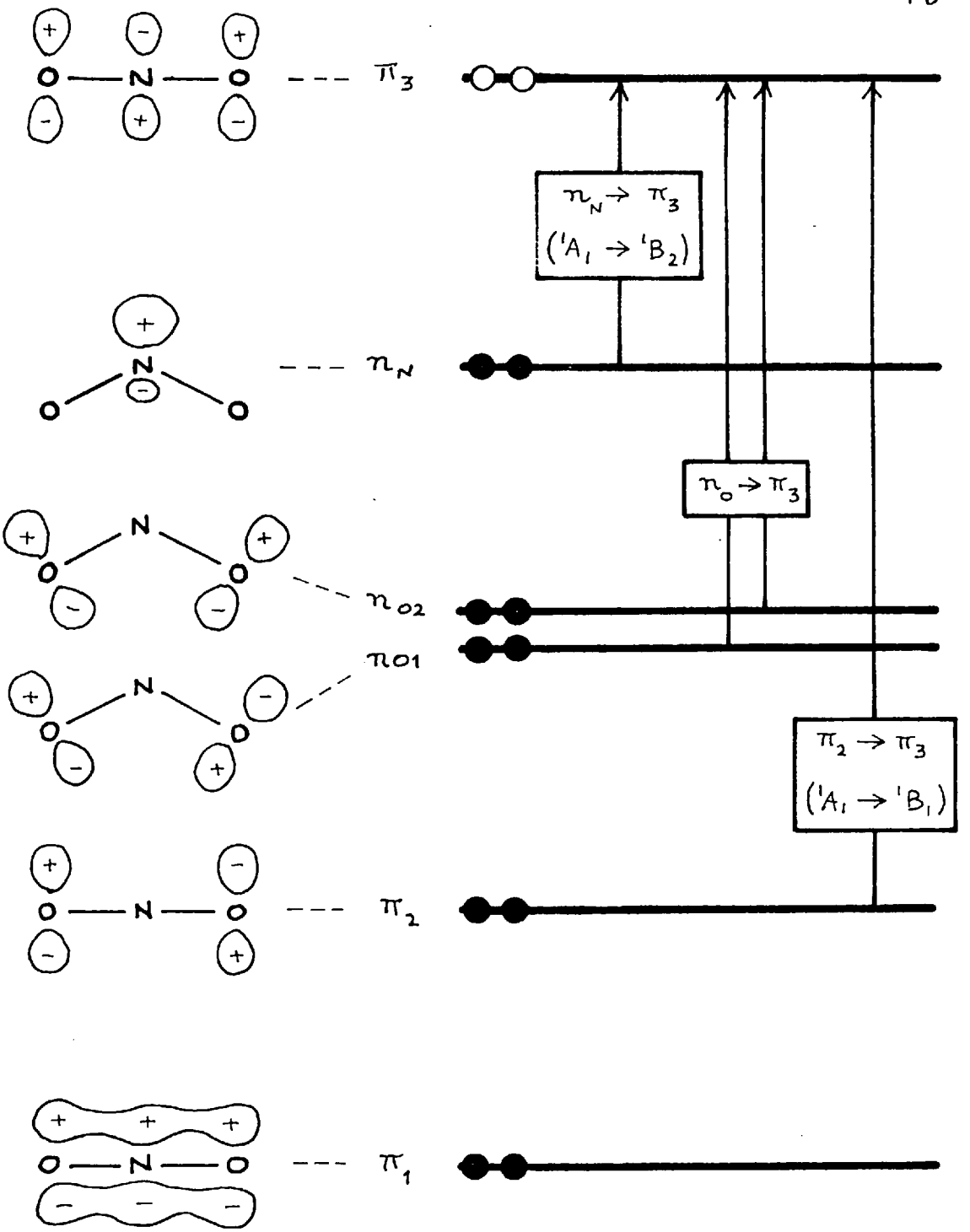


FIGURE 6.2. MOLECULAR ORBITALS AND ENERGY LEVELS IN THE NITRITE ION, (NO_2^-). (ACCORDING TO J.W. SIDMAN, REFS 25 AND 26).

(iii) The band at 27 kcm^{-1} is reported to be absent in crystalline silver nitrite (Ref.24). The Ag--N distance in the crystal is shorter than would be expected for a purely ionic compound (Ref.29), which suggests that the electrons are contained in a covalent bond between these two atoms.

The weak shoulder at 33.5 kcm^{-1} in nitrite spectra is ascribed to excitation of an electron from a non-bonding orbital on oxygen (n_{01}) to the anti-bonding π-orbital π_3 (Ref.25).

6.6.2. The strong band at 47.4 kcm^{-1}.

The strong band at 47.4 kcm^{-1} is assigned by Sidman to transition from the oxygen π-orbital π_2 to the molecular antibonding orbital π_3 ($^1A_1 \longrightarrow {}^1B_1$). Earlier workers (notably Friedman, Ref.23) have regarded this as a charge-transfer band, but there are two pieces of evidence against this view:

(i) The frequency at the maximum of the band in dilute aqueous solution ~~(28,200 cm^{-1})~~ is very close to that in crystalline sodium and potassium nitrites ~~(28,600 and 27,630 cm^{-1} respectively, at 20°C)~~.

(ii) The band is polarised in the plane of the nitrite ion (Ref.24). If it were due to charge transfer absorption, the plane of polarisation would be perpendicular to the plane of the ion (Ref.9).

The knowledge summarised in this Chapter is used as a basis for the interpretation of the author's spectroscopic results, which are described in Chapter 14.

REFERENCES TO CHAPTER 6.

1. Franck, Kuhn and Rollefson, Z. Physik, (1927), 43, 155.

2. Kondratjew, Z. Physik, (1938), 39, 191.

3. L.E. Orgel, Quart. Revs. Chem. Soc., (1954), 8, 422.

4. R.F. Barrow and A.D. Caunt, Proc. Roy. Soc., (1953), A219, 120.

5. W. Martienssen, J. Phys. Chem. Solids, (1957), 2, 257.

6. Klemm, Z. Physik, (1933), 82, 529.

7. von Hippel, Z. Physik, (1936), 101, 680.

8. E. Rhodes and A.R. Ubbelohde, Proc. Roy. Soc., (1959), A251, 156.

9. S.F. Mason, Quart. Revs. Chem. Soc., (1961), 15, 287.

10. H. McConnell, J. Chem. Phys., (1952), 20, 700.

11. J.N. Murrell, Quart. Revs. Chem. Soc., (1961), 15, 191.

12. G.P. Smith and C.R. Boston, J. Chem. Phys., (1961), 34, 1396.

13. D. Meyerstein and A. Treinin, Trans. Farad. Soc., (1961), 57, 2104.

14. K.S. Krishnan and A.C. Dasgupta, Nature, (1930), 126, 12.

15. E.V. Sayre, J. Chem. Phys., (1959), 31, 73.

16. G. Rodloff, Z. Physik, (1934), 91, 511.

17. H. Schaumann, Z. Physik, (1932), 76, 106.

18. R.L. Sass, R. Vidale and J. Donohue, Acta Cryst., (1957), 10, 567.

19. S.P. McGlynn and M. Kasha, J. Chem. Phys., (1956), 24, 481.

20. K.L. McEwen, J. Chem. Phys., (1961), 34, 547.

21. G.P. Smith and C.R. Boston, Discuss. Farad. Soc., (1961), 32, 14.

22. J.A. Friend and L.E. Lyons, J. Chem. Soc., (1959),1572.

23. H.L. Friedman, J. Chem. Phys., (1953), 21, 319.

24. W.G. Trawick and W.H. Eberhardt, J. Chem. Phys., (1954), 22, 1492.

25. J.W. Sidman, J. Amer. Chem. Soc., (1957), 79, 2669.

26. J.W. Sidman, J. Amer. Chem. Soc., (1957), 76, 2675.

27. H.E. Ungnade and R.A. Smiley, J. Org. Chem., (1956), 21, 993.

28. E.G. Vassian and W.H. Eberhardt, J. Phys. Chem., (1958), 62, 84.

29. Strukturbericht, IV, 41 and 153.

CHAPTER 7.

PREVIOUS STUDIES ON THE MELTING PROCESS IN IONIC CRYSTALS.

A brief but critical summary is given here of the methods used by earlier workers to investigate the structures of ionic melts and to derive information about the changes which accompany fusion of an ionic crystal.

7.1. Diffraction techniques.

Levy et al.(Ref 1) have carried out X-ray and neutron diffraction experiments on fused alkali halides, and have expressed their results in the form of radial distribution curves referred to either the metal nucleus or the halogen nucleus as origin. The following general conclusions can be drawn:

a) Each cation has only anions as nearest neighbours, and vice versa, as in the crystal. For a given substance, the most probable distance between each cation and its nearest-neighbour anions (corresponding to the first maximum in the radial distribution curve) is shorter in the melt than in the crystal by about 0.1 - 0.2 A. This distance in the melt is therefore intermediate between the values for the crystal and for the ion-pair in the vapour phase (Ref 2).

b) The average coordination number of anions around cations (or vice versa) is smaller in the melts than in the corresponding crystals. Values in the range 5.5 to 5.6 were recorded for the alkali halides, compared with 6 for

the rock-salt structure and 8 for the room-temperature caesium chloride structure. However, calculations made by Furukawa suggest that the value 5.6 (which refers to lithium halides) is subject to large experimental errors and should be nearer to 4 (Ref 3). This reduction in coordination number accounts for the volume increase which is frequently observed when an ionic crystal is fused (see also Section 7.3), and is consistent with the result stated in paragraph a) above. In crystal transitions which involve a change in coordination number (such as the b.c.c. to f.c.c. change in caesium chloride) the shorter anion-cation distance is always associated with the smaller coordination number (the reduction being 0.09 A in the case cited (Ref 13, pp 519 and 523)).

c) The most probable distance between a given anion and the anions forming the second coordination shell around it is <u>larger</u> in the melts than in the corresponding crystals.

d) No peaks appeared in the distribution curves at values of r greater than about 5A. This means that, considering a cation as centre, ordering is discernible in the first shell of anions and in the next shell of cations but beyond this the distribution of neighbours relative to the reference ion is completely random.

The reduction in the most probable nearest-neighbour anion-cation distance on fusion can be understood in general terms. The Coulomb forces acting on a given ion due to interaction with its neighbours balance out in an alkali halide crystal because of the symmetry of the arrangement. This symmetry is lost when the crystal is fused, causing it to approach more closely to some of its neighbours than to others (Ref 2).

Diffraction experiments have also been carried out on fused sodium nitrate (Refs 4,5), potassium nitrate (Ref 5), sodium nitrite (Ref 4) and on the fused carbonates and sulphates of lithium, sodium and potassium (Ref 6). The diffraction spectra were converted to radial distribution curves having the hetero-atom (X) of the anion as origin. Again, the curves showed no peaks at r-values greater than about 5A, showing that the ordered region around a given anion is limited to a sphere of this radius.

The first peak in each distribution curve corresponded to the X-O distance in the anion, which could be derived with an accuracy of about ± 0.1A. Within these limits, the values obtained were the same as the X-O distance in the crystalline salts. The areas under the peaks gave the coordination number of O around X, and these agreed (within ± 15%) with the values expected for the formulae NO_3^-, NO_2^-, $CO_3^=$ and $SO_4^=$.

The second peak in the distribution curves corresponded to contact between the cations and the oxygen atoms of the oxy-anion. This peak was prominent and well- resolved for the melts of $NaNO_3$, Na_2SO_4, K_2SO_4, Na_2CO_3 and K_2CO_3, showing that the cation-oxygen contact distance is a very common one in these melts.

At larger values of r the radial distribution curves showed one or sometimes two further peaks, but these were very broad and poorly resolved, and could not be assigned unambiguously to any particular atom-pairs. This is a consequence of the lack of definite structure in the liquid at these distances, and is not due merely to the failure of experimenters to record reflections over a sufficiently large range of values of $\sin\Theta/\lambda$. (Ref 6).

Attempts have been made to find the relative populations of the situations in which the cation is in contact with one, two or three oxygen atoms in these melts containing oxy-anions (Refs 4,6). However, the information provided by the diffraction experiments is much too scanty for any firm conclusions to be drawn from this evidence alone. There would be more object in examining a melt such as caesium iodate, in which the diffraction pattern would be dominated by the heavy atoms. It should then be possible to pick out the peaks corresponding to the distances Cs..I, I..I and Cs..Cs.

7.2. Changes in electrical conductivity on melting.

For alkali-metal halides, nitrates and nitrites, the specific electrical conductivity increases on fusion by a factor of the order 10^3 to 10^4 (Ref 7). This clearly demonstrates the greater freedom of movement of ions in the melts; in the crystals only those ions which are adjacent to a Schottky defect are capable of movement when an electric field is applied, but in the melts all ions are mobile (considering a time-average over a period of 10^{-6} second).

In some salts, notably the silver and cuprous halides, the conductivity increases on fusion by only 20 to 30 times (Refs 7,8). This is attributed to the high degree of disorder of the cations in the solid; for example, in the high-temperature modification of AgI only three-quarters of the available (equivalent) cation sites are occupied, and the cation lattice can be regarded as already 'liquid' below the melting point. Fusion of the crystal corresponds to positional disordering of the anion lattice. The conductivity of silver nitrate increases by 500 on fusion,

suggesting that some cation disordering is also present in this salt below its melting-point (Ref 8).

The activation energy for electrical conductivity in alkali halides, nitrates and nitrites falls from about 30 to about 3 kcal/mole on fusion (Ref 7). This suggests that counter movement of ions towards the two electrodes occurs by a cooperative mechanism in the melts, whereas in the crystals an ion moving into a vacant site has to displace its neighbours against the relatively high restoring forces of the rigid lattice.

The ratio of the activation energy for viscous flow to that for electrical conductivity, E_η / E_σ, provides some insight into the structural difference between 'low-melting' and 'high-melting' salts. The ratio is in the range 3.1 to 7.6 for fused alkali halides but is much nearer to unity (0.7 to 1.4) for low-melting salts such as alkali-metal nitrates, nitrites, dichromates and thiocyanates (Ref 7). This implies that conductivity and viscous flow require similar movement of the ions in the low-melting salts but that different mechanisms are involved for these two processes in the halides.

7.3. Volume changes on fusion.

The molar volumes of the alkali halides increase on fusion by amounts varying from 29% (LiF) to 10.5% (CsCl). For nitrates of univalent cations the corresponding change is sometimes (but not always) smaller. Table 7.1 gives some values for the two groups of compounds.

TABLE 7.1. Volume changes on fusion for some halides and nitrates.

Salt	100. $\Delta V_f/V_s$	Salt	100. $\Delta V_f/V_s$
LiF	29.4 (a)		
LiBr	24.3 (a)	$LiNO_3$	21.4 (b)
NaCl	25.0 (a)		
NaBr	22.4 (a)	$NaNO_3$	10.7 (b)
KBr	16.6 (a)	KNO_3	3.3 (b)
RbBr	13.5 (a)	$RbNO_3$	-0.2 (b)
CsCl	10.5 (a)		
CsBr*	9.9* (a)	$CsNO_3$	12.1 (b)
AgBr	8.2 (a)	$AgNO_3$	0.7 (c)

* Extrapolated, using the values for CsCl, RbCl and RbBr.

(a) Ref 9.

(b) Ref 10.

(c) Ref 11.

The low values of $\Delta V_f/V_s$ obtained for some of the nitrates can be interpreted in the following way. In the crystals the nitrate ions are constrained to occupy certain sites, with the three-fold axes along fixed directions, and the cations are restricted to their

lattice points. When the salt is fused these constraints no longer apply, and it may be possible for the ions to arrange themselves so that the density of packing is higher in some micro-regions than it is in the crystal. (Since these relatively dense regions will have irregular shapes, spaces will appear between them as they are packed together in the liquid and this prevents the overall density of the melt from actually exceeding that of the crystal). This type of volume economy can apply only to salts containing non-spherical ions, and so could be the cause of the differences in the values of $\Delta V_f/V_s$ for nitrates and halides.

If this picture is correct, the proportion of the total volume of a melt which is actually occupied by the ions should be greater for a melt containing non-spherical ions than for one containing only spherical ions. In Table 7.2 some data have been collected to test this hypothesis. The volume of the nitrate ion was calculated on the assumption that it rotates freely about its three-fold axis, taking the N-O bond length as 1.2A (Ref 12) and the contact radius of the oxygen atom as 1.4A (Refs 3 and 13). The volume obtained was 36.0 A^3, or 21.7 ml/mole. The alternative assumption that the nitrate ion is free to rotate about <u>any</u> axis would not be justified; Furukawa has shown that if the nitrate ion in sodium nitrate melt effectively occupied a spherical cavity of radius 2.6A, the molar volume of the salt just above the melting-point would be at least 37% higher than the actual value (Ref 3). The volumes of the spherical alkali-metal and halide ions were calculated from the crystal radii given by Pauling (Ref 13). The halide ion whose volume is nearest to that of the nitrate ion was found to be Br^- (31.1 A^3, or 18.7 ml/mole), so the alkali bromides have been selected for comparison with the nitrates in order to minimise any effect due to

differences in anion-cation size-ratio. (The volumes of Cl^- and I^- are 15.0 and 25.3 ml/mole, respectively).

TABLE 7.2. Volume of the ions (V_o) expressed as a % of the total volume, for solid and liquid bromides and nitrates.

V_L for caesium bromide was calculated from densities reported by van Artsdalen et al.(Ref 14). All other molar volumes were taken from Refs 9 and 10.

Cation	100. (V_o/V_s)		100. (V_o/V_L)	
	bromide	nitrate	bromide	nitrate
Li^+	70.2	70.0	56.5	57.6
Na^+	58.0	59.4	47.3	53.6
K^+	51.3	52.8	44.0	51.2
Rb^+	49.3	49.9	43.7	50.1
Cs^+	49.0	53.9	44.5	48.0

Table 7.2 shows that, for salts of Li^+, Na^+, K^+ and Rb^+ in the solid state, the volume of the ions as a fraction of the total volume is the same for the bromide of a given cation as for the nitrate, within about 1%. However, for the corresponding melts (V_o/V_L) is higher for the nitrates than for the bromides, the difference being greatest (6 - 7%) for the salts of sodium, potassium and rubidium. Reference to Table 7.1 shows that these three cations are just the ones whose nitrates have small volume changes on fusion compared with the bromides. $\Delta V_f/V_s$ for lithium nitrate is only 3% less than that for lithium bromide, and the difference between the (V_o/V_L) values for the two salts

is correspondingly small (1.1%). These results provide striking confirmation for the hypothesis put forward above.

The caesium salts provide an exception which proves the rule. (V_o/V_s) for solid caesium nitrate is 5% higher than that for solid caesium bromide. In the melts the difference is only 3.5% (in the same sense). The conclusion is that ion association is less important in the melting of caesium nitrate than in the other alkali nitrates (because a packing arrangement more economical than that in the bromide has apparently already been achieved in crystalline caesium nitrate). This is confirmed by two other observations:

a) The volume increase on fusion for caesium nitrate is greater than that of either the chloride or the bromide (Cs^+ being the only cation for which this is so).

b) The melting-point of caesium nitrate is markedly higher than those of the other alkali-metal nitrates. Table 7.3 shows that the same is not true for any of the caesium halides, so the effect cannot be ascribed to the normal dependence of lattice energy on anion-cation radius ratio. These exceptional properties of caesium nitrate do not seem to have been correlated before.

TABLE 7.3. Melting-points of the alkali-metal chlorides, bromides, iodides and nitrates (Refs 7,14).

	Cl^-	Br^-	I^-	NO_3^-
Li^+	613	549	465	257
Na^+	801	745	659	308
K^+	776	735	723	334
Rb^+	722	692	647	312
Cs^+	645	636	630	410

Several groups of workers (Refs 10,15) have calculated values for (V_o/V_s) for nitrates on the assumption that the nitrate ion can be regarded as an oblate spheroid with semi-axes 0.95A and 1.88A (the corresponding volume being 18.5 A^3). These dimensions are undoubtedly too small; the values used by the author (semi-axes 1.4 and 2.6 A, volume 36.0 A^3) are consistent with the cation-oxygen distances found in nitrate melts by X-ray diffraction (Refs 4,5), and with the radius of the oxide ion $O^=$ (1.4A) given by Pauling (Ref 13). The smaller figures quoted above were obtained by calculating the N...N distance between neighbouring nitrate ions in the calcite-type lattices of lithium nitrate and sodium nitrate (parallel and perpendicular to the three-fold axis), plotting these against cation radius r and extrapolating to r = 0. This seems a dubious procedure; its invalidity can be demonstrated by using it to find the radii of Cl^- and Br^- from the Cl...Cl and Br...Br distances in the chlorides and bromides of lithium and sodium. The values obtained are again too low, namely $r(Cl^-)$ = 1.51A (cf. Pauling's 1.81A), and $r(Br^-)$ = 1.66A (cf. 1.95A).

7.4. Heat and entropy changes on fusion.

The molar heats of fusion of alkali halide crystals fall within the range 5 - 8 kcal/mole, and those of lower-melting salts such as alkali nitrates and thiocyanates are between 2 and 4 kcal/mole (Refs 16,17). Førland (Ref 18) has calculated that the energy required to interchange an anion and a cation in the sodium chloride crystal is about 200 kcal/mole. Comparison of these energies provides strong support for the conclusion from the diffraction experiments (Section 7.1) that the anions in ionic melts have only cations as nearest neighbours and vice versa.

The difference of some 2 to 4 kcal/mole between the heats of fusion of alkali halides and those of low-melting nitrates and thiocyanates can be attributed to the more economical packing of ions in the melts of the latter group, i.e. to the same effect which is responsible for the relatively small volume increase on fusion of these salts. This statement is not strictly rigorous because it implies that the energy associated with the different degrees of freedom in the melt (such as positions of the ions, vibration about these positions and ionic rotation) can be treated as independent and additive, and that the heat of fusion can be written as a sum of separate terms:

$$\Delta H_f = \Delta H_{positional} + \Delta H_{rotation} + \Delta H_{vibration} + \Delta H_{association} \quad (7.1)$$

An analagous expression for the entropy of fusion is obtained by dividing each term in this equation by the melting temperature in ^{o}K:

$$\Delta S_f = \Delta S_{positional} + \Delta S_{rotation} + \Delta S_{vibration} + \Delta S_{association} \quad (7.2)$$

(see Ref 17). This partition of the enthalpy and entropy of fusion into independent terms is permissible in a dilute gas but is not a good approximation in a condensed ionic medium in which the energy levels associated with one set of degrees of freedom are strongly dependent on the energies present in the other sets, e.g. the energies of the vibrational states (referring to lattice vibrations as well as to internal vibrations of a polyatomic ion) are strongly dependent on the positions of the ions.

Entropies of fusion for alkali halides, nitrates and thiocyanates fall in the range 4 to 10 e.u./mole, and no systematic difference exists between the values for the 'high-melting' and those for the 'low-melting' groups. The low melting-points of the second group are approximately compensated by low heats of fusion, so the ratio $\Delta H_f/T_f$ is roughly the same throughout; for example, ΔS_f for potassium thiocyanate (m.p. 175°C) is 7.6 e.u./mole, and that for potassium chloride (m.p. 776°C) is 6.2 e.u./mole (Ref 17). In the author's opinion, this fact has not yet been adequately explained. Plester et al. (Ref 17) suggested that the formation of association complexes in the melt makes a significant contribution to ΔS_f for potassium thiocyanate but not for potassium chloride. However, the formation of these complexes must be an exothermic process, so $\Delta S_{assoc.}$ in equation 7.2 would be <u>negative</u> and would tend to make ΔS_f <u>less</u> for the thiocyanate than for the chloride. However, the discussion of entropy of fusion of ionic crystals in terms of specific processes such as rotation, association, positional randomisation and vibration is not likely to be very profitable because of the interdependence of the sets of energy levels associated with these processes.

7.5. Spectroscopic methods.

These are extremely important because, in contrast to the thermodynamic methods mentioned above, they frequently give direct information about the <u>immediate environment</u> experienced by a single ion.

Mention has already been made of the application of Raman and ultra-violet spectroscopy to the study of the melting process (Chapter 2, Sections 2 and 3). Infra-red spectroscopy has also been used; Hexter (Ref 19) measured the absorption spectrum of a single crystal of sodium nitrate

from 2500 to 4500 cm^{-1}, and recorded some bands which he assigned as combinations between the frequencies of the librational movements of the nitrate ions and the first overtone ($2\nu_3$) of the degenerate stretching mode of the ion. These combination bands disappeared on fusion of the sample, and Hexter concluded that the librations do not occur in the melt (i.e. the melt offers no resistance to rotation of a nitrate ion about its three-fold axis). This work forms an interesting complement to that of Kracek (Ref 20), who noted that X-ray reflections due to sodium nitrate crystal planes containing only oxygen atoms were present at room temperature but absent between 275°C and the melting-point (308°C). This was interpreted as due to randomisation of the nitrate ions with regard to rotation about their three-fold axes; Hexter's results show that this randomisation is not free rotation but something more restricted, e.g. the ion may assume one of several equivalent orientational positions but remains in one such position for a time which is long compared with the period of the librational mode.

REFERENCES TO CHAPTER 7.

1. H.A. Levy, P.A. Agron, M.A. Bredig and M.D. Danford, Ann. N.Y. Acad. Sci., (1960), 79, 762.

2. A.R. Ubbelohde, Liversidge Lecture, Proc. Chem Soc., (1960), 332.

3. K. Furukawa, Discuss. Farad. Soc., (1961), 32, 53.

4. K. Furukawa, Sci. Reps. Res. Inst., Tokohu Univ., (1960), A12, 150.

5. V.I. Danilov and S.Ya. Krasnitskii, Dokl. Akad. Nauk. S.S.S.R., (1955), 101, 661.

6. J. Zarzycki, Discuss. Farad. Soc., (1961), 32, 38.

7. J.P. Frame, E. Rhodes and A.R. Ubbelohde, Trans. Farad. Soc., (1959), 55, 2039.

8. C. Tubandt and E. Lorenz, Z. phys. Chem., (1914), 87, 513.

9. H. Schinke and F. Sauerwald, Z. anorg. Chem., (1956), 287, 313.

10. Idem, ibid., (1960), 304, 25.

11. Davis, Rogers and Ubbelohde, Proc. Roy. Soc., (1953) A220, 14.

12. Sass, Vidale and Donohue, Acta Cryst., (1957), 10, 567.

13. L. Pauling, "The Nature of the Chemical Bond", 3rd edition, Cornell Univ. Press, Ithaca, N.Y. (1960).

14. Yaffe and van Artsdalen, J. Phys. Chem., (1956),60,1125.

15. W. Bues, Z. phys Chem., (N.F.), (1957), 10, 1.

16. Handbook of Chemistry and Physics, Rubber Publishing Co, (1961), p 2313.

17. D.W. Plester, S.E. Rogers and A.R. Ubbelohde, Proc. Roy. Soc., (1956), A235, 469.

18. T. Førland, U.S. Office of Naval Research, Report No. 69.

19. R.M. Hexter, Spectrochim. Acta., (1958), 10, 291.

20. Cracek, Posnjak and Hendricks, J. Amer. Chem Soc., (1931) 53, 1183, 2609, 3339.

E X P E R I M E N T A L

S E C T I O N

CHAPTER 8

EXPERIMENTAL TECHNIQUES - GENERAL.

The materials, techniques and apparatus described in this Chapter were common to all parts of the experimental work.

8.1. Materials.

The following list gives the sources and purities of the materials used.

Potassium nitrate: Judactan Analytical Reagent, containing less than 0.0005% chloride and less than 0.002% heavy metals (Pb).

Sodium nitrate: Judactan Analytical Reagent, containing less than 0.003% anionic and less than 0.002% cationic impurities.

Rubidium nitrate: Johnson, Matthey & Co., 99.9% pure. The salt was recrystallised once from distilled water before shock-drying (see Section 8.2.1).

Caesium nitrate: Judex Laboratory Reagent, 99.8% pure. The substance was recrystallised once from distilled water before shock-drying.

Silver nitrate: Hopkin & Williams Ltd., Analytical Reagent, not less than 99.9% pure. The maximum limits of impurities were: (sulphate + chloride), 0.006%; alkali metals, 0.05%; heavy metals (Pb), 0.0005%.

Thallous nitrate: British Drug Houses, Ltd., not less than

99.8% pure. The salt was recrystallised once from distilled water.

Ammonium nitrate: Hopkin & Williams Ltd., Analytical Reagent, containing not less than 99.0% NH_4NO_3. The maximum limits of the impurities were: (chloride + sulphate + phosphate + silicate), 0.02%; nitrite, 0.0005%; (Fe + Pb), 0.0003%.

Sodium nitrite: British Drug Houses Ltd., Analytical Reagent, containing not less than 98.0% $NaNO_2$. The nitrate ion content was not known, but the maximum limits of the other impurities were: (chloride + sulphate), 0.02%; (Fe + Pb + K), 0.01%. A sample of this salt was further purified by zone-refining (see Section 8.2.2).

Potassium nitrite: Riedel - De Haen A.G., Hanover, Analytical Reagent. The sodium ion and nitrite ion contents were not known, but the upper limits of the other impurities were: (chloride + sulphate), 0.02%; (Pb + Fe + Ca), 0.01%. A sample of this material was zone-refined (see section 8.2.2).

Nitric acid: this material was prepared by distillation of a mixture of Judactan A.R. potassium nitrate (70 grm) and A.R. conc. sulphuric acid (50 ml) in an all-glass apparatus. A guard-tube containing silica gel prevented the contamination of the distillate by atmospheric moisture. A sample of 10 ml of nitric acid was collected, after rejection of the first 5 ml of distillate. A stream of dry oxygen was bubbled through the acid before it was used, to reduce the concentration of dissolved oxides of nitrogen; the yellow colour was almost completely discharged by this means. No precipitate was formed when a drop of the acid was added to a dilute aqueous solution of barium nitrate, which showed that the amount of sulphuric acid present was negligible (less than 10^{-4} moles per litre).

Mixtures corresponding to the compositions $HNO_3.H_2O$ and $HNO_3.3H_2O$ were prepared by weighing, using small, glass bottles fitted with ground glass stoppers. A solution of concentration 0.24N was prepared by diluting the pure acid (1.508 grm.) to 100 ml. with distilled water, in a standard flask.

Iso-propyl nitrate: a sample of 99% purity was kindly supplied by the Chief Superintendent, E.R.D.E., Waltham Abbey, and was not further purified before use. This substance was chosen as an example of a covalent nitrate. It is less easily detonated than methyl and ethyl nitrates, and was therefore used in preference to these. It is a sweet-smelling, colourless, mobile liquid, boiling at 102°C.

8.2. Purification techniques.

8.2.1. Shock drying (Ref.1.)

All the crystalline nitrates listed above were dried by this technique before use. A sample (~ 20 grms.) of the salt to be dried was ground to a powder with a pestle and mortar, and loaded into a Pyrex tube fitted with a B24 ground-glass cone. This was connected to an all-glass gas line, which was evacuated by a rotary oil-pump. A liquid nitrogen trap was situated between the sample tube and the oil-pump. No grease was used in the ground glass joint; a PTFE sleeve (Loughborough Glass Co., Ltd.) served to make the joint air-tight. The use of the sleeve ensured that the salt was not contaminated with vacuum grease during the drying process.

The sample was pumped for ten minutes at room temperature. It was then heated, still under the action of the pump, to a temperature below the melting point of the salt but above the highest of its transition temperatures. Heating was carried out by placing the sample tube in a thermostatted melt-

bath, described in more detail below (see Section 8.3.) Pumping was continued for ten minutes. The tube was then removed from the thermostat and immediately plunged into liquid nitrogen in a Dewar vessel. This caused the sample to pass rapidly through its transitions, causing the small, crystalline particles to break up still further and permitting the release of any entrained water. The sample tube was then removed from the liquid nitrogen and allowed to warm up to room temperature, when the moisture was removed by the pump. The heating and cooling cycle was repeated five times.

Silver nitrate and thallous nitrate were found to darken slowly when kept at temperatures above 160°C. A sample of silver nitrate was dried by repeated shock-cooling from room temperature, and remained colourless throughout the operation; this sample was used in the experimental work. Some drying was essential for this salt, as the AnalaR material was moist. Thallous nitrate, on the other hand, appeared quite dry after recrystallisation from distilled water, and was used in the experiments without further purification.

8.2.2. Zone refining.

The samples of sodium and potassium nitrites which were available commercially were not of such high purity as the nitrates; apart from moisture, they were thought to contain nitrate ions as impurities. Reference to the appropriate phase diagrams (Ref.2.) showed that nitrate ions depressed the freezing points of both nitrites, but that solid solutions were formed. This means that the nitrate ions could not be removed by a single recrystallisation, even in principle, and that a multiple recrystallisation technique would be required. Repeated crystallisation from water would be tedious and also inefficient, because both nitrites are very soluble in water at room temperature ($NaNO_2$, 85 grm/100 g water at 21°C., KNO_2 300 grm/100 g water at 20°C.) (Ref.3.).

It was thought that zone-refining would be a convenient method for the purification of these materials. By this technique, multiple recrystallisation can be carried out from the melt with no loss of material at each stage. Potassium nitrate has been successfully purified in this way (Refs 7,8).

The object of the method is to produce a small molten zone in a solid column of the salt, and to cause this zone to pass slowly from one end of the column to the other. Impurities which depress the freezing point of the substance in the column are concentrated in the liquid zone, and are carried to the end of the column, where the zone is allowed to freeze. If the impurity is not soluble in the solid phase of the host substanc a single pass is, in principle, sufficient to remove it completely; in practice, however, some of the impurity is retained by occlusion and it is necessary to pass the zone several times (in the same direction). If the impurity is soluble in the solid but depresses its melting-point, passage of the liquid zone effects some purification, and in theory complete separation can be achieved only by making an infinite number of passes. The efficiency of the separation for a given number of passes depends on the value of the ratio

$$\frac{\text{(solubility of the impurity in the liquid phase)}}{\text{(solubility of the impurity in the solid phase)}} .$$

If this ratio is large the efficiency is high, and the impurity passes in the direction of movement of the zone. If the ratio is unity no separation is achieved, and if it is less than unity the impurity tends to move against the direction of movement of the zone. This is a very slow process, since a given impurity molecule can move not more than one zone-length per pass. (Ref 4)

A simple zone-refining apparatus was designed and constructed. It is illustrated in Figure 3.1. The Pyrex tube containing the sample to be purified was mounted

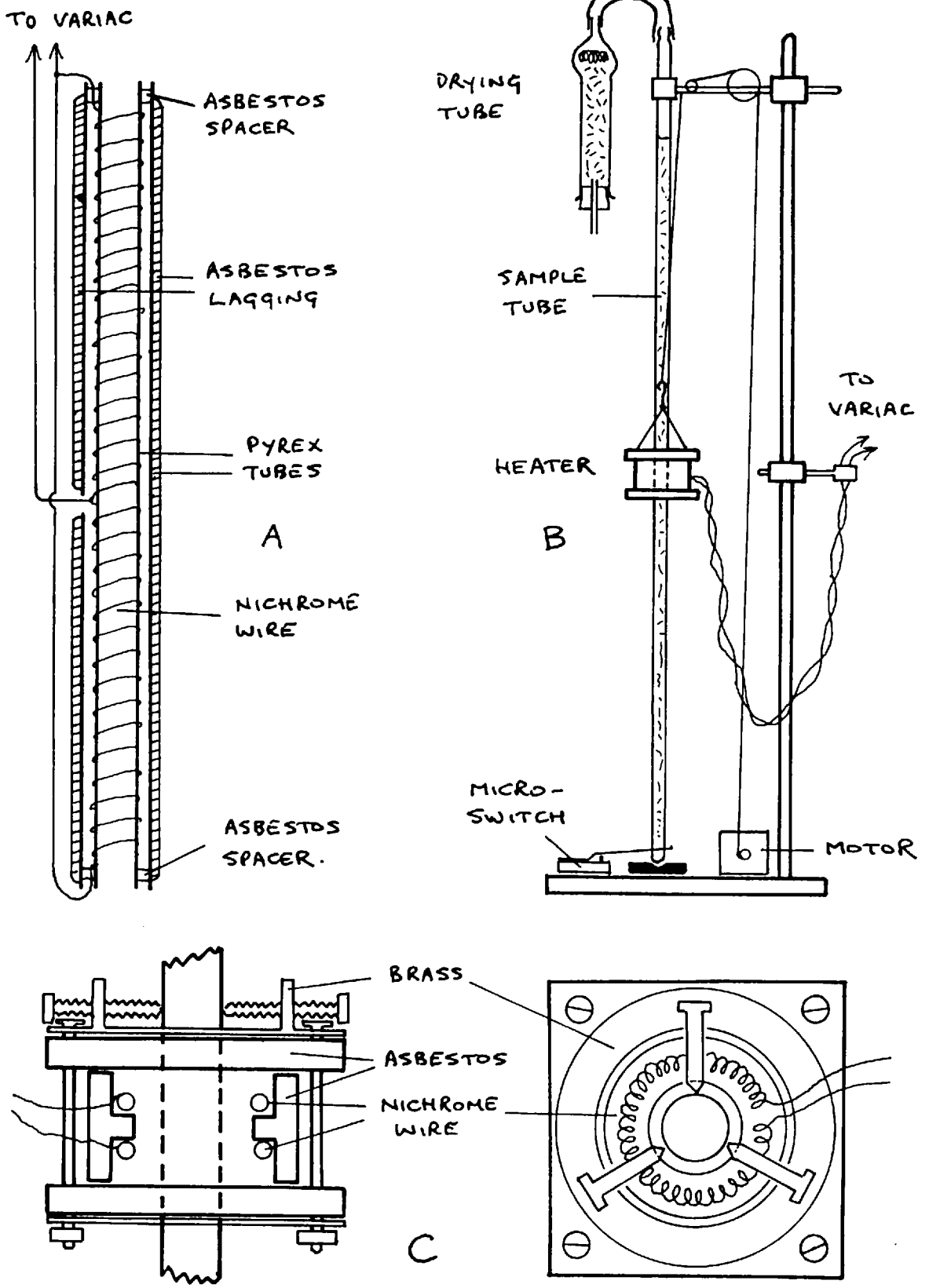


FIGURE 8.1. ZONE-REFINING APPARATUS.

vertically. The tube was closed at the bottom, and the open top end was fitted with a guard-tube filled with silica gel to prevent access of atmospheric moisture. The heater consisted of two turns of nichrome spiral fire-element wire, and had a resistance of 16 ohms at room temperature. It was mounted in a carriage which could slide freely up or down the sample tube. Three centering-screws on the carriage ensured that the tube was heated evenly from all sides. The heater was suspended from a thin wire, which ran over two pulleys to the chuck of a synchronous motor ("Sangamo", model S7, final speed one revolution per hour). When the motor was energised, the heater moved downwards under its own weight. The chuck was designed so that the heater passed from top to bottom of the column in 24 hours. When it reached the bottom it operated a micro-switch which cut off the power to the heater and the motor. The heater was then wound back to the top of the column by hand, a new zone started, and the cycle of operations repeated as many times as desired.

The fused zone was passed from top to bottom of the column because the melts of sodium and potassium nitrites are less dense than the corresponding solids, as is commonly the case. There was therefore no danger of the containing tube being burst when the liquid zone froze at the end of each pass. It is necessary to pass the zone from the bottom to the top of the tube when refining salts for which the melt is denser than the solid (as it is, for example, in the case of rubidium nitrate).

The power supply to the heater was controlled by a "Variac" transformer. The voltage was adjusted until it was just sufficient to maintain a liquid zone; excessive heating was avoided, as it could cause decomposition of the melt. In the case of potassium nitrite (m.p. 423°C) the power required was 25 watts. The length of the liquid zone was 1 cm.

The sample tube was 150 cm. long, and 7 mm. in internal

diameter. The salt was loaded into it as a powder, melted in the electric furnace (Figure 8.1 A) and allowed to re-freeze, giving a compact column of salt.

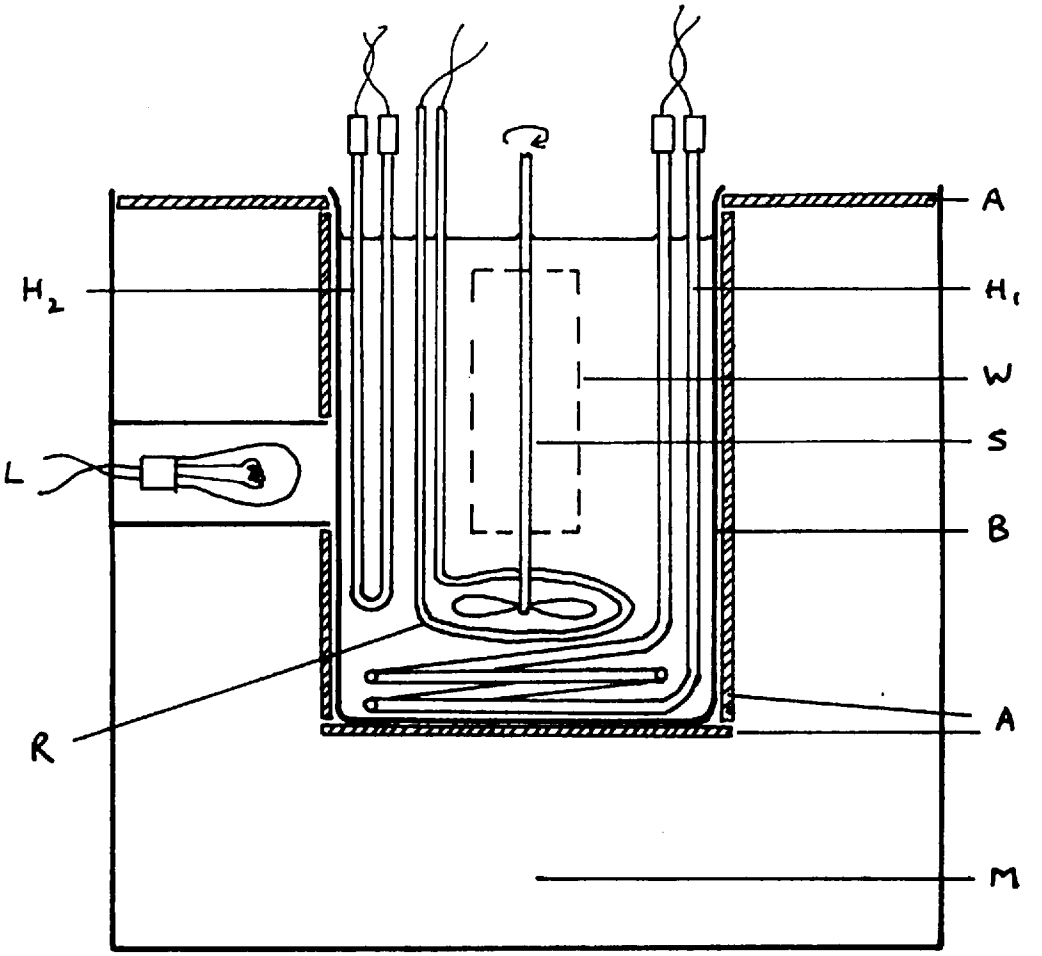
In the purification of sodium nitrite the liquid zone was passed down the column ten times. A sample taken from the middle of the column was found to have a melting-point 0.5°C higher than that of the original Analar salt; the melting-points were 281.0 and 280.5°C, respectively.

It has not been possible to deduce the minimum impurity concentration from this freezing-point difference, because the latent heat of fusion of sodium nitrite is not known. A rough calculation can be made by assuming that sodium nitrite has the same heat of fusion as sodium nitrate (3.8 kcal/mole); the value obtained is 0.4 mole % of impurity soluble in the liquid salt but not in the solid.

Seven passes of the molten zone were made in the case of potassium nitrite. The refined salt melted at 423.4°C, compared with 422.7°C for the original material. The latent heat of fusion of potassium nitrite is also unknown; if it is assumed to be 3.8 kcal/mole, the minimum concentration of the impurity is calculated to be 0.3 mole %.

8.3 The melt bath.

During the conductivity and density measurements described in Chapters 9 and 10, the experimental cells were immersed in a thermostatted bath containing the ternary eutectic KNO_3 (53 weight %):$NaNO_2$(40%):$NaNO_2$(7%), (m.p. 142°C; Ref 5). The melt is pale yellow, and is water-clear if Analar salts are used. It etches Pyrex slowly at temperatures above 350°C, and if it is kept in a Pyrex beaker for one or two



A	ASBESTOS BOARD
B	PYREX FIVE-LITRE BEAKER
H_1	MAIN HEATER
H_2	AUXILIARY HEATER
L	LAMP
R	RESISTANCE THERMOMETER
S	MOTOR-DRIVEN STIRRER
W	OBSERVATION WINDOW.
M	MICAFILL (THERMAL INSULATION)

FIGURE 8.2. THE MELT BATH.

months at this temperature a dense, white precipitate slowly forms, and this makes observation difficult. The precipitate is probably silica. However, it is easily removed by filtering the melt through glass wool, and if this is done regularly the same melt can be used indefinitely.

The container used for the melt-bath was a Pyrex five litre beaker.. This had to be replaced about every three months, when etching had made it difficult to see the measuring apparatus through the observation window.

The motor-driven stirrer was made from stainless steel. The two heaters (H_1 and H_2) (G.Bray & Co Ltd., Leeds) were sheathed in inconel, a nickel alloy which appeared to be unattacked after immersion in the melt for two years at temperatures between 250°C and 450°C. The helical heater H_1 had a maximum output of 1,500 watts, and was powered from a "Variac" transformer. The transformer was adjusted until, at equilibrium, the temperature of the bath was 20 - 50° below the required value. The remaining power was supplied by the hairpin-shaped heater H_2 (maximum output 250 watts), which was energised from an electronic control unit. The controller had the resistance thermometer R (platinum, 36 ohms at room temperature) and a set of decade resistance cans (Muirhead & Co Ltd.) in the ratio arms of a Wheatstone's bridge circuit. The controller supplied 250 watts to the heater until the resistance thermometer immersed in the bath had almost the same resistance as the decade chain. For the final stage of the heating process the power supplied to H_2 was proportional to the out-of-balance current in the bridge circuit, so that the equilibrium temperature was approached slowly and was not overshot. This "proportional control" applied over about the final 2° of the heating process. With this arrangement, the bath temperature could be maintained constant to within 0.1°C for periods of the order of one hour, and within $\pm$0.5°C for days.

The equilibrium bath temperature could be changed by resetting the decade resistance chain, and adjusting the power supply to H_1 if necessary. The decade chain could be set to any value from 0 - 111 ohms, in steps of 0.1 ohm. This increment corresponded to a change in the bath temperature of about 0.6°C.

The temperature controller was made in the electronic workshop of the Chemical Engineering Department, Imperial College, to the design of Mr. L. Tyley.

The melt-bath described above can be used between about 150°C and 500°C. Oxygen is evolved from the melt at temperatures above 400°C. It has viscosity and surface tension similar to those of water; it is odourless, does not evaporate or creep and is not inflammable. In these respects it is superior to the oils conventionally used in thermostats. Its only disadvantage is that it is an extremely vigorous oxidising agent. If the melt at 350°C comes into contact with wood, rubber or plastic they take fire immediately and burn violently. It is therefore necessary to ensure that, if the beaker containing the melt is accidentally broken, the melt does not run out onto any wooden or plastic surface. This is most easily done by placing beneath the bath a metal tray capable of holding the whole of the melt.

Metal parts which are to be kept permanently immersed in the bath should be made from stainless steel or inconel. Brass, copper and aluminium are all oxidised slowly, but can be used for periods of a few months. Ceramics and refractory oxides such as alumina are not attacked.

.4. Temperature measurement.

The temperature of the bath was measured to ± 0.1°C with

a "Pallador" thermocouple (Pt + 10%Rh/Au + 40%Pd), (Johnson, Matthey & Co., Ltd.). The couple was enclosed in a thin Pyrex sheath and immersed in the bath to a depth of at least six inches. The leads were each soldered to copper wires, and the junctions formed were enclosed in Pyrex tubes which were kept in ice in a Dewar vessel. A little silicone oil was put in each tube, to promote thermal contact.

The E.M.F. of the couple was measured to ± 2 microvolts with a "Cambridge" potentiometer (W.G. Pye & Co., Ltd), standardised with a Weston cell (Muirhead & Co., Ltd).

This thermocouple can be used to measure temperatures up to 1,000°C. It has a thermo-E.M.F. about six times that of the (Pt / Pt + 13%Rh) couple, rising from about 43 microvolts per °C at 0°C to 62 microvolts at 450°C. This thermo-E.M.F. is similar to that of the iron/constanan couple. The Pallador couple thus combines the advantages of these two couples, in that it has a high thermo-E.M.F. and yet remains accurate and reliable at high temperatures because the metals of which it is made are not liable to corrosion.

Since the E.M.F. of the Pallador couple is very sensitive to small variations in the composition of the wires, it is necessary to calibrate each couple before use, rather than to rely on the values of thermal E.M.F. supplied by the makers. The couple was to be used to measure temperatures between 275°C and 450°C, and it was therefore decided not to use the ice point or the steam point as 'fixed points' for calibration, because they lie too far outside this range. The sulphur point was used as one fixed point, and three other calibration points were obtained by using a set of NPL-certified mercury-in-glass thermometers as secondary standards.

The E.M.F. of the thermocouple at the sulphur point was

measured with the apparatus illustrated in Figure 8.3. With the sulphur refluxing near the top of the tube, the E.M.F. was recorded for different positions of the thermocouple tip. The E.M.F. was found to be constant over a zone of length six inches near the middle of the boiling-tube. The results are summarised in the table:

Distance of tip from top of tube (inches)	Thermo-E.M.F. (millivolts)
14	24.345
13	24.345
12	24.345
11	24.345
10	24.345
9	24.345
8	24.343
7	24.330
6	23.85

TABLE 8.1. E.M.F. of thermocouple at the sulphur point.

The atmospheric pressure was 750.0 mm. mercury at 21°C, or 747.5 mm. corrected to 0°C.

The boiling-point of sulphur in °C is given by:

$$444.6 - 0.09\ (760 - p_o),$$

where p_o is the atmospheric pressure in mms. of mercury at 0°C. (Ref.6.)

Applying this formula, the boiling point at 747.5 mms. is 443.5°C. The corresponding thermo-E.M.F. is 24.345 mv.

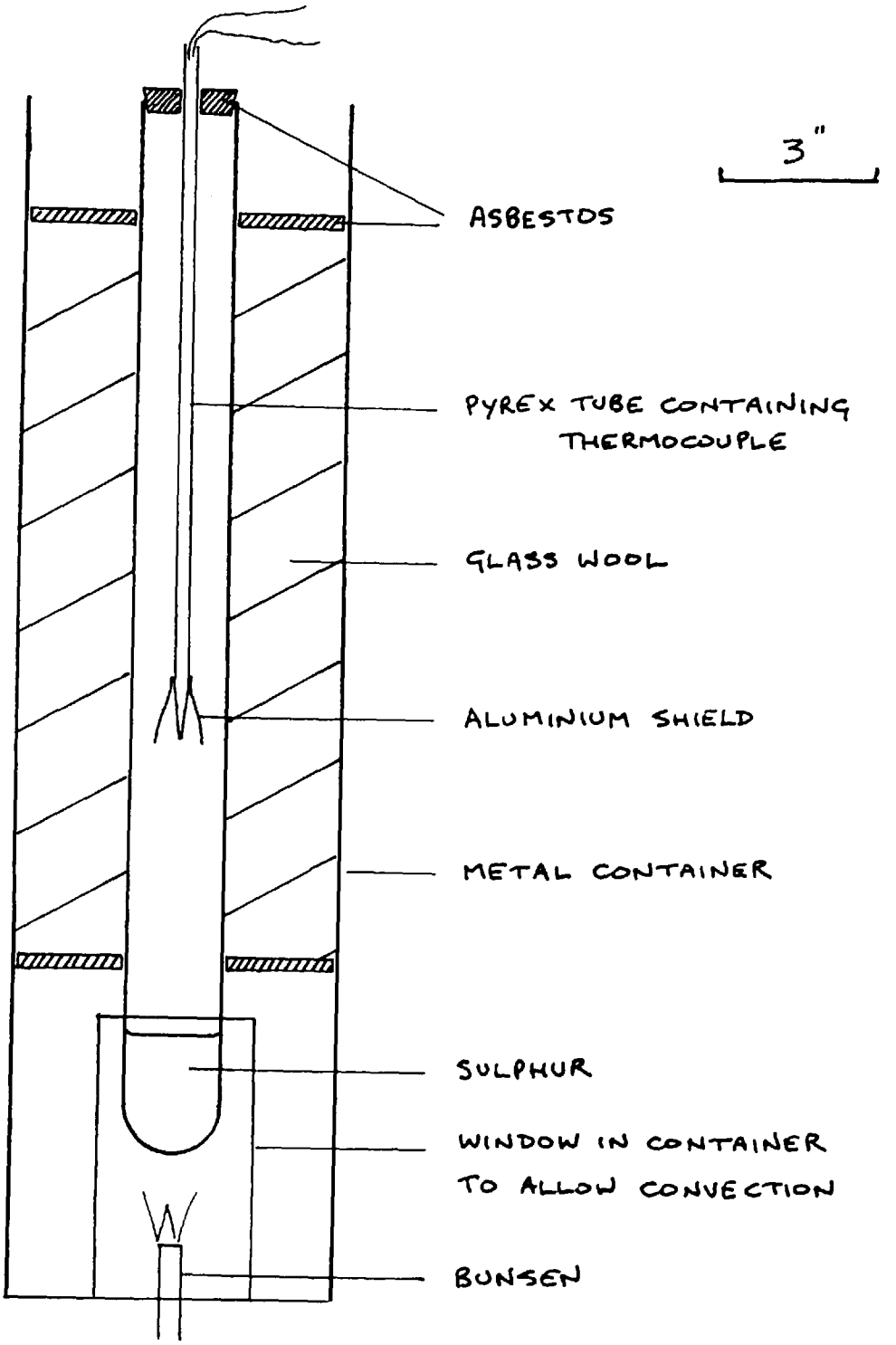


FIGURE 8.3. SULPHUR-POINT APPARATUS.

In another experiment, the E.M.F. was found to be 24.390 mv. at p_o = 756.3 mms. The boiling-point of sulphur at this pressure is 444.2°C. This result agrees with the previous one to within 0.005 mv., or 0.1°C.

To obtain the other calibration points, the thermocouple, inside its protective Pyrex sheath, was immersed in the melt bath, with the mercury-in-glass thermometer suspended beside it. The tip of the thermocouple sheath was touching the bulb of the thermometer. The bath temperature was maintained at constant values by the electronic controller described above. When thermal equilibrium was reached, the thermometer was read and the E.M.F. of the couple recorded. The thermometer readings were corrected, using the N.P.L. certificate. Three sets of readings were taken and these are tabulated below, with the figures for the sulphur point.

Temperature,(°C)	E.M.F. (mv.)
208.3	10.249
259.4	13.166
338.9	17.900
444.2	24.390

Table 8.2. Thermocouple E.M.F.'s at different temperatures.

These values were substituted into the equation

$$(E-10.249) = A.(t-208.3) + B.(t-208.3)^2 + C.(t-208.3)^3,$$

where E is the E.M.F. of the couple in mv. and t is the temperature in °C. The constants A, B and C were calculated from the three simultaneous equations obtained.

The values were:

$$A = 5.5901 \times 10^{-2}$$
$$B = 2.468 \times 10^{-5}$$
$$C = -3.21 \times 10^{-8}.$$

Values of E were then calculated at intervals of 5° from 200 to $450^{\circ}C$, and a set of graphs of E against t were drawn. Each page covered about 20°, and the plots were practically linear over this small range. These graphs were used throughout the experimental work to obtain temperatures from the measured E.M.F.'s, to the nearest tenth of a degree.

REFERENCES TO CHAPTER 8.

1. E.Rhodes and A.R.Ubbelohde, Proc. Roy. Soc., (1959), A251, 156.

2. International Critical Tables, 3, 69.

3. A.Seidell, "Solubilities of inorganic and metal-organic compounds", Van Nostrand, New York, (1940).

4. E.F.G.Herington, The Analyst, (1959), 84, 680.

5. S.I.Berul and A.G.Bergman, Izvest. Sekt. Fiz-Khim Anal., (1954), 25, 218.

6. E.Griffiths, "Methods of measuring temperature", Charles Griffin & Co., Ltd., London (1947), page 216.

7. P. Sue, J. Pauly and A Nouaille, Compt. Rend., (1957), 244, 1212.

8. J. Pauly and P. Sue, Compt. Rend., (1957), 244, 1505.

CHAPTER 9.

THE MEASUREMENT OF THE ELECTRICAL CONDUCTIVITY OF FUSED POTASSIUM NITRATE - BARIUM NITRATE MIXTURES.

9.1. Apparatus.

The conductivity cell is illustrated in Figure . A. It was made from Pyrex glass. The electrodes were of bright platinum; one was a disc 6 mm. in diameter, the other a loop of 24-gauge wire. Each electrode had a surface area of about 0.6 cm^2. Thick copper leads were welded to the platinum beyond the metal-through-glass seals, and these were connected to the leads from the conductivity bridge before measurements were made. The flow of electricity between the two electrodes was restricted by a capillary of diameter 1 mm. The space above the melt could be evacuated through the tap T_1, and air or dry nitrogen could be admitted through T_2. T_2 was a greaseless stopcock, having a PTFE diaphragm; its use prevented the possibility of tap-grease being blown into the melt when the vacuum was released.

Under operating conditions the disc electrode was about 1 cm. below the surface of the melt, and the cell had a resistance in the range 500 - 1,000 ohms.

The apparatus could also be used as a cryometer by removing the B40 cone and electrodes and replacing them by the unit illustrated in part B of the figure. It was therefore possible to measure the freezing-point of the melt before or after conductivity measurements were carried out.

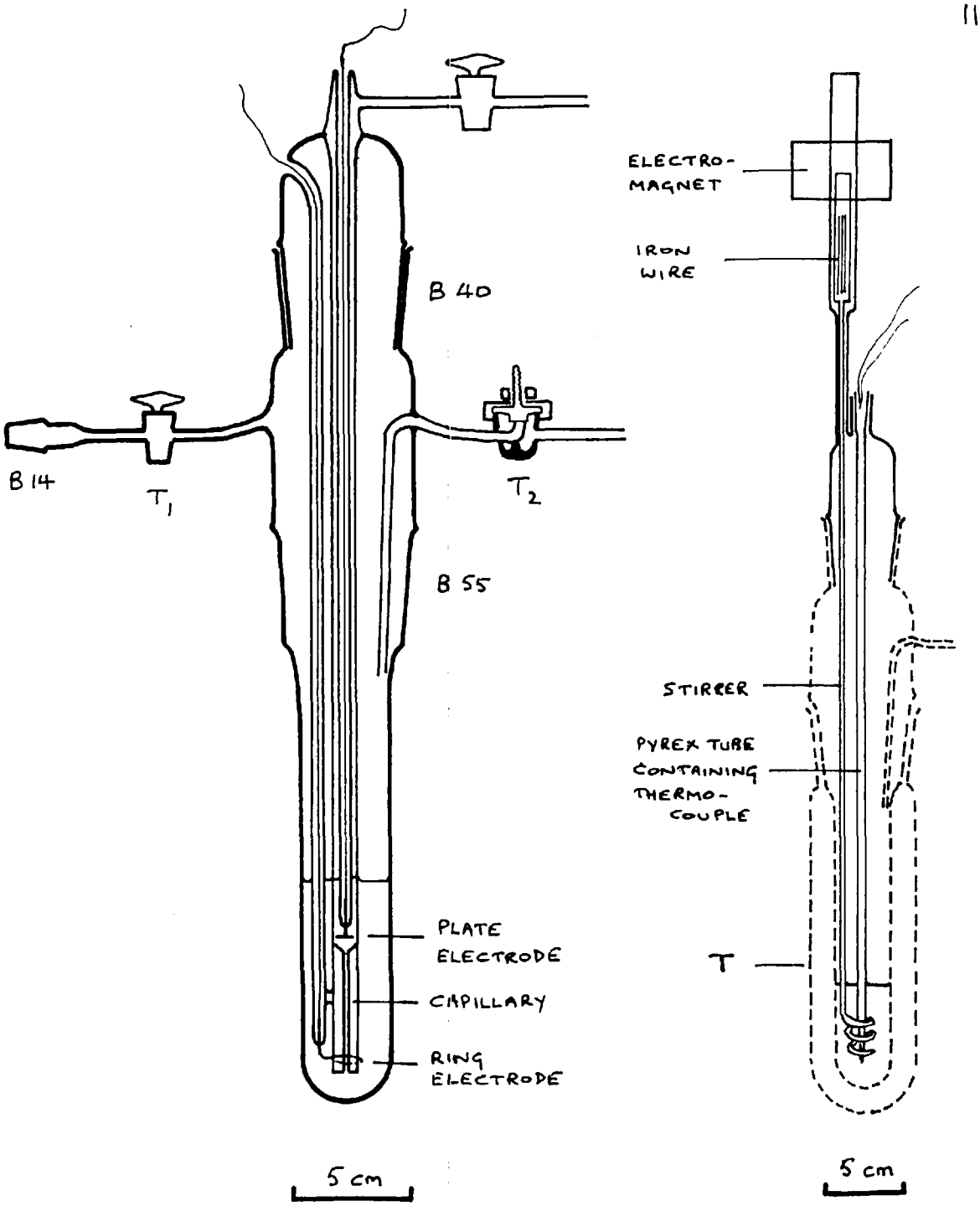


FIGURE 9.1. A - CONDUCTIVITY CELL

B - CRYOSCOPIC UNIT.

When cryoscopic measurements were being made, the large outer tube T was in position, so that there was an air space between the measuring cell and the surrounding melt-bath. This made it possible to adjust the rate of cooling of the central tube to a suitably low value. The electrical measurements were made without the tube T, i.e. with the cell immersed directly in the melt-bath.

The conductivity bridge used was a direct-reading 'transformer ratio-arm' bridge (Wayne-Kerr Laboratories, Model B221), operating at a fixed frequency of 1592 cycles per second. The bridge had controls by means of which the capacitance (or inductance) of the cell could be balanced out before the conductivity was measured. Bridge balance was registered by magic eyes. The voltage applied across the conductivity cell was 0.1 v. Since the cell had a resistance of the order of 500 ohms when filled with melt, the current was $\sim$0.2 ma., and the current density at the electrode surfaces was $\sim$ 0.3 ma/cm^2. The makers claimed that the bridge was capable of measuring conductances of 10^{-1} to 10^{-8} ohm^{-1} with an accuracy of 0.2%.

9.2 Measurement of the cell constant.

This constant was found by measuring the conductivity of the cell filled with a standard solution of potassium chloride in boiled-out distilled water. The most concentrated of the available standard solutions was chosen, as it had a specific conductivity nearest to those of the fused nitrates.

Some Analar potassium chloride was dried in an air oven at 250°C, and a sample was weighed out and dissolved in boiled-out distilled water to give a solution containing

7.1134 grm salt per 100.000 grm solution. Jones and Bradshaw (Ref. 1) have made accurate measurements of the specific conductances of potassium chloride solutions, and record that a solution containing 7.11352 grm per 100.0000 grm solution has a specific conductance of 0.111342 $ohm^{-1}cm^{-1}$.

The conductivity cell and electrodes were cleaned by boiling them in nitrating mixture and washing them thoroughly with distilled water. The cell was placed in the fused-salt thermostat at 370°C, and filled to the working capacity with potassium nitrate melt. The electrode unit was lowered into position, and left there for 24 hours to allow the electrode surfaces to become aged. The melt was poured out, and the cell and electrodes washed thoroughly with distilled water. Cleaning with nitrating mixture and distilled water was then repeated.

The cell was filled to the working level with boiled-out distilled water, and placed in a thermostat at at 25.0°C. Its conductivity was measured, and was found to be 0.089μmho. The cell was emptied and dried, filled with the standard potassium chloride solution and replaced in the thermostat. The conductivity was measured at intervals of five minutes until it reached a steady value (302.2 μmho), corresponding to the attainment of thermal equilibrium. No change could be detected in the conductivity when the electrode unit was rotated through 180°, or when a further 10 ml of solution was added. This showed that the cell-constant was not sensitive to either of these factors.

The cell-constant was calculated as the ratio

$$\frac{\text{(Specific conductance of the standard KCl solution)}}{\text{(Measured conductance of the cell filled with this solution)}}.$$

$$= \frac{0.111,342}{302.2} \times 10^6 \text{ cm}^{-1}$$

$$= 368.4 \text{ cm}^{-1}, \text{ at } 25^\circ\text{C}.$$

The correction for the conductivity of the distilled water was considered too small to be significant.

When the measurements of the fused salt conductivities had been completed, the cell constant was remeasured in the way described above. The value obtained was 369.2 cm^{-1}. This differs from the first figure by only 0.2%.

The calculation of the specific conductances of the melts was based on a mean value of 368.8 cm^{-1} at 25°C, corrected to the experimental temperature. If l_t and a_t are the length and cross-sectional area of the capillary at temperature t°C, the cell constant c_t at this temperature is given by:

$$c_t \approx \frac{l_t}{a_t} = \frac{l_o}{a_o} \frac{(1 + \alpha t)}{(1 + 2\alpha t)}$$

$$\approx c_o.(1 + \alpha t).(1 - 2\alpha t)$$

$$\approx c_o.(1 - \alpha t),$$

where c_o is the cell constant at 0°C and α is the coefficient of linear expansion of Pyrex. The cell constant at t°C can therefore be derived from that at 25° by multiplication by the factor $[1 - \alpha(t - 25)]$.

Values of the cell constant at different temperatures are listed below; it is seen that the constant changes by only 0.14% between 25° and 450°C. α was taken as 3.27×10^{-6} per degree C.

TABLE 9.1. Values of the cell constant at different temperatures.

Temperature (^{o}C)	Cell constant (cm^{-1})
25	368.8
200	368.6
300	368.5
400	368.3
450	368.3

9.3. Preliminary fused-salt conductivity measurements.

Before measurements were begun, the cell and electrodes were re-cleaned with boiling nitrating mixture, washed with distilled water and dried in an air-oven. This cleaning process was repeated whenever the melt was changed.

In order to prove the apparatus and perfect the technique before making definitive measurements, some preliminary measurements were carried out on pure potassium nitrate melts (Runs 1 - 4 and 6 - 8) and on one mixture (Run 5). The results from this work are tabulated in Appendix B (page 381).

Some of the sources of error discovered in the course of the preliminary measurements, and the steps taken to eliminate them, are described in the following paragraphs.

a) A steady evolution of small bubbles occurred from the melts above 450°C, the rate of evolution increasing with rising temperature. The bubbles were oxygen, formed in the

well-known reaction

$$2\ NO_3^- \longrightarrow 2\ NO_2^- + O_2.$$

If these bubbles entered the glass capillary or settled on the surface of the electrodes, the cell-constant was effectively increased and the conductivity measurement could be in error by as much as 50%.

This error is much larger than that caused by the corresponding changes in the chemical composition of the melt (i.e. replacement of NO_3^- by NO_2^-). Even in Run 1, in which the melt was heated from 450° to 500°C over a period of three hours and then cooled to 335°C, the freezing-point of the sample at the end of the run was only 0.35° lower than at the beginning. Reference to the phase-diagram of the system KNO_3 - KNO_2 (Ref.2) shows that this depression corresponds to a nitrite ion concentration of 0.26 mole %. The literature contains no record of conductivity measurements on KNO_3 - KNO_2 mixtures, but Bloom et al (Ref.3) have studied the liquid system $NaNO_3$ - $NaNO_2$ over the entire composition range. They found an almost linear variation of conductivity with molar composition. The specific conductivities of pure potassium nitrate and potassium nitrite melts are both known; they are respectively 0.90 and 1.37 $ohm^{-1}cm^{-1}$ at 420°C (see pages 203 and 34). Assuming that the conductivity varies linearly with composition in this system also, a simple calculation shows that the presence of 0.26 mole % nitrite in potassium nitrate should raise the specific conductivity by only 0.13%. This is barely significant, as the accuracy of the measuring bridge was ±0.2%.

In subsequent runs (including the definitive runs 9 - 12) the sample was not heated above 450°C. Changes in the composition of the melt were then entirely negligible. For

example, in Runs 2 to 4 the same potassium nitrate melt was heated and cooled through the cycle $340^{\circ} \rightarrow 440^{\circ} \rightarrow 340^{\circ} \rightarrow 460^{\circ} \rightarrow 340^{\circ}$. Each part of the cycle occupied six hours, and, in addition, the melt was kept for 48 hours at 340° and for 2 hours at 460°; it had therefore been molten for some 72 hours at the end of the series. The final freezing-point was found to be $0.15^{\circ}C$ lower than the initial one. This corresponds to an accumulated nitrite ion concentration of 0.1 mole %, which should change the conductivity by only 0.05 %.

b) In the first three runs the bridge leads were connected to the copper leads from the conductivity cell by crocodile clips. A contact resistance arose at this point, and could be up to 1% of the cell resistance. In the later runs (including the definitive ones) this source of error was eliminated by soldering the bridge leads to the cell leads.

c) Runs 2 to 4 were carried out on the same potassium nitrate melt, and covered a time period of 72 hours. Runs 6 to 9 were also carried out on a single melt, and occupied 60 hours. In both cases, the conductivity at a given temperature increased by up to 0.8% in the course of the series of measurements. The rate of change diminished as each series progressed; for example, the results for runs 3 and 4 differ by less than 0.2%, and those for runs 8 and 9 differ by 0.4% at $346.5^{\circ}C$ and by 0.1% at $434.2^{\circ}C$.

The evidence presented in paragraph (a) above shows that even these small changes are too large to be attributable to decomposition of the melts. It seems more likely that they are due to an ageing process at the electrode surfaces. For this reason, Run 9 was taken as the definitive run for pure

potassium nitrate, and the mixtures with barium nitrate were prepared by dissolving successive amounts of this salt in the potassium nitrate melt remaining at the end of Run 9. The additions were made without withdrawing the electrodes from the melt; in this way the ageing process was not interrupted, and no sudden changes could have occurred in the state of the electrode surfaces. The change in the conductivity of the cell which took place when the barium nitrate was added could therefore be ascribed entirely to the change in composition of the melt.

In the next section a detailed description is given of the experimental procedure finally adopted for the definitive measurements on pure potassium nitrate and on the mixtures.

9.4. Definitive conductivity measurements.

9.4.1. Pure potassium nitrate.

The conductivity cell and electrodes were cleaned and dried in the way described in Section 9.3. With the electrode unit removed, powdered potassium nitrate was poured into the cell from a tared beaker. The cell was closed with a B40 stopper, and pumped for two hours at room temperature. The salt was then subjected to shock-cooling and -heating cycles to complete the drying process.

The cell was clamped in the melt-bath at 400°C and the salt was melted, still under vacuum. When fusion was complete the B40 stopper was replaced by the cryometric unit (Figure 9.1B) and the freezing-point of the sample measured. It was found to be 334.5°C.

The cryometric unit was withdrawn, and replaced by the electrode unit. The thermocouple was clamped in the melt-bath so that the tip of its protective sheath touched the outside of the conductivity cell at a point opposite the middle of the capillary. The cell leads were soldered to the leads from the bridge, and runs 6, 7. 8 and 9 (the definitive one) were carried out in that order.

The following routine was followed in making the individual conductivity measurements. The temperature control unit of the melt-bath was set to the required value. When the thermocouple reading indicated that the bath had reached a steady temperature, the conductivity and capacitance controls of the bridge were adjusted until the magic eye registered balance. The bridge was re-balanced at five-minute intervals until the conductivity became constant, Finally, the electrode unit was withdrawn slightly, the melt allowed to run out of the capillary and the unit immediately replaced. This ensured that the melt inside the capillary was at the same temperature as the rest of the liquid in the cell, and also dislodged any small gas bubbles which might be adhering to the inside of the capillary or to the electrodes. The bridge was re-balanced, and if the operation had brought about no change in the conductivity the reading was taken as correct; otherwise the process was repeated after a further wait of five minutes. A satisfactory result could usually be obtained within fifteen minutes of setting the bath temperature.

9.4.2. Potassium nitrate - barium nitrate mixtures.

Some barium nitrate was crushed, oven-dried at 250°C and shock-dried. A quantity sufficient to give a solution of

concentration 5.0 equivalent % (6.69 grm) was weighed out and added to the potassium nitrate melt (98.42 grm) in the conductivity cell at the end of Run 9. The mixture was heated to 370°C, and the electrode unit was withdrawn slightly to permit a narrow Pyrex tube to be pushed through the B40 joint and into the melt. The mixture was stirred by passing dry nitrogen through this tube, until all the solid had dissolved. The tube was removed, the electrode unit pushed home and the space above the melt evacuated in order to remove some small gas bubbles which were adhering to the electrodes and to the walls of the cell. The temperature was then raised to 434°C, with the cell still evacuated. No gas evolution was observed under these conditions, which confirmed that decomposition was negligible at 434°C.

The conductivity of the melt was measured with a descending temperature sequence, over the range 434° to 332°C (Run 10).

A further 7.45 grm of barium nitrate was added, to increase the barium ion concentration to 10.0 equivalent %. The melt was again stirred by bubbling dry nitrogen through it, until all the solid had dissolved. The solution was water clear. Bubbles were removed by evacuating the space above the melt, and dry nitrogen was then admitted. Run 11 was carried out as the temperature was changed from 434° to 324°C.

Finally, a solution of approximately the eutectic composition (22.1 equivalent % barium nitrate) was made by adding 21.94 grm barium nitrate to the mixture in the cell. The mixture was stirred with a stream of nitrogen bubbles. When the solid had all dissolved, some of the melt was removed with a pipette, as the cell was now filled to above its working capacity. The mixture was heated to 434°C, and the

conductivity measured at temperatures descending to 293°C (Run 12) (the freezing point of this mixture being 288°C; Ref.4).

The results derived from this work are presented in Chapter 12, and a discussion of their significance is given in Chapter 16.

REFERENCES TO CHAPTER 9.

1. Jones and Bradshaw, J. Amer. Chem. Soc., (1933), 55, 1780.

2. International Critical Tables, 4, 71.

3. H. Bloom, I.W. Knaggs, J.J. Molloy and D. Welch, Trans. Farad. Soc., (1953), 49, 1458.

4. P.I. Protsenko and A.Ya. Malakhova, Zhur. Neorg. Khim., (1957), 2, 2145.

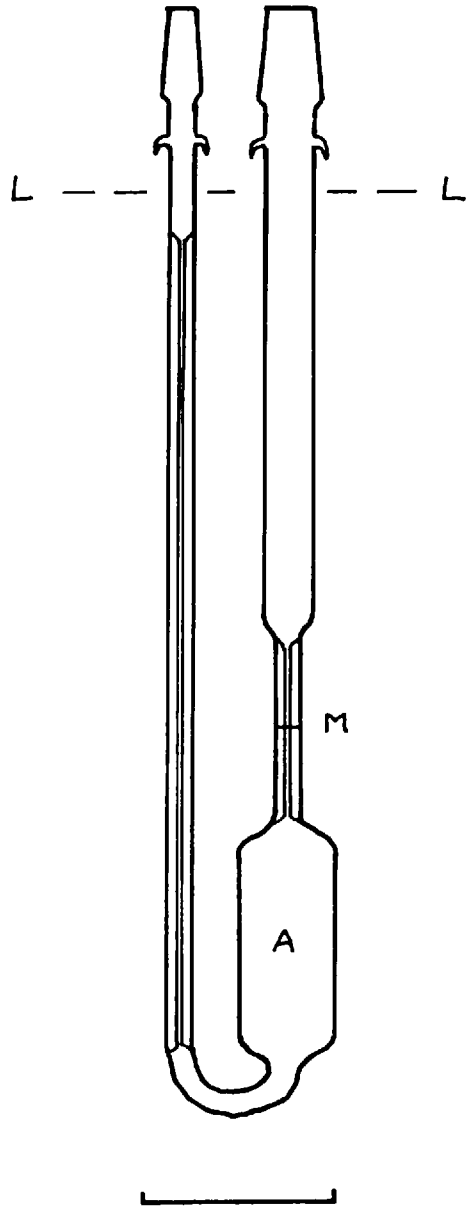
CHAPTER 10

MEASUREMENT OF THE DENSITIES OF FUSED POTASSIUM NITRITE - BARIUM NITRATE MIXTURES.

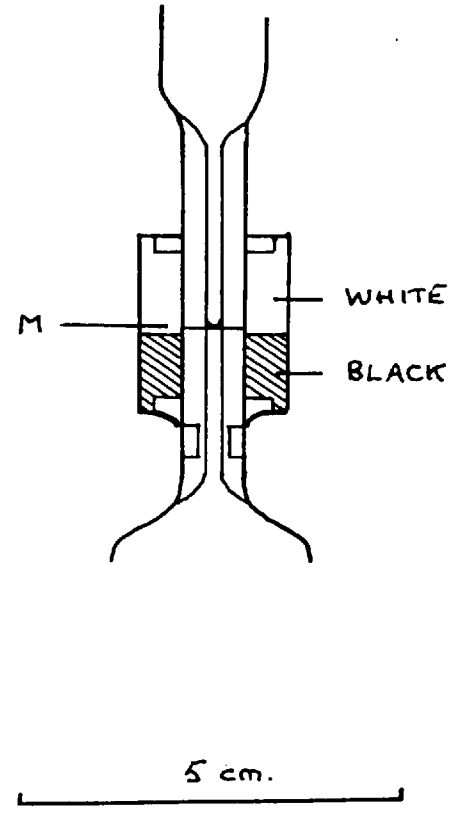
10.1. Apparatus.

The densities were measured with a manometric densitometer, first described by L.J.B. Husband (Ref.1.) A scale drawing of the densitometer is shown in Figure 10.1. The cell was made from Pyrex. The bulb A had a volume of about 20 ml., and the two capillaries were cut from the same length of "Veridia" precision-bore tubing (Chance Bros.). A fiducial mark M was scratched with a diamond on the short capillary. This mark could be viewed through a telescope against a background provided by a small ceramic plate, which was clipped onto the capillary with a Terry clip (see part (ii) of the Figure). The sighting plate was made from a black-glazed egg-cup (Woolworths), by cutting out a piece of suitable size and scraping the glaze from half of it to expose the white ceramic beneath it. This attachment was still in good condition after it had been immersed in the melt-bath for 500 hours.

The remainder of the apparatus is illustrated in Figure 10.2. The purpose of the gas-line was to produce at X an excess pressure which was continuously variable over the range 0 - 2 cms. of mercury. Nitrogen from the cylinder was dried by passing it through the liquid-oxygen trap T. B was a blow-off filled with di-n-butyl phthalate, and the pressure of the gas in the line could be adjusted roughly by raising or lowering B. Fine adjustments to the liquid level in B were made by means of the screw device S, which caused liquid to flow into B from the polyvinyl chloride tubing P. The aspirator A smoothed out the small variations in pressure which arose from the release of



(i)



(ii)

FIGURE 10.1. (i) THE DENSITOMETER

(ii) THE CERAMIC SIGHTING-PLATE.

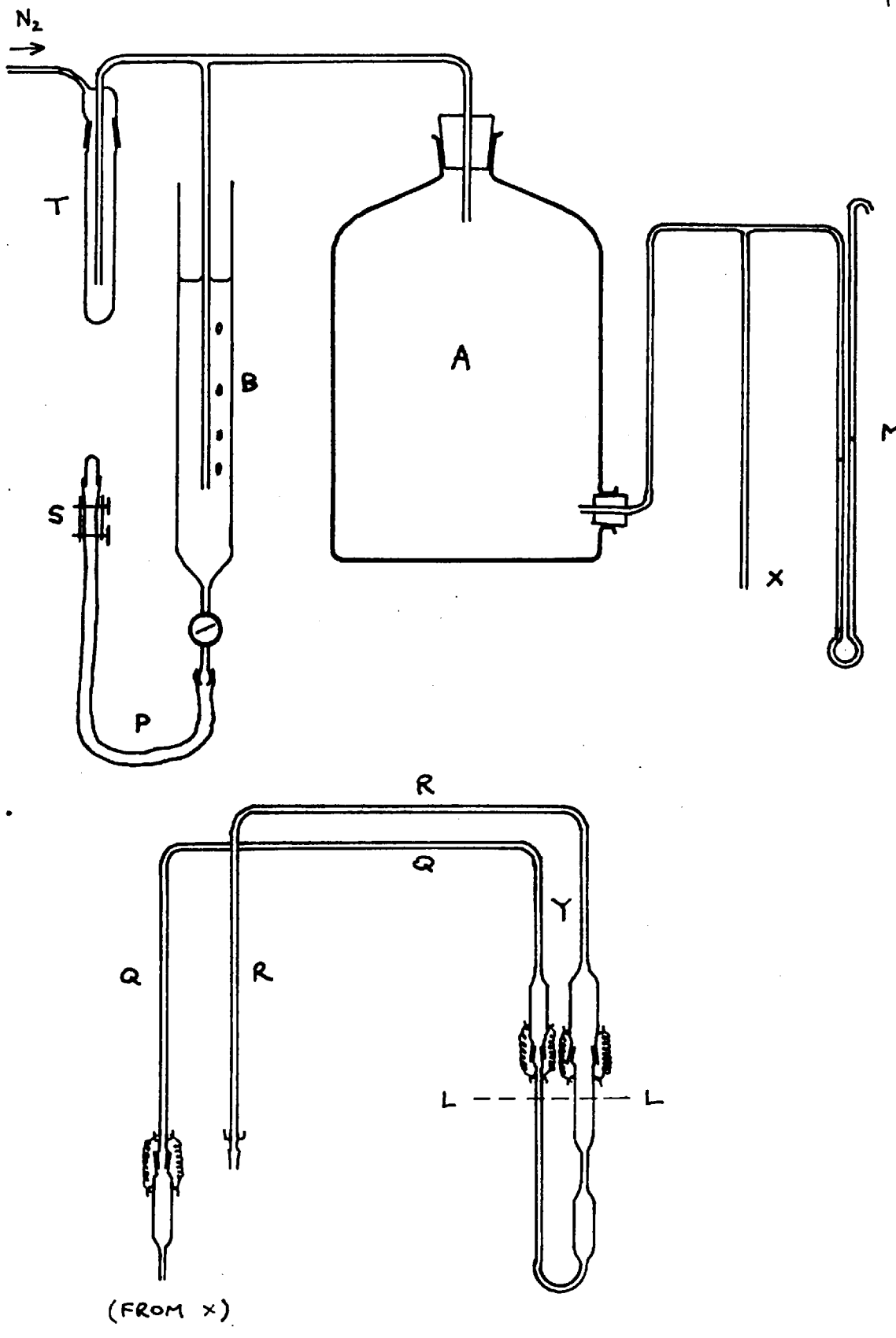


FIGURE 10.2. GAS-LINE FOR DENSITY MEASUREMENTS.

bubbles in B. The pressure in the line was registered by the manometer M, which was also filled with dibutyl phthalate. The pressure could be applied to either limb of the densitometer through the line X, by means of the spring-loaded Quickfit adaptors Q and R. When the densitometer was in use, both adaptors were attached to it and were clamped at Y. This served as a convenient means of holding the densitometer in a thermostat or melt bath, immersed to the level L. The cell was positioned as in Figure 10.2., so that both capillaries could be seen through the observation window. PTFE sleeves (Loughborough Glass Co., Ltd.) were used in the two joints between the densitometer and the adaptors, to avoid possible contamination of the melt by vacuum grease.

The levels of the menisci in the manometer could be measured to $\pm$ 0.002 cms. with a vernier cathetometer. A glass test-tube was made from the same tubing as was used for the limbs of the manometer, and filled with dibutyl phthalate. A mercury thermometer was placed inside it and it was fixed beside the manometer, touching one limb. The temperature registered by the thermometer was taken as the temperature of the manometric fluid.

10.2. Principle of the method.

It was first necessary to measure the volume of liquid, V_o, which was sufficient to fill the densitometer to the fiducial mark, with the limbs vertical. This was done by filling the cell to the mark with water in a thermostat at 25°C, and weighing. V_o at higher temperatures could then be calculated from the coefficient of expansion of Pyrex.

The cross-sectional area A of the capillaries was next determined by introducing a thread of mercury into the long capillary, measuring its length and weighing it.

The densitometer was clamped in the salt-bath thermostat with the capillaries vertical. The bulb was filled with melt, and a pressure was applied to one limb until the meniscus in the short capillary was brought to the fiducial mark. The volume of liquid in the densitometer was such that the other meniscus lay within the long capillary at this stage. The pressure required was measured with the manometer. If h is the manometric height, h' the vertical distance between the menisci in the densitometer and ρ and ρ_o the densities of the salt and the manometric fluid respectively, it is clear that

$$\rho_o h = \rho h' \qquad \text{- - - - - - - - - - - -(10.1)}$$

If M is the mass of salt in the densitometer, its density is given by

$$\rho = \frac{M}{V_o + Ah'} \qquad \text{- - - - - - - - - -(10.2)}$$

(where it is assumed that the pressure was applied to the short capillary). V_o and A have the meanings defined above.

Eliminating h' between equations (10.1) and (10.2) and rearranging, we have:

$$\rho = \frac{M}{V_o}\cdot\left(1 - \frac{A\rho_o h}{M}\right) \qquad \text{- - - - - - - - -(10.3)}$$

If the pressure is applied to the short capillary to bring the meniscus to the mark, the corresponding expression is:

$$\rho = \frac{M}{V_o}\cdot\left(1 + \frac{A\rho_o h}{M}\right) \qquad \text{- - - - - - - - -(10.4)}$$

The density of the salt can therefore be calculated if M, V_o, ρ_o and A are all known and if h is measured.

10.3. Assessment of the error in ρ produced by errors in the meausrement of M, V_o, A, ρ_o and h.

Taking logarithms of the expression (10.4) for ρ,

$$\log(\rho) = \log M - \log V_o + \log (1 + A\rho_o h/M).$$

Differentiating,

$$\frac{d\rho}{\rho} = \frac{dM}{M} - \frac{dV_o}{V_o} + \frac{d(1 + A\rho o h/M)}{(1 + A\rho_o h/M)} .$$

If A = 0.03 cm^2, ρ_o = 1, h = 20cm and M = 50 grm, the term $(A\rho_o h/M)$ is about 0.012. We may therefore write, with very little loss of accuracy,

$$\left|\frac{\delta\rho}{\rho}\right| = \left|\frac{\delta M}{M}\right| + \left|\frac{\delta V_o}{V_o}\right| + \left|\delta\left(\frac{A\rho o h}{M}\right)\right|, \quad - - - - - \quad (10.5)$$

where $\delta\rho$ is the maximum possible error in ρ which could be produced by errors δM, δV_o, etc., in the quantities on the right-hand side of equation (10.5). The proportional error in ρ is seen to equal the sum of the proportional errors in M and in V_o plus the absolute error in $(A\rho_o h/M)$.

M is about 50 grm, and can be measured to 0.001 grm. $|\delta M/M|$ is therefore 0.00002.

V_o is about 20 ml, and δV_o is certainly less than 0.01 ml. (see section 10.4.1). $|\delta V_o/V_o|$ is then 0.0005.

The value of $|\delta(A\rho_o h/M)|$ is calculated to be 0.0001, assuming the following values and maximum errors for A, ρ_o and h:

A	= 0.03 cm^3,	δA	= 0.00012 cm^2,
ρ_o	= 1,	$\delta\rho_o$	= 0.0002,
h	= 20 cm,	δh	= 0.01 cm.

The value of $\left|\frac{\delta\rho}{\rho}\right|$ is therefore:

$$0.00002 + 0.0005 + 0.0001,$$

$$= 0.0006, \text{ or } 0.06\%.$$

If $\rho \sim 2$, this corresponds to an absolute error in the density of 0.001.

Several points emerge from the above discussion:

(a). The weighing error is entirely negligible. In this respect the manometric technique is at an advantage over methods which involve weighing a metal bob immersed in the melt; in these methods, appreciable weighing errors can arise from convection currents, from gas bubbles adhering to the bob and from uncertainty about the depth of immersion of the suspension-wire.

(b). The manometric height h need be measured to only $\pm$ 0.01 cm. to give densities accurate to 0.01%. This accuracy is easily achieved; in the present experiments h was measured to $\pm$ 0.005 cm.

(c). The major part of the total error arises from the uncertainty in V_o. Since the same value of V_o (suitably corrected for thermal expansion) was used throughout the series of experiments, this error is systematic. The residual error, which gives rise to the scatter in the experimental points, is of the order 0.01%. The method is therefore extremely well suited for observation of <u>changes</u> in density, e.g. those accompanying compositional changes.

The error in the temperature measurement was less than 0.1°C. This corresponds to an uncertainty of 0.00008 in a melt density, which is negligible compared with the total absolute error. It could cause scatter of up to 0.005% in experimental points.

10.4. Calibration of the densitometer.

This involved the measurement of the volume V_o and the area of cross-section of the capillaries, A.

10.4.1. Measurement of V_o.

The densitometer was cleaned with boiling nitrating mixture, washed with distilled water, dried and weighed. The black and white sighting screen was attached to the short capillary, and the cell was clamped in a water thermostat. The thermostat temperature could be measured with a N.P.L. -certified mercury in glass thermometer whose scale was marked in intervals of $0.1^{\circ}C$. The position of the cell was adjusted until the long capillary was vertical, using plumb-lines and viewing the instrument from two directions at rightangles to each other. The densitometer was filled roughly to the fiducial mark with boiled-out distilled water. The water was poured down a funnel inserted into the wide limb of the densitometer, which prevented the upper part of the cell from becoming wet.

The cell was allowed to reach thermal equilibrium with the bath, the water was added or taken away with a pipette until the meniscus in the short capillary was opposite the fiducial mark, which was viewed through a telescope. The temperature of the thermostat was noted and the densitometer withdrawn, dried on the outside and weighed. The volume of water in it was calculated from its mass and from the density values in the literature. (Ref.2)

The temperature of the thermostat was raised, the densitometer replaced in it, and some water removed until the level was again correct. The cell was reweighed, and V_o again calculated. This process was repeated four more times. The results of all these experiments are tabulated below.

Temperature (°C)	Mass of water (grm.)	Volume of water (ml.)
23.22	20.317_1	20.367_7
24.55	20.309_5	20.366_7
26.00	20.300_7	20.365_6
27.24	20.295_8	20.367_5
28.52	20.287_1	20.366_2
29.69	20.277_1	20.363_2

TABLE 10.1. Volume of water required to fill the densitometer.

The change in V_o due to thermal expansion of the cell is negligible over the temperature range shown in the table; it is about 0.0002 ml. per °C.

After the fused salt density measurements had been completed, V_o was re-measured, as it was thought that it might have increased slightly because of the etching action of the melts. In this second series of determinations, three sets of measurements were made. In all of them it was noticed that the two menisci were not at the same vertical level, the meniscus in the long capillary being the higher. The cell was several times cleaned with nitrating mixture, but the difference in levels was still observed. The vertical distance between the menisci, Δh, was measured with a cathetometer, and V_o was obtained by subtracting the volume $A.\Delta h$ from the volume of water in the densitometer, (where A is the cross-sectional area of the capillaries). The difference in levels was probably a contact-angle effect.

In the last two experiments of this series, great care was

taken to dry the upper parts of the capillaries with a bunsen flame after the water had been added. The results of these experiments were:

Temperature (°C)	Mass of water (grm)	Volume of water (ml)	$A.\Delta h$ (ml)	V_o (ml)
22.23	20.328_8	20.374_7	0.012_4	20.362_3
20.56	20.330_0	20.368_3	0.009_3	20.359_0
19.62	20.324_9	20.359_3	0.002_0	20.357_3

TABLE 10.2. Values of V_o near 20°C.

These values of V_o are all lower than the initial value of 20.367 ml., by up to 0.008 ml. This difference is significant, since an error of 0.008 in V_o would give rise to an error of ± 0.001 in the salt densities (which would, however, be systematic).

It was considered very unlikely that the volume of the densitometer had really decreased in the course of the measurements of fused salt densities; if anything it would be expected to increase, because the melts have a slight etching action. It is much more probable that, in the first set of determinations of V_o, the upper parts of the densitometer had not been dried properly, so that the volume of the water adhering to them had been included in V_o. This would be a systematic error, because the cell was not emptied between the six determinations.

The drying of the upper parts of the densitometer was carried out with the greatest care during the last two experiments of the second set. The mean of the results of

these two experiments was therefore adopted for use in calculating the fused salt densities. This value was

$$V_o = 20.358 \text{ ml. at } 20^\circ\text{C.}$$

It was probably accurate to ± 0.005 ml.

Values of V_o at higher temperatures t were calculated by adding $3\,(V_o)_{20^\circ}.\alpha.(t - 20)$ to the value at 20°C, where α is the coefficient of linear expansion of Pyrex (3.27×10^{-6} per °C) The results are shown in the table.

Temperature (°C)	$3\alpha(V_o)_{20^\circ}(t - 20)$ (ml.)	$(V_o)_{t^\circ}$ (ml.)
20	-	20.358
320	0.059	20.417
330	0.061	20.419
340	0.063	20.421
373	0.069	20.427
410	0.077	20.435
440	0.083	20.441

TABLE 10.3. Values of V_o at experimental temperatures.

10.4.2. Measurement of the cross-sectional areas of the capillaries.

The densitometer was cleaned with dilute aqueous potassium hydroxide and then with nitrating mixture, washed thoroughly with distilled water and dried with a stream of nitrogen flowing through it.

Some mercury (triple distilled) was filtered through a sintered glass plate, and a thread of it was introduced into the long capillary of the densitometer. The cell was clamped in a horizontal position, and the length of the thread measured with a travelling microscope, from crown to crown of the two menisci. The height of each meniscus was also measured. The mercury was poured into a tared beaker and weighed. The room temperature was measured, and the density of mercury at this temperature was found from the standard tables. (Ref.2.)

The volume of the mercury column was taken to be

$$V = \pi a^2 l + V_1 + V_2 , \quad \text{- - - - - - - -} \quad (10.6)$$

where a is the radius of the capillary, l is the length of the column between the two circles of contact and V_1 and V_2 are the volumes of mercury in the caps. The caps were assumed to be sections of spheres, so that V_1 and V_2 were given by:

$$V_i = \pi h_i^2 \left(\frac{1}{2} \cdot \frac{a^2}{h_i} + \frac{h_i}{6} \right) \quad \text{- - - -} \quad (10.7)$$

(i = 1, 2), where h is the height of the cap.

The mass of mercury was 2.6993 grm., and the room temperature was 23.6°C. The corresponding density is 13.5370 grm /cm^3. The total volume V is therefore 0.1994 cm^3, by division. The values of the other parameters were:

$$l = 6.24 \text{ cm},$$
$$h_1 = 0.044 \text{ cm},$$
$$h_2 = 0.048 \text{ cm}.$$

Equations (10.6) and (10.7) were combined and a was calculated. The value obtained was

$$a = 0.1005 \pm 0.0002 \text{ cm}.$$

If the coefficient of linear expansion of Pyrex be taken as 3×10^{-6} per $^{\circ}C$, the change in a for a temperature change of $400^{\circ}C$ is 0.0001 cm. Since this is within the experimental error of the value given above, no account was taken of it.

The cross-sectional area A of the capillaries was calculated. and was

$$A = 0.0317 \text{ cm}^2.$$

10.5. Measurement of the density of di-n-butyl phthalate (ρ_o).

The densitometer was cleaned and dried, and filled to the fiducial mark with dibutyl phthalate (British Drug Houses Ltd. reagent grade). The liquid was poured in slowly through the funnel which reached to the top of the short capillary. Great care was taken to prevent the phthalate from touching the upper parts of the densitometer limbs.

The densitometer was clamped in a water thermostat and adjusted with the help of two plumb-lines until the capillaries were vertical. When thermal equilibrium had been reached, liquid was added or removed with a pipette until the meniscus in the short capillary was exactly opposite the fiducial mark (viewed through a telescope). The temperature of the bath was measured with a N.P.L.-certified mercury thermometer reading to $0.1^{\circ}C$. The densitometer was removed, dried and weighed.

The experiment was carried out at seven temperatures betwe 19° and 25°. The density was calculated at each temperature by dividing the mass of the dibutyl phthalate by the value of V_o previously obtained (20.358 ml.). The densities are tabulated below. They are accurate to ± 0.0002; this accuracy is well within that required for the determination of

fused salt densities to ± 0.001 (see page 130).

Temperature (°C)	Density of dibutyl phthalate (ρ_o).
19.0_7	1.0466
19.6_6	1.0461
20.4_8	1.0453
21.4_7	1.0446
22.5_7	1.0437
23.6_0	1.0428
24.8_3	1.0417

TABLE 10.4. Density of dibutyl phthalate.

A graph of density against temperature was plotted, (see Figure 10.3), and was used to find ρ_o at the temperature of the manometer during experimental work.

10.6. Experimental procedure for the measurement of the density of a liquid mixture of potassium nitrate and barium nitrate.

Measurements were made on mixtures covering the concentration range 0 - 50 equivalent % barium, in steps of 5%, and at set temperatures between the liquidus and 440°C. Above this temperature some gas evolution occurred, and would have vitiated results. For mixtures containing more than 50 equivalent % barium, the liquidus temperature was above 440°C (see Figure 10.4).

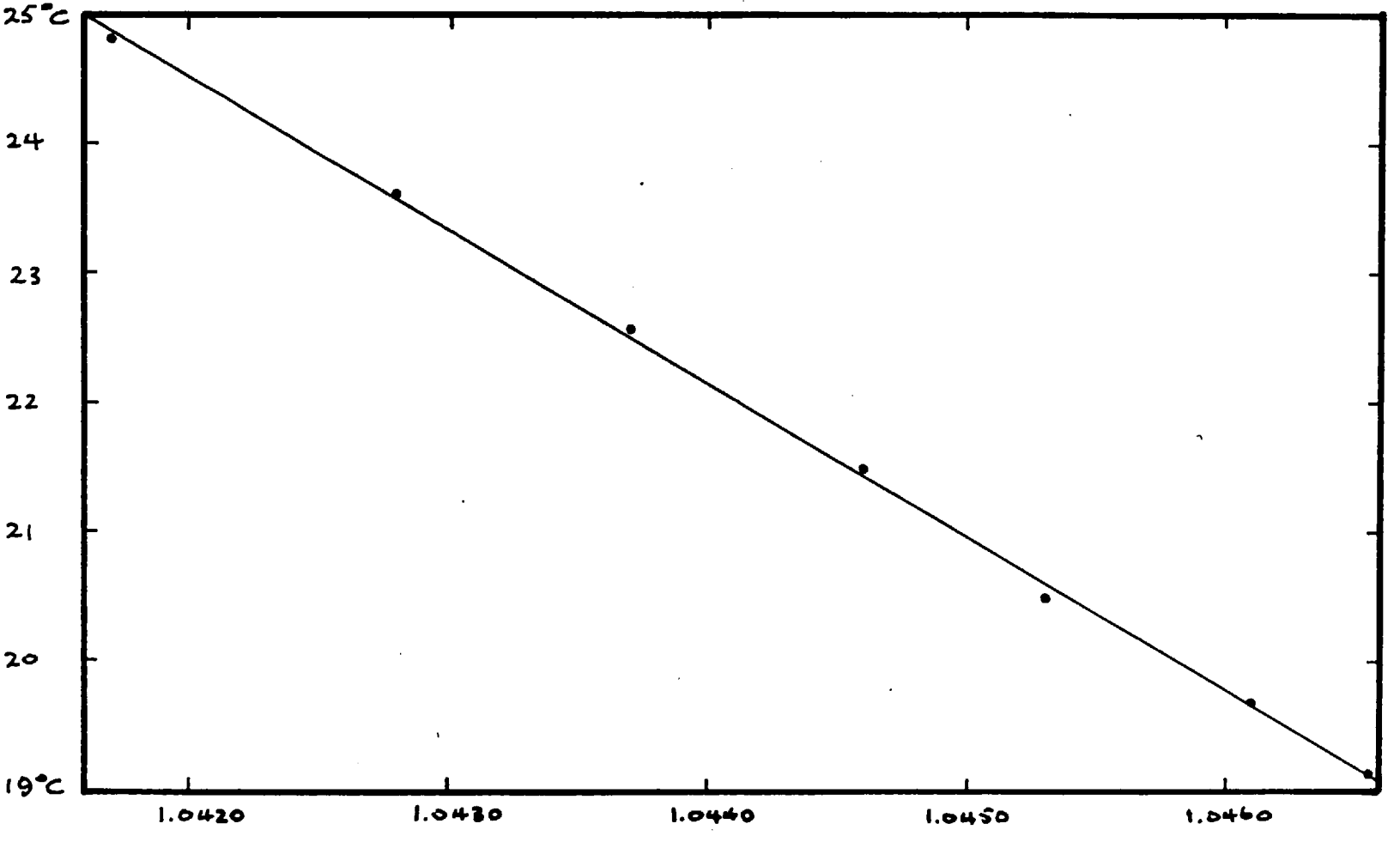


FIGURE 10.3. DENSITY OF DI-n-BUTYL PHTHALATE AS A FUNCTION OF TEMPERATURE.

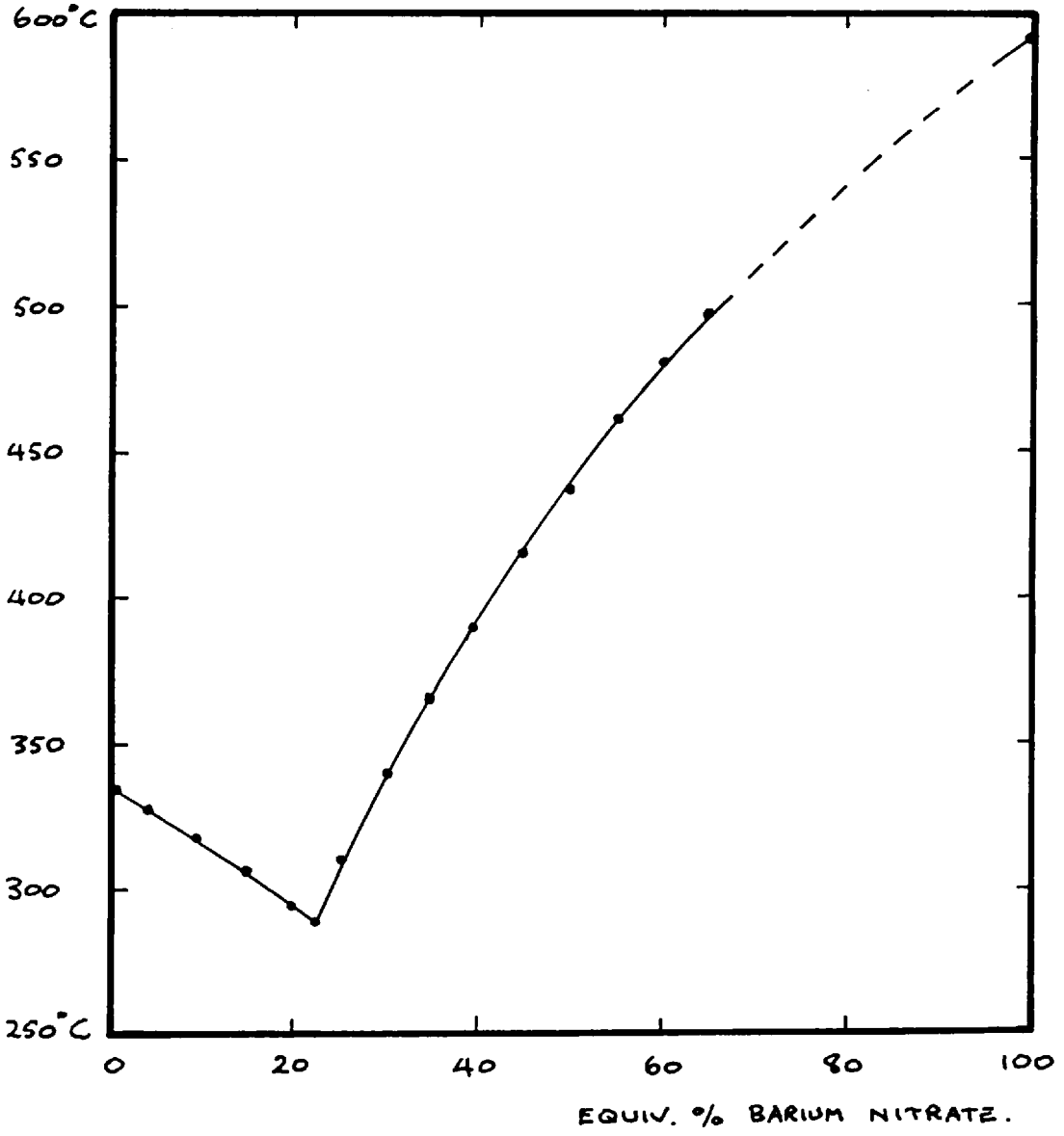


FIGURE 10.4. FREEZING-POINT DIAGRAM FOR THE SYSTEM POTASSIUM NITRATE - BARIUM NITRATE.

The same experimental pattern was followed for all the mixtures. The densitometer was cleaned with hot nitrating mixture, washed with distilled water and dried at 250°C. It was cooled to room temperature with a stream of dry nitrogen flowing through it.

Some barium nitrate was crushed, oven-dried and shock-dried. A suitable amount was placed in a weighing bottle and weighed. A tared Pyrex funnel was lowered into the wide limb of the densitometer until its tip reached the upper end of the short capillary. The barium nitrate was poured from the bottle into the funnel, when it ran down through the capillary and into the bulb of the densitometer. The capillary became blocked from time to time, but gentle tapping with a glass rod was usually sufficient to free it. Sometimes a stiff wire had to be used to release the blockage; in this case the mass of salt adhering to the wire was found by weighing. The bottle and funnel were finally reweighed, and the mass of barium nitrate in the cell found by difference.

The funnel was washed, dried and reweighed. Some powdered, shock-dried potassium nitrate was placed in a 100 ml. beaker, which was then weighed. The funnel was put into the densitometer as before, and potassium nitrate poured in until the densitometer bulb was full of powdered salt. The ceramic sighting-plate was clipped into position on the short capillary. The adaptor Q was attached to the narrow arm of the cell, which was then immersed in the salt bath thermostat at 340°C. The salt mixture melted. It could be stirred by squeezing a rubber bulb which was fitted by a Quickfit joint onto the open end of the adaptor Q. More potassium nitrate was poured down the funnel, with the cell still in the melt-bath, until the liquid level was approximately at the fiducial mark. The funnel was withdrawn and weighed. The beaker was reweighed, and the mass of potassium nitrate in the densitometer found by difference. This last stage of the filling process, with the densitometer

in the melt-bath, was the most difficult one, and took several hours to complete. The funnel frequently became blocked at a point opposite the liquid level in the melt-bath. The blockage was released by lowering the cell further into the bath until the solid plug of salt fused and ran down into the densitometer. The cell was then withdrawn as far as possible without the contents solidifying , and the upper parts allowed to cool before a further addition of salt was made.

The mixture was stirred until in became completely liquid, the thermostat temperature being raised if necessary. Both limbs of the densitometer were connected to a rotary oil pump and the space above the melt was evacuated. This was a convenient way of removing the large number of small gas bubbles (probably air) which adhered to the walls of the densitometer at this stage.

The vacuum was released, the adaptors Q and R fitted to the densitometer and one of them attached to the gas line. The cell was adjusted to an accurately vertical position with the aid of a plumb line hanging in front of the observation window. The cell was positioned so that the whole of the long capillary was immersed in the melt bath, its upper end being ½" - 1" below the surface. The thermostat was regulated to the lowest of the set values at which measurements were being made. The nitrogen flow to the gas line was turned on, and the bubbler B raised until the meniscus in the short capillary of the densitometer was roughly opposite the fiducial mark. If the cell had been filled to the best advantage, the other meniscus was now near the lower end of the long capillary, with the pressure applied above it. The gas flow rate was adjusted by means of the needle valve V until the bubbling caused no fluctuations in the liquid levels in the manometer.

The apparatus was left to attain thermal equilibrium, the bath temperature being read at intervals of one minute until

it remained constant within $\pm 0.05^{\circ}C$ for ten minutes. Fine adjustment was then made to the gas pressure in the line, using the clamp C, until the meniscus (viewed through a telescope) was accurately opposite the fuducial mark. The cathetometer telescope was then set so that the image of the meniscus in one limb of the manometer was tangential to the cross-wire. The apparatus was left for a further five minutes, with continuous observation of the bath temperature. If during that time the temperature had remained steady to $\pm 0.05^{\circ}C$ and the menisci remained in the same positions, the manometer levels were read and the bath temperature and manometer temperature were taken. If the meniscus levels had changed, the gas pressure was readjusted and the apparatus left for a further five minutes. This procedure was continued until satisfactory readings were obtained.

The bath temperature was raised to the next set value, and the melt in the densitometer allowed to expand. The gas pressure was adjusted, or changed to the other limb if necessary. When thermal equilibrium had been re-established, the readings were taken in the same way as before.

This cycle of operations was repeated until one meniscus was near the top of the long capillary when the other was at the fiducial mark. The adaptor R on the wide limb was then removed, and the rubber bulb fitted at the end of the other adaptor Q. With the aid of the bulb, the meniscus in the long capillary was depressed and some melt caused to flow up the short capillary and into the wide limb of the densitometer. An amount of melt equal in volume to the long capillary (~ 0.5 ml) was removed with a tared pipette, which was cooled and reweighed. The mass of mixture remaining in the densitometer was calculated by difference. Density measurements were continued, the pressure being applied to the long capillary for the first determination. For potassium nitrate, measurements could be made over a temperature range

of 60°C before it became necessary to remove some salt. This range increased steadily with barium concentration, since the coefficient of thermal expansion of the melt decreased correspondingly. For no mixture was it necessary to make more than one withdrawal of salt to cover the required temperature range.

When density measurements on each mixture were completed, the melt was usually poured from the densitometer into a tared beaker and weighed. The densitometer was cooled, washed on the outside and weighed, and the total mass of the melt found, as a check. It was always less than the mass of salt originally added. The discrepancy was always less than 0.007 grm., and may have been caused by splashing as the salt was poured into the beaker. Pouring had to be carried out quickly, otherwise the salt solidified inside the densitometer; this was undesirable, because it was then very difficult to re-melt the salt without breaking the densitometer.

This discrepancy in the mass of salt was not serious; an error of 0.007 grm. in M corresponds to an error of only 0.0004 in the salt density. The mass of salt originally weighed into the densitometer was used throughout in calculating the melt densities from the experimental observations.

The densities are presented on pages 212 et seq.

REFERENCES TO CHAPTER 10.

1. L.J.B.Husband, J. Sci. Instrum., (1958), 35, 300.

2. Perry, "Chemical Engineers' Handbook", McGraw Hill, New York, 1950.

CHAPTER 11

ULTRA-VIOLET SPECTROSCOPY OF NITRATES AND NITRITES.

A set of experiments was carried out to record the absorption spectra of pure nitrates and nitrites in the frequency range 54,000 cm^{-1} to 24,000 cm^{-1}, at temperatures from 15°C to a maximum of 500°C. This temperature range includes the melting-points of all the salts examined, and also includes some transition points between solid phases.

The measurements were made with a recording spectrophotometer, and the salts were in the form of thin polycrystalline or liquid films, supported between two flat plates of Spectrosil. The plates were held in a stainless steel frame which could be heated to 500°C in a thermostat unit built into the spectrophotometer.

The pure salts studied, their melting-points and transition temperatures and the temperature range of the spectroscopic observations are listed in Table 11.1.

Some measurements were made on fused mixtures of potassium nitrate and barium nitrate. These are detailed in Table 11.2. The freezing-point diagram for this system is shown on page 140.

Finally, an examination was made of nitric acid and its aqueous solutions, and of iso-propyl nitrate. Details are given in Table 11.3. The cell temperature was lowered to -70°C in the study of the nitric acid solutions, in order to include their freezing-points in the experimental range. The freezing-point diagram for the system nitric acid - water is shown on page 146.

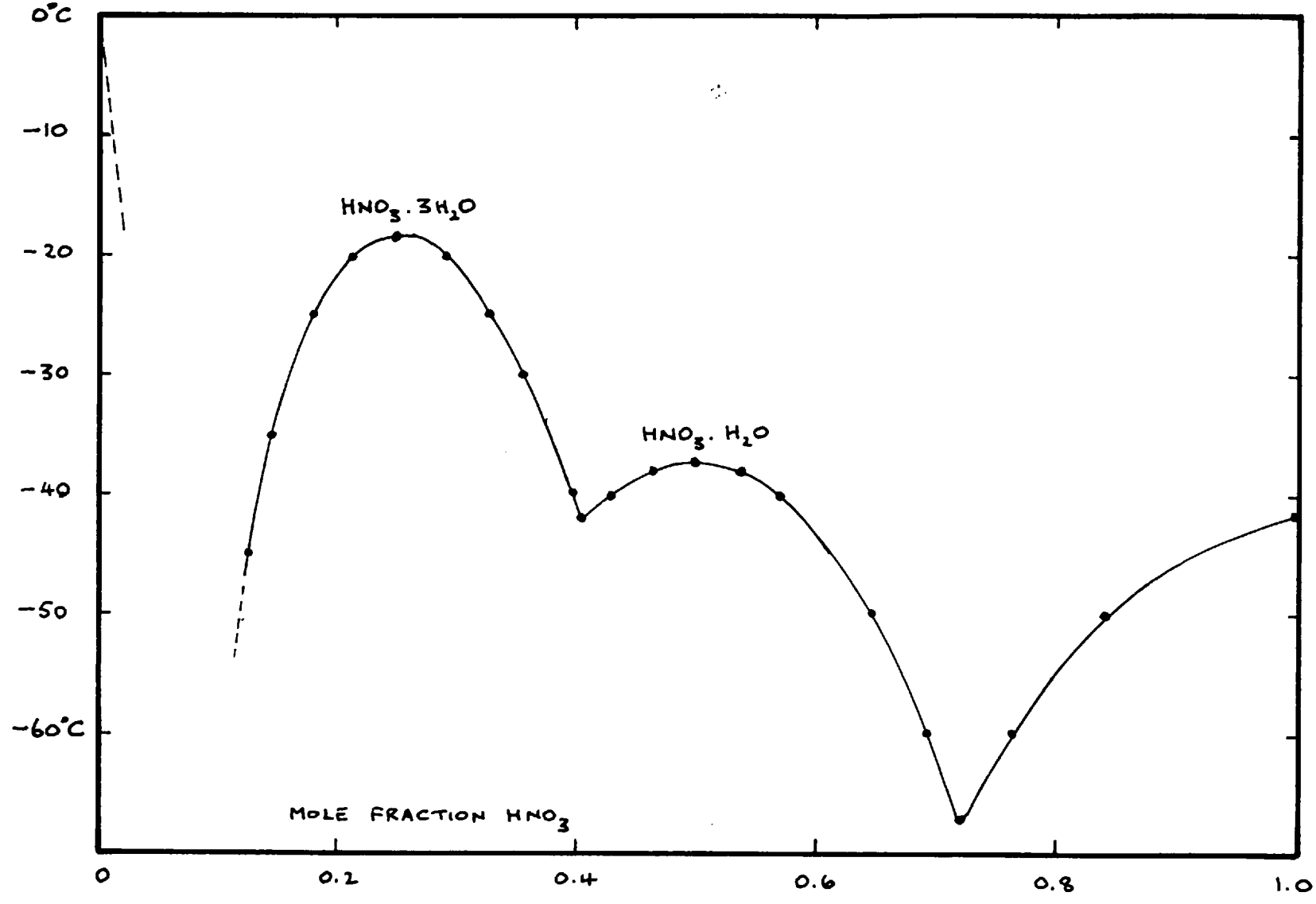


FIGURE 11.1 FREEZING-POINT DIAGRAM FOR THE SYSTEM WATER - NITRIC ACID.

TABLE 11.1. Salts examined by u-v spectroscopy.

Salt	Melting-point (°C)	Transition-points (°C)	Temp. range covered (°C)
$NaNO_3$	~308	275.5(d)	15 - 400
KNO_3	334.5 ± 0.1(a)	127.5(c)	15 - 440
$RbNO_3$	312.3 ± 0.5(c)	161(c) 220(c) 282.7(c)	15 - 420
$CsNO_3$	~408	153.1(c)	15 - 430
NH_4NO_3	168.6 ± 0.1(a)	35(d) 85(d) 125(c)	15 - 175
$AgNO_3$	208.1 ± 0.5(c)	158.1(c)	15 - 240
$TlNO_3$	206.6 ± 0.2(a)	75(d) 145(d)	15 - 220
$NaNO_2$	281.0 ± 0.2(b)	none	15 - 380
KNO_2	420.2 - 423.4 (b)	40-50(c)	15 - 430

(a) Obtained cryoscopically.
(b) Determined with a melting-point tube in the fused-salt thermostat.
(c) Determined optically, as described in Chapter 15.
(d) From the literature (see Table 15.1).

Equivalent % barium in mixture.	Liquidus temp. (°C)(Ref.2)	Range of measurements (°C)
10	318	330 - 450
20	294	320 - 450
35	364	370 - 450
50	437	440 - 460

TABLE II.2. Potassium nitrate - barium nitrate mixtures studied spectroscopically.

Substance	Freezing-point (°C) (Ref.3.)	Temperature range covered (°C)
HNO_3	- 41.3	20
$HNO_3.H_2O$	- 37.3	-54 to +20
$HNO_3.3H_2O$	- 18.5	-30 to +20
0.24N HNO_3	-	20
$(CH_3)_2CH.ONO_2$	-	20

TABLE II.3. Coverage of spectroscopic examination of nitric acid (pure and in aqueous solutions), and iso-propyl nitrate.

II.1. The spectrophotometer.

The instrument used was the S.P.700 recording spectrophotometer (Unicam Instruments Ltd., Cambridge). The

optical system is illustrated in Figure II.2. It incorporated hydrogen and tungsten lamps, a quartz prism and a diffraction grating, and a photo-electric cell and a lead sulphide detector. By selecting suitable combinations of these sources, monochromators and detectors, spectroscopic measurements could be made within the range 54,000 cm^{-1} to 2,800 cm^{-1}. In the work described here, the frequency range was restricted to 54,000 to 24,000 cm^{-1}; this required the use of the hydrogen lamp as source, the prism as monochromator and the photo-cell as detector.

Spectra were normally obtained by the 'double beam' technique. The light from the monochromator was split into two beams of equal intensity by the bank of mirrors M, and one beam was passed through the sample and the other through a reference unit. The reference unit contained no salt (or other sample), but was otherwise identical with the sample unit. A synchronous motor bearing a slotted metal disc was mounted between the monochromator and the sample and reference compartments. When the motor was running, the disc allowed pulses of light to pass through sample and reference cell alternately. These pulses were directed onto the photo-multiplier, and by use of suitable electronic circuits the two signals were separated, and a voltage was produced which was proportional to the ratio

$$\frac{\text{(intensity of light from sample cell)}}{\text{(intensity of light from reference cell)}} = \frac{I}{I_o} .$$

This voltage was applied to a chart recorder (Honeywell Brown Ltd), which displayed the % transmission of the sample.

The instrument could be made to scan a frequency range automatically. The prism was mounted on a table to which a metal arm was fixed. This arm was pressed by a spring against a metal cam, which could be rotated slowly by a

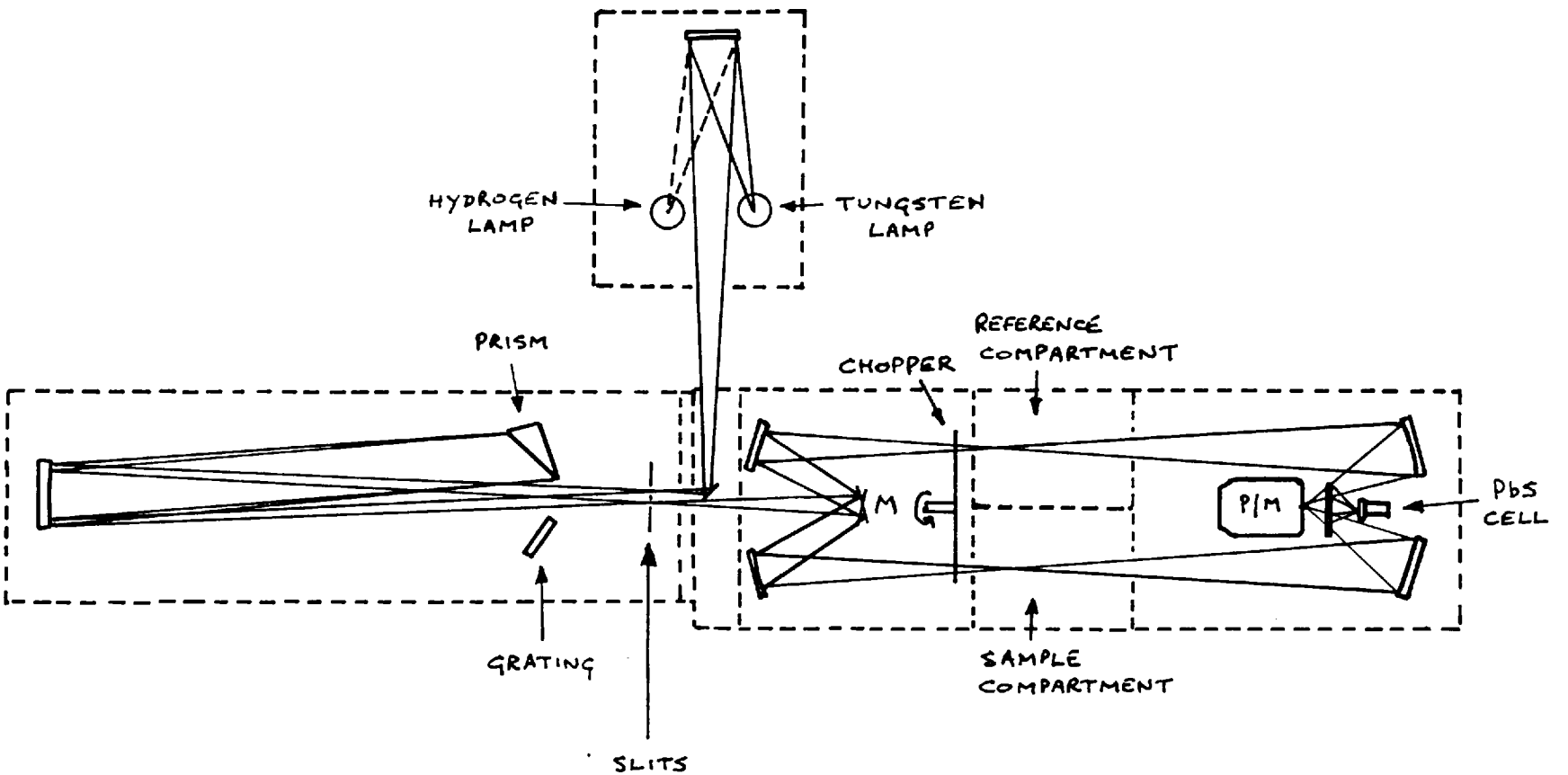


FIGURE 11.2. OPTICAL SYSTEM OF THE SP700 SPECTROPHOTOMETER

(UNICAM INSTRUMENT CO., LTD.)

synchronous motor. The shape of the cam was such that, if it was rotated at constant speed, the movement of the arm caused the prism to rotate and the frequency of the light passing the exit slit of the monochromator varied linearly with time. If at the same time the recorder chart was in motion, the % transmission of the sample was plotted as a linear function of frequency.

The cam was ganged to a microswitch device which caused two marker pens on the recorder chart to be actuated at intervals; by operating a selector switch the pens could be made to mark integral multiples of either 1,000 cm^{-1} or 200 cm^{-1}. The frequency was also displayed visually, on a set of dials geared to the cam. The cam, microswitch device and frequency display dials could not normally be disengaged from each other.

The instrument scanned from high to low frequencies. Five scanning speeds were available, and could be selected by a gear-change unit. The speeds were 250, 750, 2200, 6700 and 20,000 cm^{-1} per minute. A fast reverse speed (30,000 cm^{-1} per minute) could be engaged to re-wind the cam to its original position after completion of a scan. The cam-drive motor could also be declutched and the operating frequency changed manually, using a milled wheel attached to the drive.

Four recorder chart speeds were provided; they were 40, 80, 120, and 160 inches per hour.

The output signal from the detector could be damped if the trace on the chart was marred by excessive electronic 'noise'. Three levels of damping were available.

During a frequency scan, the intensity of the reference beam (I_o) was maintained at a constant level by means of a servo-motor, which caused the slits in front of the light

source to open or close as required. The instrument could be operated at five different reference beam intensities, one of which was selected by a switch. The lowest value of I_o corresponded to the smallest slit-width at a given frequency, and this gave rise to the highest resolution when a spectrum was scanned. However, when the lowest intensity was selected the 'noise' to 'signal' ratio in the output to the recorder was highest, because the 'noise' intensity was independent of I_o. Thus high resolution could be obtained only at the cost of a high noise level, and maximum damping of the signal to the recorder was then required. High damping caused the pen response to be sluggish, so that peaks tended to be recorded at too low a frequency. The highest resolution was therefore used only when it was really necessary (e.g. in separating a multiplet from a mercury arc into its components), and it was always used in conjunction with the highest damping and lowest scanning speed.

In scanning the spectra of the nitrates and nitrites, the middle settings for resolution, scanning speed and damping were used. High resolution was not required, since the spectra were broad, smooth peaks at the experimental temperatures involved.

The full-scale deflection of the recorder pen usually represented 100% transmission. It could be made to represent 10% transmission by switching in an attenuator. This caused a tenfold reduction in the amplification factor of the reference signal from the photo-multiplier, but did not alter this factor for the sample signal. The servo mechanism caused the slits to open until the reference signal (after amplification) regained its original level. As a result, the voltages supplied to the recorder were increased by a factor of ten, so that the scale of the chart now represented the transmission range 0 - 10%. The attenuator was used when a scan on range 0 - 100% had shown the presence of a

peak whose minimum transmission was less than 10%. By re-scanning on the 0 - 10% scale, the curvature in the region of the peak was increased, and this made it possible to measure the frequency of maximum absorption more accurately.

If a scan was carried out over the full range of the instrument with no sample in position, 100% transmission should have been recorded throughout. In practice, the line obtained showed deviations from this value in some frequency regions. The line could be made straight by adjusting a set of sliding resistances, each of which controlled a frequency range of 2,000 cm^{-1}. The full movement of each slider corresponded to a pen movement over 20% of the chart scale. A standard transmission was selected arbitrarily (90% was usually chosen), and the frequency range scanned through by hand, the resistances being adjusted in turn until the pen registered the standard transmission at all frequencies (within a tolerance of 1%). The standard line so obtained was known as the base-line, or 100% line. The re-setting process was normally carried out about every three months.

The entire base-line could be moved exactly onto the 100% line of the chart scale by adjusting a potentiometer (the 100% control).

When the lid of the sample compartment was opened, a shutter automatically moved across the exit port of the compartment and prevented light from reaching the photo-multiplier by this route. The pen position then corresponded to 0% transmission, at all frequencies. The pen could be moved exactly onto the 0% line of the chart scale by adjusting a second potentiometer (the 0% control).

The spectrophotometer could be used as a single-beam instrument if desired. In this case the slit-width was controlled manually, and could be set to any value from

0.0 to 2.0 mm. The deflection of the recorder pen was proportional to the energy of the sample beam.

This setting was particularly useful for recording the sharp lines in the emission spectrum of the hydrogen lamp, which were used to check the frequency scale of the instrument. The procedure for this is described in the next section.

11.2. Checking the calibration of the frequency scale.

11.2.1. Normal adjustment.

With the instrument at the 'single beam' setting, the emission spectrum of the hydrogen lamp was measured from 15,400 to 15,000 cm^{-1}, using slit-width 0.02 mm, resolution control 4, damping control 2 and scan speed 5 (the slowest speed). This frequency range includes the red line of the Balmer series of the hydrogen atomic spectrum. The frequency of this line has been measured accurately, and is recorded in the literature as 15,237 cm^{-1} (Ref. 4).

The position of this line was measured on the frequency scale provided by the marker pens on the recorder. If the measured frequency deviated from 15,237 cm^{-1}, an adjustment was made to a screw which rotated the prism turntable relative to the cam-following arm. The spectrum was re-scanned, and adjustment continued until the instrument recorded the line within 20 cm^{-1} of the correct frequency.

The setting was checked, and re-adjusted if necessary, before the spectroscopic examination of each salt.

II.2.2. Effect of ambient temperature fluctuations.

When the bulk of the experimental work had been finished (up to run number 1366), it was found that the frequency calibration was sensitive to changes in the ambient temperature near the cam, monochromator and cam-following arm. In particular, the calibration drifted just after the instrument had been turned on, because some of the electronic units were housed near the monochromator and the heat generated from these warmed up the surrounding parts. A second source of heat inside the main chassis was the scanning motor.

An experiment was performed to measure the order of magnitude of this thermal drift in the frequency calibration. The main switch of the instrument was turned on, and within two minutes a scan was made from 15,400 to 15,000 cm^{-1}, using the instrument settings given above. The Balmer line was recorded at 15,086 cm^{-1}. The same region was re-scanned at intervals of fifteen minutes. The frequency at which the line was recorded increased steadily with time; after two hours it was 15,160 cm^{-1}. The rate of drift increased if the scanning motor was left running between readings.

In assessing the errors caused by thermal fluctuations, two effects have to be considered:

(a) The heat output from the valves housed in the main chassis was steady. If the instrument was turned on but no scans carried out, the temperature of the chassis would be expected to rise smoothly until thermal equilibrium was attained with the surroundings, after which it would remain constant. The frequency calibration would therefore change during the initial warming-up period, but not subsequently. If the cam was set to record the Balmer line at 15,237 cm^{-1}

before the chassis had reached thermal equilibrium, any frequency measurements made after equilibration would be in error. This error would be constant for a series of measurements provided the chassis temperature returned to its equilibrium value between scans. It would not give rise to 'scatter' in the results, and would have no effect on the difference between two measured frequencies.

It is estimated that the maximum systematic error which could arise in this way was 100 cm^{-1}.

In the experimental work on nitrates and nitrites described in Chapter 14, the cam setting was never changed, and the main switch of the instrument was never turned off, while a particular sample was being examined. Any error from the source described here was therefore completely systematic for each sample; it could not affect the sizes of the steps in the plots of frequency against temperature, nor could it influence the slopes of the linear portions of the plots.

(b) The scanning motor generated heat only when it was running, i.e. when a scan was being made. The temperature of the spectrophotometer chassis would therefore rise during a scan and fall to its equilibrium value afterwards. If another scan was made immediately after the first, before the temperature had returned to its equilibrium value, there would be a relative error between the two results. If further scans were made at unequal intervals, the chassis temperature would vary irregularly and the results would show 'scatter'.

This is believed to be the source of the scatter (of the order ± 50 cm^{-1}) in the plots of frequency against temperature shown in Chapter 14.

The sources of error described in (a) and (b) influenced all the results for nitrates and nitrites, with the exception of those described in the next two paragraphs.

In order to reduce the temperature fluctuations causing the calibration drift, a fan was mounted behind the instrument and the front and back panels were removed. A stream of air was blown over the electronic units and past the cam-following arm and monochromator. In thirty minutes, the frequency at which the Balmer line was recorded fell from 15,160 to 15,142 cm^{-1}, and remained within 5 cm^{-1} of this for three hours. The effect of running the scanning motor was now much smaller; when the motor was run for 35 minutes, the Balmer line frequency appeared to increase by only 10 cm^{-1}, and when the motor was switched off the line returned to its original position in 45 minutes.

The fan-cooling was used to stabilise the calibration while a set of experiments was carried out to measure accurately the frequencies of maximum absorption of the alkali nitrates just above their melting-points. In these experiments the Balmer line was drawn immediately before and immediately after each salt spectrum, and the result was accepted only if the line appeared within 10 cm^{-1} of the correct value on both occasions. In this way the total error due to (a) and (b) above was reduced to 20 cm^{-1}. The results of these experiments are given on page 446.

11.2.3. Effect of cam mis-shaping; standardisation of the frequency scale using lines from the mercury-arc spectrum.

The results of the carefully-made experiments mentioned in the previous paragraph were found to be significantly different from a similar set of results for alkali nitrate melts which had recently appeared in the literature (Ref.5). The differences were all about 100 cm^{-1}, the present results

being the lower in every case. The approximate constancy of this difference suggested that it was due to a calibratic error in one or both sets of measurements.

This stimulated a further experiment to check the calibration of the Unicam instrument. An independent frequency standard was used in the range which included the maximum of the weak band of the nitrates, so that the result for these salts need no longer be based on the instrument-makers' assertion that the frequency scale would be correct at all values if it was set at 15,237 cm^{-1}.

When this experiment was begun, the main switch of the spectrophotometer had been on for one week, with the fan-cooling operating. Thermal drifts were therefore minimised.

The Balmer line was recorded three times, at intervals of five minutes. The measured frequencies were respectively 15236, 15236 and 15237 cm^{-1}. The cam was therefore correctly set according to the makers' specification. The lamp-house was uncovered, and a mercury arc-lamp was mounted above it. An aluminium plate was positioned to reflect light from the lamp through the slit. Scans were made in range 27,000 to 33,000 cm^{-1}; the strongest lines emitted by the lamp were recorded, and their positions measured on the frequency scale of the instrument. The measured frequencies were compared with values taken from the literature (Refs. 6 and 7). Several scans were made for each group of lines; the measured frequencies, and the standard ones, are listed in TABLE II.4.

Finally, the Balmer line was again recorded three times, at five minute intervals. It was found at 15240, 15238 and 15234 cm^{-1}. Since these and the initial values all lay

TABLE 11.4. Frequencies of lines in the spectrum of the mercury arc.

Measured frequency * (cm^{-1})	Standard frequency * (cm^{-1})	(Measured) − (Standard)
27247 27246 27247	27298	-51
27308 27308 27308	27361	-53
27338 27338 27336	27396	-60
29838 29838 29843 29851 29846	29927	-85
31884 31892 31890	31933	-42
31943 31952 31950	31993	-42

* in air.

within 3 cm^{-1} of the correct value, it was assumed that the cam had remained set to the makers' specification throughout the experiment.

It is clear from the results in the table that, when the scale was set to read correctly at 15,237 cm^{-1}, the reading was too low in the range 27,000 to 33,000 cm^{-1}.

All the results presented in Chapter 14 (and Appendix C) have been adjusted to allow for this discrepancy due to cam mis-shaping. The corrections at 31.8 kcm^{-1}, 29.8 kcm^{-1} and 27.3 kcm^{-1} were +40 cm^{-1}, +85 cm^{-1} and +55 cm^{-1} respectively; at intermediate frequencies the correction was found by linear interpolation between these values.

This source of error affects only the <u>absolute</u> value of the frequency at an absorption maximum; in a series of scans on the same substance at different temperatures, the error would be systematic and would not affect the accuracy with which <u>changes</u> in the position of the maximum could be measured.

After correction for the effect of cam mis-shaping, the accurate values of E(2) for sodium and rubidium nitrates were in satisfactory agreement with those obtained by Smith et al., but some discrepancy remained in the case of potassium and caesium nitrates. Both sets of results are shown in the table on page 238, where some possible causes of the differences are suggested.

11.3. The sample and reference thermostat units.

The thermostat units were built to fit into the sample and reference compartments of the spectrophotometer. They

were designed to maintain a salt sample at any temperature from 20° to 450°, while allowing free passage to the ultra-violet beam.

The design was based on that of Rhodes and Ubbelohde (Ref.8), but several improvements were made; the cell described here differs from theirs in the following respects:

(a). The copper block was nickel plated. This prevents flaking of the copper due to atmospheric oxidation at the higher temperatures.

(b). The units were cooled by water jackets, which prevented the ambient temperature around each thermostat from rising more than 2°C above room temperature. This prevented excessive heating of the surrounding structural units of the spectrophotometer (see page 168).

(c). Steps were taken to reduce temperature gradients in the sample, by winding heating-wires round the tubes through which the ultra-violet beam passed (see page 175).

The sample unit is illustrated to scale in Figure 11.3; the reference unit was its mirror image.

The block A was built up from nickel-plated copper laminations. The nickel plating prevented atmospheric oxidation of the copper at the higher temperatures. The block was heated by means of four flat heating-elements (Figure 11.3, part J), sandwiched in pairs between the laminations. The heaters were made from nichrome wire (0.025" x 0.002"), wound on mica formers, and were insulated from each other and from the block by mica sheets. The four heaters in each block had a total resistance of 120 ohms at room temperature. The block was earthed with a thick copper wire.

KEY TO FIGURE 11.3.

A Copper block.

B Positions of heaters. Two heaters were placed in each of the positions indicated.

C Space occupied by stainless steel sample holder (for detailed drawing see Figure 11.4).

G Holes occupied by resistance thermometer and thermocouple.

J One of the flat heaters. The heater was made from nichrome wire wound on mica.

T Sindanyo tubes to allow passage of the light beam. Spectrosil windows were set into each tube; their positions are shown in Figure 11.4.

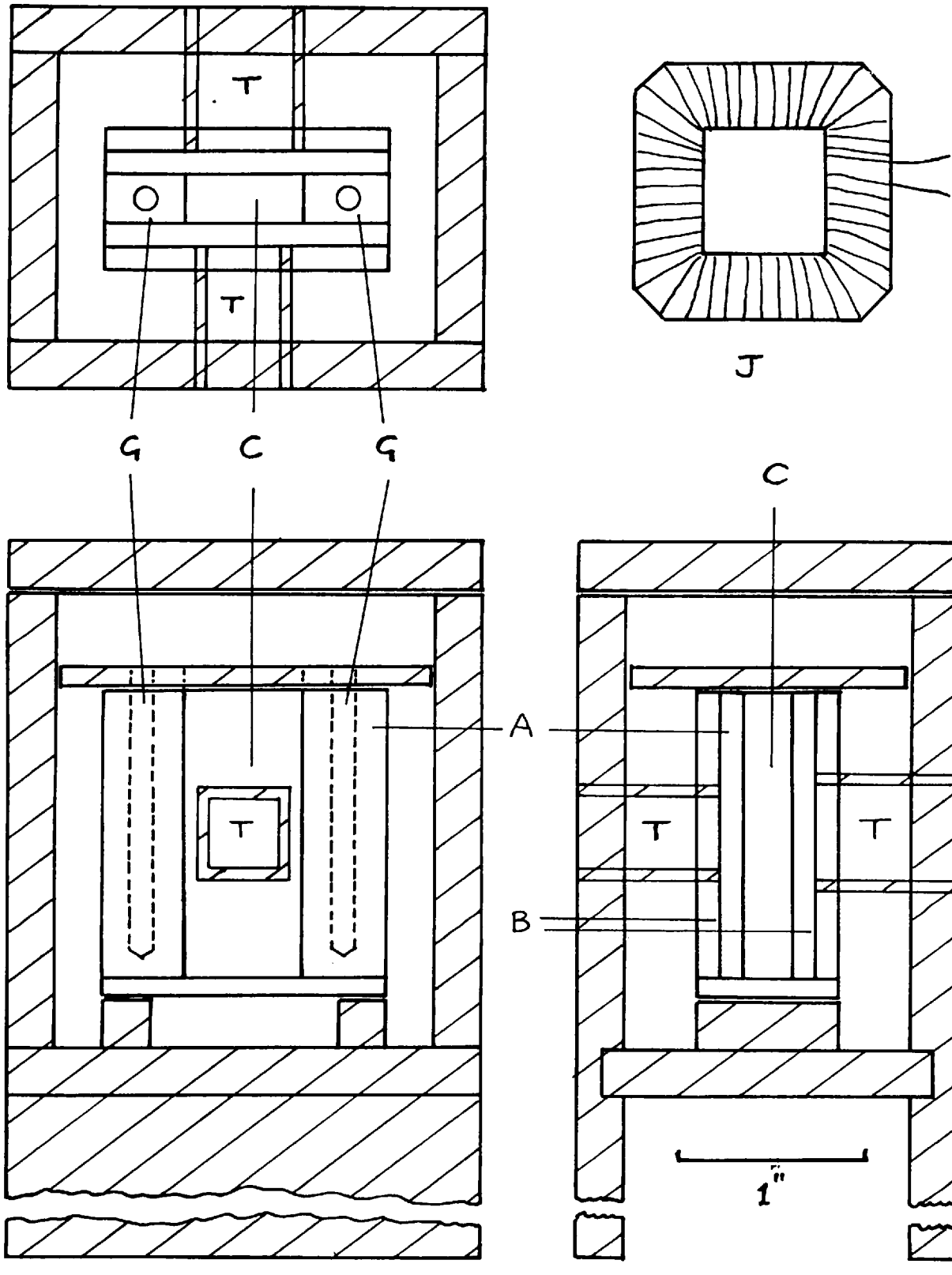


FIGURE 11.3. SCALE DRAWING OF SAMPLE THERMOSTAT.

(FOR KEY, SEE PREVIOUS PAGE).

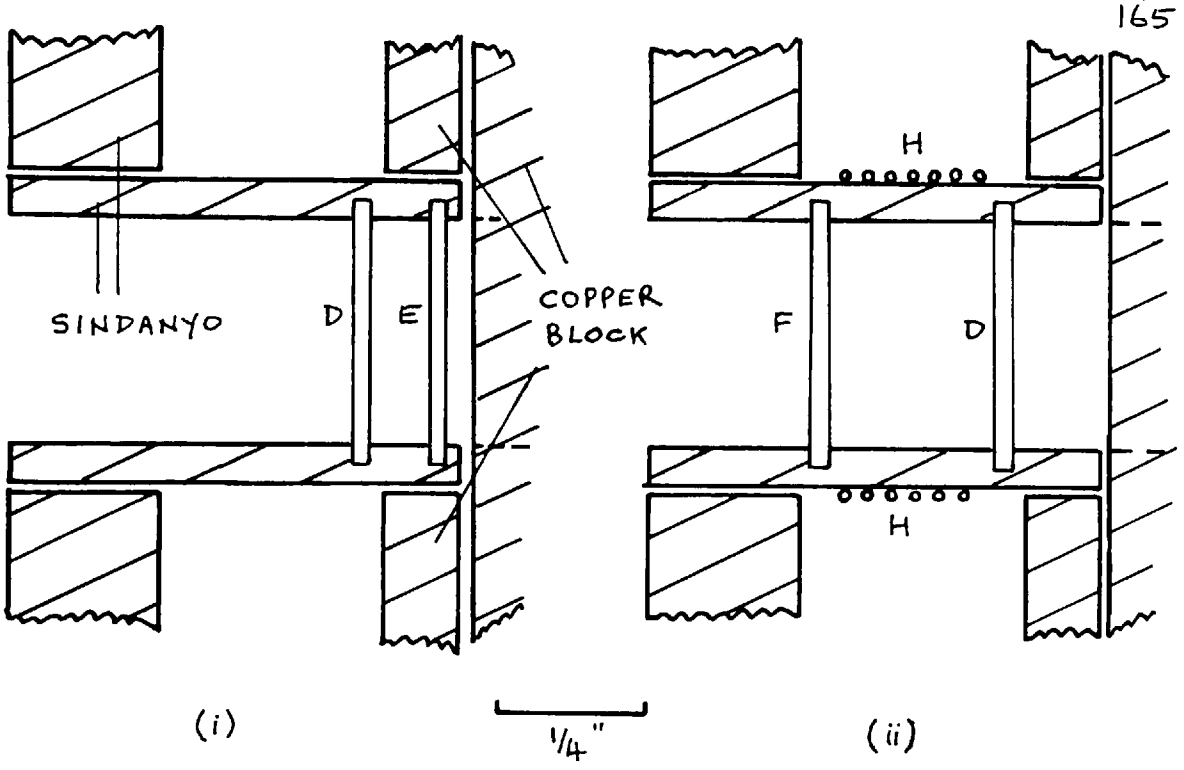
KEY TO FIGURE 11.4.

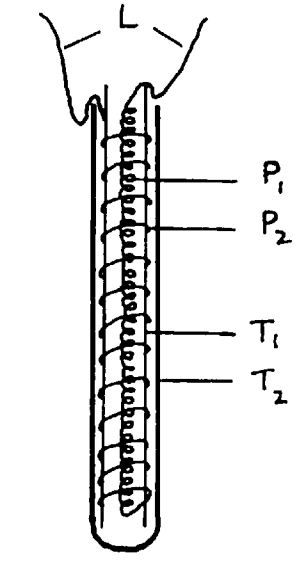
(i) Section of one of the Sindanyo tubes through which the ultra-violet beam entered the thermostat, showing the Spectrosil windows D and E in their original positions.

(ii) The same, after modification. One window was moved from E to F, and the heating wire H wound around the Sindanyo tube between the windows. The 'exit' tube was modified in a similar way.

(iii) Diagram of the resistance thermometer made by the author. The thermometer consisted of two helices of 47-gauge platinum wire, one inside the other (P_1 and P_2). The helices were separated from each other by a Pyrex tube T_1 and the whole assembly enclosed in a second tube T_2. The leads L were of gold wire, which was welded onto the platinum.

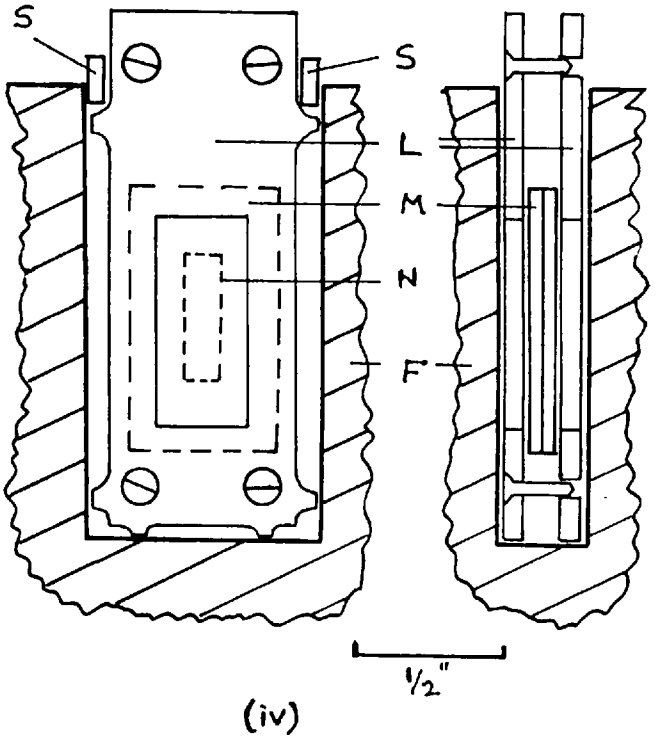
(iv) The stainless steel sample holder L in position in the thermostat. The salt sample was sandwiched between the Spectrosil plates M. The rectangle N shows the size and position of the ultra-violet beam. The silica spacers S kept the holder equidistant from the walls of the copper block.





(iii)

(NOT TO SCALE)



(iv)

FIGURE 11.4. DETAILS OF ABSORPTION CELL FOR FUSED SALTS (FOR KEY, SEE PREVIOUS PAGE).

A stainless steel holder (Figure 11.4, part iv) could be lowered into the central space in the block. The holder supported a pair of flat "Spectrosil" plates (Thermal Syndicate), which had sandwiched between them a thin film of the salt to be examined.

Two holes drilled into the block were used to accomodate a Pallador thermocouple and a platinum resistance thermometer, respectively. The thermocouple was used to measure the temperature of the block to within 0.1°C, in conjunction with a "Cambridge" potentiometer (W.G. Pye & Co) and a Weston standard cell (Muirhead). The calibration of the thermocouples in the sample and reference thermostats is described on page 182. The resistance thermometers in the two blocks were connected to separate electronic temperature controllers, which regulated the power supply to the heaters. Each controller incorporated a Wheatstone's bridge circuit, with the platinum resistance thermometer in one ratio arm and a chain of decade resistance boxes in the other. The resistance chain on the 'sample' controller also included an oil-immersed slide wire of resistance 1 ohm, so that the resistance of this chain could be varied continuously.

The power supplied by the controller was constant when the out-of-balance current in the bridge circuit was above a certain value, but was proportional to this current for the last 1°C of the heating process. The equilibrium temperature was therefore approached gradually and without overshoot.

The controllers maintained the block temperatures constant to ±0.01°C for five minutes, or to ±0.1° indefinitely. The temperatures were changed by altering the settings of the resistance chains; the 'reference' temperature could be changed by increments of 0.7°C, but the 'sample' temperature

could be set to any value by means of the slide wire.

Two sets of resistance thermometers were used in the course of the experimental work. The first pair were made by the author, and one of them is illustrated in Figure 11.4, part iii. It was made from about one metre of 47-gauge platinum wire, wound non-inductively on a Pyrex former, the whole being enclosed in a Pyrex sheath. The thermometer had a resistance of 35 ohms at room temperature.

The second pair of thermometers was obtained commercially (Degussa, Hanau, W.Germany), and each had a resistance of 100 ohms at room temperature. They were also made from platinum wire enclosed in a Pyrex capsule. When these thermometers were installed, another resistance box was added to the decade chain in each temperature controller; the resistances could then be varied from 0 to 1,111 ohms, and the smallest increment on the reference controller now represented a temperature change of 0.25°C.

The copper blocks were mounted in Sindanyo containers, the interspace being filled with exfoliated mica ("Micafill").

The sample and reference units, as illustrated in Figure 11.3, were installed in the two compartments in the spectrophotometer. Four brass tubes were sealed through the side-walls of each compartment; three of these were used to admit the leads to the resistance thermometers, thermocouples and block heaters, and the compartments could be flushed with dry nitrogen through the fourth.

The makers of the instrument had specified that the ambient temperature inside the compartments should not rise above 35°C. A Pallador thermocouple was used to measure this ambient temperature when the blocks were heated.

The unit containing the two compartments was unscrewed from the chassis of the spectrophotometer and withdrawn for the time of this experiment, to prevent possible damage to the rest of the instrument.

The blocks were thermostatted at 175°C, whereupon the air temperature rose to 45°C. The compartments were flushed with dry nitrogen from a cylinder, but even with a gas flow-rate of one cubic foot per minute the equilibrium air temperature could not be reduced below 40°C.

Since this method of cooling was clearly ineffective as well as uneconomical, brass water jackets were designed to fit over the sides and top of each Sindanyo unit. Water was passed through the two jackets in series, at a rate of one litre per minute.

The jackets controlled the ambient temperatures very effectively; even with the blocks at 450°C, the equilibrium temperature inside the compartments was only 2° above room temperature.

11.4. Measurement of temperature gradients in the original thermostat unit.

Two Sindanyo tubes were recessed into each copper thermostat block, to provide a clear path for the ultra-violet beam. It was essential that these tubes should not mask off any part of the beam; otherwise the electrical signal from the photomultiplier was distorted, and this caused irregularities in the trace drawn by the recorder pen. Since the beam diverged on its passage through the thermostat, the 'exit' tube had a larger cross-section than the 'entry' tube.

Heat losses could occur from the central part of the sample, by radiation or by convection through the Sindanyo tubes. Two Spectrosil windows were slotted into each tube to reduce the convective losses; in the original design they were at the positions marked D and E in part (i) of Figure 11.4 .

Some experiments were carried out to measure the temperature gradients in the sample, and the temperature difference between the sample and the thermostat block, at different block temperatures. A knowledge of these gradients and differences is essential in assessing the significance of spectroscopic measurements made on salt films in the region of their melting points or transition points.

The measurement of the gradients is described below, and their influence on the accuracy of the spectroscopic measurements is discussed in Section 11.8.

11.4.1. Temperature differences between different parts of the sample.

The sample space was explored with a two-junction thermocouple consisting of a piece of 36-gauge alumel wire, 1.5 cm long, with chromel wires welded to its ends. The chromel wires were connected directly to a potentiometer, and the couple generated 0.040 mv per ^{o}C of temperature difference between its junctions.

The two junctions were placed between a pair of the Spectrosil plates used for holding salt samples. Care was taken to see that equal lengths of the chromel wires were between the plates; this reduced the possibility of unequal

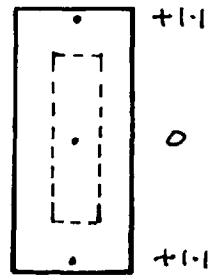
cooling of the junctions by conduction of heat along the wires. The plates were mounted in the steel holder, which was lowered into the 'sample' thermostat.

The E.M.F. of the couple was measured at different block temperatures, adequate time being allowed for thermal equilibrium to be reached at each setting. The gradients were explored by moving the junctions to different positions in the sample space.

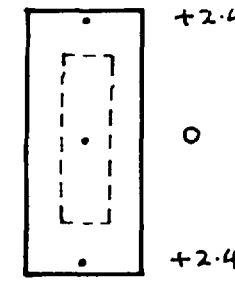
During these experiments the temperature difference between the top and bottom of the sample was found to be sensitive to the exact position of the steel holder relative to the copper block. The maximum difference noted was $1^{\circ}C$, when the block was at $400^{\circ}C$. After some experimentation this temperature difference was shown to be smallest, and to vary least, if the holder was filed to the shape shown in Figure 11.4, part (iv); contact with the copper block could then occur only through the small projections. Silica spacers were used to keep the sides of the holder equidistant from the block. Under these conditions the temperature difference between the top and the bottom of the sample space was not greater than $0.1^{\circ}C$ for block temperatures up to $400^{\circ}C$.

This holder was used, with the silica spacers, during the whole of the spectroscopic work on salt films.

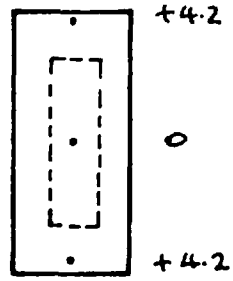
The final temperature differences between the centre and the edge of the sample space are shown in part (i) of Figure 11.5, in which the large rectangles represent the window in the steel holder and the numbers are temperatures in $^{\circ}C$ relative to the central spot. The position of the beam profile is also marked; the dimensions of the beam as it passed through the sample were 1/8" x 7/16".



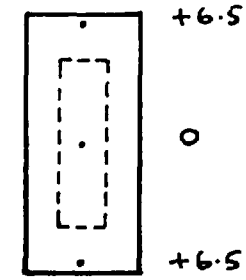
BLOCK TEMPERATURE = 100°C



BLOCK TEMPERATURE = 200°C

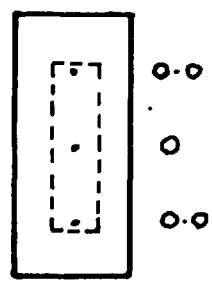


BLOCK TEMPERATURE = 300°C

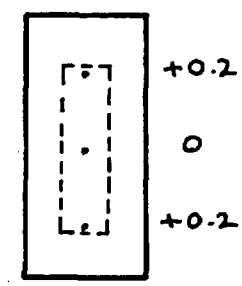


BLOCK TEMPERATURE = 400°C

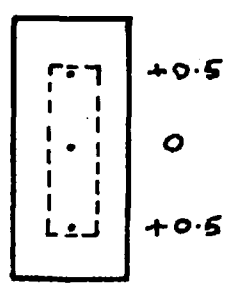
(I) ORIGINAL CELL DESIGN



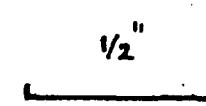
BLOCK TEMPERATURE = 100°C



BLOCK TEMPERATURE = 200°C



BLOCK TEMPERATURE = 300°C



(II) MODIFIED APPARATUS.

FIGURE 11.5. TEMPERATURE GRADIENTS IN THE SAMPLE SPACE.
THE LARGE RECTANGLES REPRESENT THE WINDOW IN THE STEEL SAMPLE-HOLDER; THE SMALL RECTANGLES ARE THE BEAM CROSS-SECTION. THE NUMBERS ARE THE TEMPERATURES AT THE POINTS MARKED, RELATIVE TO THE CENTRAL SPOT.

A second technique was used to measure the temperature difference between the centre and edge of the illuminated part of the sample at 334°C.

Two Spectrosil plates with a thin film of potassium nitrate between them were mounted in the steel holder and placed in the 'sample' thermostat. Using the 0 - 100% transmission scale and with the recorder chart in motion, the % transmission of the sample was measured at a fixed frequency (38.8 kcm^{-1}) while the block temperature was raised from 330° to 340°C at a steady rate of 1° every three minutes.

The % transmission showed practically no variation as the block temperature increased from 330 to 335.0°C. A change in transmission was recorded as the temperature passed through the range 335.0 to 336.4°C, the rate of change increasing with rising temperature, and above 336.4°C the transmission again became steady. The change between 335.0 and 336.4° corresponded to melting of the sample from its edges towards the centre; it occurred between the same limits when the heating rate was reduced to 1° every five minutes, which indicates that the system was in thermal equilibrium throughout both experiments.

The fact that the change in % transmission accelerated with rising temperature shows that the temperature gradient was steepest at the periphery of the sample, becoming shallower towards the centre. Assuming that the potassium nitrate had a sharp melting temperature, the centre and edge of the illuminated part of the sample must have differed in temperature by 1.4°C (i.e. 336.4 - 335.0). Interpolation between the results in Figure 11.5, part (i) gives a difference of 5.0°C at this block temperature;

however, these figures refer to the whole of the sample space rather than just the illuminated part. This confirms the earlier conclusion that the temperature gradient was steepest in the peripheral parts of the sample which were outside the beam cross-section.

In order to obtain some realistic values of the temperature differences in the illuminated part of the sample for block temperatures other than 334°C, the results in part (i) of Figure 11.5 were multiplied by the ratio 5.0/1.4. The values so obtained are tabulated in Section 11.7, and provided the basis for any corrections applied during the spectroscopic work. The significance of the gradients with respect to the spectroscopic results is discussed in Section 11.8.

The freezing-point of potassium nitrate was measured very carefully during the work on conductivity, and was found to be 334.5°C (see page 121). We can therefore derive the additional information that the centre of the sample was at 334.5°C when the block temperature was 336.4°, i.e. the block was 1.9° hotter than the centre of the sample.

11.4.2. Temperature differences between thermostat block and sample.

It was important to have a knowledge of the temperature difference between the block and the centre of the sample (at different block temperatures) in order to be able to calculate the sample temperature from the block temperature during the spectroscopic work. The direct measurement of the sample temperature during spectroscopy would have been extremely difficult.

The tip of a calibrated Pallador thermocouple was sandwiched between two Spectrosil plates, which were mounted in the steel holder and placed in the thermostat. The position of the tip of the couple was adjusted until it was at the centre of the rectangular cross-section of the light beam. The junction of a similar thermocouple was in a hole drilled in the copper block (see Figure 11.3). The E.M.F.s of the two couples were measured, at different block temperatures, and the temperature difference between the two points calculated.

The results are summarised in Table 11.5; ΔT is the temperature difference in ^{o}C, the block being hotter than the sample throughout.

TABLE 11.5. Temperature difference between block and centre of sample (ΔT).

Block temperature (^{o}C)	20	100	200	300	400	450
ΔT (^{o}C)	0.0	0.0	0.3	2.3	4.2	5.2

In the melting experiment described at the end of Section 11.4.1, ΔT was found to be $1.9^{o}C$ at a block temperature of $334^{o}C$. This is less than the value obtained by interpolation between the results in Table 11.5 (2.9^{o}). The lower figure is believed to be the more significant; the results in the table were measured with a 0.5 mm air gap between the Spectrosil plates, whereas in the melting experiment the conditions were exactly those which obtained

during spectroscopy (when the gap was of the order 0.05 mm, and was filled with salt).

In order to obtain a set of values of ΔT which correspond to the value 1.9° at $334^{\circ}C$, the figures in Table 11.5 have been multiplied by the ratio 2.9/1.9. The resulting temperature differences are listed in the Table in Section 11.7, and were used during the spectroscopic work to calculate sample temperatures from block temperatures when required. The circumstances under which it was necessary to apply this correction to the block temperatures are defined in Section 11.8.

11.5. Improvement of thermostat design.

The data in Sections 11.4.1 and 11.4.2 refer to the original design of the thermostat, which was used for the work on alkali-metal nitrates and on potassium nitrate - barium nitrate mixtures. When this work was finished, some modifications were made to the 'sample' thermostat with the aim of reducing the temperature gradients in the sample. The new design is shown in Figure 11.4, part (ii). One of the Spectrosil windows was moved to F from its original position at E, and a Nichrome heating wire was wound around the Sindanyo tube. Similar changes were made to the 'exit' tube from the thermostat. The aim was to heat the air between each pair of windows and so prevent heat losses from the centre of the sample.

The two auxiliary heaters had a combined resistance of 40 ohms, and were connected in series with the main block heaters. A variable resistance was connected in

parallel with the auxiliary heaters, so that the current through them could be varied relative to the main heater current; however, the best performance was obtained when the shunt resistance was infinite.

11.6. Measurement of thermal gradients in the improved thermostat unit.

The temperature gradients were again explored, using the chromel - alumel thermocouple described in Section 11.4.1. On this occasion the gradients were measured over that part of the sample which fell within the beam cross-section rather than over the whole area of the window in the steel holder. The two junctions were positioned between the Spectrosil plates, which were mounted into the steel holder and lowered into the thermostat. The tungsten lamp of the spectrophotometer was turned on, and the slits opened to their maximum width (2.0 mm). The frequency was set to a value in the visible range, and the light passing through the cell was focussed by a convex lens so that an image of the thermocouple junctions was formed on a white card placed near the exit port of the compartment. It was then possible to see the positions of the junctions relative to the light beam.

The gradients were measured at different block temperatures; the values obtained are shown in part (ii) of Figure 11.5.

At the end of Section 11.4.1 an experiment was described which enabled temperature gradients to be deduced from the changes in % transmission of a film of potassium nitrate as it was heated slowly from 330 to 340°C. The experiment

was repeated using the modified thermostat unit. Fusion of the nitrate film occurred as the block temperature passed through the range 333.5 to 334.3°C. Applying the reasoning used in Section 11.4.1, the difference in temperature between the centre and the edge of the illuminated part of the sample was 0.8°C (which is consistent with the trend shown in part (ii) of Figure 11.5), and the temperature difference between the block and the centre of the sample was 0.2°C (the sample being the hotter).

The temperature gradients and differences in the modified thermostat are about one-fifth of the corresponding values in the original unit, which demonstrates the inprovement brought about by the change in design.

For convenience of reference, the finally-adopted values of the temperature gradients in both forms of the apparatus are tabulated concisely in the next Section.

11.7. Summary of temperature gradients in the original and in the modified thermostat unit.

The symbols in Table 11.6 have the following meanings:

ΔT = (block temperature) - (temperature at centre of sample)

δT = (temperature at upper or lower edge of the illuminated part of the sample) - (temperature at centre of sample)

ΔT_{mean} = (block temperature) - (mean sample temperature).

By 'mean sample temperature' is meant the mean of the temperatures at the edge and at the centre of the illuminated part of the sample.

TABLE 11.6.

Original apparatus (used for the work on $NaNO_3$, KNO_3, $RbNO_3$, $CsNO_3$ and KNO_3 - $BaNO_3$ mixtures).

Block temp. (°C)	ΔT (°C)	δT (°C)	ΔT_{mean} (°C)
100	0.0	+0.3	-0.15
200	+0.2	+0.7	-0.15
300	+1.5	+1.2	+0.9
334	+1.9	+1.4	+1.2
400	+2.8	+1.8	+1.9

Modified apparatus (used for the work on NH_4NO_3, $AgNO_3$, $TlNO_3$, $NaNO_2$ and KNO_2).

Block temp. (°C)	ΔT (°C)	δT (°C)	ΔT_{mean} (°C)
100	(0.0)	0.0	0.0
200	(-0.1)	+0.2	-0.2
300	(-0.2)	+0.5	-0.45
334	-0.2	+0.8	-0.6

Figures given in brackets were estimated by interpolation.

11.8. Influence of temperature gradients on the accuracy of the spectroscopic measurements on salt films.

The gradients in the sample and the temperature difference between the block and the sample must be considered separately.

11.8.1. Temperature gradients in the sample.

The data tabulated in the previous Section show that the centre and edge of the illuminated part of the sample differed in temperature by not more than $2^{o}C$ at block temperatures up to $400^{o}C$.

For a salt film consisting of a single crystalline phase, or for a molten film, this temperature gradient is entirely insignificant. In temperature ranges which did not include transitions or melting-points, E(2) decreased with rising temperature by about 2 to 3 cm^{-1} per ^{o}C for all the salts examined. If two parts of a homogeneous sample differed in temperature by $2^{o}C$, E(2) for the two regions would differ by about 5 cm^{-1} and the measured value E(2) would correspond to the average temperature over the area of the sample. The uncertainty in E(2) from this source is negligible compared with the scatter of ~ 50 cm^{-1} arising from fluctuations in the setting of the frequency calibration (see page 156).

E(2) changed abruptly in the region of transition-points and melting-points. If a sample was part liquid and part solid, the values of E(2) for the two zones might differ

by up to 400 cm^{-1}; a scan carried out on such a sample would give an absorption band which was much broader than that of an all-solid or an all-liquid sample and which had a maximum intermediate between the two. If spectra were drawn at 1° intervals in the region of a melting-point or transition-point the presence of the gradients would cause the change in E(2) to be spread over a small range of block temperatures.

In spite of this difficulty, the value of the abrupt change in E(2) at a melting-point, $\Delta E(2)$, was easily found. E(2) was measured for the solid and for the liquid at temperatures extending over a range of $50^{o}C$ on either side of the melting-point, but no measurements were made within 2° of this point. E(2) was plotted against temperature, when the values for solid and liquid fell on two straight lines. These were extrapolated to the melting-point, and $\Delta E(2)$ were read from the scale. This very small extrapolation involved practically no loss of accuracy. Similar considerations apply at the polymorphic transition points.

The temperature gradients in the sample must be taken into consideration when solid-state transitions are being studied by observing changes in % transmission at constant frequency (as described in Section 11.13). The way in which corrections were applied is described in Chapter 15 (Section 15.1).

11.8.2. Temperature differences between block and sample.

Mean sample temperatures could be calculated from the measured block temperatures by subtracting the increment ΔT_{mean}. As Table 11.6 shows, this correction term would be less than 2°C for block temperatures up to 400°C. Since dE(2)/dT was of the order 2 - 3 cm^{-1} per °C, a correction of 2° to the temperature is equivalent to a correction of 5 cm^{-1} to E(2), which is only one-tenth of the scatter due to short-term calibration changes. The advantage to be gained by applying this correction is clearly negligible. Throughout Chapter 14, where the results of this work are presented, E(2) has therefore been plotted directly against the temperature of the thermostat block. Over a small temperature range near a melting-point or transition-point, the correction would be virtually constant, so would not in any case affect the accuracy with which $\Delta E(2)$ could be measured. The correction to the block temperature has been applied in the case of the accurate values of E(2) for alkali nitrate melts (page 238), for which the error due to calibration changes was less than the general value. Even here, the correction has only marginal significance; it was 2°C for caesium nitrate and 1°C for sodium, potassium and rubidium nitrates.

When transitions were studied by the 'constant frequency' technique (Section 11.13 and Chapter 15), the values of ΔT and δT in Table 11.6 were used to calculate absolute transition temperatures (or transition ranges) from the measured block temperatures. Details are given in Chapter 15.

11.9. Calibration of the Pallador thermocouples used in the sample and reference thermostats.

These two couples and the couple used during the conductivity and density measurements were enclosed in identical protective sheaths of Pyrex and immersed side by side in the melt-bath, with their tips six inches below the surface. The bath was heated to 520°C, and the couples were annealed at this temperature for twelve hours.

The bath was thermostatted at various temperatures between 520° and 140°C, and the E.M.F.s of the three couples were measured at each temperature. The couples were transferred to an oil-filled thermostat, and measurements were continued from 140° to 20°C. Finally, the couples were compared at the ice-point.

Between 520°C and 0°C, the E.M.F.s did not differ by more than 0.035 mv. at any one temperature.

The thermocouple which had been used in the conductivity and density determinations was then re-calibrated at the steam-point, the naphthalene-point and the sulphur-point. The temperatures and E.M.F.s at the standard points are given in Table 11.7.

TABLE 11.7. E.M.F. of calibrated thermocouple at the Fixed Points.

Temperature (°C)	E.M.F. (mv)
0.00	0.006
100.2_1	4.580
218.0_6	10.838
444.5_6	24.448

Using the differences obtained in the comparison experiment the E.M.F.s of the other two couples were calculated at these temperatures. The results are shown in Table 11.8.

TABLE 11.8. E.M.F.s of 'sample' and 'reference' thermocouples.

Temperature (^{o}C)	E.M.F. of sample couple (mv)	E.M.F. of reference couple (mv)
0.00	0.004	0.005
100.2_1	4.609	4.601
218.0_6	10.849	10.840
444.5_6	24.456	24.423

Equations of the type

$$E - E_o = At + Bt^2 + Ct^3 \qquad - - - (11.1)$$

were fitted to these two sets of E.M.F.-values, where E is the E.M.F. in millivolts at temperature t^{o}C. The values of the constants so obtained are tabulated below.

TABLE 11.9. Calibration parameters for 'sample' and 'reference' thermocouples.

	Sample couple	Reference couple
E_o	0.004	0.005
A	4.2171×10^{-2}	4.2021×10^{-2}
B	4.0278×10^{-5}	4.1053×10^{-5}
C	-2.569×10^{-8}	-2.708×10^{-8}

These constants and equation (11.1) were used to calculate values of E for each couple, at 5° intervals, over the range 0° to 500°C. Graphs of temperature against E.M.F. were plotted, each page covering 20°C. These graphs were used throughout the experimental work to derive temperatures from the measured E.M.F.s.

Standard procedures were used for the calibration of the first thermocouple at the steam-, naphthalene- and sulphur-points; the experiments are described in detail in Appendix A (page 375).

11.10 Preparation of salt samples for spectroscopy.

Two Spectrosil plates (25 x 13 x 1 mm) were cleaned with hot aqueous potassium hydroxide solution, then with hot nitric acid. They were washed with distilled water and dried.

The plates were laid on a small electric hotplate and heated to a temperature just above the melting-point of the salt to be examined. A few crystals of the salt were sprinkled on one plate, and when they had melted the second plate was placed on top. A little manipulation was usually necessary to remove gas bubbles from the molten film. In this way, samples of thickness 4 - 20 microns were obtained. Thicker films (up to 150 microns) were prepared by using spacers of platinum - iridium foil between the plates.

The sample was frozen and cooled, and excess salt scraped from the edges of the plates. When the spectroscopic examination was finished, the extruded salt was wiped away with moist paper tissues, and the plates and salt weighed. The plates were then re-separated on the hotplate, cooled, washed, dried and reweighed. The mass of salt in the film

was found by difference, and its thickness calculated by dividing the mass by the product of the density and the area of the plates.

This thickness determination was carried out after rather than before the spectroscopic examination because salt was usually extruded from between the plates when the sample was melted in the spectrophotometer.

11.11. Procedure for obtaining absorption spectra of salt films.

The spectrophotometer was switched on and allowed to warm up for at least thirty minutes. The hydrogen lamp was turned on about five minutes before scanning was begun.

The sample thermostat temperature was set to the required value, and the reference thermostat brought to within $5^{\circ}C$ of the same temperature.

The salt sample, between Spectrosil plates, was mounted in the stainless steel holder and placed in the sample thermostat. Two clean Spectrosil plates were mounted in a similar holder and placed in the reference thermostat. It was found to be necessary to separate these plates slightly, by means of a piece of platinum wire; this prevented the occurrence of interference phenomena between the adjacent surfaces.

The hydrogen lamp was used as light source, the prism as monochromator and the photocell as detector, and the recorder was set to display transmission on the 0 - 100% scale.

The frequency was set to a value at which the sample was known to have no absorption (26,000 cm^{-1} for the nitrates,

20,000 cm^{-1} for the nitrites). The 100% control was set so that the recorder pen was at the 100% mark of the chart scale. The lid of the sample compartment was opened, when the shutter cut off the light in the sample beam (see page 153). The 0% control was then adjusted until the pen moved to the 0% mark of the chart scale. Since the 0% control influenced the position of the pen over the whole of its range of movement, it was usually necessary to make a second adjustment to the 100% control. Setting the pen to the chart scale in this way was tantamount to assuming that the proportion of the sample beam lost by scattering was the same at all frequencies.

The reverse gear of the cam drive was engaged, and the cam wound back to a position corresponding to the upper limit of the frequency range to be covered. Forward gear was engaged, suitable scanning-speed, resolution, signal damping and chart speed selected and the scan begun. The sample block temperature was measured while the scan was being made.

At the end of the scan, the thermostat temperatures were set to new values. The 0% and 100% controls were readjusted in the way described above and, after a wait of ten minutes to allow the sample to reach thermal equilibrium, another scan was made. This procedure was continued until the desired temperature range had been covered.

Scans were made at intervals of $2^{\circ}C$ in the vicinity of transition-points and melting-points; otherwise, the intervals were 15 - 20°. The examination of a substance was usually begun at room temperature, and the temperature gradually raised through the melting-point. About six scans were made just above the melting-point, and the sample re-frozen. Several more scans were made just below the freezing-point and at temperatures descending to room temperature, to confirm the reversibility of the changes observed on heating.

Finally, the sample was re-melted, and scans carried out at temperatures increasing by intervals of 10°C until accurate plotting of spectra was rendered impossible by the evolution of gas bubbles in the melt. These bubbles were islands of low absorption, and their growth and movement to the edge of the melt film caused irregularities in the trace recorded on the chart.

The reduction of the sample beam intensity by scattering and reflection from solid films varied over a wide range according to the thickness and state of fragmentation of the sample. If a thin film of melt was cooled just below its freezing-point in the thermostat unit, the loss by scattering from the solid so formed was as little as 5%; for thicker samples, it was 10 - 15%. Losses remained at these levels if the sample was cooled, but increased abruptly if the solid underwent a transition to a new crystalline modification. The greatest losses by scattering occurred during the study of ammonium nitrate; this substance undergoes three transitions when cooled from its freezing-point to room temperature, and losses were up to 86%. It was necessary to use the 0 - 10% transmission scale (see page 152) to record the maximum of the small peak with sufficient accuracy.

Some details of the experimental procedure for the different substances are outlined in the following paragraphs.

II.11.1. The crystalline nitrates.

For practical reasons, the weak band at ~ 33 kcm^{-1} and the strong band at 40 - 50 kcm^{-1} were studied separately.

The weak band at ~ 33 kcm^{-1}.

For the frequency region 40,000 to 26,000 cm^{-1}, film

thicknesses were used which gave 50 - 80% absorption at the maximum of the weak band. Measurements made on different samples showed that the position of the maximum did not depend on the thickness of the film at a given temperature. This is shown by the results for sodium nitrate (see Appendix C, page 387), which were obtained with five samples of thickness 21μ, 28μ, 40μ, 49μ, and 57μ. For this reason, no precautions were taken to prevent the thickness of the sample from changing on fusion.

The frequency of maximum absorption for the small peak, E(2), was found from the recorded spectra in the following way. Chords were drawn across the top of the peak, parallel to the frequency axis. The midpoints of these chords lay on a straight line, which was extrapolated to cut the absorption curve. The frequency corresponding to the point of intersection was read from the scale (see Figure 11.6). This measuring process could be carried out with a reproducibility of $\pm$ 10 cm^{-1}. The scatter in the experimental results is of the order $\pm$ 50 cm^{-1}, and is probably due mainly to changes in the frequency calibration of the spectrophotometer. The causes of these changes are discussed on page 155.

In the spectra of silver and thallous nitrates near their melting-points, and also in the spectra of the nitric acid solutions, the edge of the strong band overlapped with the weak band to such an extent that it became impossible to measure E(2) accurately. In these cases the band was characterised by the parameter E'(2), which is defined as the frequency on the low-energy side of the weak band for which the extinction coefficient is a constant (arbitrary) fraction of that at the band maximum. The transmission I/I_o corresponding to E'(2) is given by

$$\log (I/I_o) = k. \log (I/I_o)_{max.} ,$$

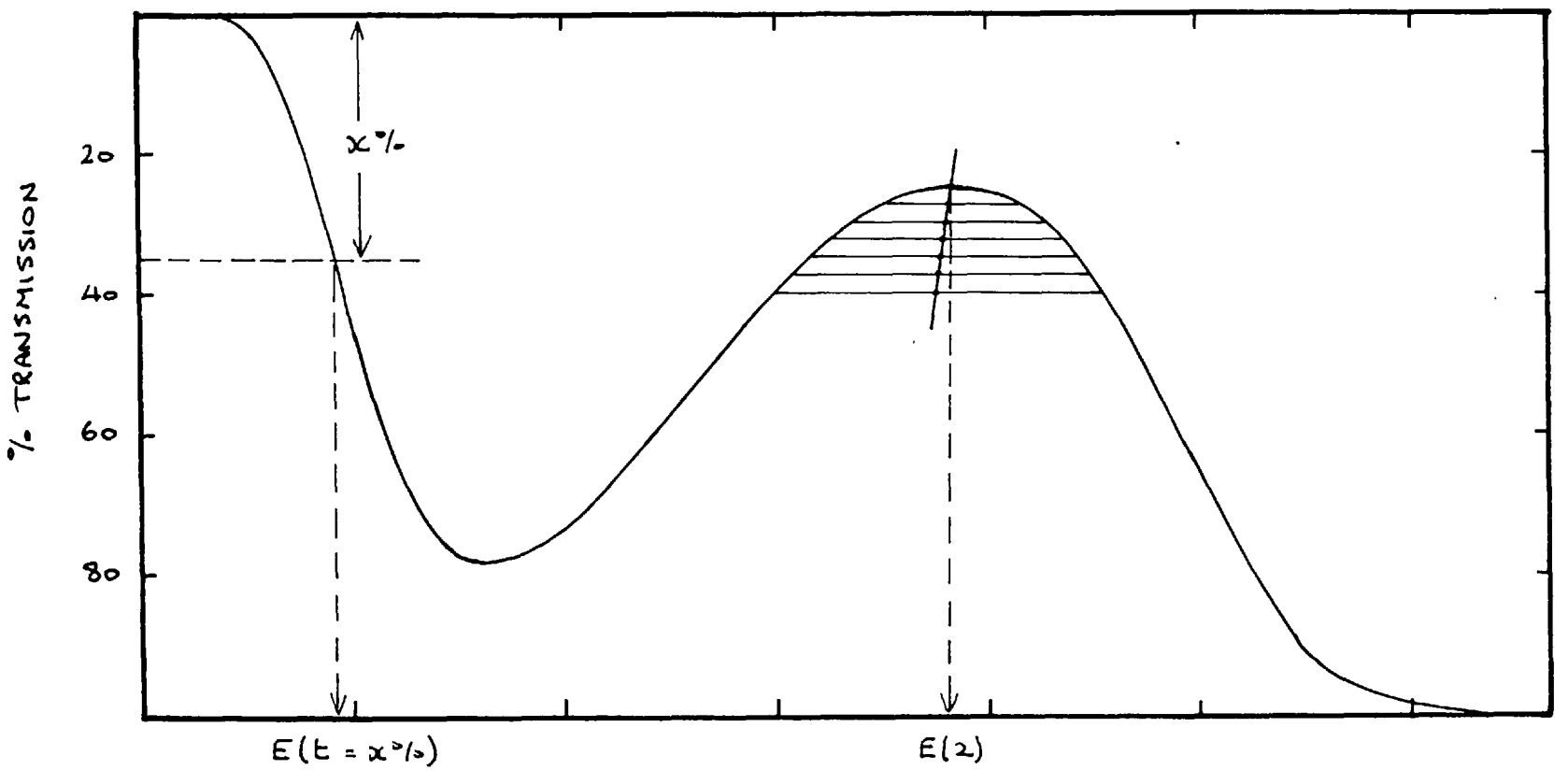


FIGURE 11.6. DIAGRAM SHOWING METHOD OF MEASUREMENT OF E(2) AND E(t = x%)
(THE SPECTRUM ILLUSTRATED IS THAT OF SODIUM NITRATE AT 15°C)

where k is a constant (usually taken as 0.3 or 0.5) and $(I/I_o)_{max}$ is the transmission at the maximum.

Variations in the extent of overlap between the strong and weak bands have a smaller effect on E'(2) than they do on E(2). The changes in E'(2) with rising temperature therefore provide a more reliable indication of the true movements of the weak band than do the corresponding changes in E(2).

The strong band at 40 - 50 kcm^{-1}.

In the range 54 - 35 kcm^{-1}, the thinnest obtainable samples ($\sim 4\mu$) were used in order to obtain maximum transmission. Even with these samples, 100% absorption was recorded for all the nitrates from 50 to about 40 kcm^{-1}. Some transmission was recorded in the range 54 to 50 kcm^{-1}, but a later set of experiments (see page 194) showed that this was entirely spurious for potassium and caesium nitrates. It was probably spurious for all the other materials studied.

It was therefore not possible to measure the frequency of the maximum of the strong band (which occurs at 50 kcm^{-1}, with a molar extinction coefficient of 10,000 litres/mole. cm.; see page 67). Measurements on the low-energy edge of this band could be made at frequencies up to $\sim$40 kcm^{-1} and for extinction coefficients up to $\sim$300 litres/mole. cm. The movements of this low-energy edge could not be taken as an indication of the corresponding movements of the band maximum, but it was considered desirable to record them because of the influence they might have on the position of the maximum of the weak band. In particular, an abrupt shift of the strong-band edge to lower frequency would increase the extent of overlap between the two bands, and this would tend to displace the maximum of the weak band to higher frequency. It was therefore necessary to show that the observed changes in E(2) reflected the real movements of the weak band, and that

they were not due merely to changes in the extent of overlap.

For the alkali nitrates overlap was slight, and the strong-band edge moved to higher frequency at the melting-point (except for rubidium nitrate, for which no abrupt shift was recorded). This shift to higher frequency would tend to cause E(2) to decrease on fusion; since E(2) in fact increased on melting, there is no possibility that this change was caused by the movement of the strong-band edge.

For silver and thallous nitrates, overlap between the two bands was more marked, and the changes in E(2) were influenced strongly by the movements of the strong-band edge. The way in which the true movements of the weak band were deduced from the experimental observations on these salts is described in detail on pages 269 and 277.

The position of the steep edge of the strong band at about 40,000 cm^{-1} depended on sample thickness, as would be expected from Beer's law. In order to establish the direction in which this edge was displaced when the salts melted, it was necessary to obtain spectra of solid and liquid films containing the same mass of salt per unit area. This was done in the following way.

The frequency was set manually to a value on the steep edge so that the % transmission was 30 to 50%. The salt was heated through its melting-point, when the % transmission changed abruptly. The salt was held two degrees above its melting-point for a few minutes, during which time the transmission usually increased slightly as salt was extruded from between the plates. When a steady condition was reached, the salt was cooled to a few degrees below its freezing-point, and then re-melted. The % transmission of the melt was noted. The freezing and re-melting process was continued

until the transmission of the melt reached a constant value, within a tolerance of 1%.

Three scans were then carried out on the melt, with the temperature not more than 5° above the melting-point. The sample was frozen, and three scans made on the solid just below the freezing-point. Two more scans were made on the liquid, as a check, and finally the salt was frozen and scans carried out at intervals of $10 - 20^{\circ}$ down to room temperature. For each scan, the 100% control was adjusted so that 100% transmission was recorded at 25,000 cm^{-1}.

The absorption edge was characterised by measuring the frequency corresponding to a given % transmission, E(t = x%). Values of x were chosen arbitrarily; x = 4% was convenient for silver and thallous nitrates (where overlap with the weak band was marked), and x = 10%, 30% and 50% were suitable values for the alkali nitrates.

It is certain that the mass of salt per unit area of sample remained constant during the examination of a solid sample, but it is problematic whether the corresponding liquid film had the same mass per unit area or the same thickness as the solid. The actual behaviour probably lies between these limits, and both possibilities have been considered in discussing the results.

Since it is desirable to compare the frequencies at which solid and liquid films have the same extinction coefficient, E(t = x%) for the liquid may be compared directly with the same parameter for the solid if the mass per unit area remains constant on fusion, but if the thickness remains constant an allowance must be made for the density difference between solid and liquid. The way in which this correction was applied is described on page 242.

11.11.2. Nitric acid and its hydrates.

Spectra were obtained in the range 40,000 - 25,000 cm^{-1}. The pure acid and the hydrates $HNO_3.H_2O$ and $HNO_3.3H_2O$ were examined between Spectrosil plates, in the same way as the fused salts. In order to obtain the spectra of the solid hydrates, the sample cell was cooled to -70°C, by pouring liquid nitrogen into it. A fast scanning-speed was used, because the cell warmed up at a rate of about 3° per minute.

At the low temperatures some frost formed on the windows of the thermostat unit, and caused scattering of the sample beam. When scattering losses were particularly high, the spectra were scanned with instrument set to record 0 - 10% transmission on the full chart scale (see page 152). This improved the accuracy with which the frequency of the maximum of the weak band could be measured.

The absorption spectrum of the 0.24N aqueous solution of nitric acid was obtained with the solution in a silica cell of path-length 1 mm. A similar cell filled with distilled water was placed in the reference compartment.

11.11.3. Iso-propyl nitrate.

Attempts were made to obtain a spectrum of a thin film of the pure liquid, supported between two Spectrosil plates. A spectrum was obtained, but the thickness of the film probably changed significantly during the time of the scan because liquid was lost by evaporation. For this reason, a dilute solution of the substance was prepared, in cyclo-hexane (Hopkin & Williams, Ltd., "Spectrosil" quality). The solution contained 1.89 grm. iso-propyl nitrate per 100 ml. Its spectrum was obtained using a silica cell of 1 mm. path-length; a similar cell, filled with pure cyclo-hexane, was

placed in the reference compartment.

II.11.4. Sodium and potassium nitrites.

These were examined in the frequency range 40,000 - 20,000 cm^{-1}, using the technique already described for the nitrates. Sample thicknesses were chosen to give 70 - 90% absorption at the maximum of the band at $\sim$27,000 cm^{-1}. The frequency at the maximum was found by drawing a line through the midpoints of chords drawn across the top of the peak (see page 189).

II.12. Measurement of the true transmission in the range 54,000 - 50,000 cm^{-1}.

For all the nitrates studied, no light was transmitted between 40,000 and 50,000 cm^{-1}, but up to 40% transmission was recorded at 54,000 cm^{-1}. In the early studies this transmission was taken at its face value, and was believed to represent the high-energy edge of the strong band (which has a maximum at $\sim$50,000 cm^{-1} in aqueous solution (Ref.9)).

Suspicion was aroused when this 'high-energy edge' showed little or no variation with temperature, and when the edge appeared in the same position for nitrites and even for bromides and iodides.

Spurious transmission could be recorded in this region in the following way. When light from the hydrogen lamp passed through the monochromator, the emergent beam always contained some white light reflected directly from the front surface of the prism (see page 150 for a diagram of the optical system). The intensity of this white light was proportional to the width of the slits in front of the lamp. When the operating

frequency was changed from 50,000 to 54,000 cm^{-1}, the slit servo-motor opened the slits in order to maintain the reference beam energy at the standard level. This opening of the slits was necessary because losses occur in this frequency range through absorption by atmospheric oxygen.

Because of this increase in slit-width, the proportion of white light in the sample and reference beams increased sharply when the frequency was changed from 50,000 to 54,000 cm^{-1}. Since the nitrates and nitrites transmit some light at frequencies below 40,000 cm^{-1}, some of this white light would reach the detector when a spectrum of one of these salts was recorded, even if the sample absorbed all the light in the range 50,000 - 54,000 cm^{-1}.

Some experiments were performed to confirm this interpretation.

(i) A piece of aluminium foil was placed in the sample thermostat, between two Spectrosil plates. A spectrum was run, beginning at 54,000 cm^{-1}. No transmission was recorded at any frequency. This showed that the effect was not caused by scattering of light round the sample and into the detector unit.

(ii) A sample of potassium nitrate was made up, and its spectrum recorded from 53,500 cm^{-1} to 48,000 cm^{-1}, using resolution control 3. The transmission at 53,500 was 17%, and the corresponding slit-width was 1.75 mm. The spectrum of the same sample was recorded using resolution control 5 (which corresponded to a lower reference beam energy). The slit-width at 53,500 was 0.64 mm., and the transmission was 23%.

This showed that the transmission recorded in this region depended on the slit-width.

In order to reduce losses by atmospheric absorption, the entire optical path of the spectrophotometer was flushed with oxygen-free nitrogen. Since this increased the available energy from the lamp in the range 54,000 - 50,000 cm^{-1}, the slit-width was correspondingly reduced by the servo-motor; in one experiment, the slit-width was reduced from 1.8 mm. to 0.42 mm. at 54,400 cm^{-1}, using a nitrogen flow-rate of one cubic foot per minute. The spectrum of a sample of potassium nitrate was drawn under these conditions; the transmission recorded at 54,000 cm^{-1} was only 8%.

Some experiments were carried out to measure the true transmission of samples of potassium and caesium nitrates in this difficult region.

Extensions were built onto the sample and reference thermostat units to allow silica cells to be placed in the paths of the two beams, in addition to the salt sample.

A pair of silica cells of 1 mm. path-length were cleaned with chromic acid and washed. They were filled with distilled water, and positioned in the sample and reference compartments. Two clean Spectrosil plates were placed in each thermostat, mounted in stainless steel holders. The 100% transmission line was scanned, and adjustments made until a straight line was obtained (see page 153).

The optical path of the spectrophotometer was flushed with nitrogen until the slit-width at 54,400 cm^{-1} reached a steady value (0.70 mm in the experiment on potassium nitrate, 0.64 mm for the caesium nitrate). The Spectrosil plates in the sample compartment were replaced by the salt sample, and a scan was carried out using resolution control 5 (corresponding to the lowest reference beam intensity).

The water in the 1 mm cell in the sample compartment was

then replaced by 1% potassium bromide solution. A second scan was carried out, with the salt sample still in position.

Finally, the salt sample was removed and replaced by two clean Spectrosil plates. A third scan was carried out, to obtain the absorption spectrum of the potassium bromide solution.

The spectra recorded in these three scans are illustrated in parts (i), (ii) and (iii) of Figure 11.7, (which refers to a potassium nitrate sample).

It has been shown that the extinction coefficient of an aqueous bromide solution is greater than 3,500 litres/mole.cm. at frequencies between 48 and 55 kcm^{-1} (Ref.10). Application of Beer's law shows that the % transmission of a 1 mm cell containing a 1% solution of potassium bromide is less than 0.01% if the extinction coefficient is greater than 400 litres /mole.cm. It follows that, in the present experiment, the cell containing the bromide solution absorbs virtually all the light whose frequency lies in the range 48 - 55 kcm^{-1}; the transmission recorded in this region must be due entirely to stray light of lower frequency.

It can be seen from scans (i) and (iii) that all the light absorbed by the bromide solution below 50 kcm^{-1} would be absorbed by the nitrate film. The true transmission of the nitrate film is therefore equal to the <u>difference</u> between the transmissions recorded in spectra (i) and (ii). The true spectrum is illustrated in part (iv) of the figure (see Ref.11).

These experiments were carried out on potassium nitrate and on caesium nitrate, at 20°C. In both cases, the true transmission was $0 \pm 0.2\%$ between 40,000 and 54,000 cm^{-1}. Since the uncorrected spectra of all the nitrates and

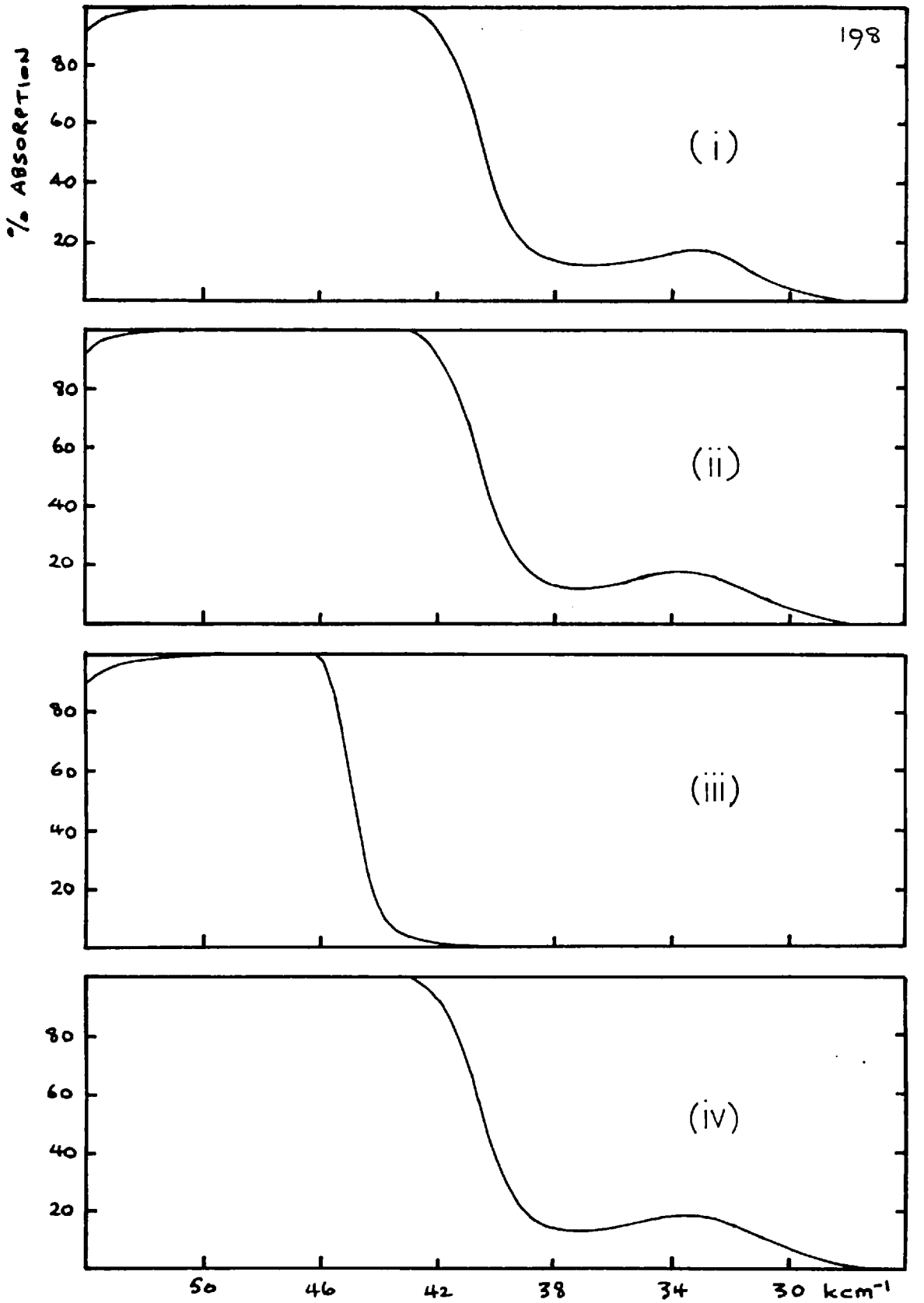


FIGURE 11.7. STAGES IN THE MEASUREMENT OF THE TRUE ABSORPTION SPECTRUM OF POTASSIUM NITRATE.

nitrites studied were practically identical from 54,000 to 50,000 cm^{-1}, it is unlikely that any of these salts had any true transmission in this range.

11.13. Spectroscopic observations at constant frequency.

Information about crystal transitions could be obtained by recording the % absorption of a sample at a constant frequency.

A salt sample was placed in the thermostat unit at room temperature. The instrument was set to record % transmission at a frequency on the steeply rising edge of the strong band ($\sim$ 40,000 cm^{-1}), and the recorder chart was set in motion. The sample was heated at a rate of $\sim 20^{o}C$ per minute, until it melted.

In temperature ranges in which a single phase was present in the sample, the % transmission decreased linearly with increasing temperature (corresponding to the movement of the edge of the strong band to lower frequencies). When a phase-change took place, the % transmission altered abruptly. The temperatures at which these abrupt changes were observed were upper limiting values for the transition temperatures.

If the sample was then cooled back to room temperature the changes were observed in reverse, at slightly lower temperatures. In this way, the transition temperatures could be 'bracketed'. If the heating and cooling cycle was repeated in the region of each transition with a smaller rate of temperature change (about 1° per minute), the size of the 'bracket' could be reduced to about $1^{o}C$, or less in some favourable cases. At block temperatures above $200^{o}C$, the accuracy with which transition temperatures could be determined was limited by the existence of temperature gradients in the sample. The corrections required are discussed on page 299.

The method described above was a very convenient one for the detection of crystal transitions, and was applied to all the salts listed in Table II.1, from 15°C to the melting-points. This was done as a preliminary to the measurement of spectra, so that the abrupt changes in E(2) which occurred at the transition-points could be determined accurately.

REFERENCES TO CHAPTER II.

1. International Critical Tables, 4, 7.

2. P.I. Protsenko and A.Ya. Malakhova, Zhur. Neorg. Khim., (1957) 2, 2145.

3. International Critical Tables, 4, 217.

4. "Handbook of Chemistry and Physics", Rubber Publishing Co., (1953 edition), p. 2519.

5. G.P. Smith and C.R. Boston, J. Chem. Phys., (1961) 34, 1396.

6. "Handbook of Chemistry and Physics", Rubber Publishing Co., (1953 edition), p.2507.

7. International Critical Tables, 5, 299.

8. E. Rhodes and A.R. Ubbelohde, Proc.Roy.Soc.,(1959), A251, 156.

9. D. Meyerstein and A. Treinin, Trans. Farad. Soc., (1961), 57, 2104.

10. E. Rabinowitch, Revs. Mod. Phys., (1942), 14, 112.

11. H.L. Friedman, J. Chem. Phys., (1953), 21, 319.

RESULTS

CHAPTER 12.

RESULTS: ELECTRICAL CONDUCTIVITIES OF FUSED POTASSIUM NITRATE - BARIUM NITRATE MIXTURES.

12.1. Tabulation of results.

Table 12.1. shows the specific and equivalent conductivities of pure potassium nitrate melt (run 9) and of mixtures containing 5.0, 10.0 and 22.1 equivalent % barium nitrate (runs 10 to 12 respectively). The results are listed in order of increasing temperature; the serial number in the first column of each table indicates the order in which the measurements were made.

The parameter actually measured during the experimental work was the conductivity of the cell (K). The specific conductivity of the melt (σ) was derived by multiplying K by the appropriate value of the cell constant c (as tabulated on page 118). The equivalent conductivity (Λ) was then calculated from σ, using the relationship

$$\Lambda = \sigma . V_e, \qquad (12.1)$$

where V_e is the equivalent volume of the mixture at the temperature of the conductivity measurement. The values of V_e used here were derived from the author's density measurements on potassium nitrate - barium nitrate melts, which are presented in Chapter 13.

TABLE 12.1.

Run 9 (pure potassium nitrate)

Serial number	Temp. (°C)	Cell condy. (mmho)	Specific condy. ($ohm^{-1}cm^{-1}$)	Equiv. vol. (ml)	Equiv. condy. ($ohm^{-1}cm^{2}$)
1	337.2	1.702	0.6270	54.025	33.873
11	337.2	1.701	0.6266	54.025	33.852
2	339.9	1.729	0.6369	54.086	34.447
10	339.9	1.733	0.6384	54.086	34.528
9	346.5	1.794	0.6609	54.237	35.845
8	358.4	1.898	0.6992	54.507	38.111
7	374.2	2.034	0.7493	54.867	41.111
6	388.6	2.158	0.7950	55.195	43.880
5	402.5	2.277	0.8386	55.511	46.551
4	418.2	2.406	0.8861	55.868	49.504
3	434.2	2.543	0.9365	56.233	52.662

Run 10 (potassium nitrate + 5.00 equiv. % barium nitrate)

Serial number	Temp. (°C)	Cell condy. (mmho)	Specific condy. ($ohm^{-1}cm^{-1}$)	Equiv. vol. (ml)	Equiv. condy. ($ohm^{-1}cm^{2}$)
10	332.0	1.612	0.5938	53.310	31.655
9	337.2	1.658	0.6108	53.426	32.632
8	339.9	1.681	0.6192	53.486	33.118
7	346.5	1.738	0.6402	53.634	34.336
6	358.4	1.842	0.6785	53.899	36.570
5	374.2	1.978	0.7286	54.252	39.528
4	388.6	2.100	0.7736	54.573	42.217
3	402.5	2.217	0.8165	54.884	44.812
2	418.2	2.353	0.8666	55.234	47.865
1	434.2	2.489	0.9166	55.591	50.954

TABLE 12.1 . (continued)

Run 11 (potassium nitrate + 10.01 equiv. % barium nitrate)

Serial number	Temp (°C)	Cell condy. (mmho)	Specific condy. ($ohm^{-1}cm^{-1}$)	Equiv. vol. (ml)	Equiv. condy. ($ohm^{-1}cm^{2}$)
11	324.0	1.479	0.5448	52.546	28.627
10	332.0	1.547	0.5699	52.720	30.045
9	337.2	1.592	0.5864	52.833	30.981
8	339.9	1.613	0.5942	52.892	31.428
7	346.5	1.671	0.6155	53.035	32.643
6	358.4	1.771	0.6524	53.293	34.768
5	374.2	1.906	0.7021	53.636	37.657
4	388.6	2.027	0.7467	53.949	40.283
3	402.5	2.145	0.7900	54.250	42.857
2	418.2	2.282	0.8404	54.588	45.875
1	434.2	2.422	0.8920	54.939	49.005

TABLE 12.1. (continued)

Run 12 (potassium nitrate + 22.10 equiv. % barium nitrate)

Serial number	Temp. (°C)	Cell condy. (mmho)	Specific condy. ($ohm^{-1}cm^{-1}$)	Equiv. vol. (ml)	Equiv. condy. ($ohm^{-1}cm^{2}$)
14	293.0	1.090	0.4015	50.505	20.277
13	300.0	1.144	0.4214	50.646	21.342
12	308.0	1.209	0.4453	50.807	22.624
11	316.0	1.273	0.4689	50.969	23.899
10	324.0	1.339	0.4932	51.131	25.217
9	332.0	1.402	0.5164	51.295	26.488
8	339.9	1.467	0.5404	51.452	27.804
7	346.5	1.520	0.5599	51.585	28.882
6	358.4	1.617	0.5957	51.826	30.872
5	374.2	1.747	0.6435	52.145	33.555
4	388.6	1.864	0.6866	52.436	36.002
3	402.5	1.977	0.7283	52.717	38.393
2	418.2	(2.102)	-	-	-
1	434.2	(2.237)	-	-	-

The results given in brackets are subject to some uncertainty, because of gas evolution in the conductivity cell.

σ and Λ for ionic melts are normally expressed as functions of temperature by the equations

$$\sigma_x = (\sigma_o)_x . \exp\left\{-(E_\sigma)_x/RT\right\} \qquad (12.2)$$

and

$$\Lambda_x = (\Lambda_o)_x . \exp\left\{-(E_\Lambda)_x/RT\right\} , \qquad (12.3)$$

where σ_x and Λ_x are the specific and equivalent conductivities of a mixture containing an equivalent fraction x of barium nitrate. $(\sigma_o)_x$, $(\Lambda_o)_x$, $(E_\sigma)_x$ and $(E_\Lambda)_x$ are parameters characteristic of each mixture.

Figure 12.1 shows plots of $\log_{10}(\sigma_x)$ against 1/T (°K), for pure potassium nitrate melt and for the three mixtures. Figure 12.2 shows corresponding plots of $\log_{10}(\Lambda_x)$ against 1/T. In both sets of graphs the lines of best fit through the experimental points are curves rather than straight lines; in all cases the plots become steeper as the temperature is lowered. In order to allow a comparison of the slopes of the lines to be made for the different mixtures, straight lines have been fitted to the upper and lower parts of each curve, by the method of least squares. Values of $(\sigma_o)_x$, $(E_\sigma)_x$, $(\Lambda_o)_x$ and $(E_\Lambda)_x$ have been derived, and are listed in Table 12.2.

12.2. Accuracy of the conductivity results.

The manufacturers of the bridge claim that it is capable of measuring conductivities to $\pm 0.2\%$. The determination of the cell constant involved a conductivity measurement, so the accumulated uncertainty in the specific conductivities of the melts is 0.4%. However, any error in the cell constant would affect the conductivities of the melts systematically,

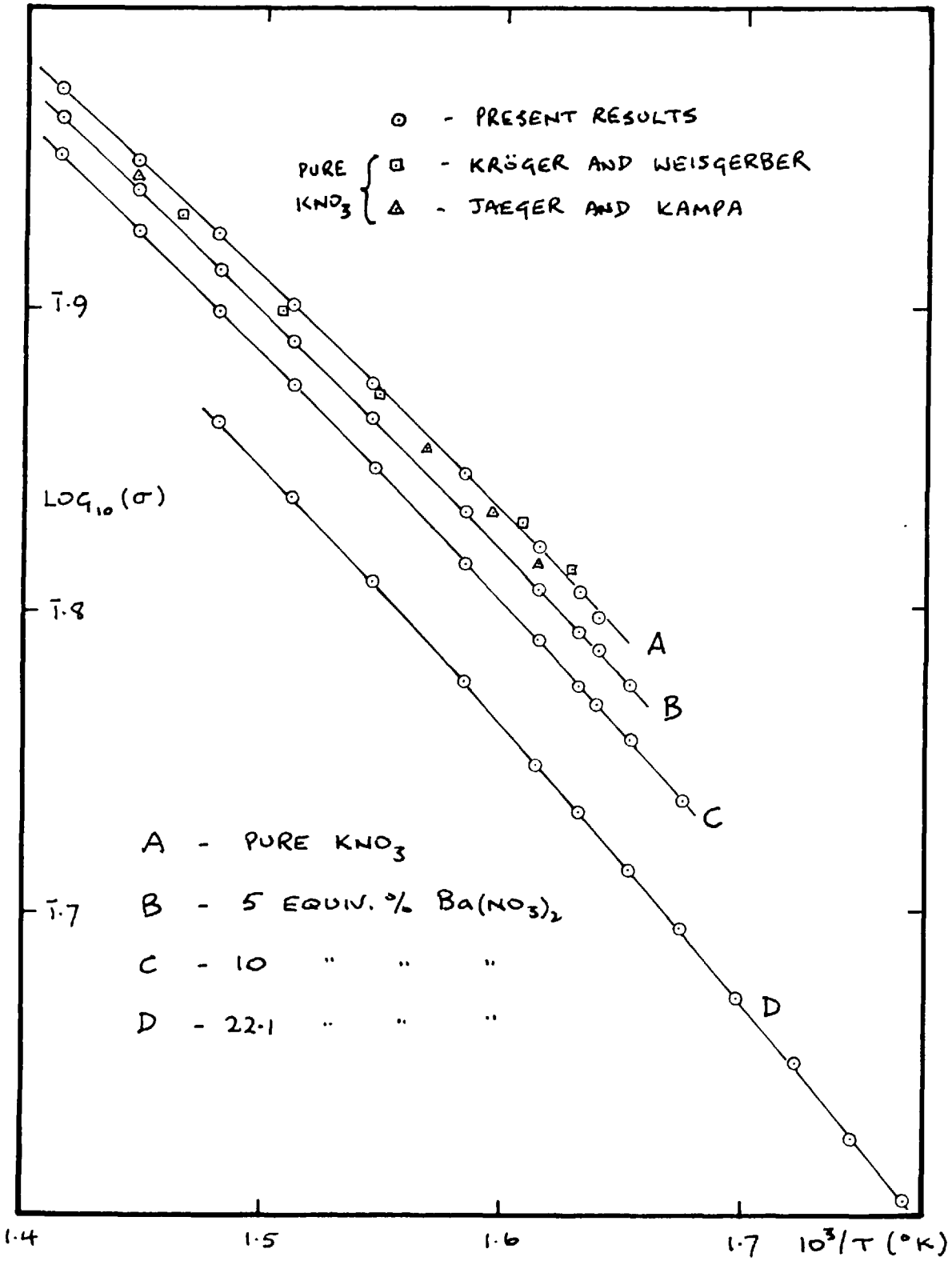


FIGURE 12.1. PLOTS OF LOG_{10}(SPECIFIC CONDUCTIVITY) AGAINST 1/T (°K) FOR KNO_3 - $Ba(NO_3)_2$ MIXTURES.

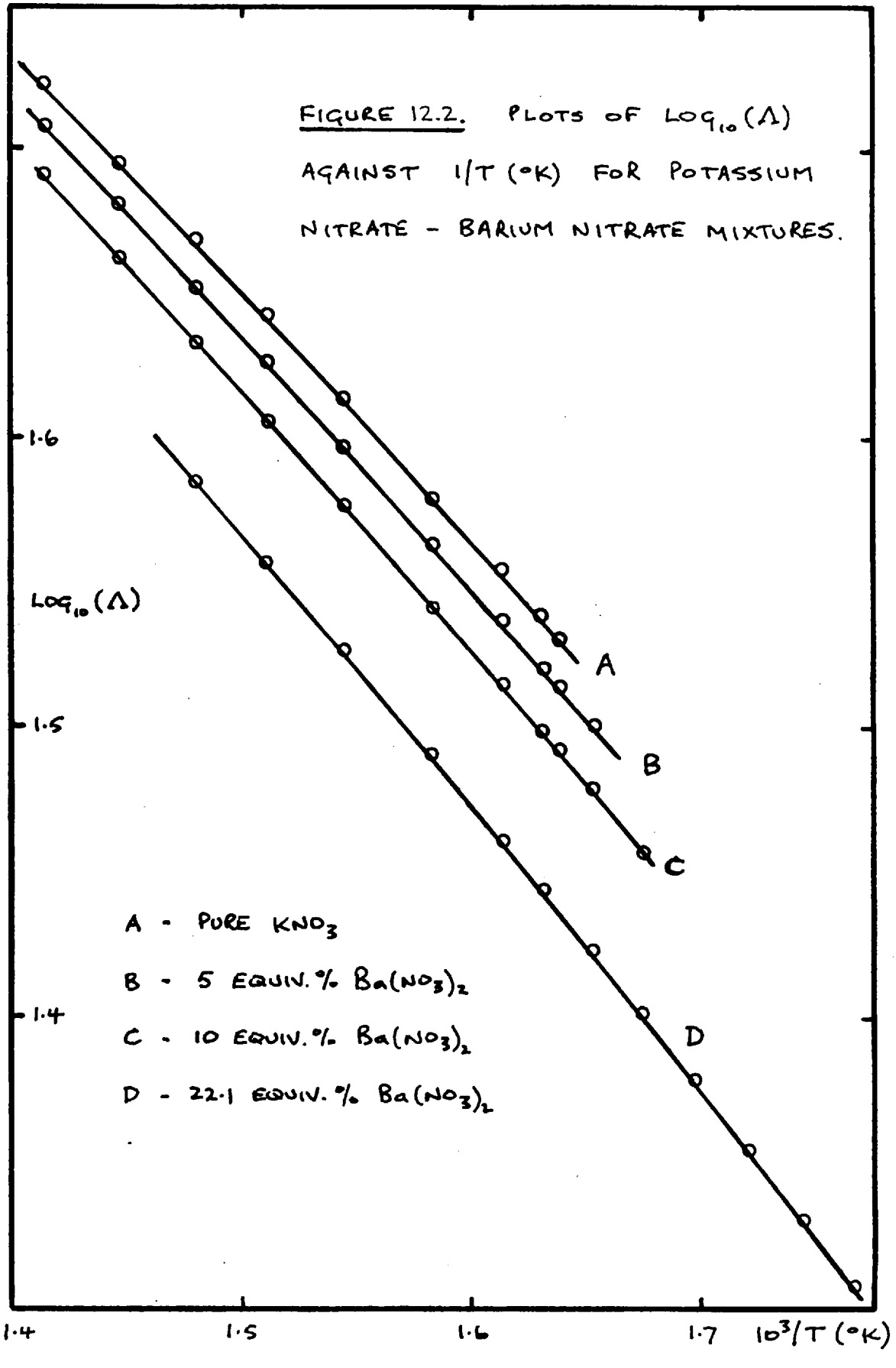


FIGURE 12.2. PLOTS OF $\log_{10}(\Lambda)$ AGAINST $1/T$ (°K) FOR POTASSIUM NITRATE - BARIUM NITRATE MIXTURES.

so would not influence the difference between the results for any two melts.

TABLE 12.2. Conductivity parameters for potassium nitrate - barium nitrate melts.

Equiv. fraction $Ba(NO_3)_2$	Temp. range (°C)	$(E_\sigma)_x$ (kcal/mole)	$(\sigma_o)_x$ ($ohm^{-1}cm^{-1}$)	$(E_\Lambda)_x$ (kcal/mole)	$(\Lambda_o)_x$ ($ohm^{-1}cm^2$ $equiv^{-1}$)
0.000	340-389	3.61	12.5	4.00	924
	374-434	3.38	10.4	3.75	762
0.050	332-389	3.72	13.1	4.05	927
	374-434	3.49	10.9	3.85	801
0.100	332-389	3.80	13.4	4.12	927
	374-434	3.64	11.7	4.00	844
0.221	340-403	3.92	13.4	4.24	904

The maximum absolute error in the equivalent volume V_e is less than 0.05% (see page 130), so there is practically no loss of precision when equivalent conductivities are calculated from specific conductivities by use of equation (12.1).

Temperatures were measured to $\pm 0.1^\circ C$. A temperature change of $0.1^\circ C$ would cause the conductivity of a melt to change by about 0.05%, which is negligible compared to the errors due to the bridge.

The conductivities listed in Table 12.1 all refer to a frequency of 1592 cycles per second; no attempt was made to correct the results to infinite frequency by applying the extrapolation procedure mentioned on page 28. Since the current density at the electrode surfaces was extremely low (0.3 ma/cm^2), the correction required would certainly be less than 0.5%, and would affect the absolute, but not the relative, accuracy of the conductivities for the different mixtures. Since the main object of this work was to find the change in conductivity brought about by the addition of barium ions to fused potassium nitrate, the application of the correction would not have justified the expenditure of time and money which it would have involved.

To summarise: the maximum absolute error in any conductivity value is less than 1%, and about four-fifths of this error is systematic; if the difference between two conductivities is to be calculated, the errors in the individual values can be reckoned as $\pm$ 0.2%.

12.3. Comparison of the results with those of earlier workers.

The conductivity of fused potassium nitrate has been measured by Kröger and Weisgerber (Ref.1) and also by Jaeger and Kampa (Ref.2). Kröger and Weisgerber measured conductivities over a range of frequencies and made an extrapolation to infinite frequency, thereby eliminating any error due to electrode polarisation. This correction was not made by Jaeger and Kampa, nor was it made in the present work (for the reasons given in Section 12.2).

Some of the values obtained by these two groups of workers are plotted in Figure 12.1. It can be seen that the present results lie between the other two sets in the lower part of the temperature range. Above 400°C, however, the earlier values lie below the line through the author's points, the discrepancy increasing with rising temperature to a maximum of 2%. This difference cannot be attributed to the effect of polarisation in the work described here, because a correction for this would involve a small addition to the conductivities and so would increase the discrepancy. It is possible that the accumulation of gas bubbles on the electrode surfaces at temperatures above 400°C caused the earlier workers' results to be too low in this region. Special care was taken to avoid this source of error in the present investigation.

REFERENCES TO CHAPTER 12.

1. C. Kröger and P. Weisgerber, Z. phys. Chem., (neue Folge), (1955), 5, 192.

2. F.M. Jaeger and B. Kampa, Z. anorg. und allgem. Chem., (1920), 113, 27.

CHAPTER 13

RESULTS: DENSITIES, EQUIVALENT VOLUMES AND PARTIAL EQUIVALENT VOLUMES IN LIQUID POTASSIUM NITRATE - BARIUM NITRATE MIXTURES.

13.1. Densities and equivalent volumes.

The compositions of the mixtures, and the measured densities, are listed in Table 13.1. The corresponding equivalent volumes are shown in Table 13.2.

The equivalent volume is that volume of melt which contains one gram-mole of nitrate ions (with an equivalent amount of the cation mixture). If a melt contains w_1 and w_2 grams of potassium nitrate and barium nitrate respectively, the equivalent volume is related to the measured density ρ by the expression

$$V_e = \frac{E_1 E_2 (w_1 + w_2)}{\rho (w_1 E_2 + w_2 E_1)} \quad - - - - - - - - \quad (13.1),$$

where E_1 and E_2 are the equivalent weights of the two salts. The values of E_1 and E_2 used throughout this work were:

$$E_1 = 101.10 \quad \text{(potassium nitrate)}$$

$$E_2 = 130.69 \quad \text{(barium nitrate)}$$

The equivalent fraction of barium nitrate, x_2, is

defined as:

$$x_2 = \frac{w_2/E_2}{w_1/E_1 + w_2/E_2} = \frac{w_2E_1}{w_1E_2 + w_2E_1} \quad - - - \quad (13.2).$$

$100x_2$ is the equivalent % of barium nitrate in the mixture.

TABLE 13.1. Densities of potassium nitrate - barium nitrate melts.

Equiv. % $Ba(NO_3)_2$	Temperature (°C)					
	320.0	330.0	340.0	373.0	410.0	440.0
0.000	-	-	1.8691	1.8434	1.8161	1.7934
4.954	-	1.9262	1.9181	1.8918	1.8633	1.8406
9.867	1.9838	1.9757	1.9675	1.9414	1.9128	1.8898
14.963	2.0335	2.0253	2.0171	1.9909	1.9622	1.9391
19.730	2.0840	2.0749	2.0666	2.0404	2.0110	1.9879
24.704	2.1365	2.1279	2.1196	2.0935	2.0640	2.0406
29.953	-	-	2.1770	2.1498	2.1204	2.0967
34.957	-	-	-	2.2056	2.1755	2.1519
39.741	-	-	-	-	2.2298	2.2058
44.566	-	-	-	-	2.2861	2.2621
50.022	-	-	-	-	-	2.3279

TABLE 13.2

Equivalent volumes of potassium nitrate - barium nitrate melts.

Equiv % $Ba(NO_3)_2$	Temperature (°C)					
	320.0	330.0	340.0	373.0	410.0	440.0
0.000	-	-	54.092	54.843	55.668	56.373
4.954	-	53.249	53.473	54.216	55.045	55.724
9.867	52.433	52.650	52.868	53.580	54.381	55.041
14.963	51.894	52.105	52.315	53.005	53.780	54.422
19.730	51.314	51.539	51.745	52.409	53.177	53.794
24.704	50.741	50.947	51.147	51.783	52.525	53.126
29.953	-	-	50.512	51.150	51.859	52.446
34.957	-	-	-	50.527	51.228	51.789
39.741	-	-	-	-	50.615	51.164
44.566	-	-	-	-	49.993	50.524
50.022	-	-	-	-	-	49.789

13.2. Densities and equivalent volumes as functions of temperature.

The densities were expressed as functions of temperature by the equation

$$\rho = a - b.(t - 300) + c.(t - 300)^2 \quad (13.3).$$

Values of the constants a, b and c were calculated for each mixture, by the method of least squares; they are listed in Table 13.3, together with the standard deviations of the experimental points from the 'least squares' line. A simplified equation

$$\rho = a - b.(t - 300) \quad - - - - - - - - - \quad (13.4)$$

was used for the mixtures containing more than 30 equivalent % barium nitrate, because the densities of these mixtures were measured at only two or three temperatures. For the less concentrated mixtures, however, the inclusion of the third term $c.(t - 300)^2$ caused a definite reduction in the standard deviations.

It was found that the equivalent volumes could be expressed as functions of temperature by the equation

$$V_e = A + B.(t - 300) \quad - - - - - - - - - - \quad (13.5)$$

There was no evidence for supposing that the lines of best fit were curved: inclusion of the term $C(t - 300)^2$ in the expressions for V_e caused no reduction in the standard deviations. Values of A and B were found for each mixture, by the method of least squares; they are listed in Table 13.4. The table includes values of B/A, the coefficients of cubic expansion relative to the volumes at 300°C.

TABLE 13.3. Density parameters for potassium nitrate - barium nitrate mixtures.

Equivalent % $Ba(NO_3)_2$	a	10^4. b	10^7. c	Standard deviation
0.000	1.9000	7.823	1.54	0.0004
4.954	1.9508	8.310	3.14	0.0001
9.867	2.0002	8.251	2.61	0.0001
14.963	2.0500	8.274	2.52	0.0002
19.730	2.1004	8.495	3.30	0.0004
24.704	2.1528	8.298	2.07	0.0003
29.953	2.2104	8.463	2.48	0.0002
34.957	2.2641	8.024	-	0.0004
39.741	2.3176	7.986	-	-
44.566	2.3741	8.003	-	-

TABLE 13.4. Equivalent volume parameters for potassium nitrate - barium nitrate mixtures.

Equivalent % $Ba(NO_3)_2$	A (ml)	10^2. B (ml per ^oC)	10^4. B/A (per ^oC)	Standard deviation (ml)
0.000	53.179	2.275	4.28	0.01
4.954	52.574	2.248	4.28	0.002
9.867	51.998	2.170	4.17	0.002
14.963	51.473	2.103	4.09	0.005
19.730	50.914	2.057	4.04	0.01
24.704	50.348	1.980	3.93	0.01
29.953	49.739	1.932	3.88	0.005
34.957	49.154	1.883	3.83	0.005
39.741	48.599	1.833	3.77	-
44.566	48.047	1.769	3.68	-

13.3.
Equivalent volume isotherms, and partial equivalent volumes.

Figure 13.1 shows isotherms of equivalent volume, plotted as a function of composition (in equivalent %). These isotherms were found to be straight lines, within the limits of experimental error. Equations

$$V_e = C - Dx \quad - - - - - - - - - \quad (13.6)$$

were fitted to them, at different temperatures, by the method of least squares (x being the equivalent fraction of barium nitrate in the mixture). The results for the 10% mixture were not included in the least squares calculation, since they were thought to be slightly inaccurate.

Values of C and D, and of the standard deviations of the points from the straight lines, are listed in Table 13.5. It can be seen from the table that the standard deviations are of the same order of magnitude as the experimental errors in the equivalent volumes. The partial equivalent volumes of the two constituents were therefore independent of the composition of the mixture, within the range studied.

TABLE 13.5. Parameters in the equations for equivalent volume isotherms for potassium nitrate - barium nitrate mixtures.

Temperature (°C)	C (ml)	D (ml)	Standard deviation. (ml)
340.0	54.083	11.892	0.014
373.0	54.838	12.328	0.009
410.0	55.678	12.740	0.008
440.0	56.381	13.125	0.006

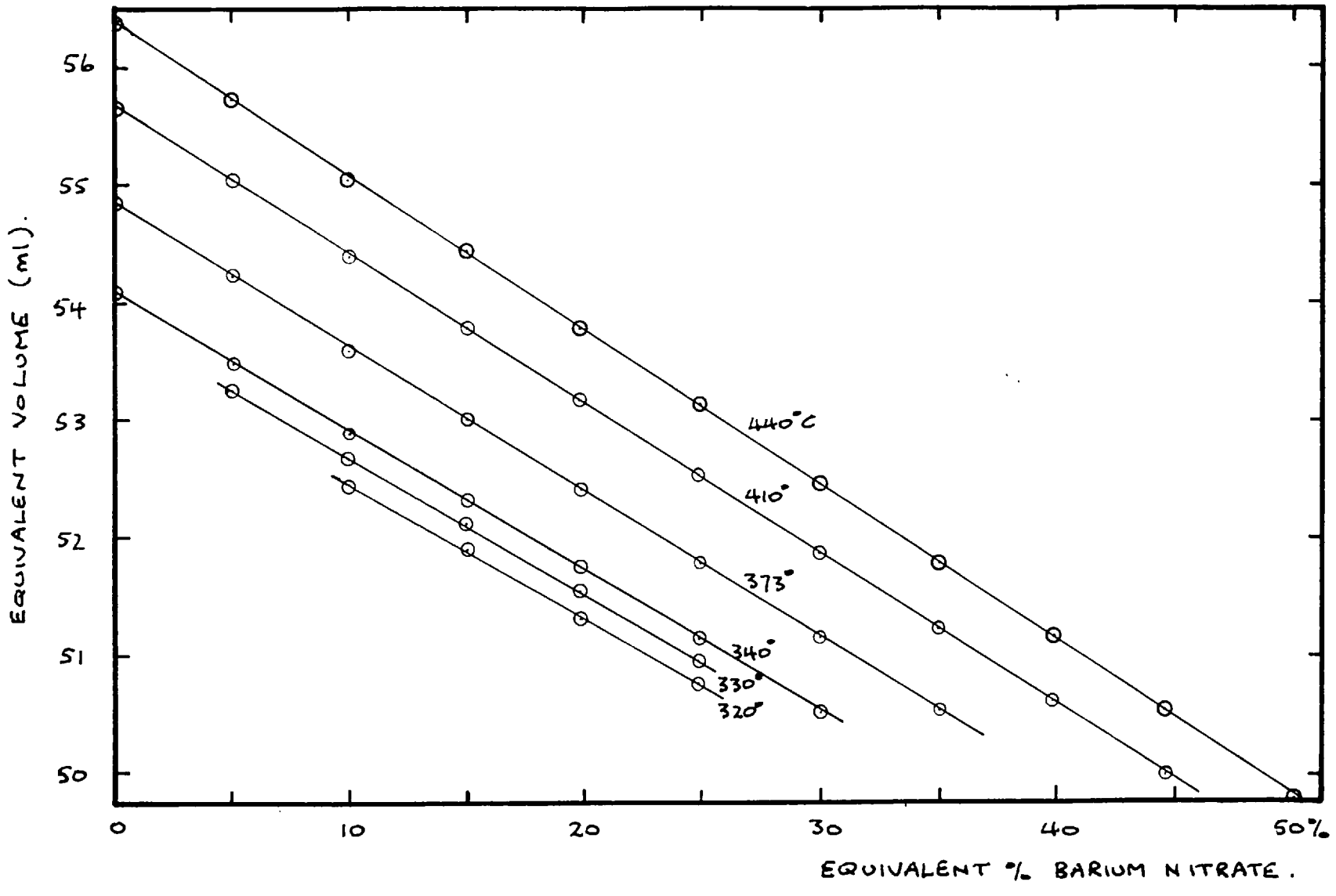


FIGURE 13.1. EQUIVALENT VOLUME ISOTHERMS FOR $KNO_3 - Ba(NO_3)_2$ MELTS.

From equation (13.6) and the parameters listed in Table 13.5, values of V_e were calculated at each temperature for $x = 0$ and $x = 1$. The values so obtained were the partial equivalent volumes of potassium and barium nitrates at these temperatures. They were found to conform (with a standard deviation of 0.02 ml) to the linear equations

$$\bar{V}_e\left[KNO_3\right] = 53.17 + 0.0229(t - 300) \quad (13.7)$$

and

$$\bar{V}_e\left[Ba(NO_3)_2\right] = 41.75 + 0.0107(t - 300) \quad (13.8)$$

where t is the temperature in ^{o}C.

If it is assumed that the equivalent volume isotherms remain linear over the entire composition range, the partial volumes obtained from these equations may be identified with the equivalent volumes, $(V_e)_l$, of pure liquid potassium and barium nitrates, respectively. The corresponding equivalent volumes of the two solids, $(V_e)_s$, have been calculated from their densities and coefficients of expansion as reported in the literature. By comparing the two sets of volumes it is possible to find the volume change, $(\Delta V)_f$, which occurs when one equivalent of solid melts, or when it dissolves in the other component to give a solution of any concentration.

Values of $(V_e)_l$, $(V_e)_s$ and $(\Delta V)_f$ at different temperatures are listed in Table 13.6, for the two salts. The $(V_e)_s$ values for potassium nitrate have been obtained by extrapolation of the expansion data above the melting-point, and the $(V_e)_l$ values for barium nitrate refer to the super-cooled liquid.

TABLE 13.6. Derived equivalent volumes of solid and liquid potassium and barium nitrates.

Potassium nitrate				
Temp. (°C)	$(V_e)_s^*$ (ml)	$(V_e)_l$ (ml)	$(\Delta V)_f$ (ml)	$(\Delta V)_f/(V_e)_s$ (%)
334.6	52.48	53.96	1.48	2.81
340.0	52.55	54.09	1.53	2.91
373.0	53.06	54.84	1.78	3.35
410.0	53.63	55.68	2.05	3.82
440.0	54.09	56.38	2.29	4.22

Barium nitrate				
Temp. (°C)	$(V_e)_s^{**}$ (ml)	$(V_e)_l$ (ml)	$(\Delta V)_f$ (ml)	$(\Delta V)_f/(V_e)_s$ (%)
288.0***	40.82	41.62	0.80	1.96
340.0	40.93	42.18	1.25	3.06
373.0	41.00	42.53	1.54	3.75
410.0	41.07	42.93	1.86	4.53
440.0	41.13	43.25	2.12	5.16
592.0***	41.44	44.88	3.45	8.31

Notes to Table 13.6.

* The values of $(V_e)_s$ for potassium nitrate were calculated from the density of the solid at 335°C and the coefficient of cubic expansion, both measured by X-ray diffraction (Ref. 1). Slightly higher values of $(V_e)_s$ are obtained from the results of dilatometric measurements due to Bredee and Cohen (Ref. 2).

** The values of $(V_e)_s$ for barium nitrate were calculated from the density at 23°C (3.244 grm/ml.; Ref 3) and

Notes to Table 13.6 (continued)

the mean coefficient of cubic expansion between 10 and 250°C, measured by X-ray diffraction.(Ref. 4).

*** 288.0°C is the eutectic temperature of the system potassium nitrate - barium nitrate, and 592.0°C is the melting-point of barium nitrate (Ref. 5).

13.4. Errors in the measured densities.

The maximum absolute error in the density values listed in Table 13.1 is estimated to be ± 0.001 (i.e. ± 0.05%; see Section 10.3, page 130, for a detailed discussion). However, the standard errors (2σ) calculated from the standard deviations (σ) listed in Tables 13.3, 13.4 and 13.5 lie between 0.01% and 0.04% (with the exception of that for the equivalent volume isotherm at 340°C, for which 2σ is 0.06%). This indicates that only a fraction of the total error of 0.05% is due to scatter of the experimental points about the 'least squares' lines; the residual error is systematic, and does not influence the relative accuracy of the results.

Temperatures were measured to ± 0.1°C. An error of 0.1°C in a given temperature is equivalent to an error of less than 0.0001 in the corresponding density. This is less than the total error by a factor of ten, and is therefore negligible.

13.5. Comparison of the present results with those of earlier workers.

Pure potassium nitrate.

Three groups of workers have measured the density of pure,

fused potassium nitrate (Refs 6, 7, 8). Table 13.7 shows the results they obtained, and also gives the results from the present work.

Temperature (°C)	Density			
	Jaeger (Ref 6)	Bloom et al (Ref 7)	Smith et al (Ref 8)	Present work.
340	1.867	1.868	1.861	1.869
373	1.842	1.844	1.837	1.843
410	1.814	1.817	1.810	1.816
440	1.791	1.795	1.788	1.793

TABLE 13.7. Density of pure potassium nitrate melt.

It is seen that the present results lie between those of Jaeger and of Bloom et al, and differ from them by not more than 0.002. However, the values obtained by Smith are consistently lower than the other three sets; they differ from the author's results by 0.005 - 0.008.

Potassium nitrate - barium nitrate mixtures.

Smith et al (Ref 8) measured the densities of three mixtures of potassium nitrate and barium nitrate. Table 13.8 lists their results at 440°C, together with the results from the present work (calculated by substituting Smith's compositions into equation 13.6, using the values of C and D given in Table 13.5).

Equiv. % $Ba(NO_3)_2$	Density at 440°C	
	Smith et al (Ref 8)	Present work
18.182	1.965	1.972
33.333	2.215	2.133
46.154	2.275	2.280

TABLE 13.8. Densities of KNO_3 - $Ba(NO_3)_2$ mixtures at 440°C.

It is seen that Smith's density values are lower than the author's by 0.005 - 0.008, which is considerably more than the maximum absolute error in the present results (±0.001). Since a similar discrepancy was recorded between the two groups of results for potassium nitrate (see Table13.7), it seems very likely that Smith et al made a wrong estimate of the volume of the platinum bob which they used in measuring the densities of the melts. However, the comparison does serve to show that no gross error has been made in calculating the densities from the experimental observations.

REFERENCES TO CHAPTER 13.

1. H.F. Fischmeister, J. Inorg. Nucl. Chem., (1956), 3, 182.

2. H.L. Bredee and E. Cohen, Z. phys. Chem., (1929),140A,391.

3. International Critical Tables.

4. L. Vegard and K.I. Roer, Avh. norske Vidensk-Akad., (1941), 1, No.17.

REFERENCES TO CHAPTER 13. (Continued)

5. P.I. Protsenko and A.Ya. Malakhova, Zh. Neorg. Khim., (1957), 2, 2145.

6. F.M. Jaeger, Z. anorg. Chem., (1917), 101, 1.

7. H. Bloom, I.W. Knaggs, J.J. Molloy and D. Welch, Trans. Farad. Soc., (1953), 49, 1458.

8. G.P. Smith, G.F. Petersen and W.M. Ewing, Oak Ridge National Report Number 2762 (1959).

CHAPTER 14.

RESULTS: ULTRA - VIOLET ABSORPTION SPECTRA OF NITRATES AND NITRITES.

14.1. Introduction.

At the outset of the research, it was hoped to measure the frequency of the maxima of the strong and the weak bands of the nitrates and nitrites as functions of temperature. However, it did not prove possible to make this measurement for the strong bands; even with the thinnest obtainable samples ($\sim 3\mu$), 100% absorption was recorded from 50 kcm^{-1} to the band edge at ~ 40 kcm^{-1}. Some transmission was recorded in the range 54 - 50 kcm^{-1}, but this was shown to be spurious.(see page 194).

Since the strong-band maxima could not be measured, the conclusions derived from this work are based mainly on the results for the weak bands of the nitrates and nitrites. The maxima of these bands could be measured conveniently for samples whose thicknesses lay in the range 3μ - 150μ.

Overlap of the weak band with the strong-band edge can cause the maximum of the former to be displaced from its true position (i.e. the position it would have if it could be recorded in isolation from the strong band). In order to allow corrections to be made for this effect, the movements of the strong-band edge with rising temperature have been recorded. For this purpose, suitable band-edge parameters have been defined by means of which the edge can be characterised. For the alkali nitrates and nitrites, overlap effects are relatively slight, but for silver and thallous nitrates

they are pronounced, and must be taken into account before the true movements of the weak band can be derived from the measured spectra.

In this Chapter the results are presented graphically. Full experimental details for each spectrum, and the value of E(2) (or other characteristic parameter) at each temperature, are listed in Appendix C (page 386). The Appendix also gives the thickness of each sample (when known) and the % absorption at the maximum of the weak band.

14.2. Changes in % absorption with rising temperature.

For all solid samples, the % absorption at the maximum of the weak band was measured to $\pm 1\%$, at temperatures between 20°C and the melting-point. Table 14.1. shows some of the results obtained.

Since the mass of salt per unit area of the solid samples remained constant as the temperature was raised, the changes in % absorption reflect corresponding changes in the molar extinction coefficients. The proportionality between $\log (I_o/I)$ and ϵ does not extend through the melting-point, because fusion of the thicker films was usually accompanied by a change in sample path-length.

The table shows that, for solid alkali nitrates, ammonium nitrate, silver nitrate and thallous nitrate, the molar extinction coefficient at the maximum of the weak band always increased with rising temperature. The integrated intensity, $\int \epsilon \, d\nu$, increased likewise.

For sodium nitrite, the % absorption at the maximum of the weak band increased with rising temperature, but for potassium nitrite a decrease was recorded.

TABLE 14.1. % absorption at the maximum of the weak band for nitrates and nitrites.

Salt	Melting-point (°C)	% absorption.	
		at 20°C	just below m.p.
$NaNO_3$ (Sample 2)	308	67	72
KNO_3 (Sample 1)	334	55	79
$RbNO_3$ (Sample 3)	310	71	77
$CsNO_3$ (Sample 4)	407	77	91
NH_4NO_3 (Sample 6)	169	(84% at 38°C)	92
$AgNO_3$ (Sample 2)	207	85	93
$TlNO_3$ (Sample 2)	207	85	91
$NaNO_2$ (Sample 1)	281	81	97.5
KNO_2 (Sample 1)	420	88	81

14.3. Estimation of sample thicknesses and molar extinction coefficients.

Sample thicknesses were found by dividing the mass of each salt film by its area and density. Since the mass of salt in a sample included a contribution from salt present in small cracks and chips at the edges of the Spectrosil plates, the values of sample thickness obtained in this way are likely to be high (the proportional error being greatest for the thinnest films). The thicknesses are recorded in Appendix C.

The accuracy with which molar extinction coefficients (ϵ) can be calculated from the % absorption data is restricted by this uncertainty in the thickness measurement.

TABLE 14.2. Molar extinction coefficients of polycrystalline films of sodium nitrate at 20°C, at the maximum of the weak band.

Sample number	% transmission at 20°C	Thickness at 20°C (microns)	ϵ (litres/ mole.cm.)
1	9	49	8.0
2	33	21	8.6
3	7	57	7.7
3*	32	25	7.5

* after fusion and re-freezing.

Table 14.2. shows values of ϵ for polycrystalline films of sodium nitrate at 20°C, calculated from the % transmission and thickness data for four different samples of this salt. It is seen that the results show a scatter of $\sim$10% about the mean value. In spite of this low accuracy, extinction coefficients calculated in this way provide a useful guide for future workers in this field.

14.4. Errors in the recorded values of E(2).

All the results presented here are subject to an absolute error of $\pm$100 cm^{-1}, with the exception of the values of E(2) recorded in Table 14.3. (which are accurate to $\pm$ 20 cm^{-1}).

Three main sources of error were encountered; they are listed below.

(i) In the plots of E(2) against temperature, the points show a scatter of the order $\pm$50 cm^{-1}. This is believed to be due to short-term changes in the frequency calibration of the spectrophotometer.(see page 156).

(ii) In addition to this random error, the results for any one salt may have a systematic error of up to100 cm^{-1}. This error remained constant during all the measurements on a given salt, so could not influence the sizes of the abrupt changes in E(2), etc., at melting-points and transition points, nor could it change the slopes of the straight-line portions of the plots of E(2) against temperature. It was due to initial mis-setting of the frequency calibration (see page 155); the setting was readjusted before the examination of each salt was begun, but was not changed during the examination.

(iii) The frequency scale was checked in the region 27 - 32 kcm^{-1}, using the lines in the spectrum of a mercury arc.

For our particular instrument, corrections of 40 - 80 cm^{-1} were required, to allow for non-linearity of the scale. These corrections have been applied to all the results presented here. For all the alkali-metal nitrates, the correction was 40 cm^{-1} over the entire temperature range, so this source of error could not have affected the accuracy with which $\Delta E(2)$ and $dE(2)/dT$ could be measured.

The accurate values of E(2) for alkali nitrates given in Table 14.3. were obtained from a special series of experiments, during which error (i) was minimised by fan-cooling the spectrophotometer chassis (particularly the monochromator and cam-following arm). Checks carried out between scans showed that error (ii) was less than 10 cm^{-1} throughout this series of experiments.

14.5. Temperature measurements.

The temperatures given in this Chapter refer to the copper block of the thermostat unit. As detailed on pages 168 to 178, this sometimes differed slightly from the mean sample temperature. A correction for this difference would have no effect on the accuracy with which E(2), $\Delta E(2)$ and $dE(2)/dT$ could be measured, as explained in Section 11.8.

The temperature difference between block and sample influences the accuracy of the transition temperatures measured by the 'constant frequency' technique described on page 199. Although the primary object of this work was to obtain the transition temperatures in terms of the block temperature (as a preliminary to the measurement of $\Delta E(2)$ at the transition-point), some corrected values of transition temperatures have also been listed (see page 309).

14.6. The nitrates.

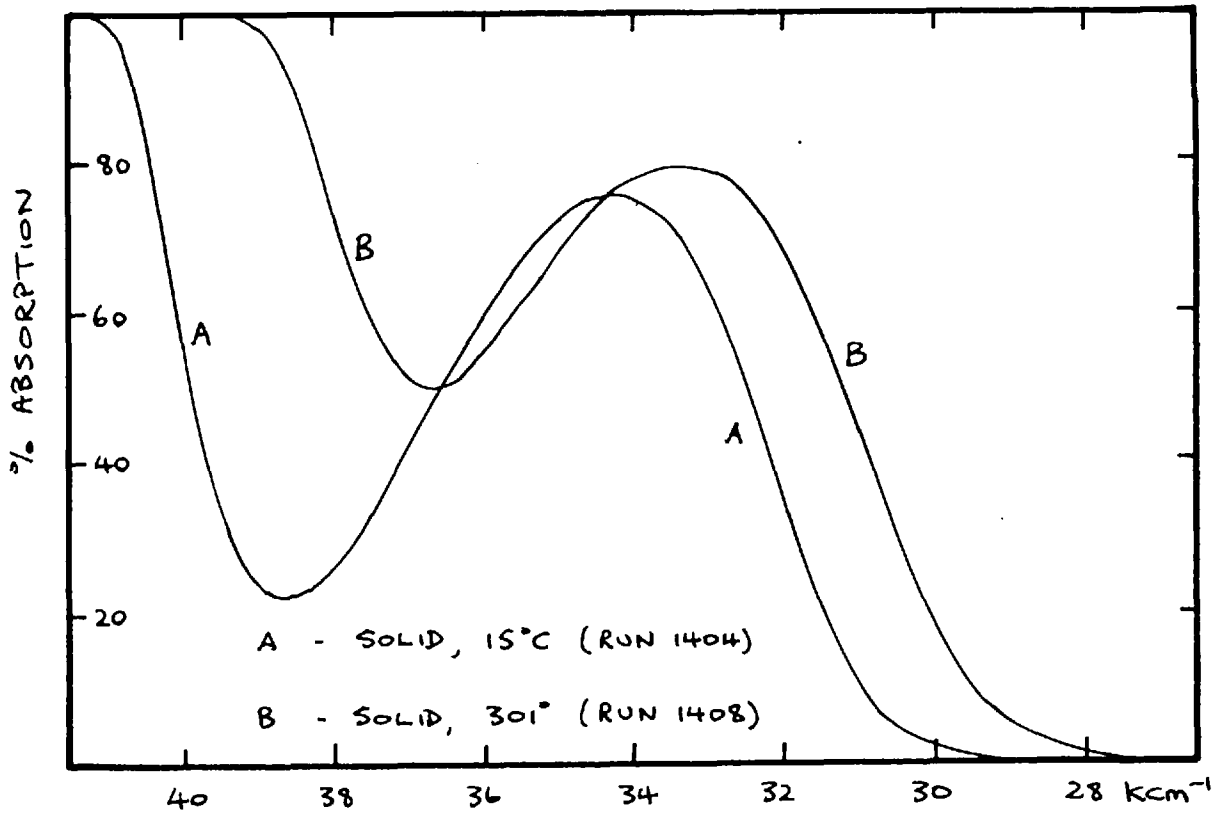
14.6.1. The alkali-metal nitrates.

The weak band at 33 kcm^{-1}.

Figures 14.1 to 14.4 illustrate some of the spectra obtained in the region of the weak band (40 - 25 kcm^{-1}). A series of shoulders were observed on the band for potassium, rubidium and caesium nitrates at 20°C. The shoulders became less distinct as the temperature was raised, and could not be distinguished above 50°C.

Figures 14.5 and 14.6 show plots of E(2) against temperature for potassium, rubidium and caesium nitrates, E(2) being the frequency at the maximum of the weak band (measured by the method described on page 189). The diagrams show that E(2) fell linearly with temperature for the different crystalline modifications of each salt and for the melts, but that abrupt changes occurred at the transition-points and the melting-points. Although changes in E(2) of either sign were observed at the transitions, E(2) always increased at the melting-point.

For potassium nitrate, there was a discrepancy of 120 cm^{-1} between the accurate value of E(2) recorded in Table 14.3. and the values for the melt obtained during the series of runs, 745 - 760. Another set of measurements was therefore made, between 40 and 340°C, in order to check the results. During these measurements the chassis of the spectrophotometer was fan-cooled, and the wave-number calibration was checked at the beginning, middle and end of the sequence. The Balmer line of the hydrogen spectrum was found to be within 20 cm^{-1} of the correct value on each occasion.



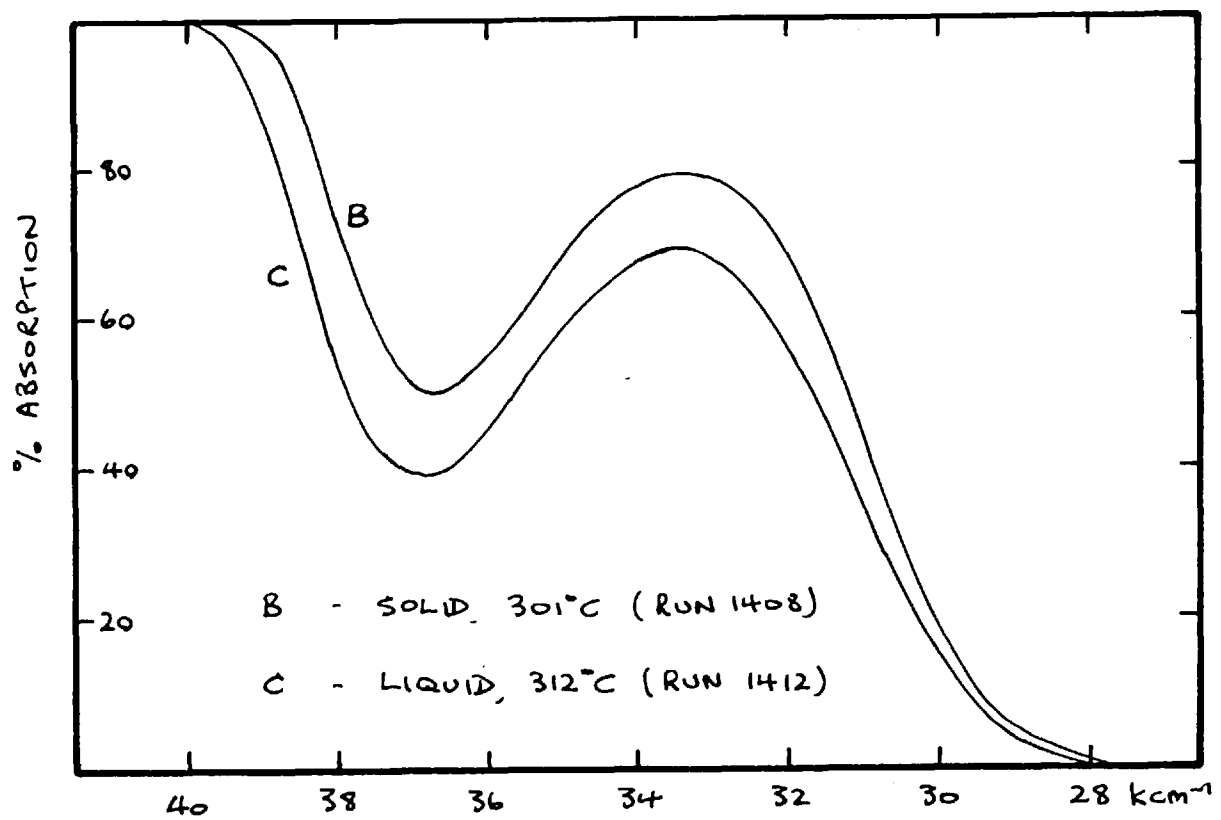


FIGURE 14.1. ABSORPTION SPECTRA OF SODIUM NITRATE.

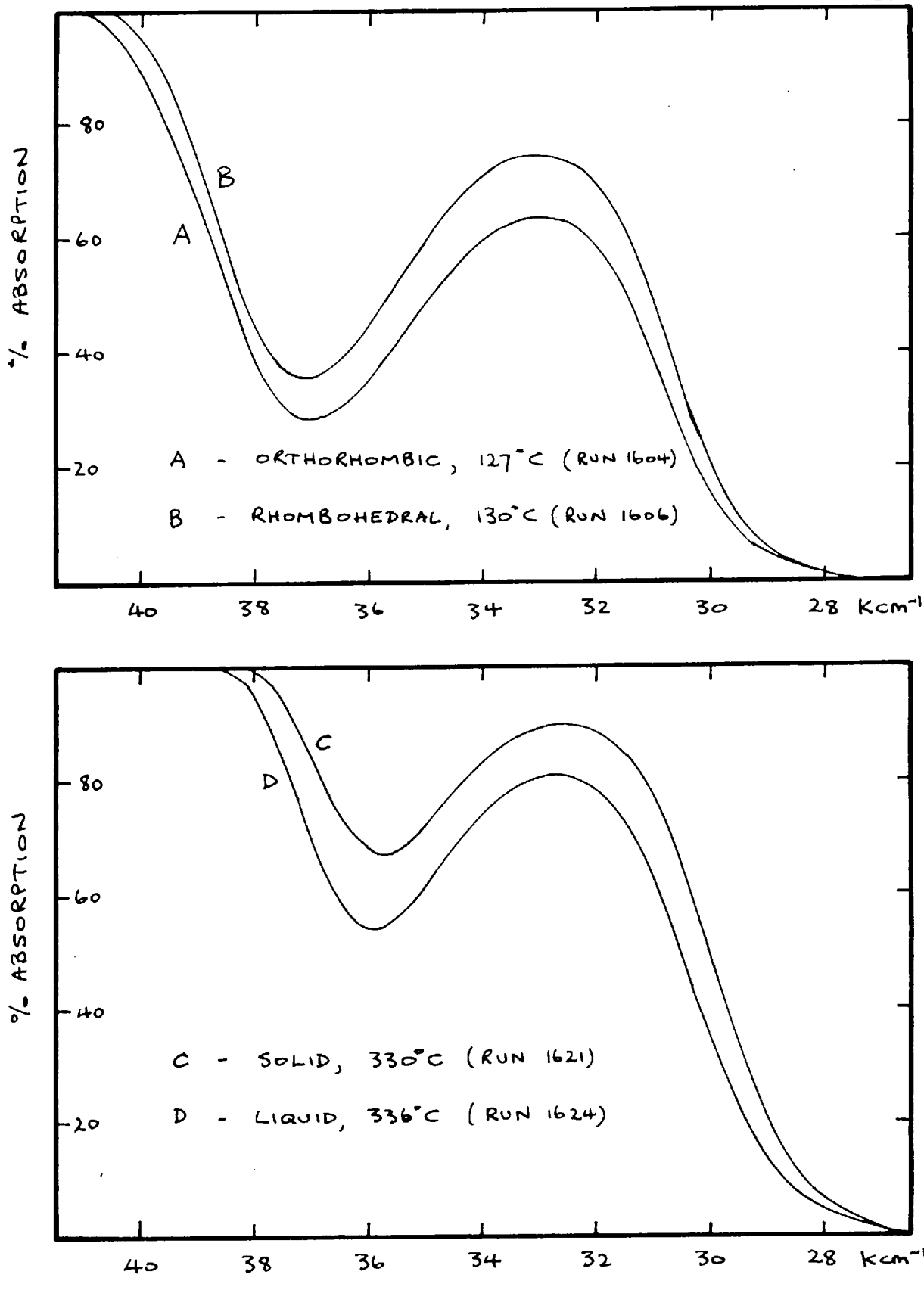
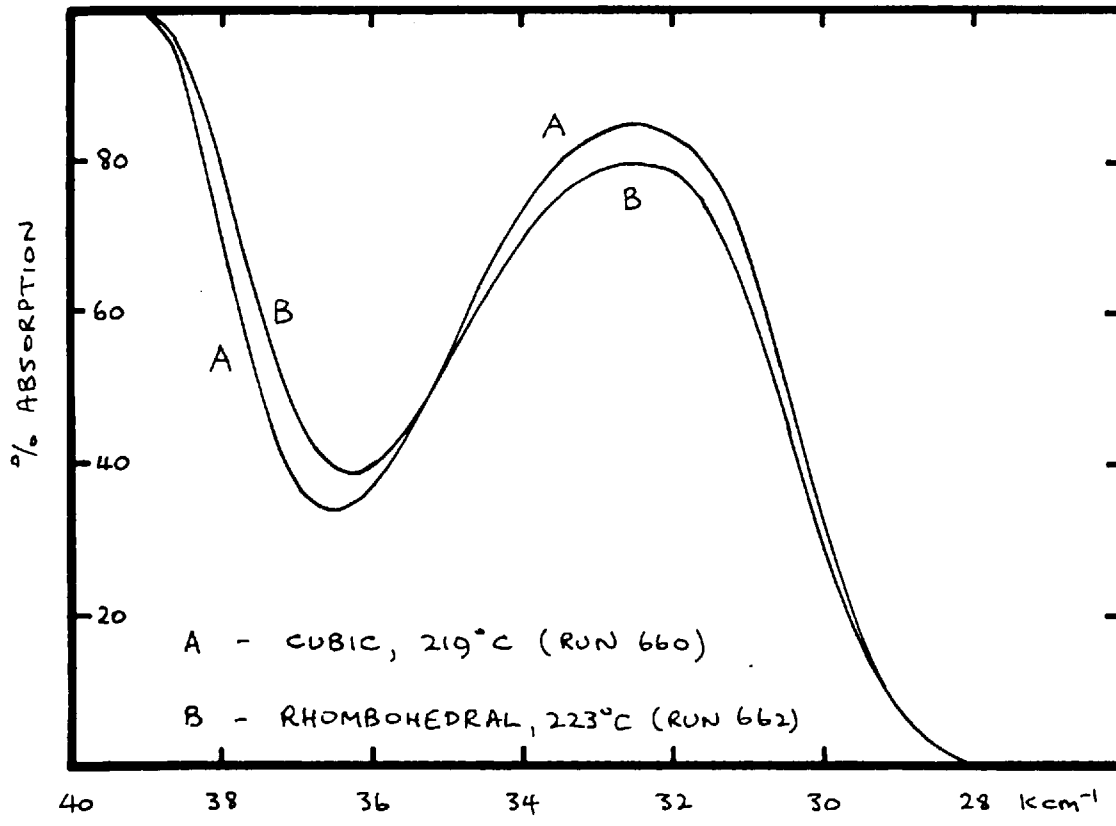


FIGURE 14.2. ABSORPTION SPECTRA OF POTASSIUM NITRATE.



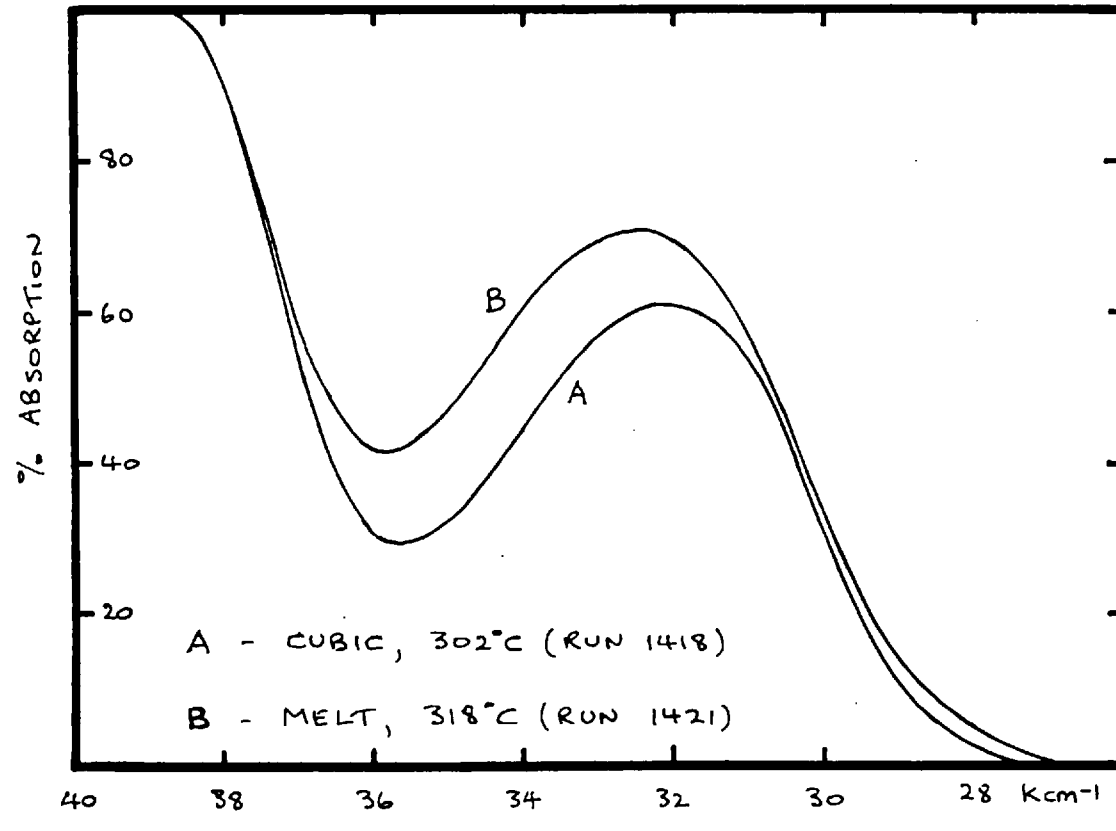


FIGURE 14.3. ABSORPTION SPECTRA OF RUBIDIUM NITRATE.

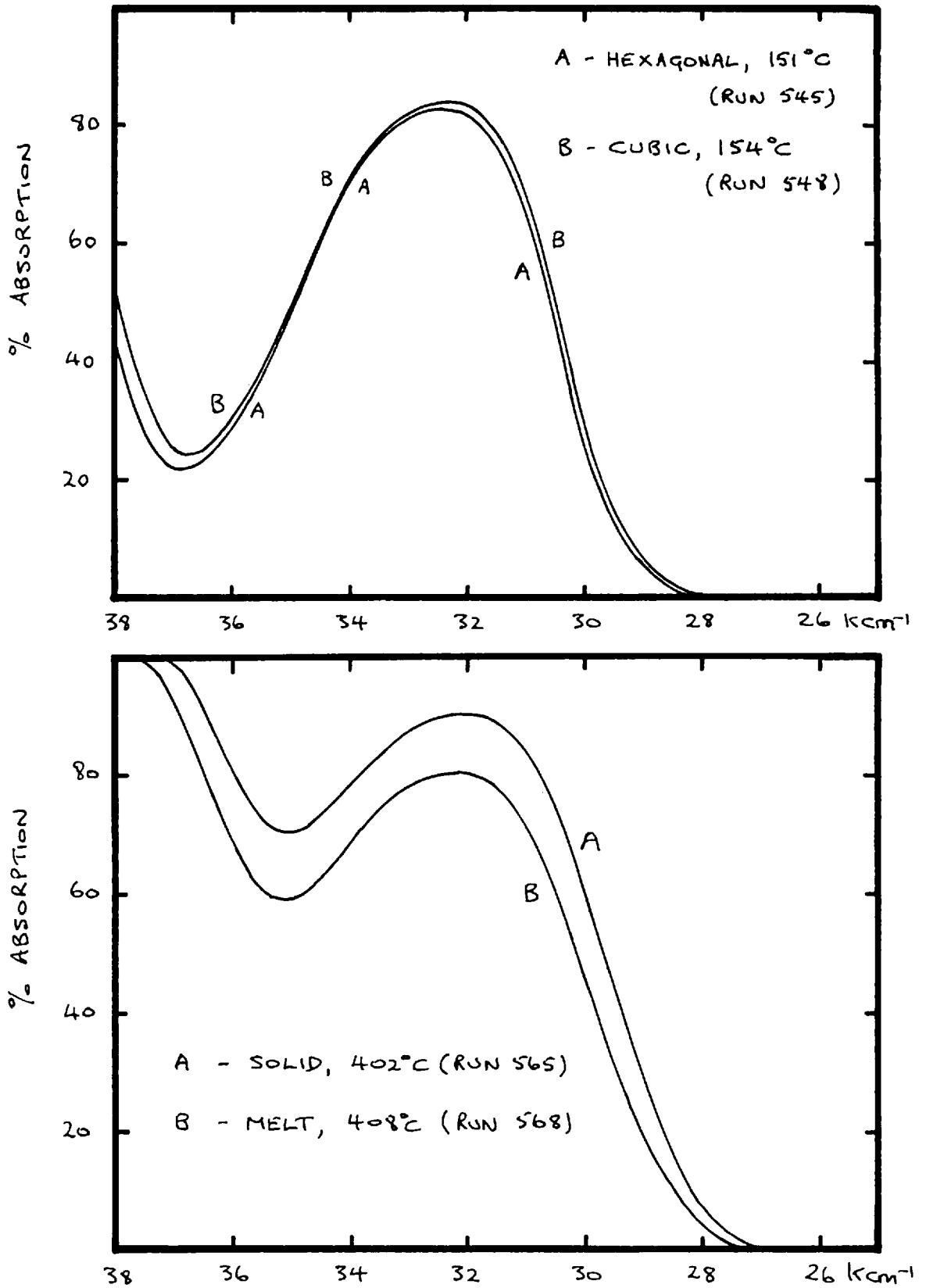


FIGURE 14.4 ABSORPTION SPECTRA OF CAESIUM NITRATE.

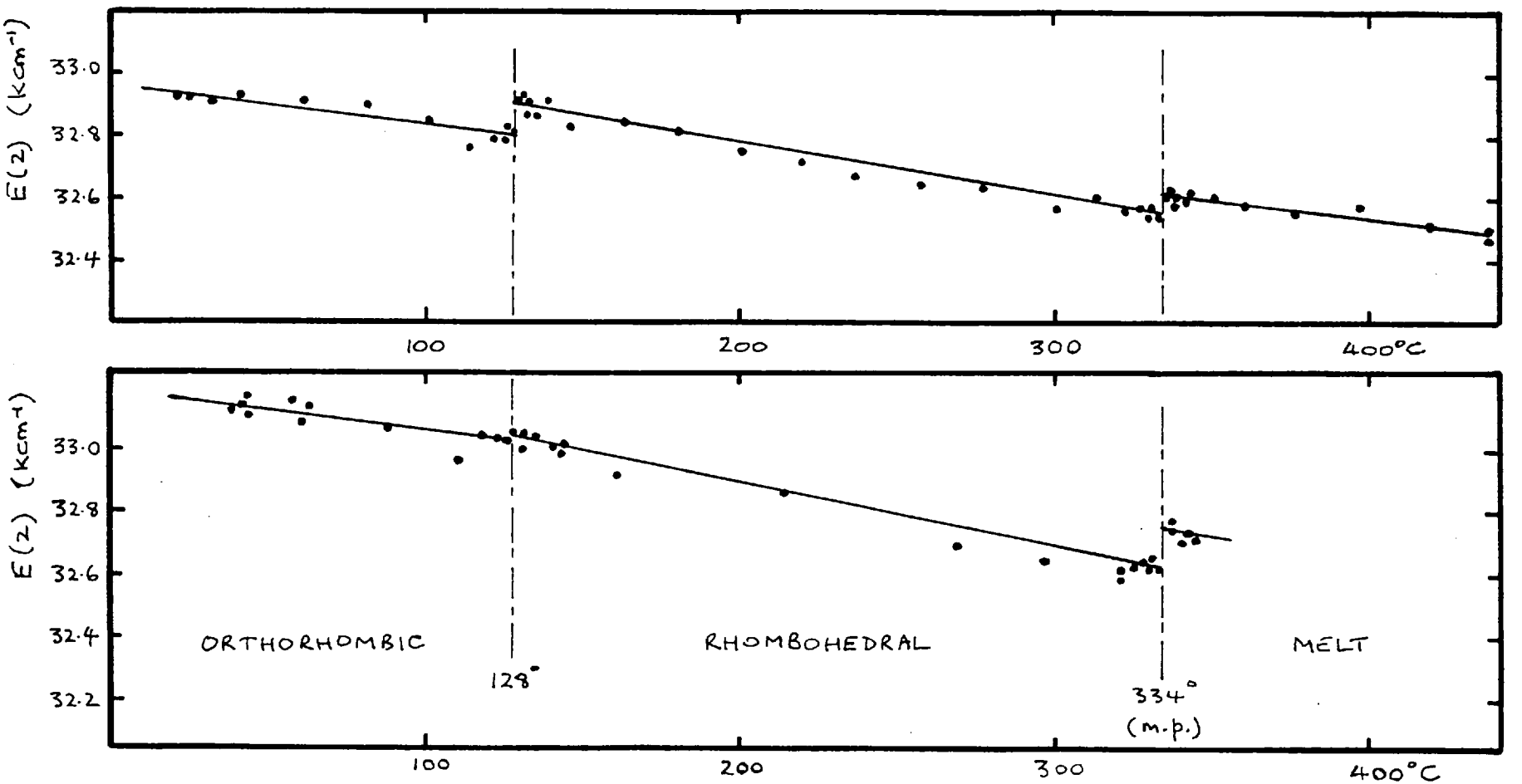


FIGURE 14.5. PLOTS OF E(2) AGAINST TEMPERATURE FOR POTASSIUM NITRATE.

UPPER GRAPH - RUNS 709 - 760; LOWER GRAPH - RUNS 1593 - 1629.

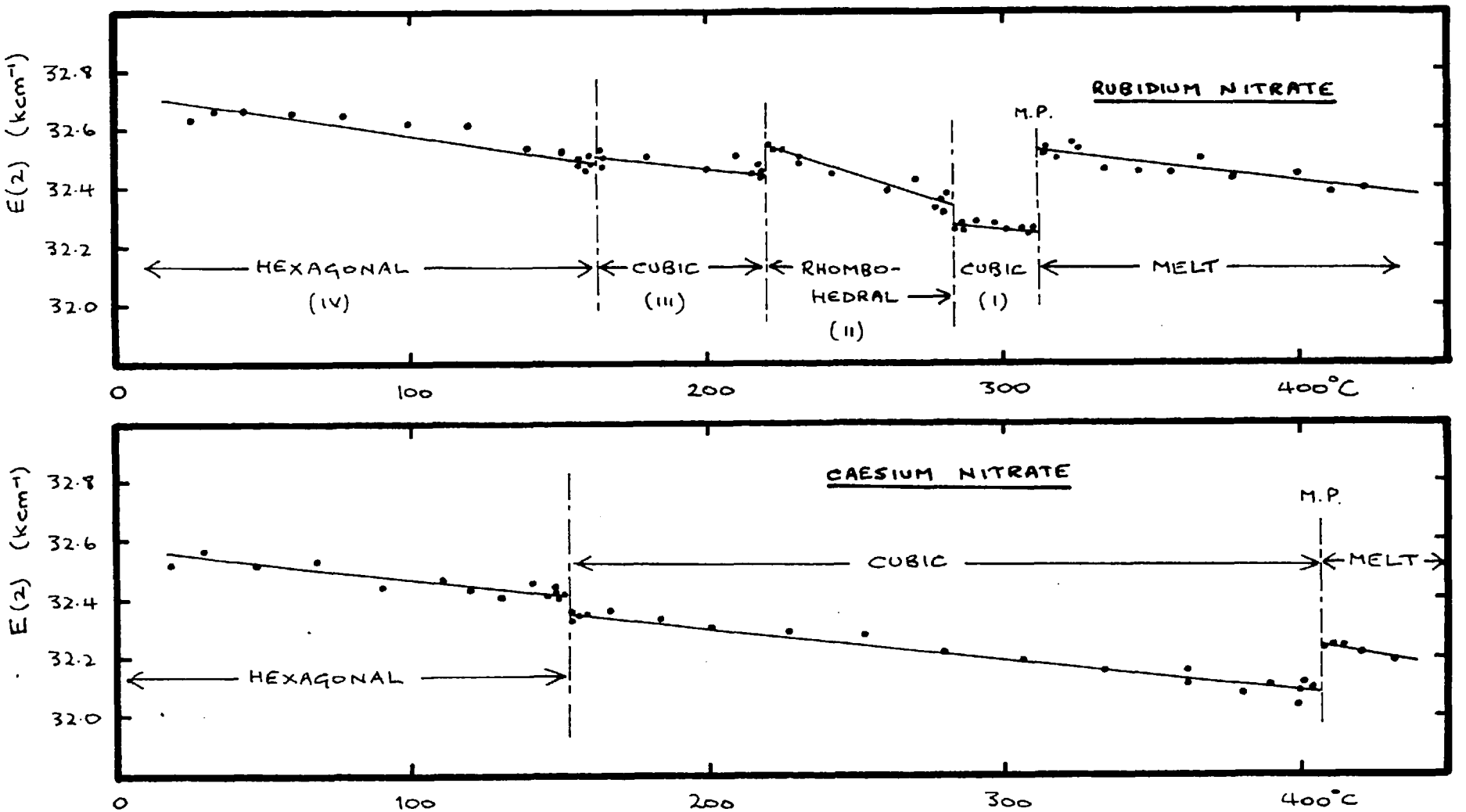


FIGURE 14.6. E(2) FOR RUBIDIUM NITRATE AND CAESIUM NITRATE.

The values of E(2) for the melt obtained during this second set of experiments agreed very well with the 'accurate value' listed in Table 14.3. This makes it practically certain that the error in the first set was due to mis-setting of the wave-number calibration, since all the experiments on potassium nitrate were carried out with salt from the same batch.

Sodium nitrate has a transition of higher order; onset of the change begins at 150°C, and a Λ-point is reached at 275.4°C (Ref.1). The plot of E(2) against temperature for this salt is shown in Figure 14.7. E(2) decreased linearly as the temperature was raised from 20°C to 150°C, but the decrease accelerated as the Λ-point was approached. The plot was again linear between 276°C and the melting-point, and E(2) increased abruptly when the salt was fused. There was no discontinuous change in E(2) in the region of the transition. A plot of the specific volume of the salt against temperature is included in the Figure; it shows similar changes in curvature near the Λ-point.(Ref.1).

TABLE 14.3. Accurate values of E(2) for alkali nitrate melts. (cm^{-1}, in air).

Salt	Melting-point (°C)	Temperature of measurement (°C)	E(2) (cm^{-1})	
			present work	Smith et al(Ref.2)
$NaNO_3$	308	311	33,520	33,520
KNO_3	334	338	32,700	32,770
$RbNO_3$	310	317	32,500	32,530
$CsNO_3$	409	416	32,160	32,280

Table 14.3. gives values of E(2) for the alkali metal nitrates just above their melting-points (see Appendix C, page 416). These results were obtained under the

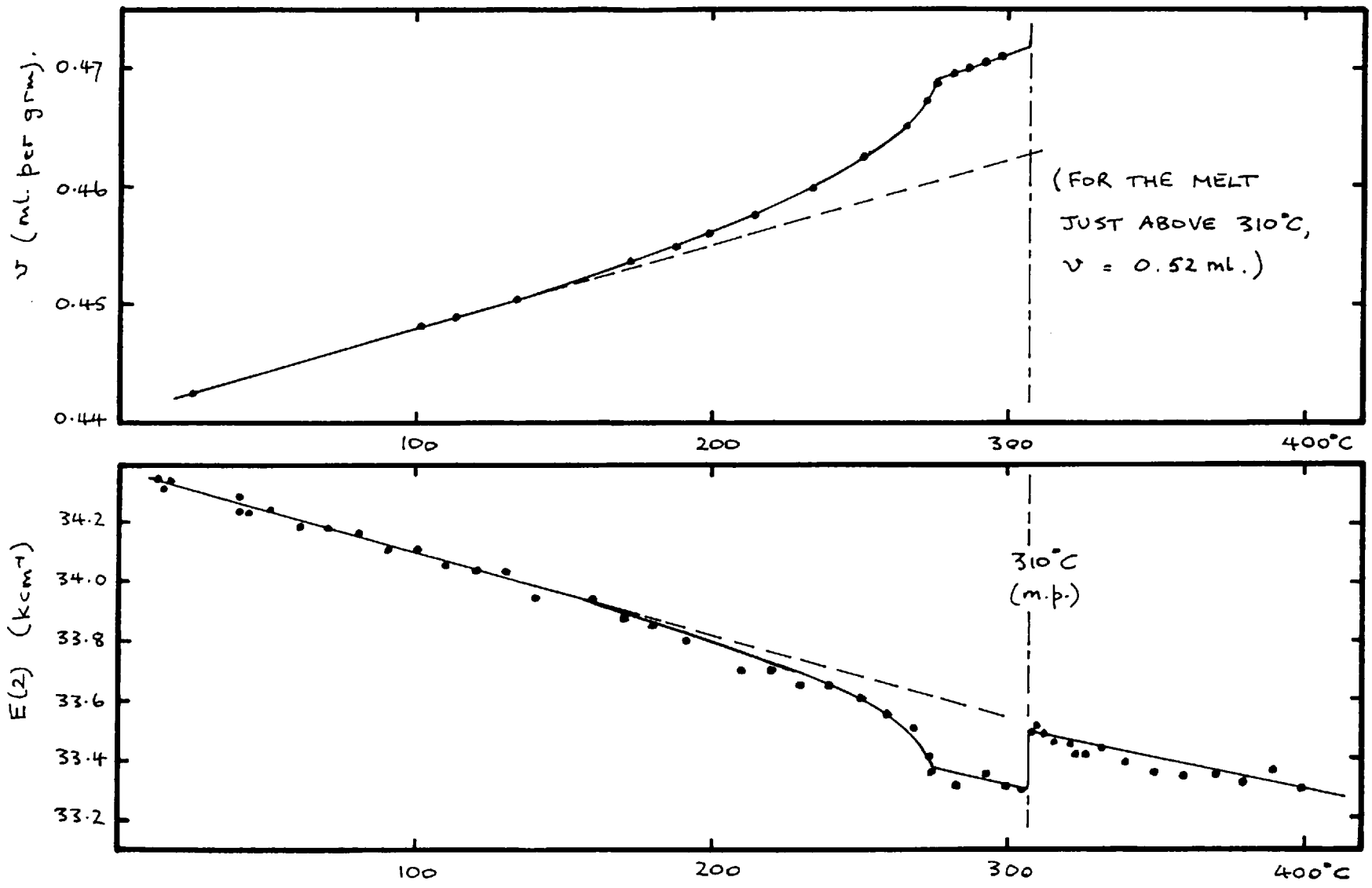


FIGURE 14.7. SPECIFIC VOLUME (v) AND E(2) FOR SODIUM NITRATE. (RUNS 383 - 425).

carefully controlled conditions described on page 157 ; they are believed to be accurate to ± 20 cm^{-1}. Each value is the mean of at least two measurements.

The temperatures given in Table 4.3. are mean sample temperatures rather than block temperatures. The corrections to the block temperatures were estimated from the data given on pages 177 - 178 ; the correction was $-1^{o}C$ for sodium, potassium and rubidium nitrates, and $-3^{o}C$ for caesium nitrate. These temperature differences correspond to changes in E(2) of ~ 3 cm^{-1} and ~ 6 cm^{-1}, respectively, and are therefore of only marginal significance.

The table includes some values reported by G.P. Smith et al. (Ref.2), who also claim to have measured E(2) with a precision of ± 20 cm^{-1}. Agreement between the two sets of results is satisfactory in the case of sodium and rubidium nitrates, but for potassium and caesium nitrates Smith's results are higher than the present ones by 70 and 120 cm^{-1} respectively. The present results for these salts are believed to be the more accurate; the value for potassium nitrate is the mean of three results (which were identical), and that for caesium nitrate is the mean of five (which had a standard deviation of 7 cm^{-1}; see page 417). The remaining discrepancy may be due to a calibration error in Smith's experiments, or to the presence of impurities in his materials (which were Reagent Grade).

These differences are too small to influence the validity of Smith's conclusions (which are mentioned on page 71), or of the author's (page 342).

The strong band at 40 - 50 kcm^{-1}.

This band has a maximum at ~ 50 kcm^{-1} for dilute aqueous solutions of nitrates (Ref. 3), but in the present work it was not possible to record the maximum; even with the thinnest obtainable samples ($\sim 3\mu$), complete absorption was registered between 50 kcm^{-1} and the steep edge at ~ 40 kcm^{-1}. Some transmission was recorded from 54 to 50 kcm^{-1}, but this was probably spurious (see page 194); the true transmission in this range was shown to be $0.0 \pm 0.2\%$ for thin samples of potassium and caesium nitrates at 20°C (page 197).

The low-energy edge of the strong band was characterised by the parameter $E(t = x\%)$, which is the frequency at which the transmission is x% (values of x being chosen arbitrarily). Clearly, this frequency depends on the thickness of the sample at a given temperature. Since sample thicknesses were known only approximately, the values of $E(t = x\%)$ given here have no absolute significance, so it was not possible to combine results obtained with different samples of the same salt; however, the variation with temperature of $E(t = x\%)$ for a particular sample is a reliable indication of the corresponding movement of the band edge.

A complication arises if we wish to follow the movement of the band edge through the melting-point. As explained on page 191, the sample was melted and re-frozen several times in the thermostat until the thickness of the film (in the molten state) reached a steady value. Scans were made first on a liquid film; this was frozen, and scans were made on the solid film so obtained. It is uncertain whether this solid film had the same thickness or the same mass per unit area as the liquid film; this would depend on whether the sample froze from the centre to the edges or vice versa. The former seems the more likely, since the centre of the sample was

known to be slightly cooler than the edge (page 178), but this situation might be reversed if the temperature of the thermostat was reduced rapidly. Both possibilities are considered in the following sections; the truth probably lies somewhere between the two extremes.

To obtain a valid comparison between solid and liquid, we must measure the frequency on the band edge for which solid and liquid have the same molar extinction coefficient. If the mass per unit area of the sample remains constant on freezing, $E(t = x\%)$ for the solid film may be compared directly with $E(t = x\%)$ for the liquid. If the thickness remains constant, $E(t = x\%)$ for the solid should be compared with $E(t = x'\%)$ for the liquid, where

$$\log (x'/100) = V_S/V_L . \log (x/100),$$

V_S and V_L being the molar volumes of solid and liquid salt respectively, at the melting-point.

Table 14.4. shows values of x' corresponding to x = 10% and 50% for the alkali nitrates, and to x = 4% for silver and thallous nitrates.

Figure 14.8 shows plots of $E(t = x\%)$ against temperature for sodium nitrate, for x = 10% and 50%. For the melt, both $E(t = x\%)$ and $E(t = x'\%)$ are plotted. The curves show variations in the region of the continuous transition similar to those recorded for E(2). The plot of $E(t = 10\%)$ is slightly steeper than that of $E(t = 50\%)$ between 20°C and 150°C; this indicates that the band edge became steeper as the temperature was raised. At the melting-point, both $E(t = x\%)$ and $E(t = x'\%)$ for the liquid were substantially higher than $E(t = x\%)$ for the solid, both for x = 10% and x = 50%. In this case there is no doubt that the band-edge moved to higher frequency when the salt was fused.

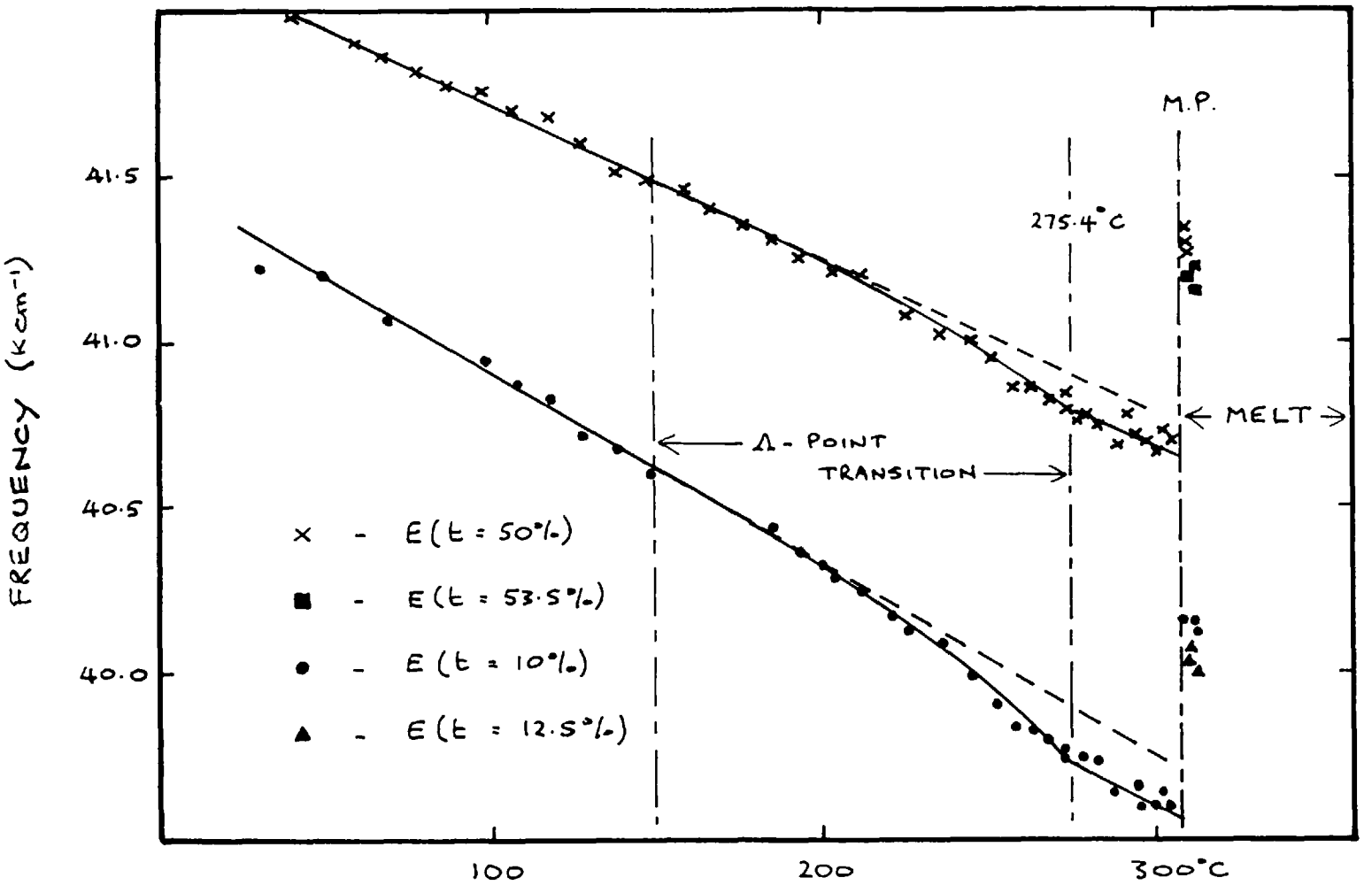


FIGURE 14.8. SPECTRAL PARAMETERS FOR SODIUM NITRATE.

TABLE 14.4. Values of V_S/V_L and x' for nitrates.

Salt	V_S/V_L	x' (x = 4%)	x' (x = 10%)	x' (x = 50%)
$NaNO_3$	0.9030(a)	-	12.5	53.5
KNO_3	0.9679(a)	-	10.8	51.1
$RbNO_3$	1.0023(a)	-	9.9	49.9
$CsNO_3$	0.8919(a)	-	12.8	53.9
$AgNO_3$	0.9931(b)	4.1	-	-
$TlNO_3$	0.9469(c)	4.7	-	-

(a) Reference 4.

(b) Reference 5.

(c) Calculated from the densities of the solid and liquid salt given in "International Critical Tables".

Figure 14.9 shows plots of E(t = 10%) and E(t = 30%) against temperature for solid potassium nitrate. The abrupt changes in these parameters at the transition-point are in the opposite sense to the corresponding change in E(2).

A separate experiment was carried out in the region of the melting-point. After melting and re-freezing twice, the sample was fused a third time and its thickness allowed to reach a steady value. Scans were carried out on the liquid film, then on the solid and finally on the liquid again. The values of E(t = 10%), E(t = 30%) and E(t = 50%) derived from the last set of measurements on the melt agreed well

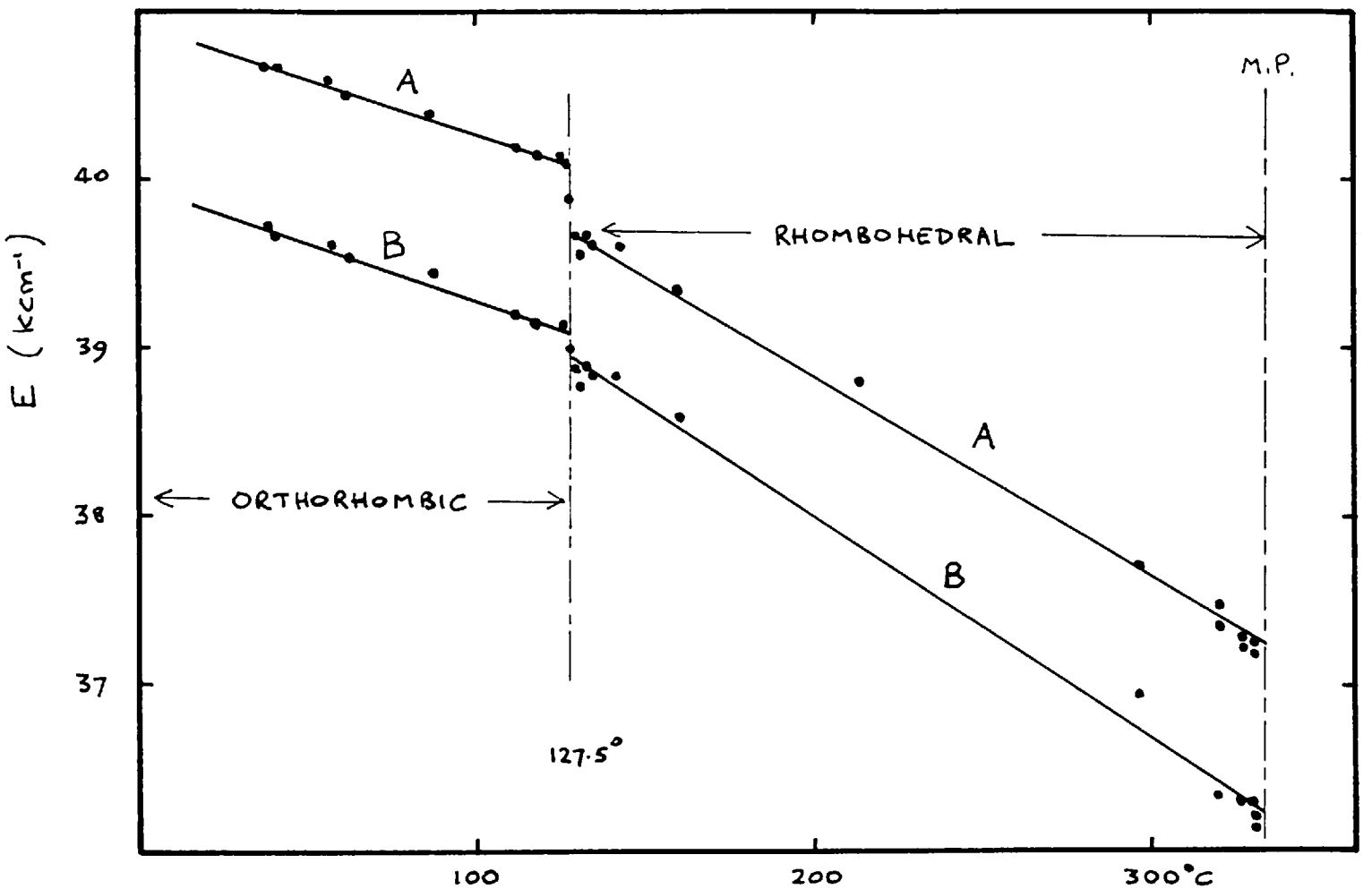


FIGURE 14.9. SPECTRAL PARAMETERS FOR SOLID POTASSIUM NITRATE.

A - E(t = 10%) B - E(t = 30%)

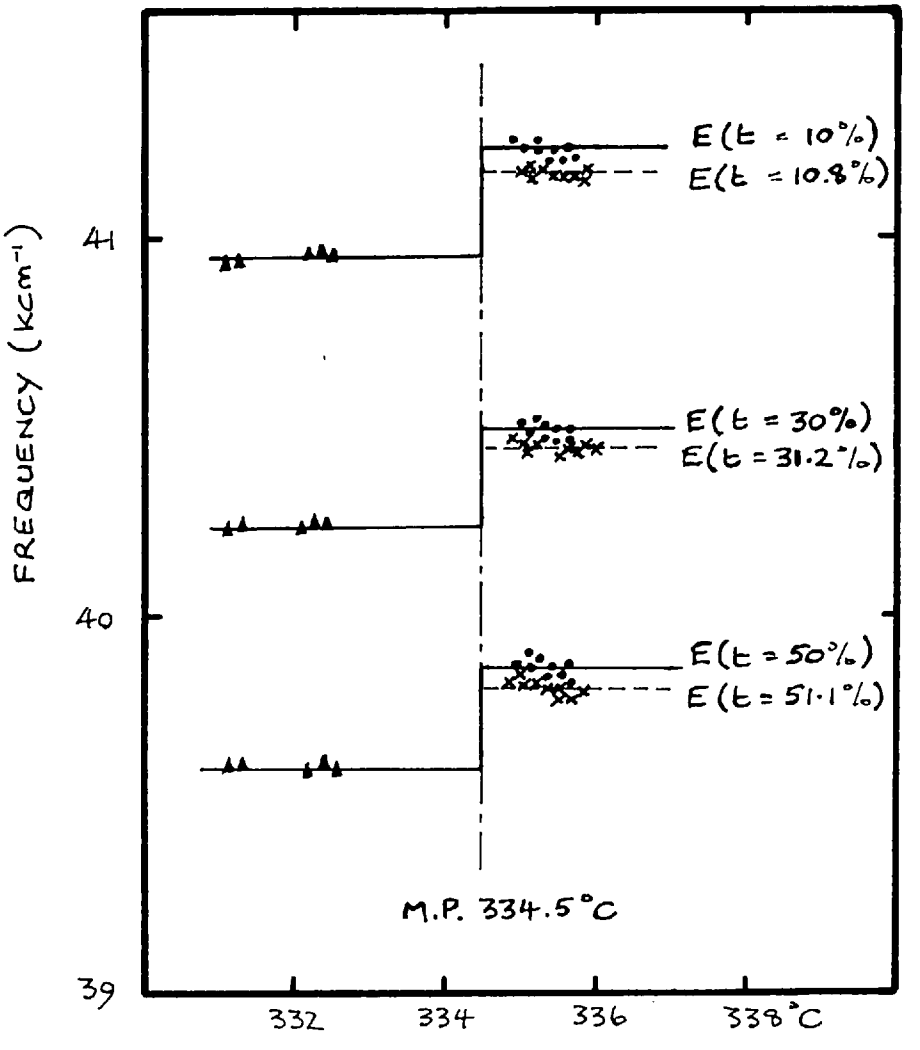


FIGURE 14.10 BAND-EDGE PARAMETERS FOR POTASSIUM NITRATE.

with those obtained from the first set, which demonstrates the reversibility of the movement of the band-edge at the melting-point. Figure 14.10 shows plots of E(t = x%) and E(t = x'%) against temperature, for x = 10, 30 and 50% and x' = 10.8, 31.2 and 51.1%. If the film retains the same thickness on fusion, the band-edge moves to higher frequency by 210 cm^{-1}; if the mass of salt per unit area of sample remains constant, the corresponding shift is 260 cm^{-1}.

For rubidium nitrate, V_S/V_L is so nearly unity that x and x' are practically identical. The overall change in E(t=10%) for the solid between 20°C and the melting-point was considerably less than the corresponding change in E(t = 50%); the band-edge therefore became less steep as the salt was heated. Abrupt changes in E(t = x%) were recorded at the transition-points; the changes depended on the value of x, and were not always in the same sense as the corresponding changes in E(2). Neither E(t = 10%) nor E(t = 50%) showed any abrupt change when the melting-point was traversed. (see Figures 14.11 and 14.12).

Figures 14.13 and 14.14 show the variation with temperature of E(t = 10%) and E(t = 50%) for solid ceasium nitrate. Both parameters were linear functions of temperature for each solid modification, and both changed in the same sense as E(2) at the transition-point. E(t = 10%) changed more than E(t = 50%) as the salt was heated from 20°C to 400°C; again, the band-edge became less steep as the temperature was raised.

A separate experiment was carried out in the region of the melting-point (using a different sample). The results are shown in Figure 14.15. Both E(t = 10%) and E(t = 50%) increased by about 100 cm^{-1} when the salt was fused; however, at the melting-point, E(t = 53.9%) and E(t = 12.8%) for the liquid were almost exactly equal to E(t = 50%) and E(t = 10%) for the solid, respectively. We conclude that, when this

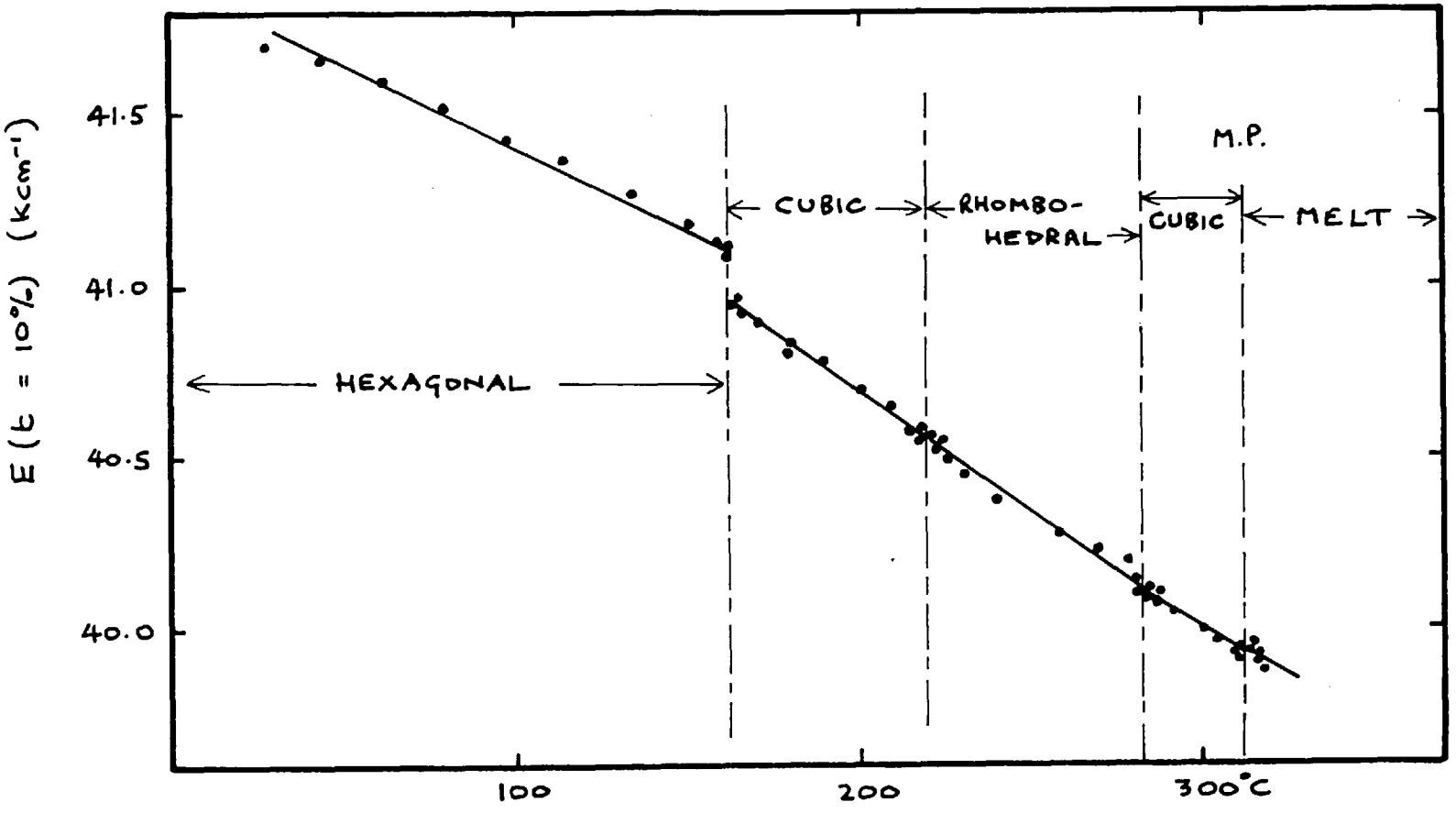


FIGURE 14.11. E(t = 10%) FOR RUBIDIUM NITRATE.

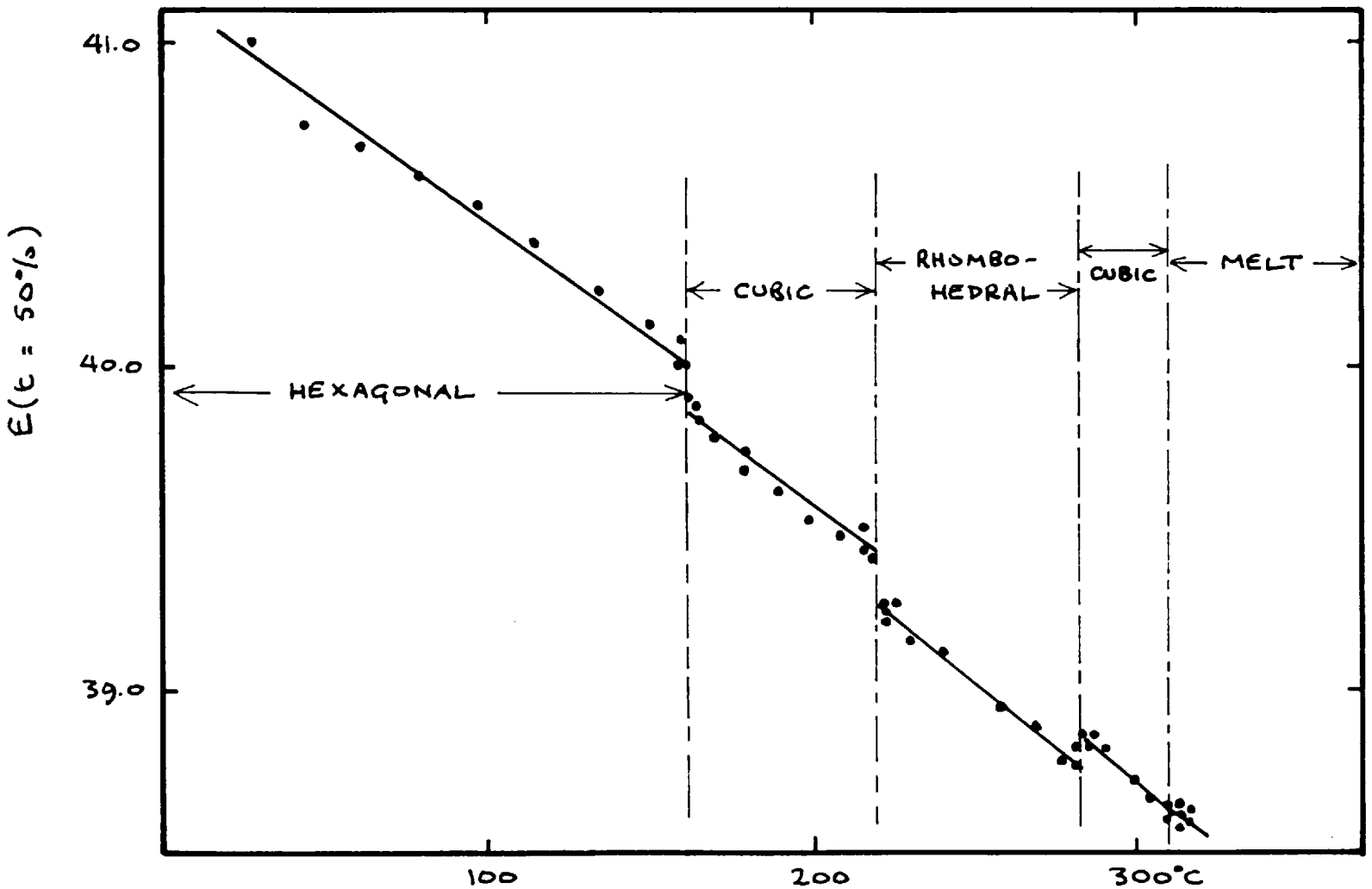


FIGURE 14.12. E(t = 50%) FOR RUBIDIUM NITRATE.

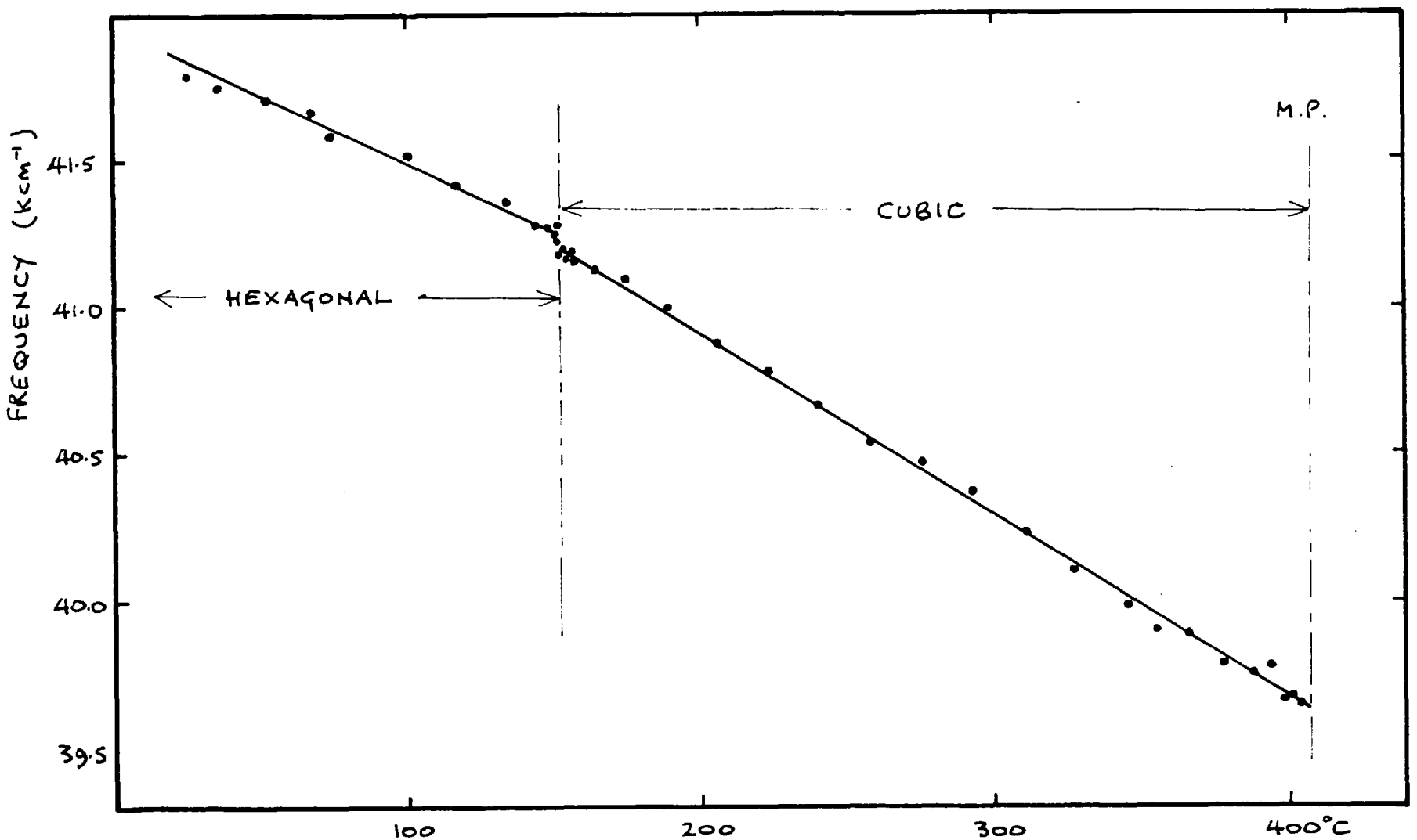


FIGURE 14.13. E(t = 10%) FOR SOLID CAESIUM NITRATE.

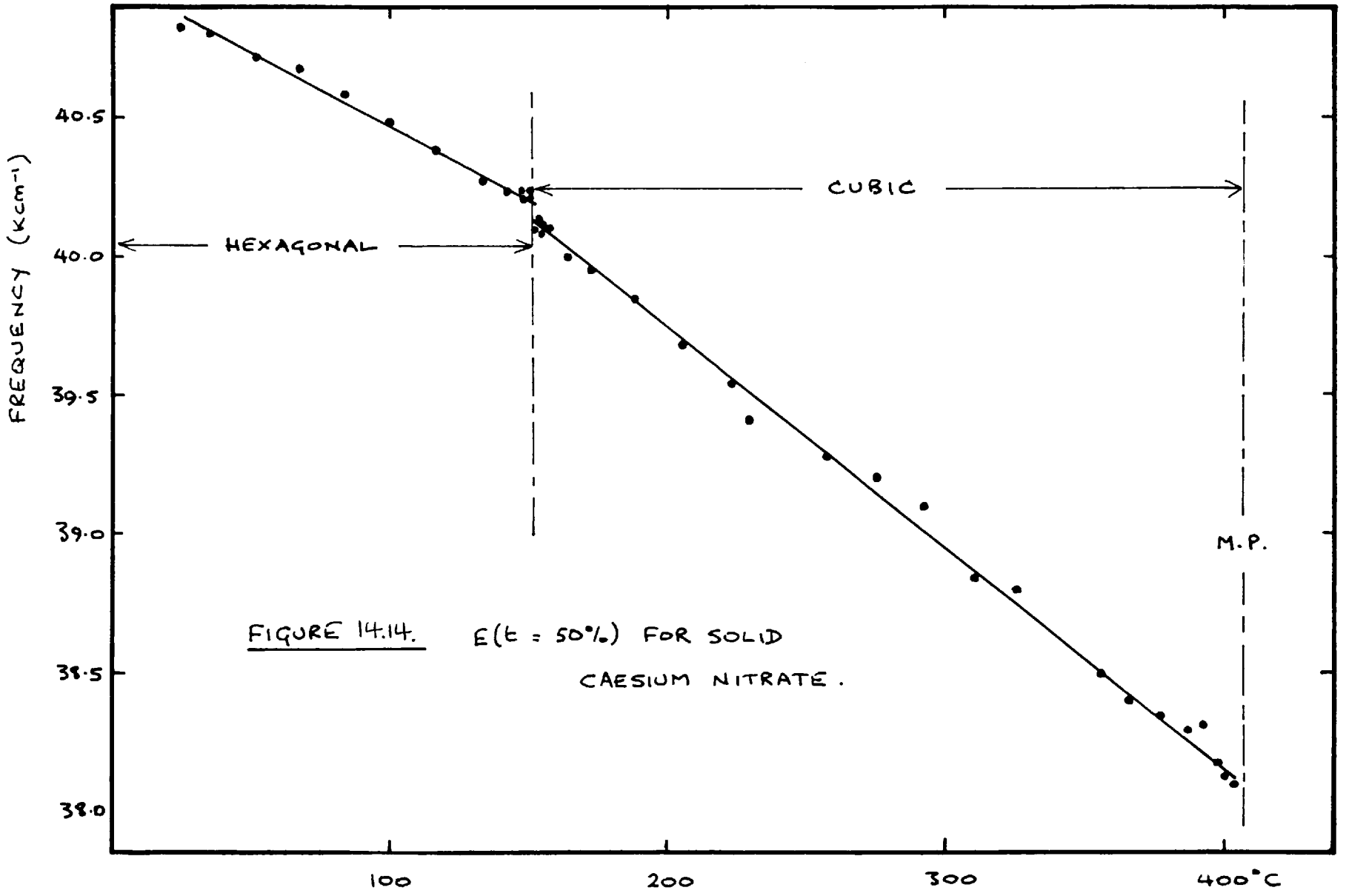
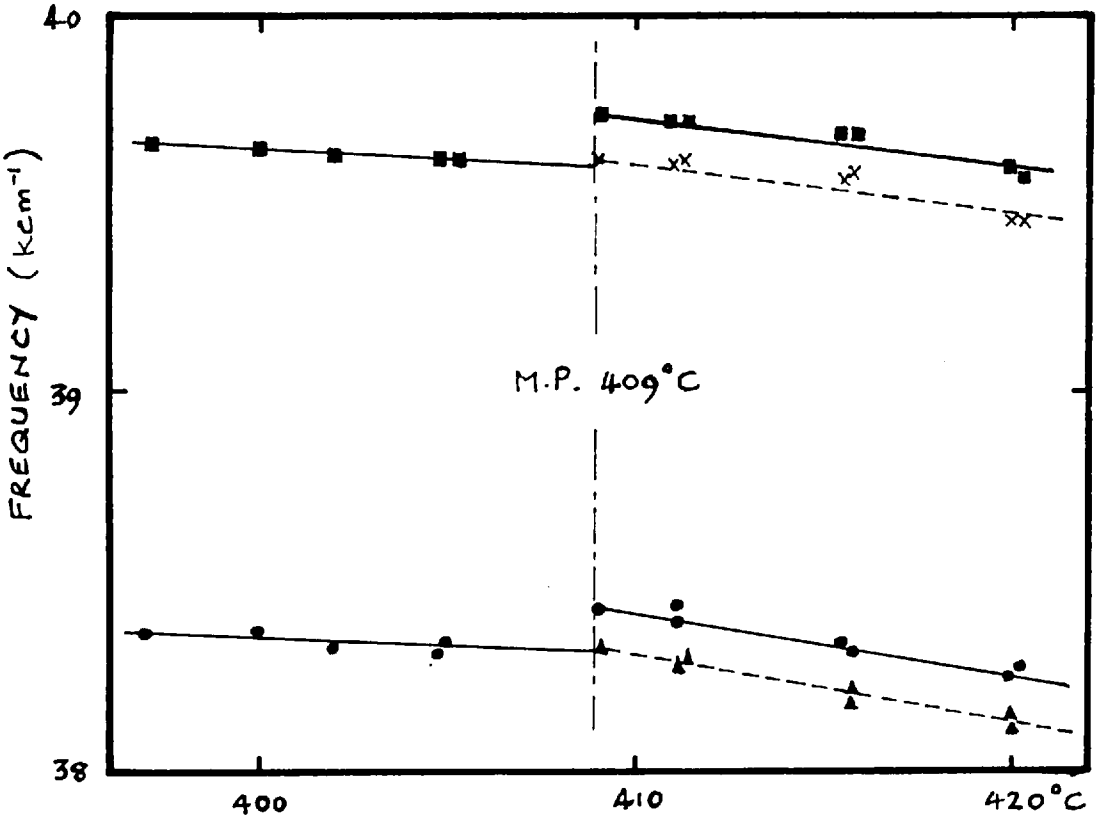


FIGURE 14.14. $\varepsilon(t = 50\%)$ FOR SOLID CAESIUM NITRATE.



● E (t = 50%)

▲ E (t = 53.9%)

■ E (t = 10%)

x E (t = 12.8%)

FIGURE 14.15 SPECTRAL PARAMETERS FOR CAESIUM NITRATE (RUNS 1580 - 1591)

salt was fused, the band-edge moved to higher frequency by between 0 and 100 cm^{-1}.

It must be emphasised that the movements of the low-energy edge of the strong band recorded above cannot be taken as an indication of the movements of the band maximum. The maximum (in aqueous solution) is at 50 kcm^{-1}, and the corresponding molar extinction coefficient is 10,000 litres/mole cm (Ref. 3). The present measurements were made at $\sim$40 kcm^{-1}, and extend only to a molar extinction coefficient of about 300 litres/mole cm.

14.6.2. Fused mixtures of potassium nitrate and barium nitrate.

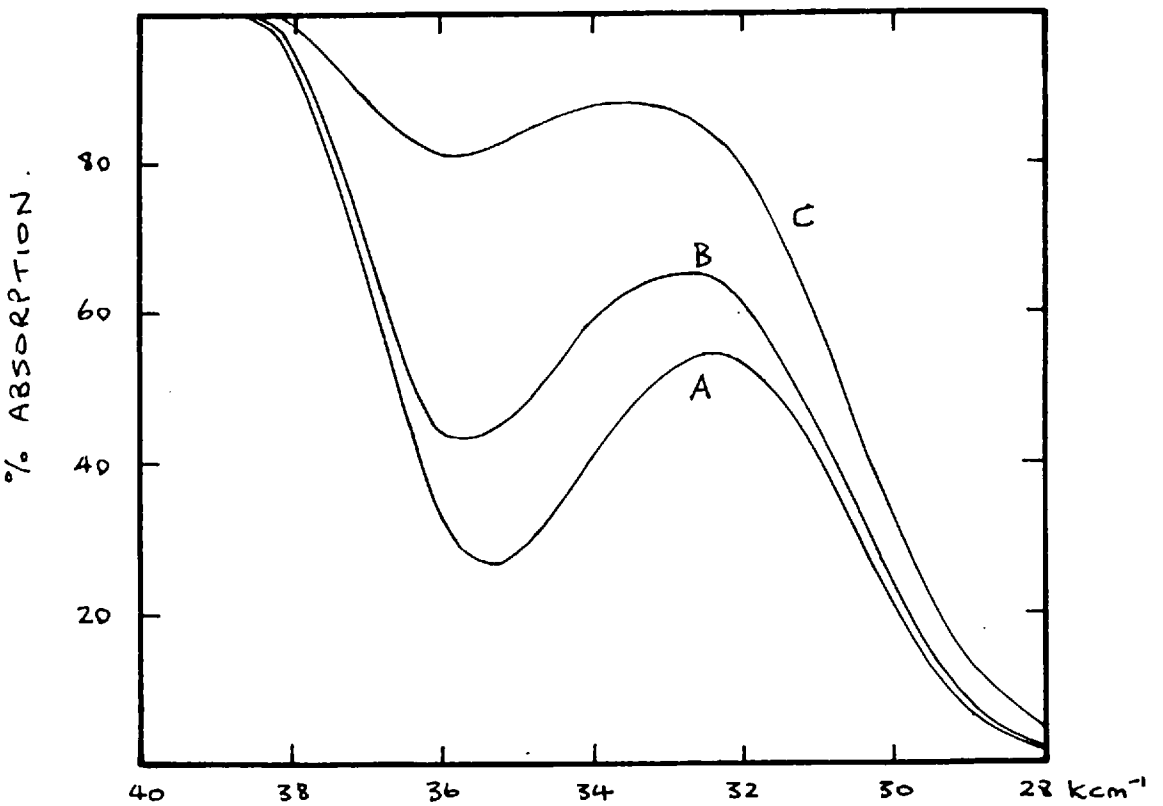
Some of the spectra obtained are shown in Figure 14.16, and Figure 14.17 shows plots of E(2) against temperature for each mixture. For a given composition, E(2) decreased linearly as the temperature was raised.

Figure 14.18 shows E(2) plotted against the equivalent fraction of barium in the mixture:-

(i) at constant temperature (440°C),

(ii) at constant equivalent volume (56.40 ml).

The values of E(2) for the different mixtures under conditions (i) and (ii) are listed in Table 14.5. The Table also shows the temperature at which the equivalent volume of each mixture is 56.40 ml (calculated from the results on page 214). When this temperature lay outside the range of the spectroscopic examination, E(2) was found by linear extrapolation of the plots of E(2) against T.

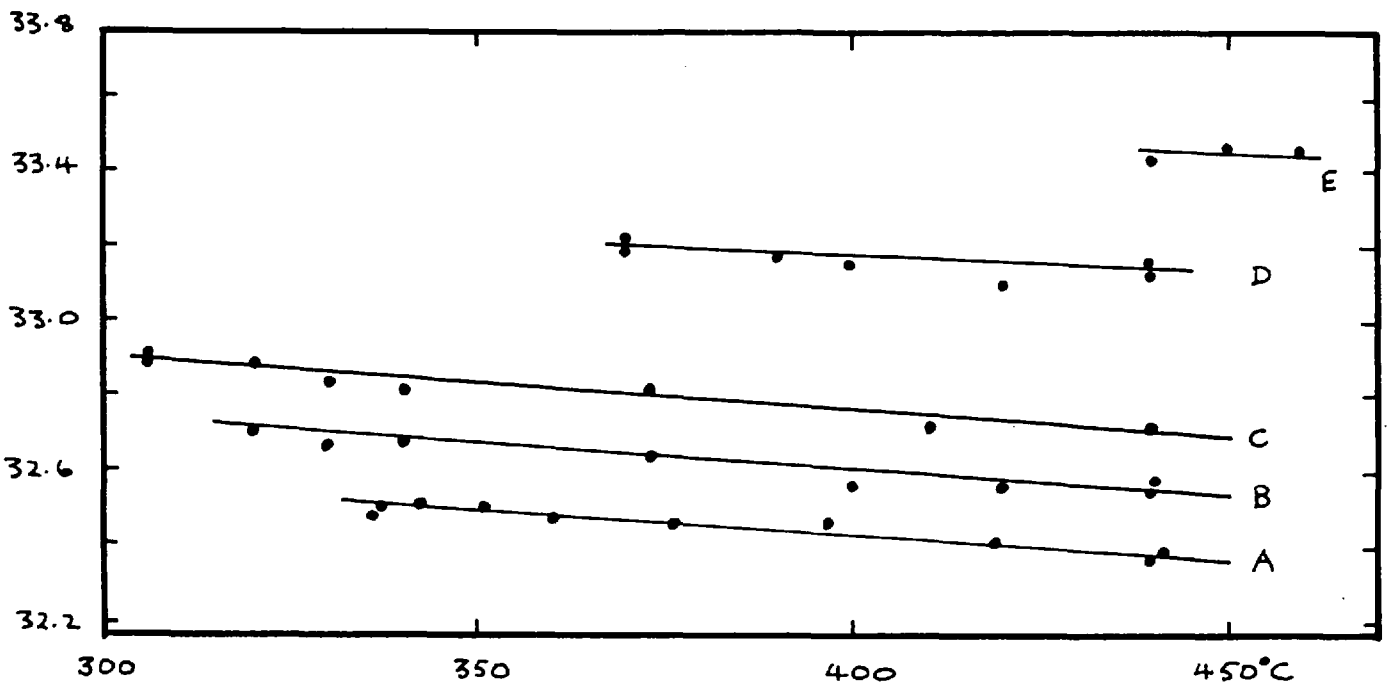


A - PURE KNO_3

B - 20 EQUIV. % $Ba(NO_3)_2$

C - 50 EQUIV. % $Ba(NO_3)_2$

FIGURE 14.16. ABSORPTION SPECTRA OF FUSED KNO_3 - $Ba(NO_3)_2$ MIXTURES.



A - PURE KNO_3

B - 10 EQUIV. % $Ba(NO_3)_2$

C - 20 EQUIV. % $Ba(NO_3)_2$

D - 35 EQUIV. % $Ba(NO_3)_2$

E - 50 EQUIV. % $Ba(NO_3)_2$

FIGURE 14.17. E(2) FOR POTASSIUM NITRATE - BARIUM NITRATE MIXTURES.

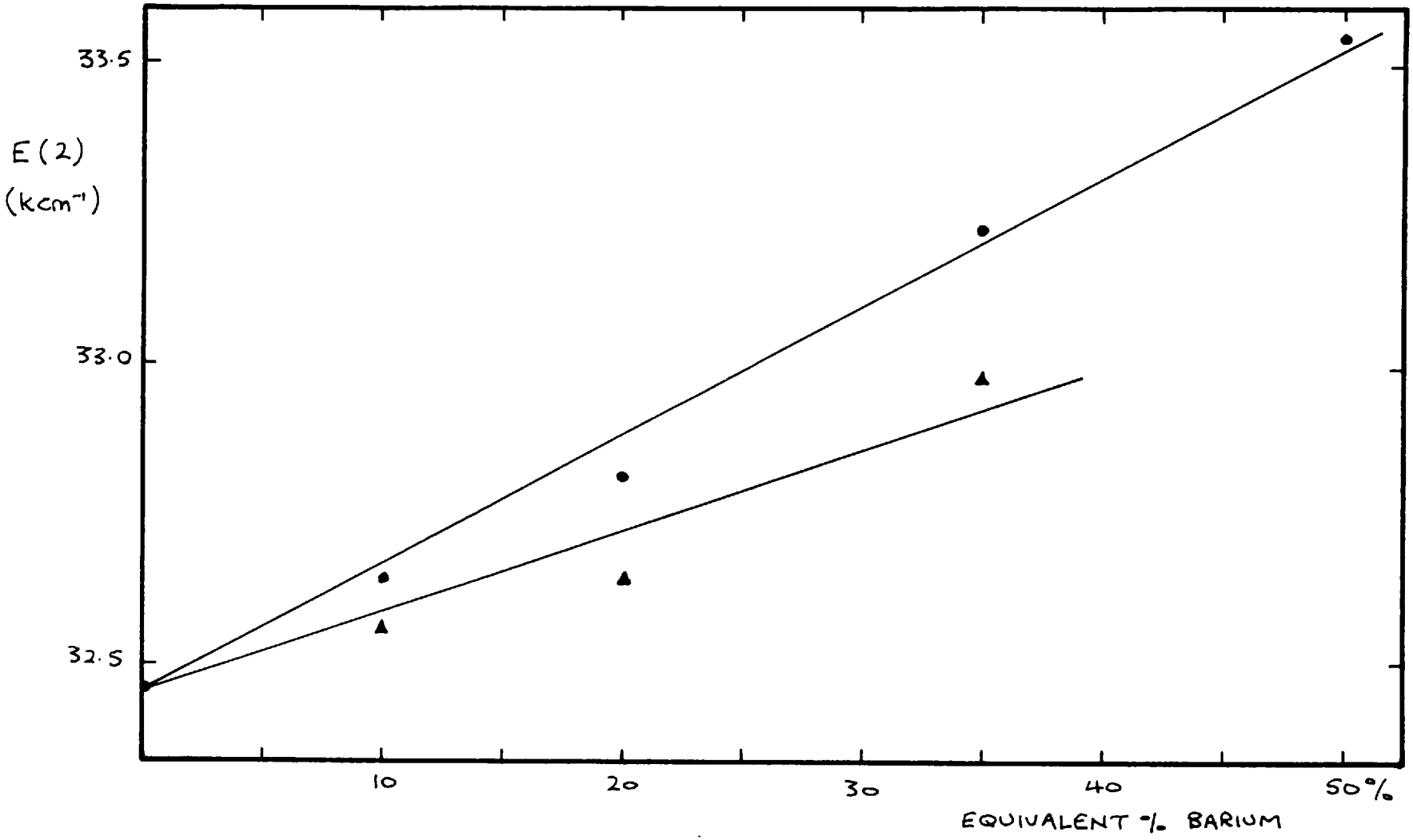


FIGURE 14.18. E(2) FOR FUSED KNO_3 - $Ba(NO_3)_2$ MIXTURES.

● - AT 440°C ▲ - AT EQUIVALENT VOLUME 56.40 ml.

TABLE 14.5. E(2) for potassium nitrate - barium nitrate mixtures.

Equiv % Ba^{++}	Temp. at which V_e = 56.40 ml.	E (2) (kcm^{-1})	
		at 440°C	at V_e = 56.40 ml.
0	440	32.42	32.42
10	503	32.60	32.52
20	567	32.77	32.60
35	685	33.18	32.93
50	-	33.50	-

14.6.3. Ammonium nitrate.

This salt has four stable crystalline modifications between room temperature and its melting-point. The crystal system and range of stability of each form is listed below.

FORM	CRYSTAL SYSTEM	RANGE OF STABILITY
(I)	cubic	125° to m.p.
(II)	tetragonal	85° to 125°
(III)	orthorhombic	35° to 85°
(IV)	orthorhombic	-18° to 35°

Some spectra of ammonium nitrate are illustrated in Figure 14.19, and they show that E(2) altered abruptly when a phase change occurred. However, the phase transformations did not all occur with equal facility; the changes (IV) $\longrightarrow$ (III) and (II) $\rightarrow$ (III) were relatively sluggish, and it was sometimes possible to superheat (IV) above 35°C and to supercool (II) below 85°C. Experiments were designed to demonstrate the relative ease with which the various transitions occurred, and these are now described in detail.

(a) Runs 993 - 1008. E(2) was measured as the sample was heated from 126°C to above the melting-point (169°C). E(2) increased abruptly on fusion, and returned to its original value when the sample was cooled to just below its freezing-point. The change in E(2) on melting is therefore reversible.

(b) Runs 1009 - 1030. Spectra were drawn as a fresh sample was cooled from 160°C through the transition temperature at 125°C. An abrupt increase in E(2) took place at 125°, indicating that the change (I) $\rightarrow$ (II) had occurred. On further cooling of the sample, E(2) underwent no abrupt change until the temperature reached 38°C, showing that form (II) can be supercooled below the (II) $\leftrightharpoons$ (III) equilibrium temperature at 85°C (see Figure 14.20).

(c) Runs 1031 - 1043. The same sample was cooled to 15°C, and left at this temperature overnight. Spectra were drawn as it was re-heated. No abrupt change in E(2) occurred at the (IV) $\leftrightharpoons$ (III) equilibrium temperature (35°C), and at 48° E(2) was still at the level characteristic of phase (IV). At 53°C E(2) increased abruptly, indicating that the change (IV) $\leftrightharpoons$ (III) had finally taken place (see Figure 14.21).

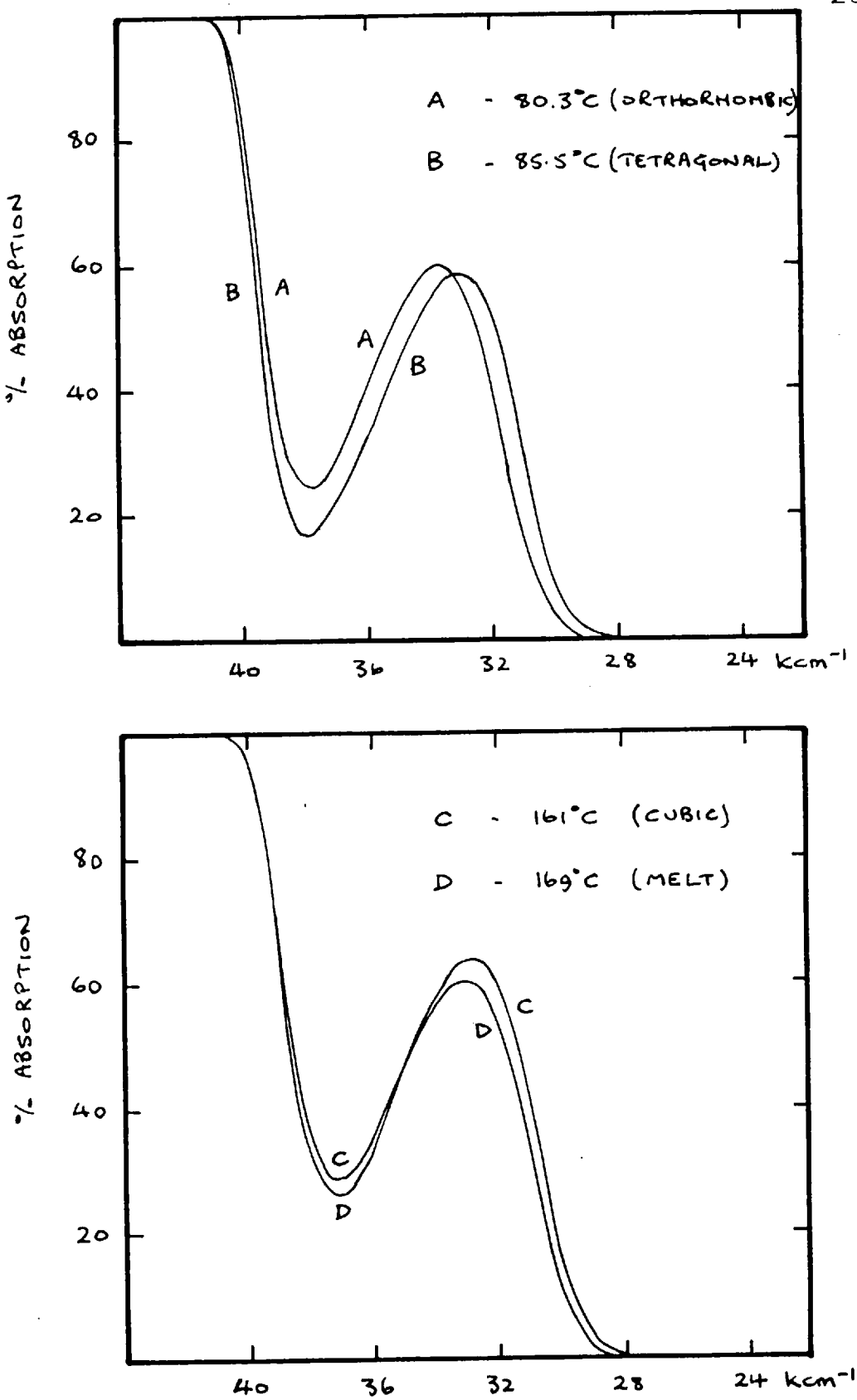


FIGURE 14.19 ABSORPTION SPECTRA OF AMMONIUM NITRATE.

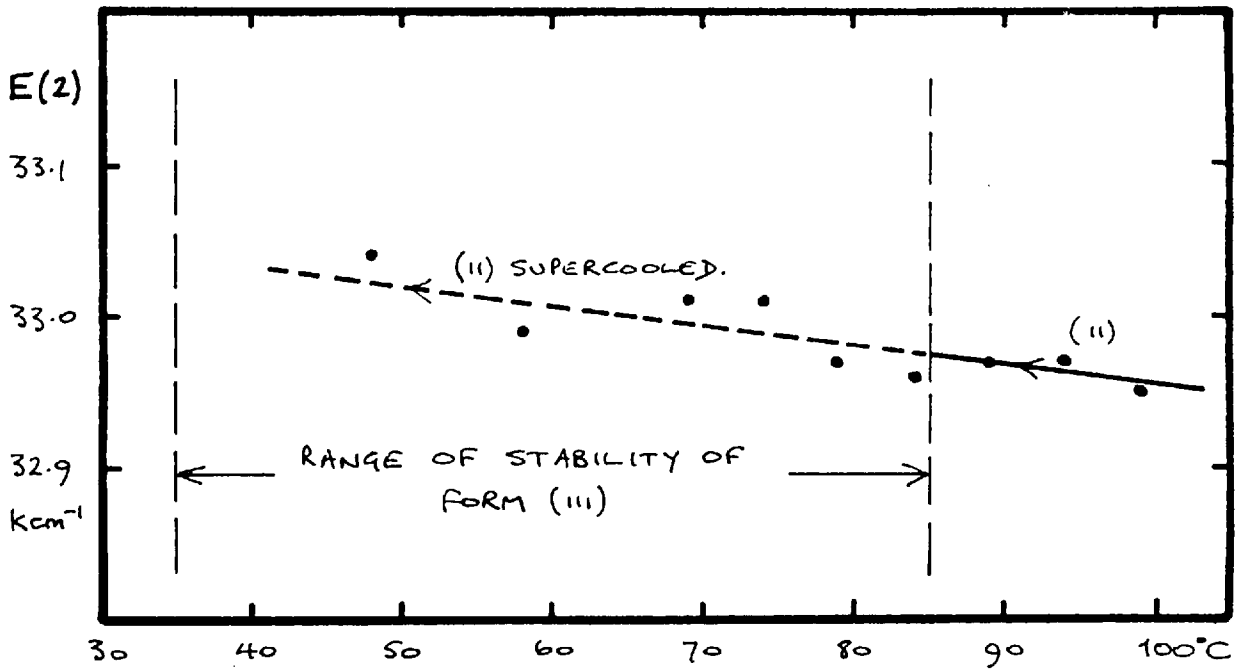


FIGURE 14.20 EXPERIMENT (b). (RUNS 1024 – 1029).

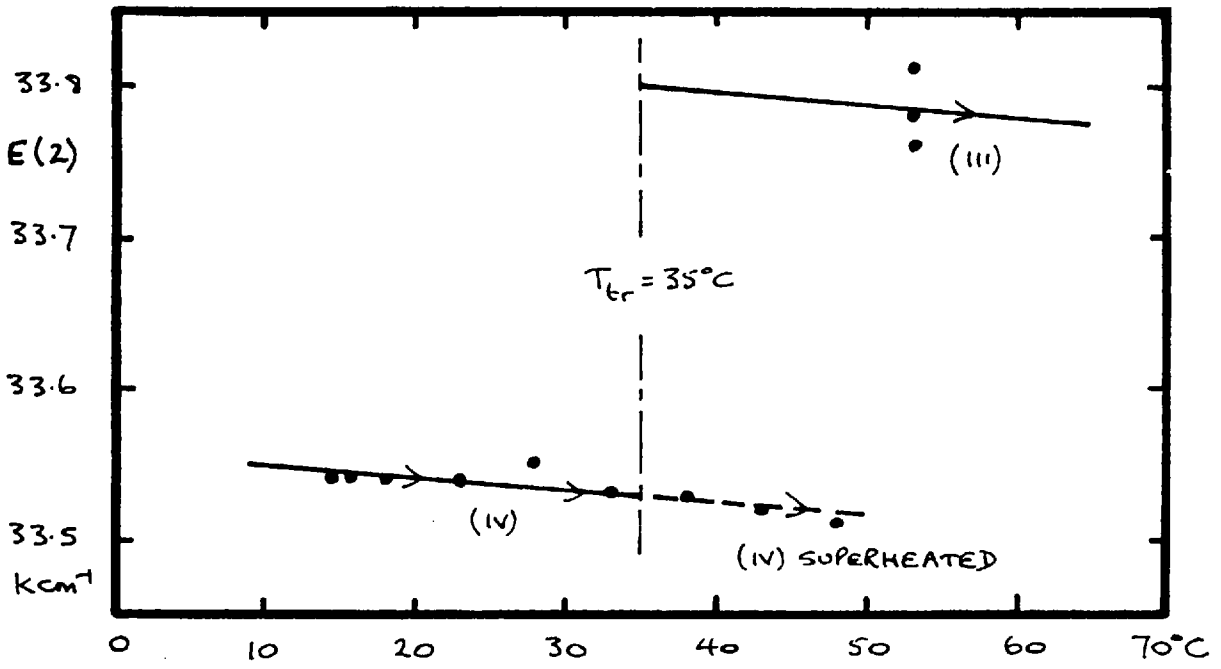


FIGURE 14.21 EXPERIMENT (c) (RUNS 1031 – 1043).

THE FULL LINES ARE TAKEN FROM FIGURE 14.24.

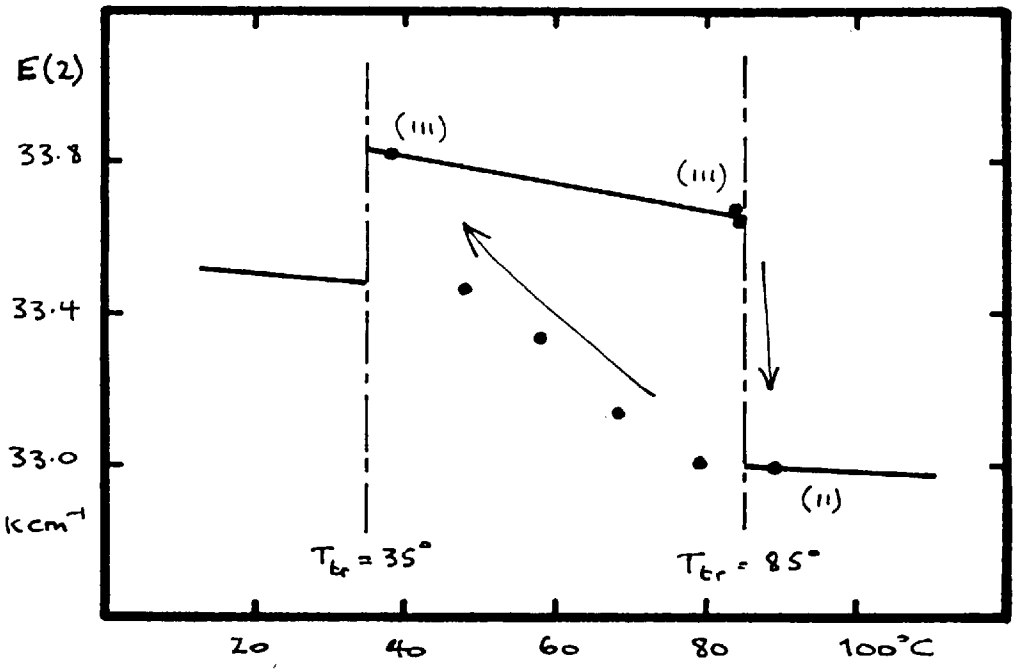


FIGURE 14.22. EXPERIMENT (d) (RUNS 1058 - 1065).

THE FULL LINES ARE TAKEN FROM FIGURE 14.24, AND THE ARROWS SHOW THE ORDER IN WHICH THE RESULTS WERE OBTAINED.

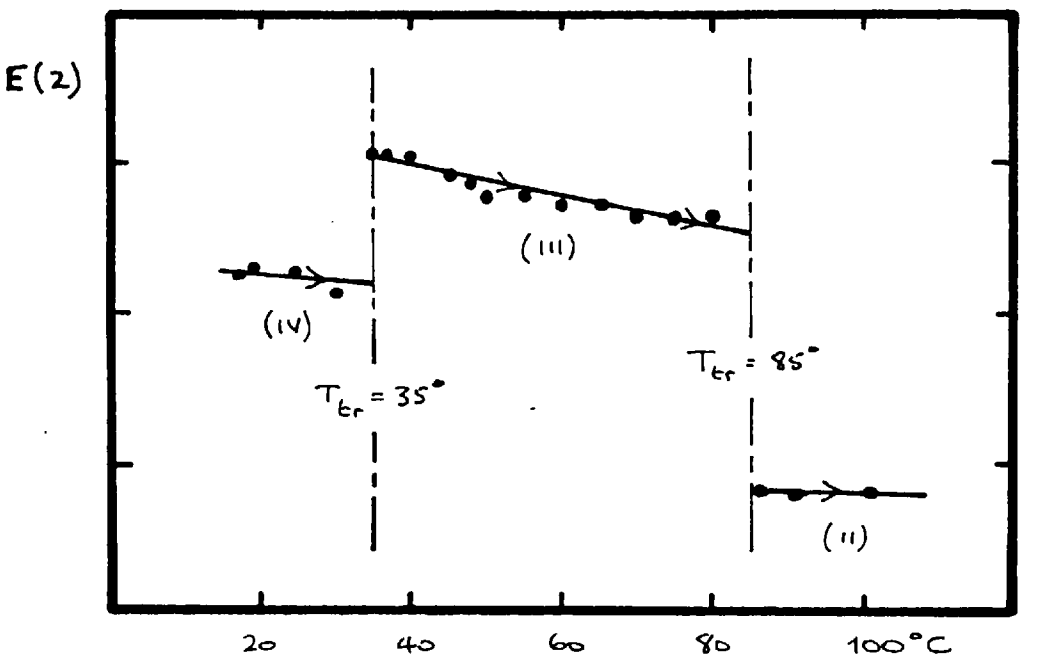


FIGURE 14.23. EXPERIMENT (e) (RUNS 1067 - 1086).

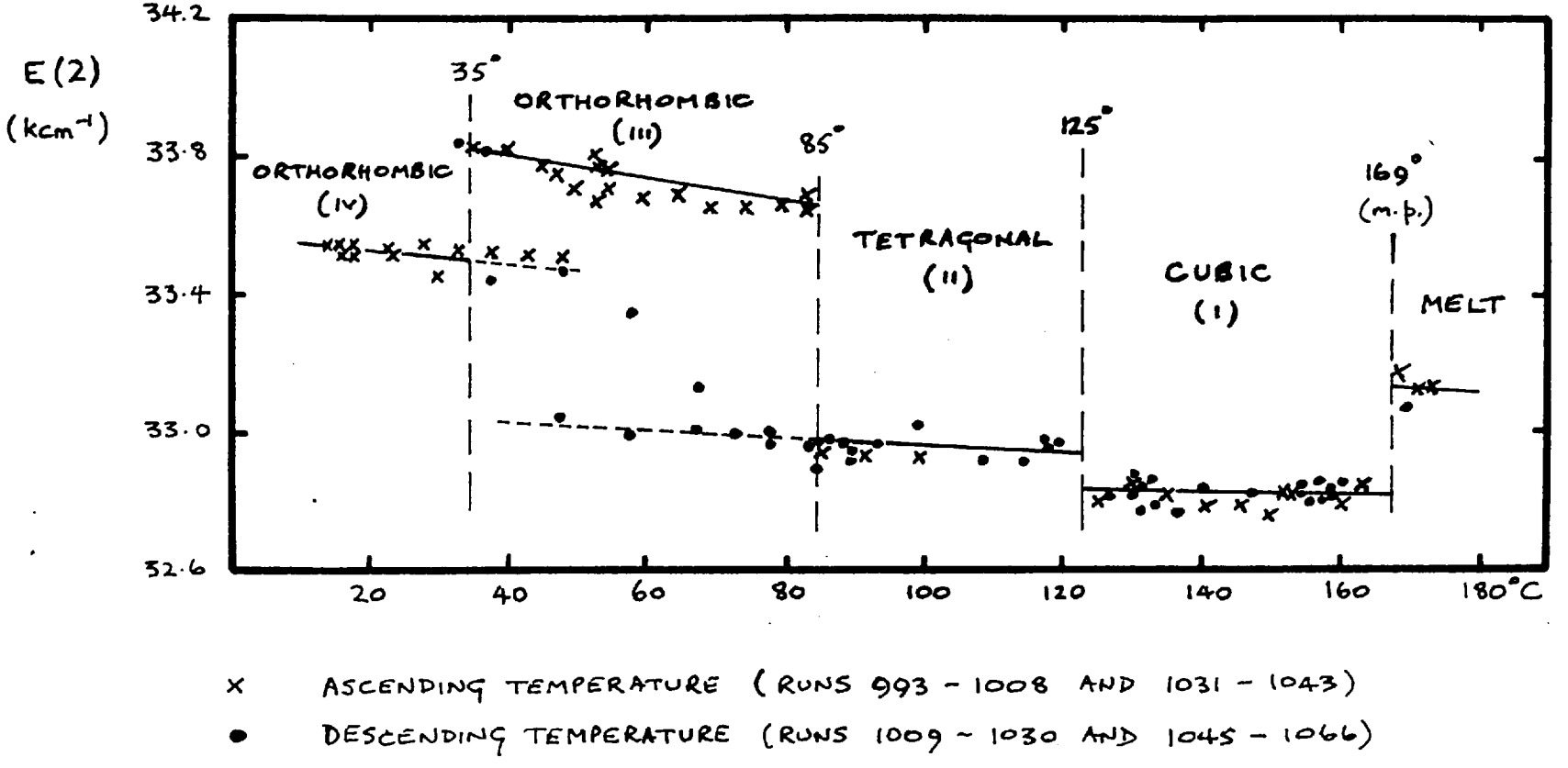


FIGURE 14.24 PLOT OF E(2) AGAINST TEMPERATURE FOR AMMONIUM NITRATE.

(d) Runs 1045 - 1066. The same sample was fused in the thermostat, and spectra were drawn as it was cooled. An abrupt increase in E(2) was recorded at 125°C, and was duly reversed when the sample was re-heated to 130°C. The salt was cooled to 85°C, at which temperature E(2) had a value characteristic of phase (II). The temperature was lowered to below 35°C and then raised to 84°C, after which E(2) had the high value associated with form (III) (Runs 1058 and 1059; see Figure 14.22). On heating the sample to 89°C, E(2) dropped abruptly by over 600 cm^{-1} as the (III) → (II) transformation took place. Runs 1061 to 1065 were then carried out as the salt was cooled from 89° to 38°C at a rate of 1°C per minute. During the 50 minutes which this occupied, E(2) gradually increased from 33.00 kcm^{-1} (characteristic of phase (II)) to 33.82 kcm^{-1} (characteristic of phase (III); see Figure 14.22). This indicates that even after the recrystallisation process had been nucleated the (II) → (III) transformation required about an hour to reach completion.

(e) Runs 1067 - 1086 were carried out on a new sample, which was heated from 19°C to 100°C. E(2) increased abruptly at 35°C and decreased abruptly by over 600 cm^{-1} at 85°C, showing that the changes (IV) → (III) and (III) → (II) had taken place at these temperatures (see Figure 14.23). The changes were complete in less than five minutes.

Figure 14.24 shows all the values of E(2) obtained in the above experiments, plotted against temperature on a single diagram.

It is clear from experiments (b), (c) and (d) that form (IV) and form (II) can be superheated and supercooled, respectively, into the temperature range in which (III) is

the most stable modification. However, in experiment (e) the changes (IV) → (III) and (III) → (II) took place without delay at the respective transition temperatures. This difference in behaviour is probably caused by a difference in the state of dryness of the two samples. The sample used in experiments (b), (c) and (d) was transferred directly from the hotplate on which it was prepared to the thermostat at 140°C, and was then melted in situ. It was again melted and re-frozen for run 1045, so would be expected to be extremely dry during runs 1061 to 1065 when the slow change from (II) to (III) was observed. In contrast, the sample used in runs 1067 to 1086 had been fused only once (during its preparation on the hotplate), and was transferred to the thermostat at 19°C. It could therefore have contained traces on moisture, which would assist the changes (IV) → (III) and (III) → (II) by allowing them to take place by way of an aqueous solution.

Experiments (b) and (d) show that transformations between forms (I) and (II) take place freely at 125°C, in either sense, irrespective of the state of dryness of the sample.

The relative slowness with which (III) grows from (II) or (IV) in a dry sample can be understood in terms of the structures of the four modifications; a detailed discussion is given in Chapter 18.

Spectrum of fused ammonium nitrate.

It has been reported in the literature that the absorption spectrum of fused ammonium nitrate in the range 50 - 38 kcm^{-1} is quite unlike that of any other nitrate . Keenan (Ref 6; quoted by Smith and Boston in Ref 7) recorded some bands in the region 38 - 45 kcm^{-1} (where the alkali nitrate melts have very strong absorption); at least three bands were found,

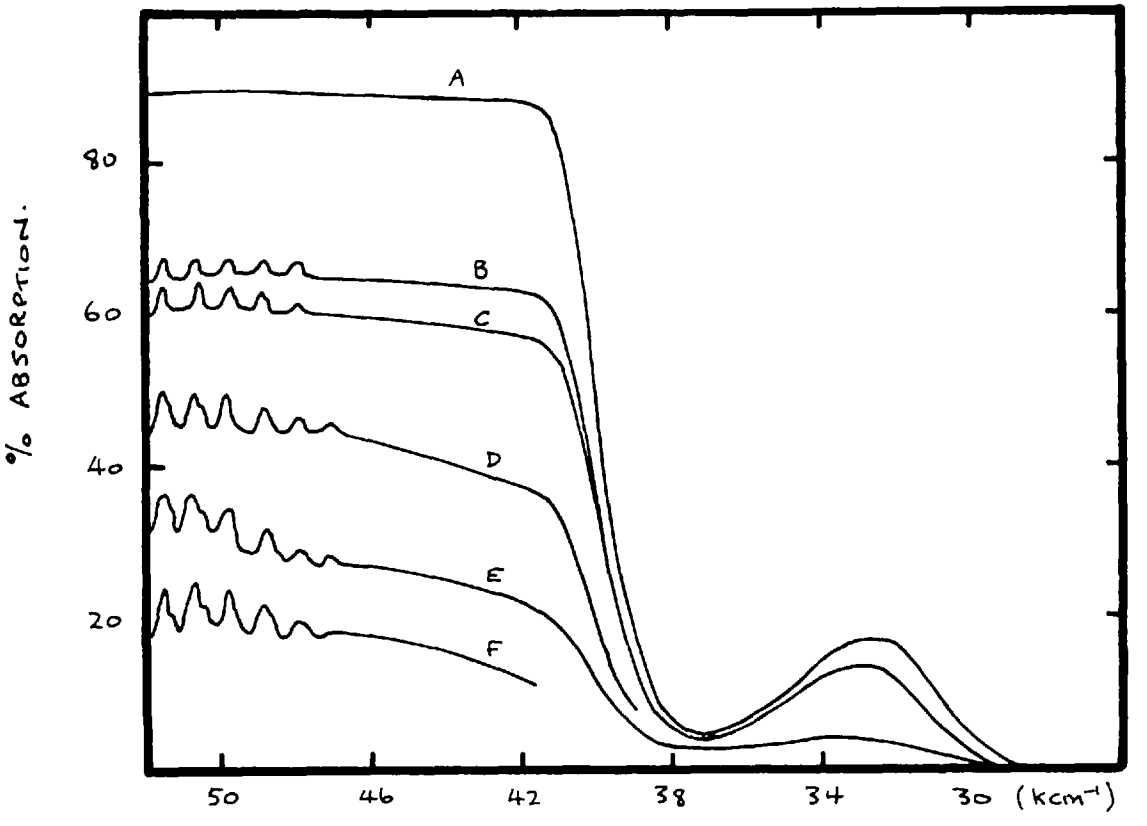
having extinction coefficients "not much greater than that of the weak band at 33 kcm^{-1}".

The experiment described below suggests that these bands were not due to ammonium nitrate but to some decomposition product, and that the spectrum of pure fused ammonium nitrate substantially resembles those of the alkali metal nitrates.

A solid sample of the salt was made up, and its spectrum recorded. The spectrum showed the weak band at 33 kcm^{-1}, and a steep absorption edge at about 40 kcm^{-1}. Complete absorption was recorded between 40 and 50 kcm^{-1}. When the sample was fused some transmission was recorded in the latter region, but this was because some gas bubbles were forming and were displacing the melt. The transmission increased as the bubbles accumulated, and the spectra began to show band structure which became more pronounced as decomposition proceded. Spectra of the melt (at 170°C) at successive stages in the decomposition are shown in Figure 14.25; the total observation period was about two hours.

The frequencies of the band maxima are listed in Table 14.6. The substance responsible for the bands can be identified with confidence as ammonia; the frequencies in Table 14.6 agree closely with the data recorded for this gas by Duncan (Ref 8), which are reproduced in Table 14.7.

The possibility that the bands are due to nitrous oxide is definitely excluded, because this gas is known to have no banded absorption in the frequency range in question (Ref 9). Nitrous oxide is the normal decomposition product of fused ammonium nitrate, and the bubbles in the molten salt film probably contained some of this gas. The ammonia would be formed by simple dissociation of the ammonium nitrate.



A - IMMEDIATELY AFTER FUSION

F - AFTER TWO HOURS.

FIGURE 14.25 ABSORPTION SPECTRA RECORDED FOR A THIN FILM OF AMMONIUM NITRATE MELT, AT SUCCESSIVE STAGES OF DECOMPOSITION (A ... F).

TABLE 14.6. Frequencies of band maxima in decomposing ammonium nitrate melt.

Run number	Frequencies of band maxima (kcm^{-1})						
981	52.35	51.52	50.60	49.76	48.86	47.85	47.00
983	52.35	51.55	50.61	49.69	48.80	47.89	-
984	52.28	51.48	50.60	49.70	48.80	47.86	-
985	52.39	51.60	50.70	49.80	48.89	48.00	-
986	52.38	51.48	50.65	49.78	48.83	47.89	47.00
987	52.38	51.52	50.65	49.75	48.84	47.90	47.03
988	52.36	51.54	50.65	49.76	48.85	47.89	-
Mean values	52.36	51.53	50.64	49.75	48.84	47.90	47.01

Leifson	Dixon	Duncan	Present work
44.247	-	-	-
45.246	-	-	-
46.157	46.140	46.126	-
-	46.200	46.202	-
47.003	47.030	47.010	47.01
-	47.090	47.069	-
47.869	47.925	47.914	47.90
-	47.975	47.962	-
48.768	48.890	48.803	48.84
-	-	48.868	-
49.686	49.790	49.712	49.75
50.556	50.675	50.663	50.64
51.440	51.600	51.555	51.53
52.317	52.407	52.501	52.36
(etc.)			

TABLE 14.7. Frequencies (kcm^{-1}) of maxima of diffuse bands in the absorption spectrum of gaseous ammonia (from Duncan (Ref 8), who quotes the results obtained by Leifson and by Dixon). The figures in the fourth column are the mean frequencies of the band maxima in the spectrum of decomposing ammonium nitrate melt, taken from the Table on the previous page.

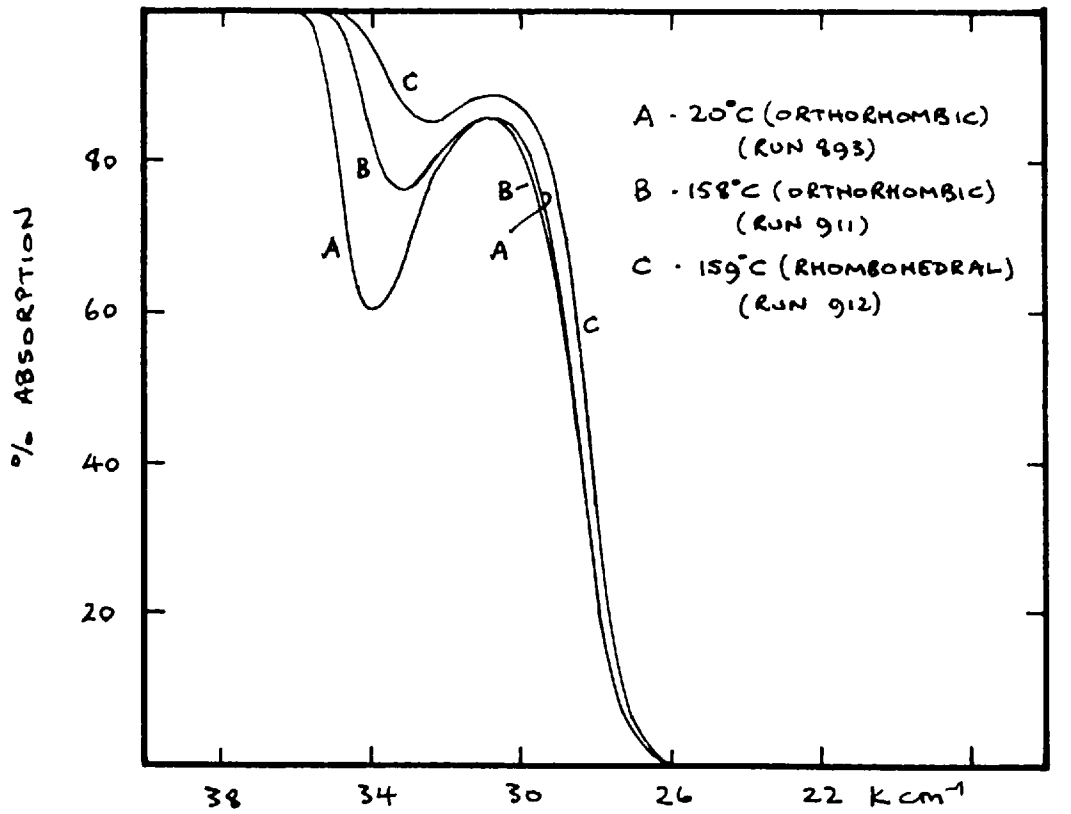
14.6.4. Silver nitrate.

Some spectra of this salt are shown in Figure 14.26. Both the maximum of the weak band and the edge of the strong band were at lower frequency than they were for the alkali-metal nitrates. As the temperature was raised, the edge of the strong band overlapped more and more with the weak band; just below the melting-point the maximum of the latter was barely discernible, and in the melt the weak band appeared only as a shoulder.

The frequency at 4% transmission, E(t = 4%), was used to characterise the low-energy edge of the strong band. Since silver nitrate undergoes only a small (0.7%) density decrease on fusion (see Table 14.4), the results for the melt may be compared directly with those for the solid salt. Part (iii) of Figure 14.27 shows that E(t = 4%) decreased linearly as the salt was heated from 20°C to the transition-point (158°C). It decreased abruptly when the transition occurred, and continued to decrease as the sample was heated further, with some acceleration as the melting-point was approached. A small, abrupt drop in E(t = 4%) took place when the sample melted.

Part (i) of the Figure shows the variation with temperature of E(2), the frequency of the maximum of the weak band (uncorrected for the effect of overlap with the strong band). E(2) increased when the solid was heated from 20°C to 158°C, decreased abruptly when the transition took place and increased further as the melting-point was approached. E(2) could not be measured above the melting-point, where the weak band appeared only as an inflexion on the edge of the strong band.

Because of the progressive overlap of the weak band by



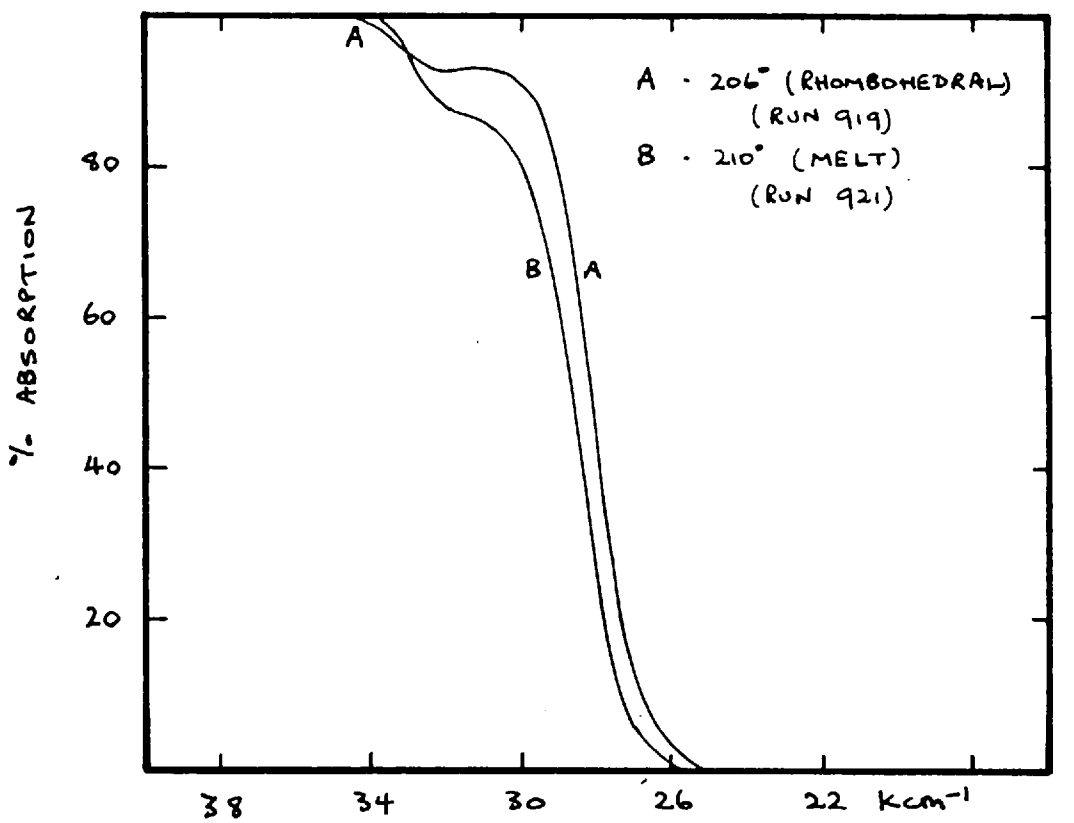


FIGURE 14.26 ABSORPTION SPECTRA OF SILVER NITRATE.

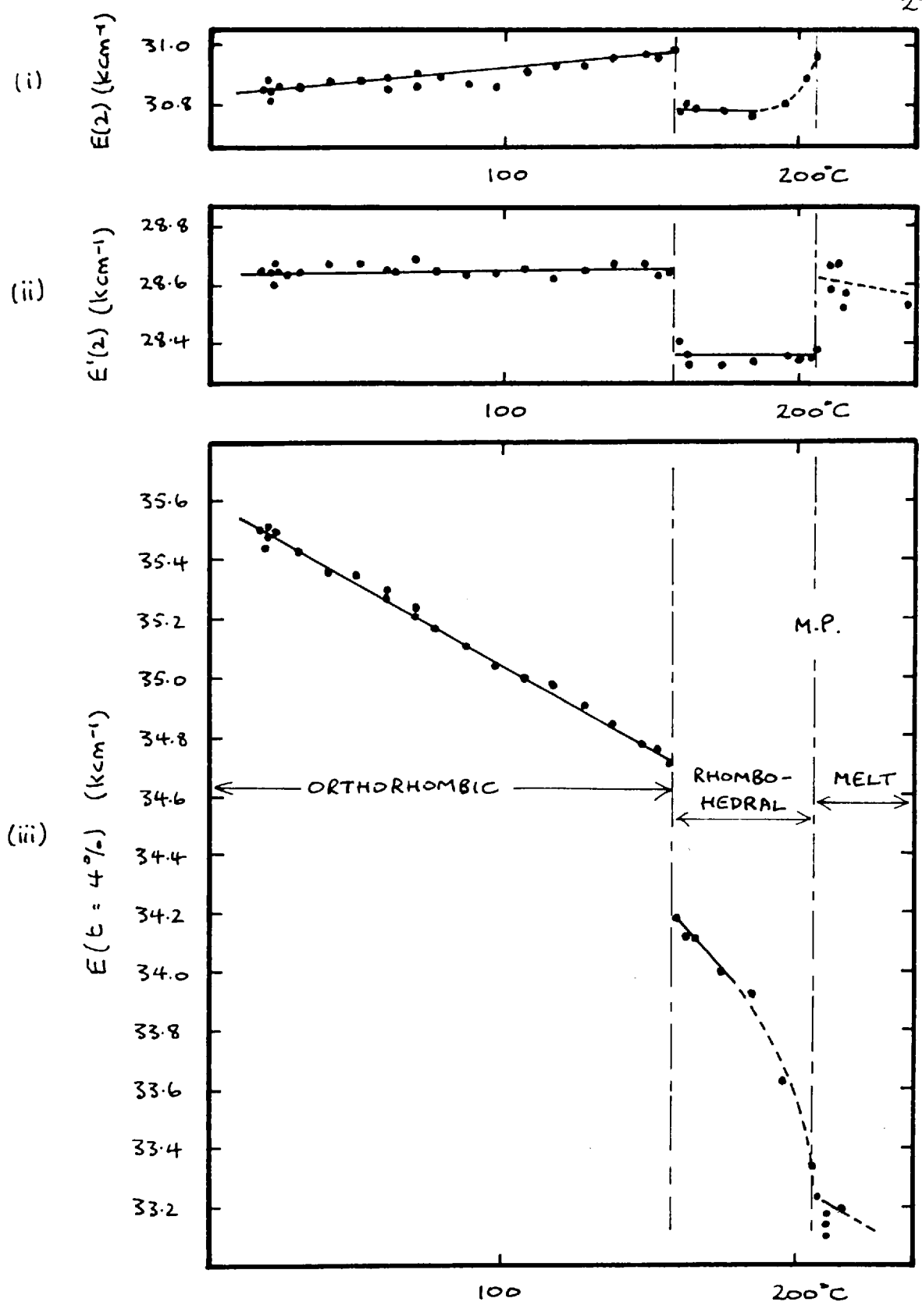


FIGURE 14.27 SPECTRAL PARAMETERS FOR SILUER NITRATE.

(RUNS 887 - 929)

the low-frequency edge of the strong band, these variations in E(2) are not a reliable indication of the changes in the frequency of the true maximum of the weak band, (i.e. of the maximum which would be observed if the weak band could be recorded separately from the strong band). If the weak band were recorded in isolation, and the edge of the strong band then superimposed on it, the maximum of the composite absorption curve, E(2), would be at higher frequency than the maximum of the weak band alone, the displacement increasing with the extent of overlap. A progressive movement of the strong band edge to lower frequency could therefore cause the composite maximum to move to higher frequency.

In the case of silver nitrate, the edge of the strong band does in fact move to lower frequency as the temperature is raised (see part (iii) of Figure 14.27). This is probably the cause of the increase in E(2) which is observed when the salt is heated from 20°C to 158°C. It is possible that the true maximum of the weak band moves to lower frequency with rising temperature, as it does for the alkali-metal nitrates.

In order to obtain more reliable information on the movements of the weak band, some measurements were made on its low-frequency edge, where the effect of overlap with the strong band is relatively slight. The parameter E'(2) is defined as the frequency on the low-energy edge of the band for which the extinction coefficient ϵ is 0.3 times the extinction coefficient at the band maximum. A plot of E'(2) against temperature is shown in Figure 14.27, part (ii). E'(2) did not change as the sample was heated from 20° to 158°C. It fell abruptly at the transition-point, remained constant between 158° and 206° and increased abruptly as the salt was fused. These changes in E'(2) are believed to be a better indication of the movements of the weak band than are the corresponding changes in E(2).

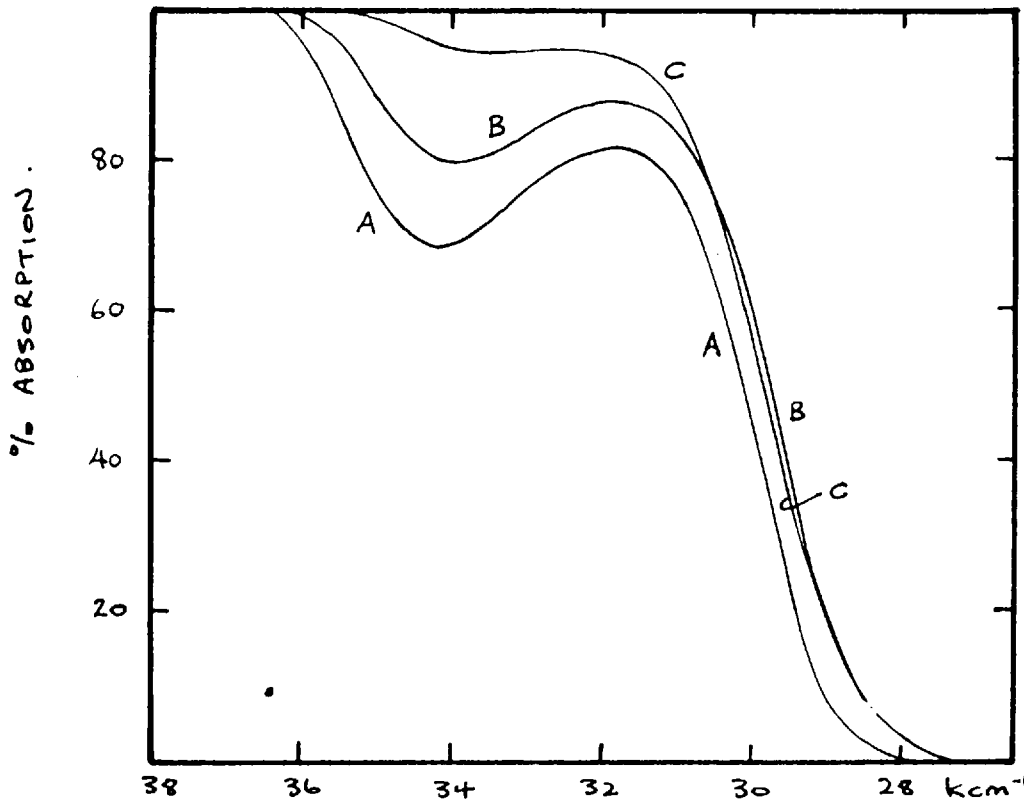
14.6.5. Thallous nitrate.

Some spectra are illustrated in Figure 14.28. Again, the observation of the weak band was seriously hampered at higher temperatures by the overlapping edge of the strong band. In the melt, the maximum of the weak band was almost obscured.

Two sets of results were obtained, using different samples (listed as samples 2 and 3 in Appendix C). In the case of sample 3, precautions were taken to ensure that the thickness (or mass per unit area) of the sample did not change on fusion. No such precautions were taken with sample 2.

The low-energy edge of the strong band was characterised by the parameter $E(t = 4\%)$, which is the frequency at which the transmission is 4%. A plot of $E(t = 4\%)$ against temperature (Figure 14.30, part (iii)) shows that the band-edge moved to lower frequencies as the salt was heated; the rate of movement ($dE(t = 4\%)/dT$) was practically the same for the three solid phases, and any abrupt changes in $E(t = 4\%)$ at the transition points were too small to be detected.

Since thallous nitrate undergoes a density increase of about 6% on freezing (see Table 14.4), an uncertainty arises as to whether the thickness or the mass of salt per unit area of the sample remains constant when a sample is frozen. $E(t_S = 4\%)$ should be compared with $E(t_L = 4.7\%)$ if the thickness is unchanged on freezing, or with $E(t_L = 4\%)$ if the mass of salt per unit area remains constant. (Subscripts S and L indicate solid and liquid salt respectively). In order to define the limits of the actual behaviour, both possibilities have been considered; part (iii) of Figure 14.30 shows that, whichever is correct, the band-edge moves to lower frequency by $\sim$1,000 cm^{-1} on fusion of the sample.



A - 20°C (RHOMBIC)

B - 204°C (CUBIC)

C - 208°C (MELT)

FIGURE 14.28 ABSORPTION SPECTRA OF THALLOUS NITRATE.

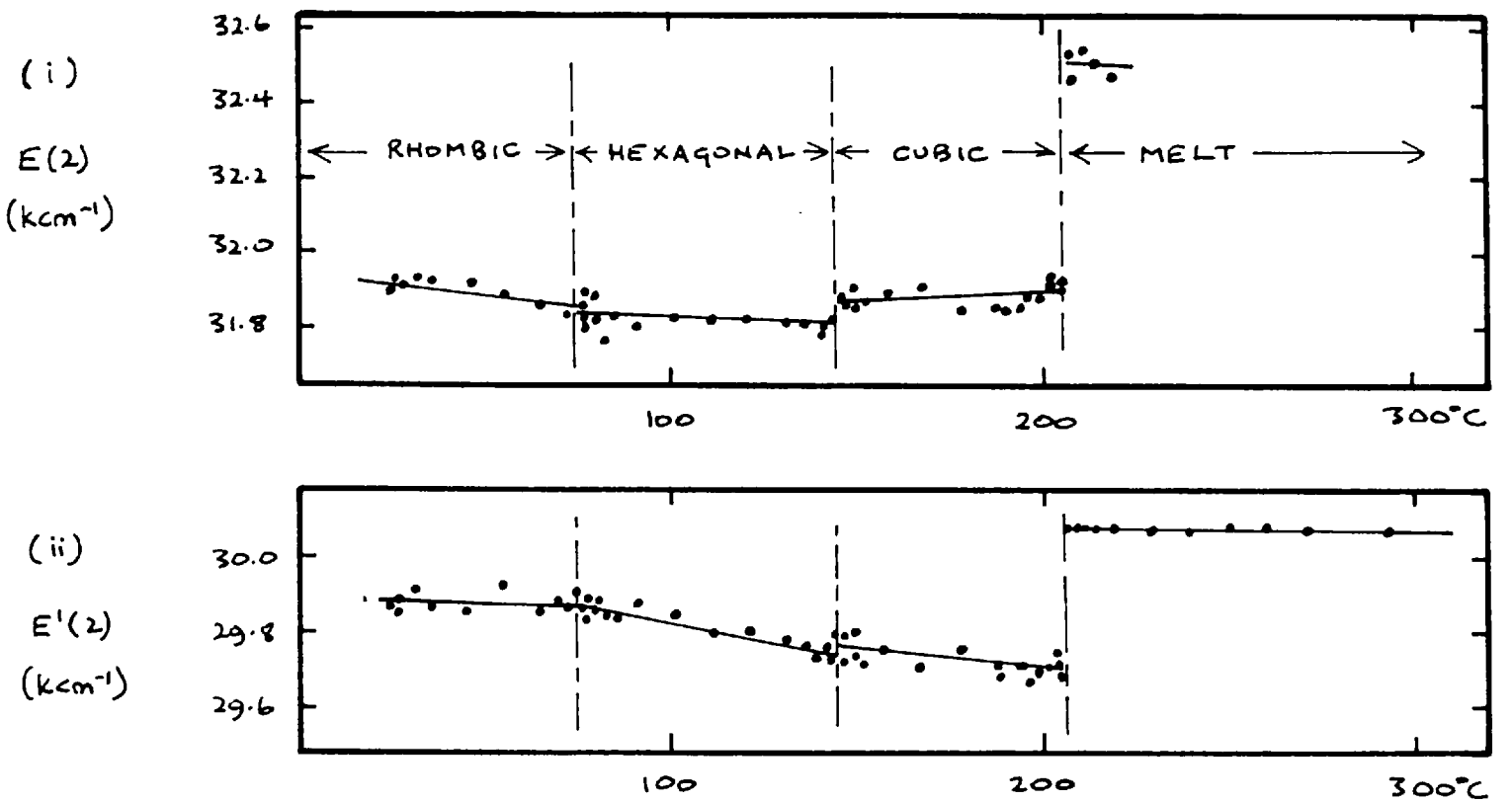


FIGURE 14.29 SPECTRAL PARAMETERS FOR THALLOUS NITRATE.

(SAMPLE 2, RUNS 781 ~ 842)

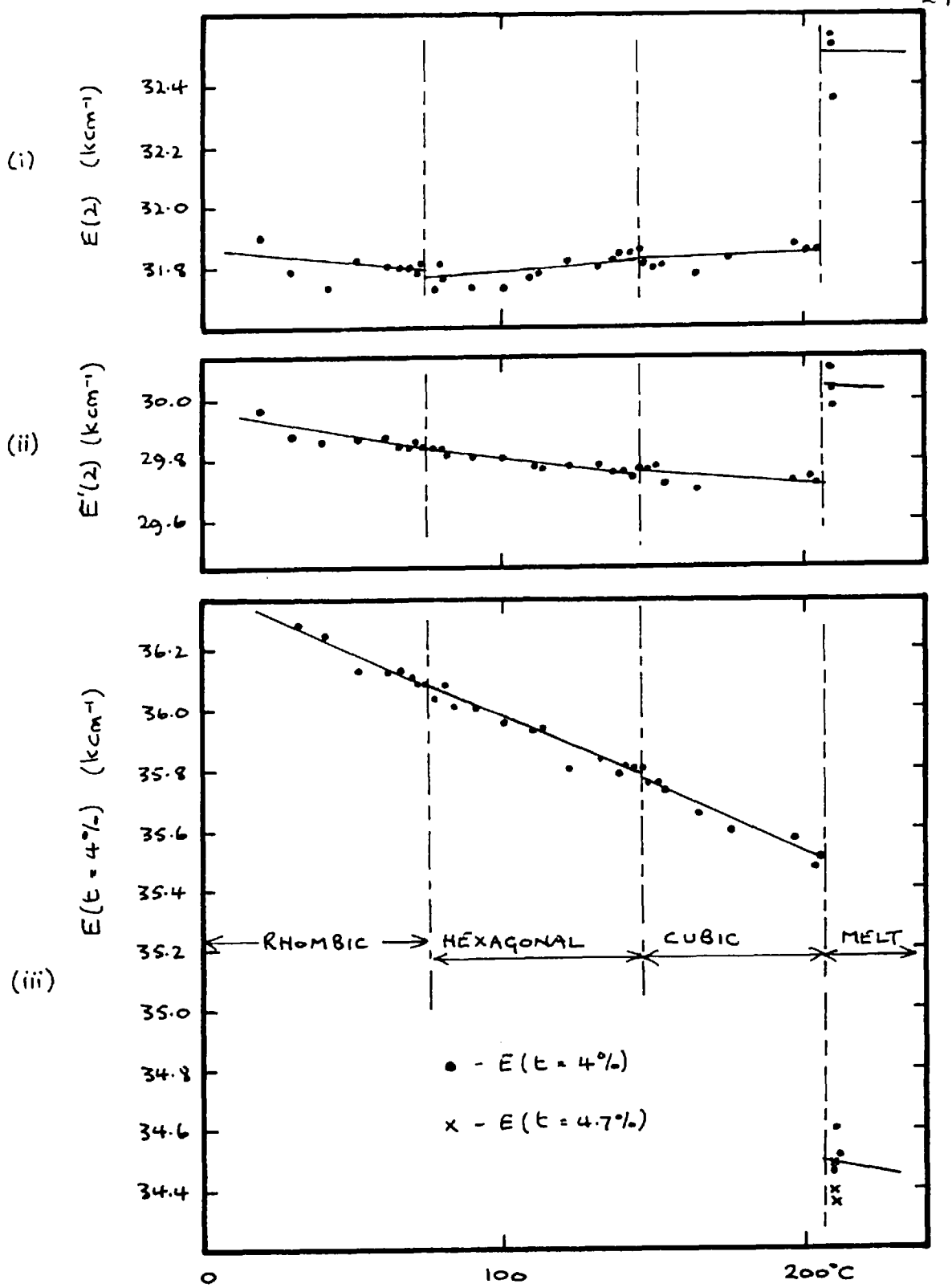


FIGURE 14.30 SPECTRAL PARAMETERS FOR THALLOUS NITRATE.

(SAMPLE 3; RUNS 846-881)

Figure 14.28 (part (i)) and Figure 14.29 (part (i)) show plots of E(2) against temperature for the two samples (E(2) being the frequency of the maximum of the weak band, uncorrected for the effect of overlap). E(2) decreased with rising temperature between 25°C and 145°C, and showed practically no abrupt change at the transition-point at 75°C. It increased by ~50 cm^{-1} at the transition-point at 145°C, continued to rise as the cubic modification was heated and increased by ~600 cm^{-1} at the melting-point.

Because of the effects of overlap, these changes in E(2) must be interpreted with caution. The increase in E(2) between 145°C and the melting-point may be caused by the progressive overlapping of the weak band by the edge of the strong band as the latter moved to lower frequency, and the large, abrupt shift of the band-edge to lower frequency at the melting-point is partly responsible for the corresponding increase in E(2).

In order to obtain a more accurate indication of the true movements of the weak band, some measurements were made on its low-energy edge, where the effects of overlap are relatively slight. This band-edge was characterised by the parameter E'(2), which is defined as the frequency at which the extinction coefficient ϵ is 0.3 times the extinction coefficient at the maximum of the weak band.

Plots of E'(2) against temperature for the two samples are shown in Figure 14.28 (part (ii)) and Figure 14.29 (part (ii)). E'(2) showed an overall decrease of 200 cm^{-1} as the salt was heated from 20°C to just below its melting-point (in contrast to E(2), which had practically the same value at these two temperatures). E'(2) decreased when the cubic modification was heated, and increased by 400 cm^{-1} at the melting-point.

These changes in E'(2) are believed to be a better indication of the true movements of the weak band than are the corresponding changes in E(2).

14.6.6. Nitric acid and its hydrates.

Pure nitric acid and solutions of composition $HNO_3.H_2O$ and $HNO_3.3H_2O$ were examined as thin films between Spectrosil plates. A dilute aqueous solution (0.24N) was examined in a silica cell of path-length 1 mm.

Figure 14.31 shows the spectra of the pure acid and of the solutions, all at 20°C. The dilute acid had a spectrum similar to those of the alkali-metal nitrates; the weak band had a maximum at 33.10 kcm^{-1}, and the edge of the strong band was at about 40 kcm^{-1}. With increasing acid concentration the weak band moved progressively to higher frequencies until in the pure acid it was present as a shoulder at 38.5 kcm^{-1} on the edge of the strong band.

The spectra of solid $HNO_3.H_2O$ and $HNO_3.3H_2O$ were also recorded. These hydrates were frozen in the copper block of the thermostat unit by cooling the latter with liquid nitrogen. The results obtained indicate that, for both hydrates, the weak band maximum moved abruptly to lower frequency on freezing. Part (i) of Figure 14.32 shows a plot of E(2) against temperature for $HNO_3.3H_2O$, and part (ii) shows a plot of E'(2) for $HNO_3.H_2O$. E'(2) is here the frequency on the low-energy edge of the weak band for which the extinction coefficient is 0.7 times the extinction coefficient at the maximum of the band. This parameter was used in preference to E(2) because the maximum of the weak band was very flat for this solution and it was difficult to measure E(2) with sufficient precision.

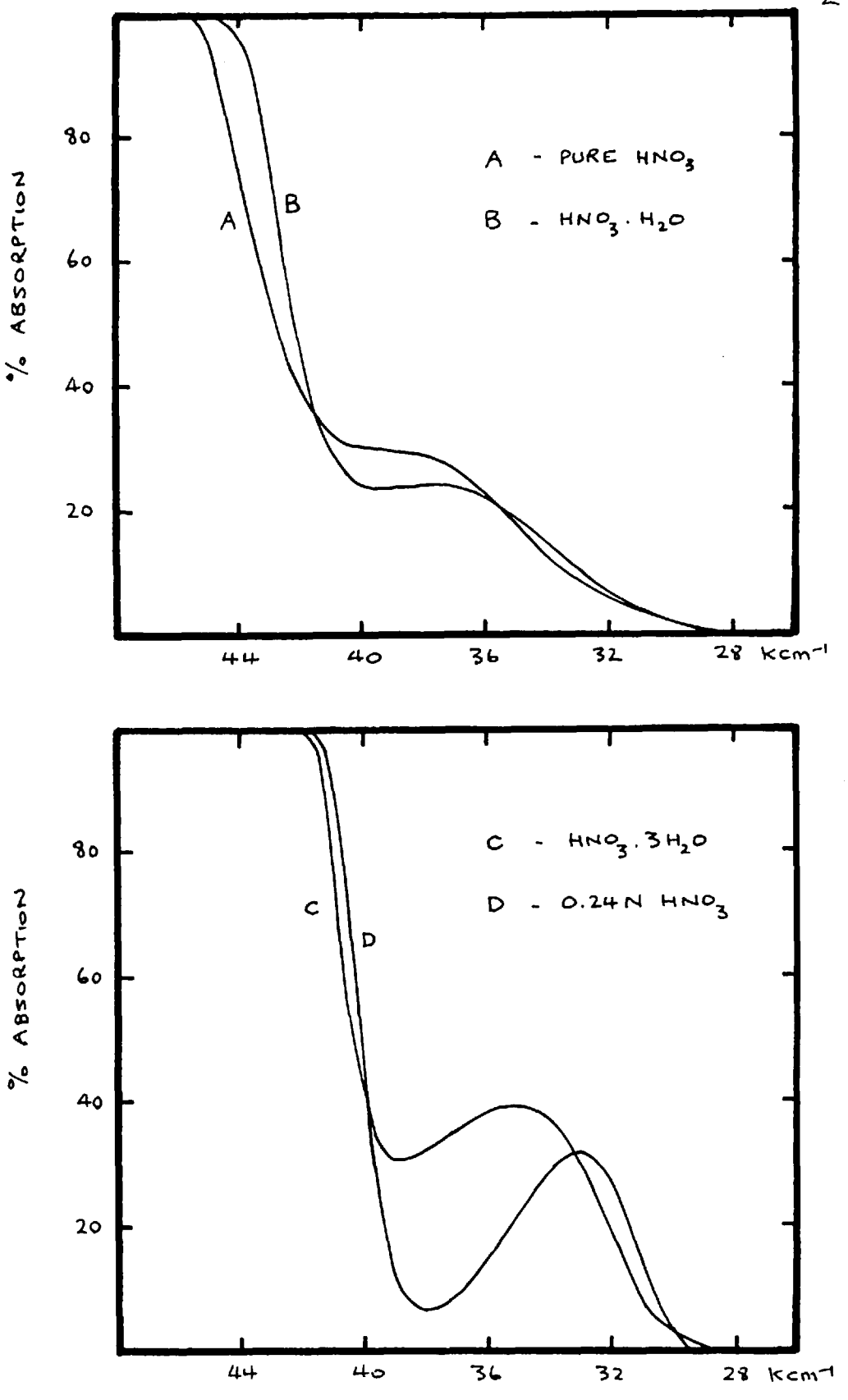
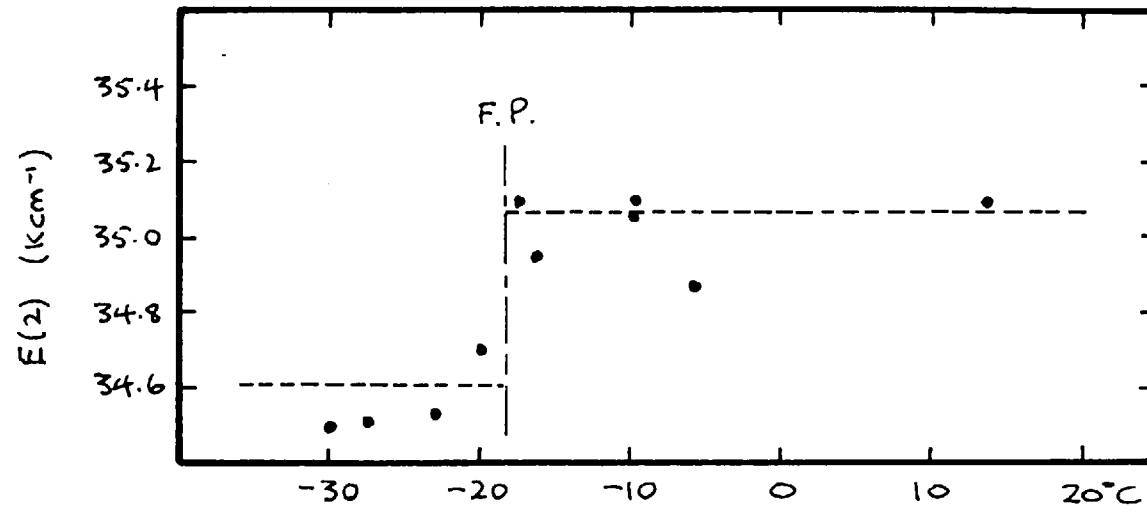
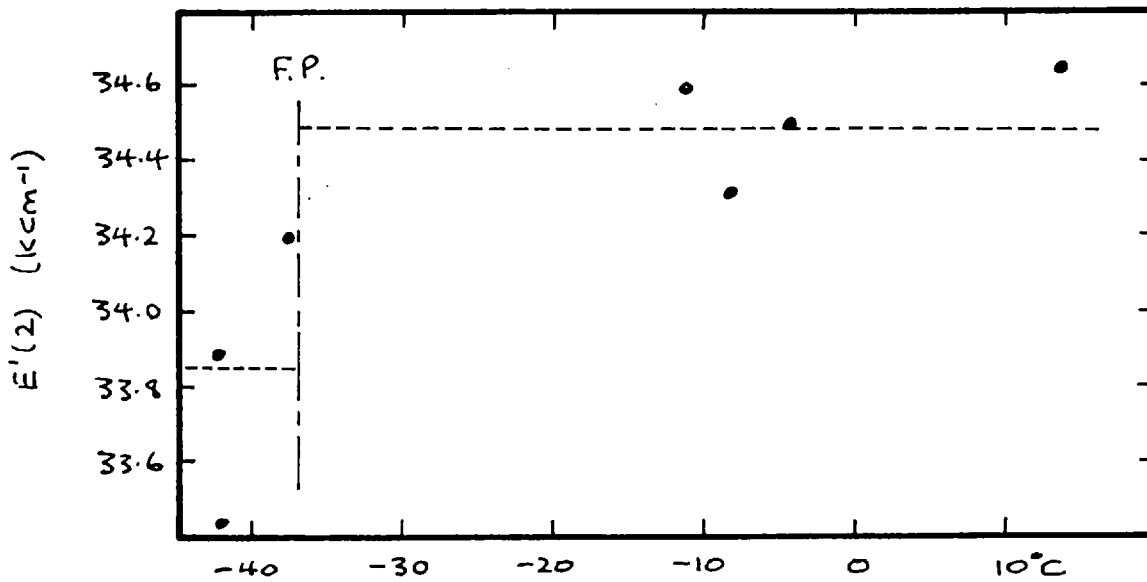


FIGURE 14.31. ABSORPTION SPECTRA OF NITRIC ACID AND ITS SOLUTIONS, AT 20°C.



(i) $HNO_3 \cdot 3H_2O$



(ii) $HNO_3 \cdot H_2O$

FIGURE 14.32 E(2) FOR $HNO_3 \cdot 3H_2O$ (PART (i))

E'(2) FOR $HNO_3 \cdot H_2O$ (PART (ii))

14.6.7. Iso-propyl nitrate.

This substance was chosen as an example of a covalent nitrate. Part (i) of Figure 14.33 illustrates the spectrum of a thin film of the pure liquid (held between Spectrosil plates), and part (ii) shows the spectrum of a 2% (w/w) solution in Spectrosol cyclo-hexane (in a silica cell of path-length 1 mm). Both spectra were measured at 20°C.

The two spectra are very similar; the edge of the strong band is at 40 - 42 kcm^{-1}, and the weak band is present as a shoulder at 38 kcm^{-1}. The spectra closely resemble that of pure nitric acid.

14.7. The nitrites.

14.7.1. Sodium nitrite.

Figure 14.34 shows the spectrum of this salt at 50°C, 271°C (solid) and 277°C (melt). Complete absorption was recorded between 50 and 40 kcm^{-1}. The band-edge at 40 kcm^{-1} was separated by a region of relatively low absorption from a well-defined band with a maximum at $\sim$28 kcm^{-1}. Some further structural features were observed in the region of room temperature:

1) There was a shoulder at $\sim$40 kcm^{-1} on the low-energy edge of the strong band, with an extinction coefficient about 0.6 times that of the weak band. The shoulder merged with the strong band when the temperature was raised to 100°C.

2) The absorption rose slowly between 38 and 34 kcm^{-1} before rising steeply when the high-energy edge of the weak

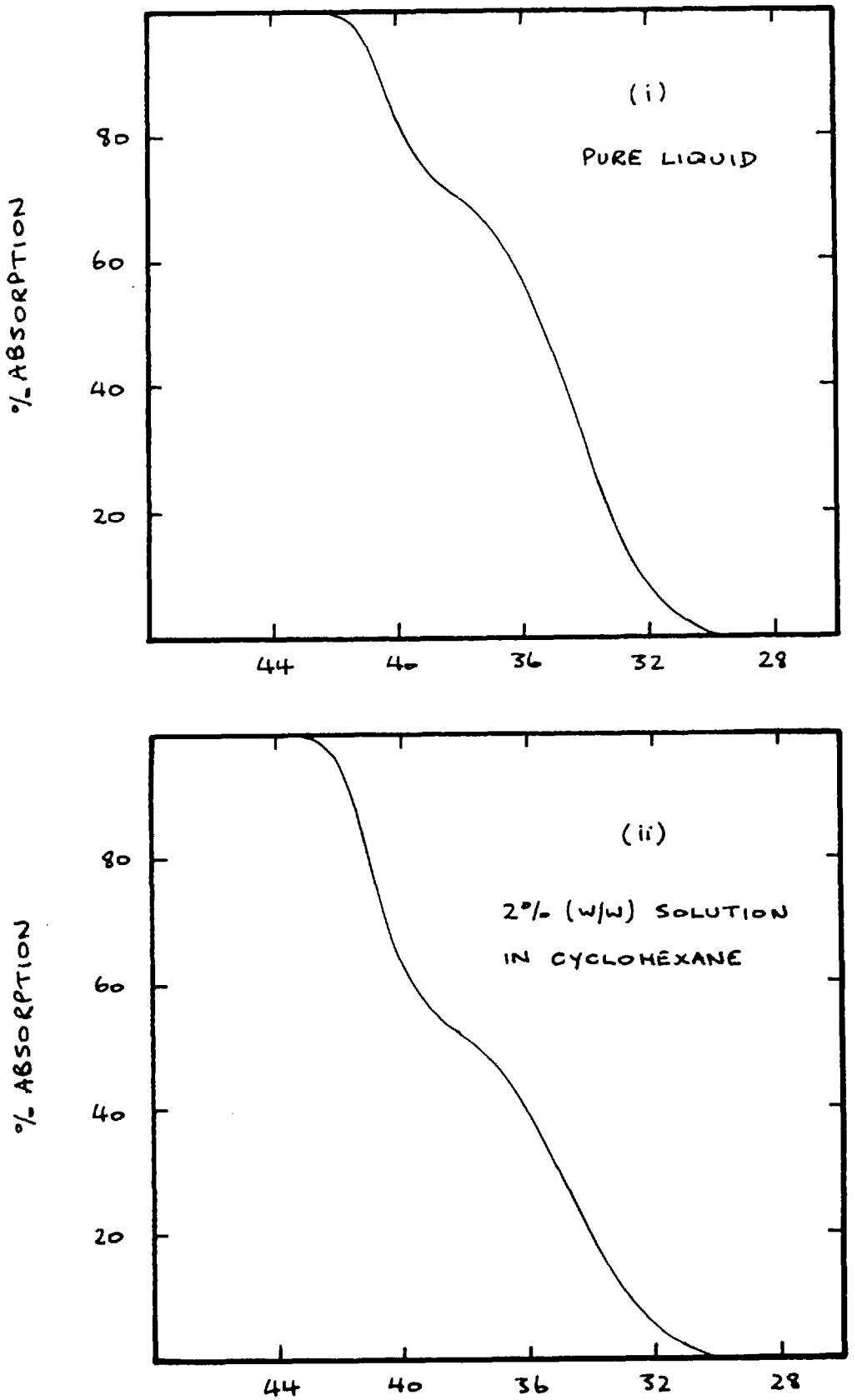
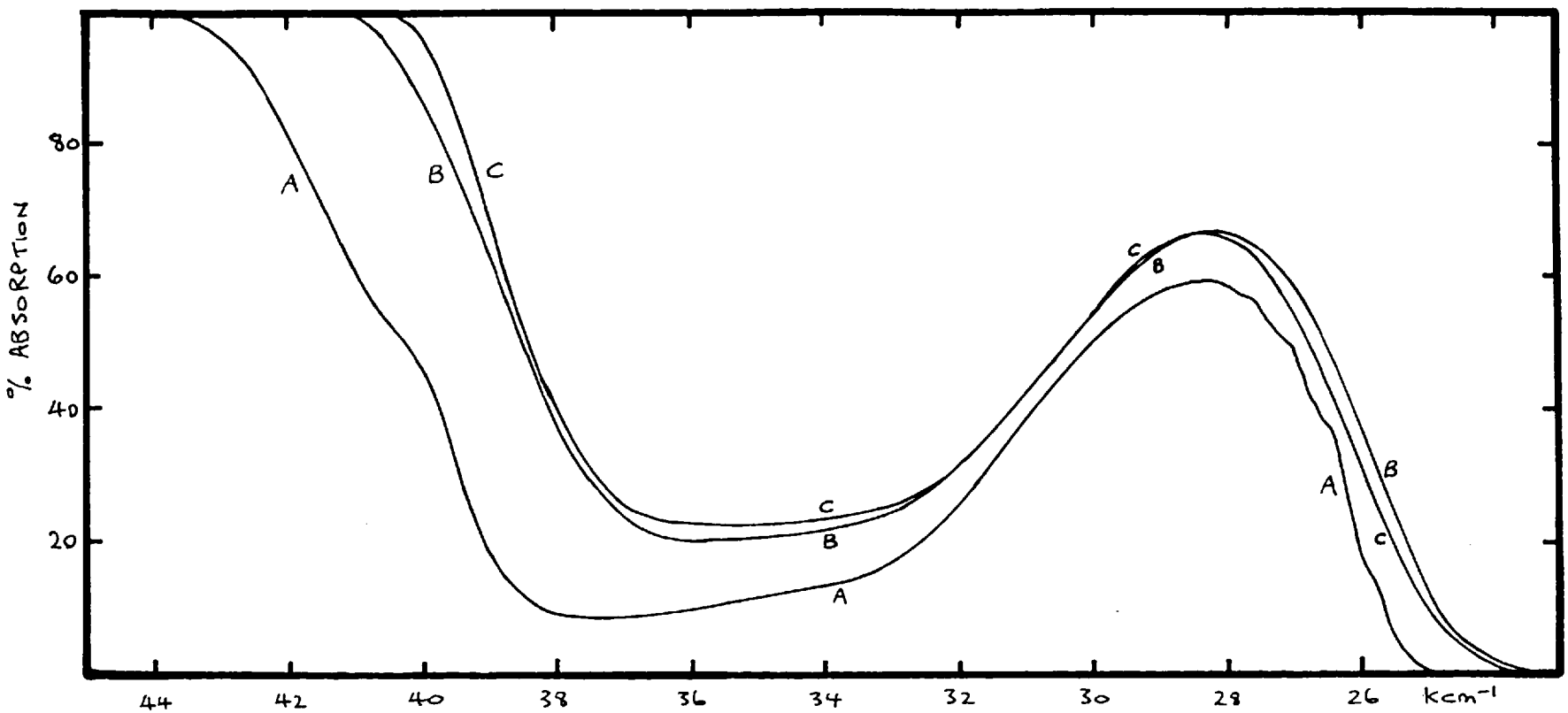


FIGURE 14.33 ABSORPTION SPECTRA OF ISO-PROPYL NITRATE.



A - SOLID AT 50°C (RUN 1233)

B - SOLID JUST BELOW M.P. (RUN 1239)

C - MELT JUST ABOVE M.P. (RUN 1240)

FIGURE 14.34 ABSORPTION SPECTRA OF SODIUM NITRITE (ZONE-REFINED SAMPLE).

band was reached. This slow rise may be identified with the shoulder at 32,300 cm^{-1} reported by Trawick and Eberhardt (Ref 10).

3) Four shoulders were observed on the high-energy side of the weak band, at 27.7, 27.1, 26.5 and 25.7 kcm^{-1}. They were smoothed out when the temperature was raised above 100°C, and probably represent vibrational structure.

All these structural features were exhibited both by the unrefined Analar sample (sample 1, Runs 1177 - 1180) and by the zone-refined samples (Sample 2; Runs 1173 - 1185, and Sample 3, Run 1233).

The % absorption at the maximum of the weak band rose steadily as the solid was heated.

Figure 14.35 shows a plot of E(2) against temperature, where E(2) is the frequency of the maximum of the weak band at 28 kcm^{-1}. The results obtained with the Analar and with the zone-refined samples are distinguished by separate symbols, but there is no significant difference between the two sets. E(2) decreased linearly as the temperature was raised from 20°C to the melting-point, and increased by about 300 cm^{-1} when the salt was fused. Sodium nitrite has no solid-solid transitions in the temperature range covered here.

The low-energy edge of the strong band was characterised by the parameters E(t = 10%) and E(t = 50%), which are the frequencies on the band-edge for which the transmission is 10% and 50%. Plots of E(t = 10%) and E(t = 50%) against temperature are shown in Figures 14.36 and 14.37 , for Runs 1233 to 1243. Both plots are linear between 20°C and the melting-point, E(t = 10%) showing the greater variation with

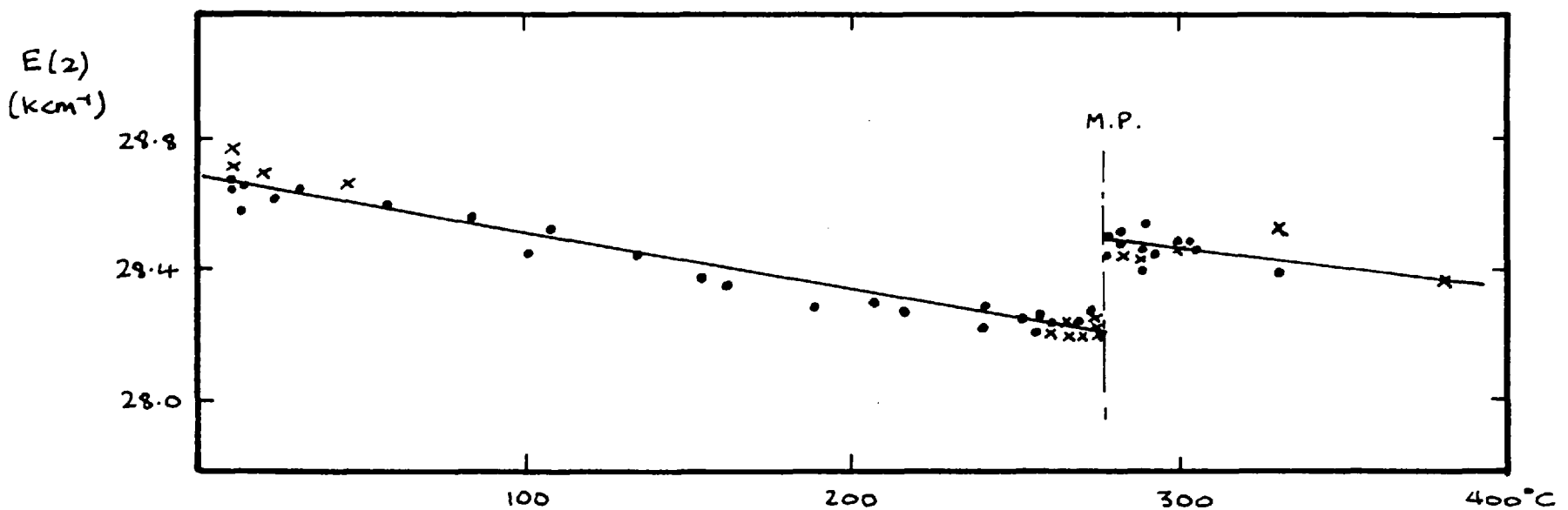


FIGURE 14.35. PLOT OF E(2) AGAINST TEMPERATURE FOR SODIUM NITRITE.

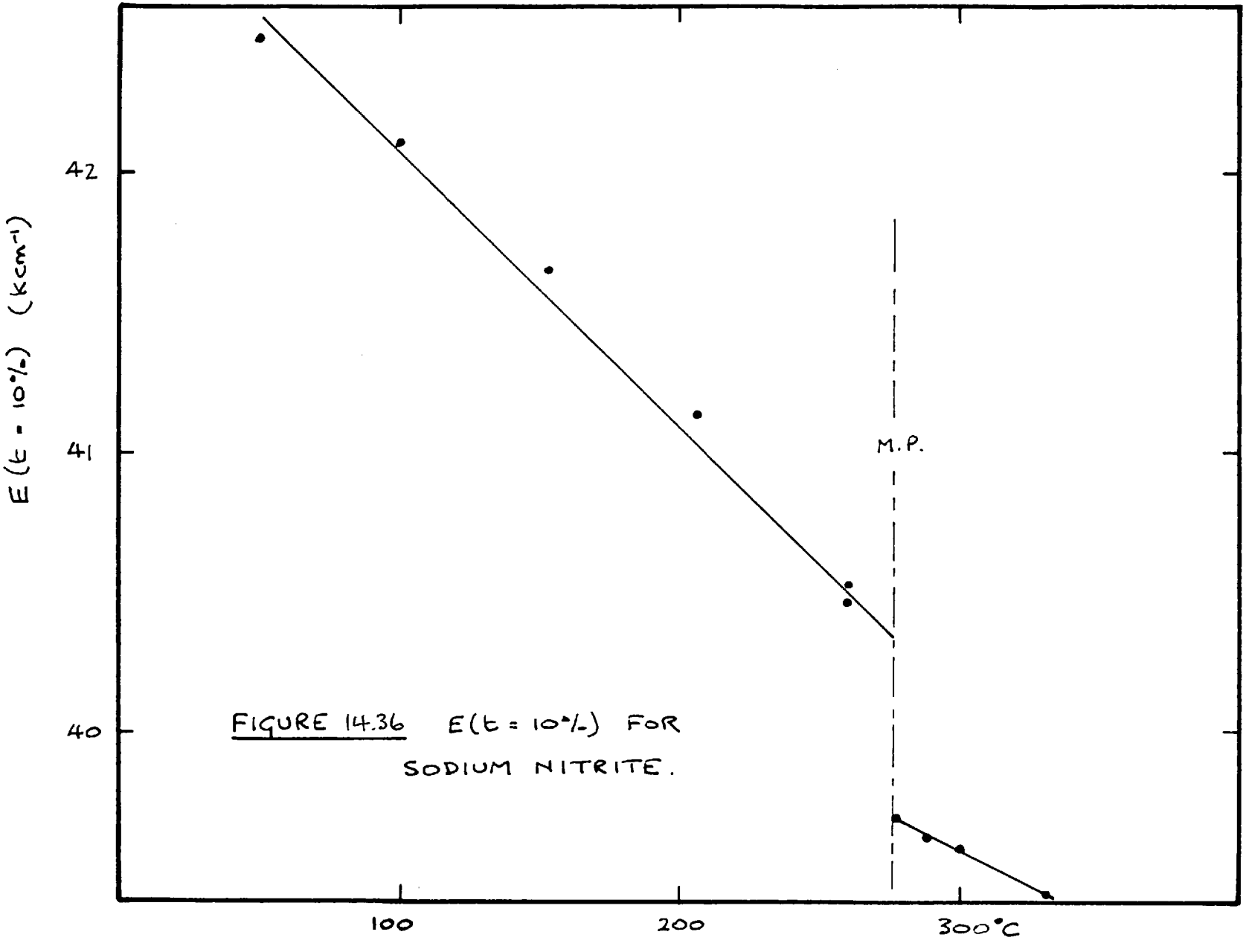


FIGURE 14.36 E(ε = 10%) FOR SODIUM NITRITE.

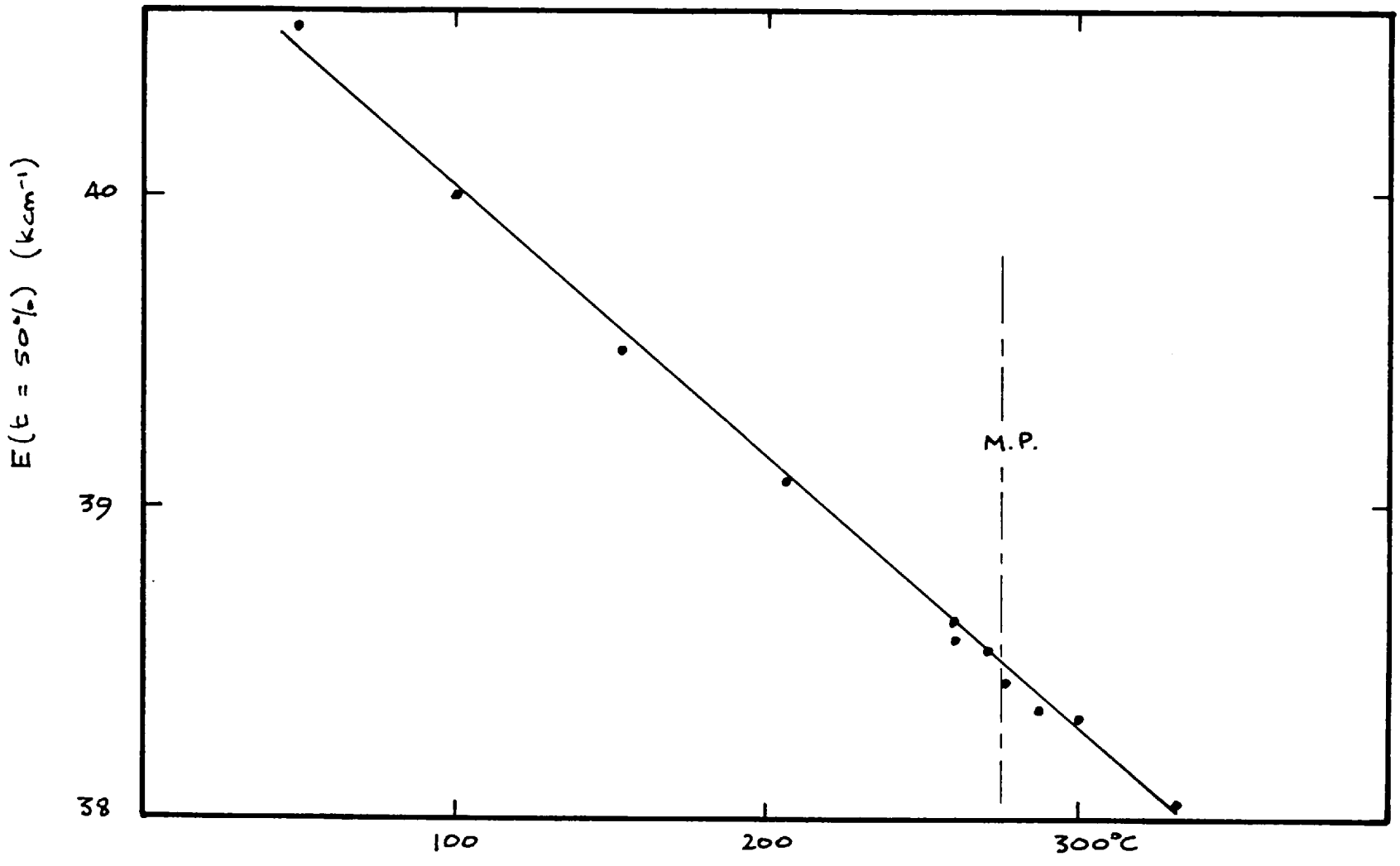


FIGURE 14.37. E(t = 50%) FOR SODIUM NITRITE.

temperature. At the melting point E(t = 10%) fell by 600 cm^{-1}, but E(t = 50%) showed no abrupt change. This shows that the band edge becomes steeper when the salt is fused, and that it moves to lower frequency only in the high-absorption region.

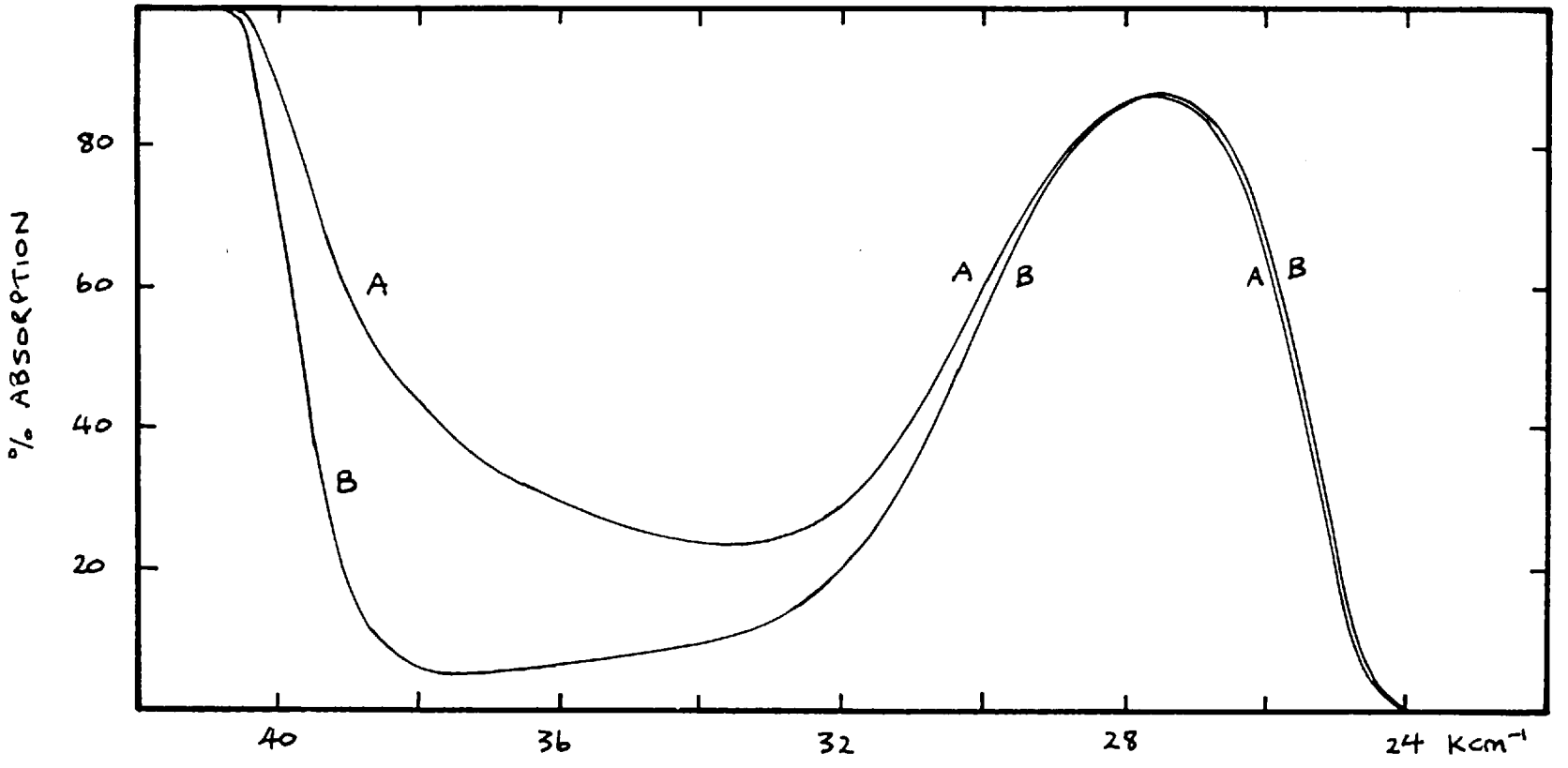
14.7.2. Potassium nitrite.

Two samples were examined; one was made up from Analar material (Sample 1), the other from zone-refined salt (Sample 2).

Some spectra are illustrated in Figures 14.38 and 14.39. They are broadly similar to those obtained for sodium nitrite, except that no structure was observed on the weak band at room temperature. The weak band had a maximum at 27.6 kcm^{-1} at 20°C.

Potassium nitrite has a transition at about 45°C. A sample of the salt obtained by freezing the melt had a clear, glassy appearance above the transition but became opaque below it; brilliant mother-of-pearl colours could be seen if the sample was scrupulously dry. Scattering losses therefore increased markedly when a sample was cooled through the transition temperature. The changes were reversed when the salt was heated above 50°C. Some hysteresis could be observed under suitable conditions; further details are given in Chapter 15.

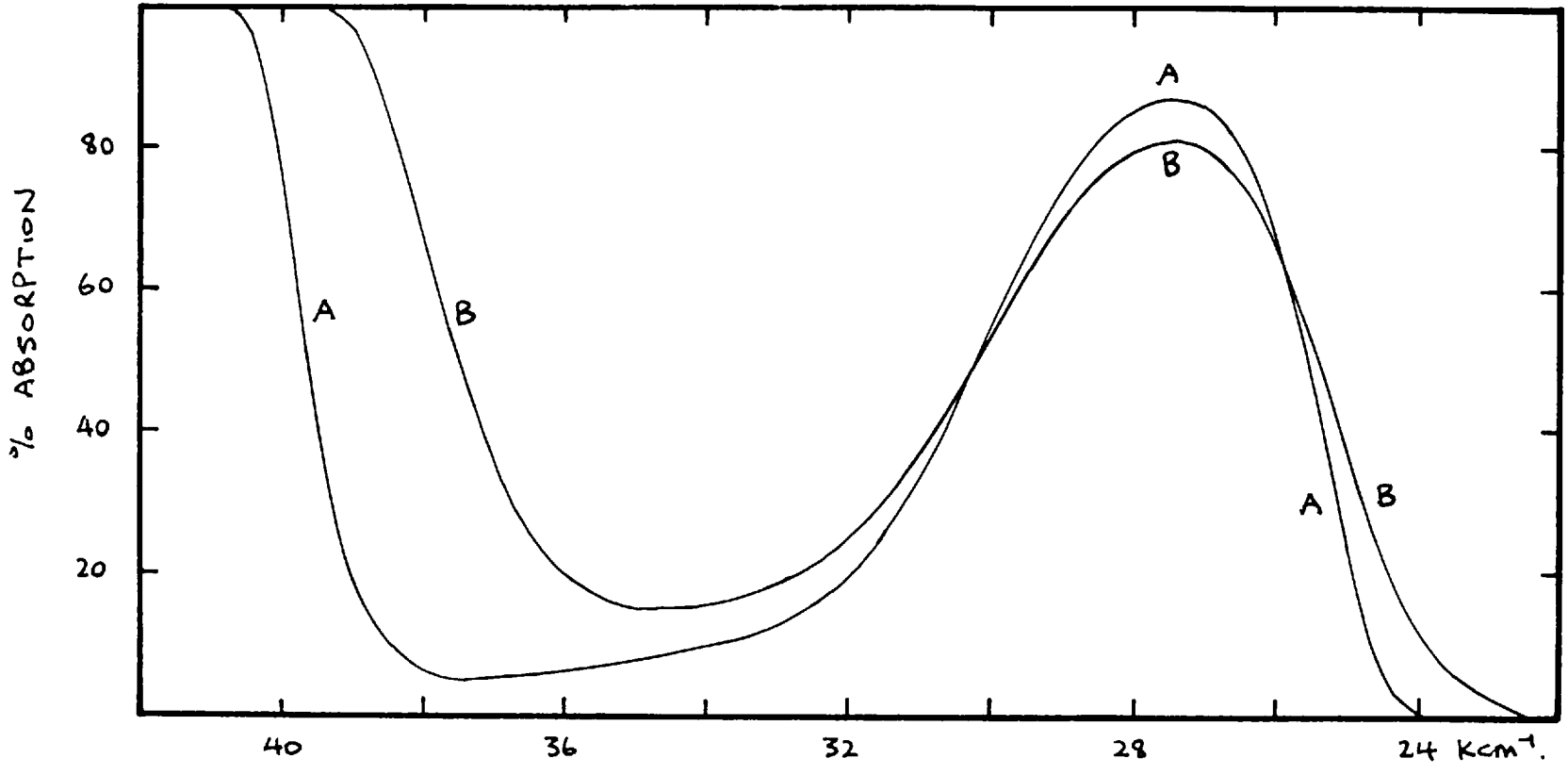
A plot of E(2) against temperature for potassium nitrite is shown in Figure 14.40. Results obtained with the Analar and zone-refined samples are plotted separately, but there is no significant difference between them. E(2) fell by about 80 cm^{-1} as the sample was heated through the transition temp-



A - 37.4°C (BELOW TRANSITION; RUN 1245)

B - 47.4°C (ABOVE TRANSITION; RUN 1246)

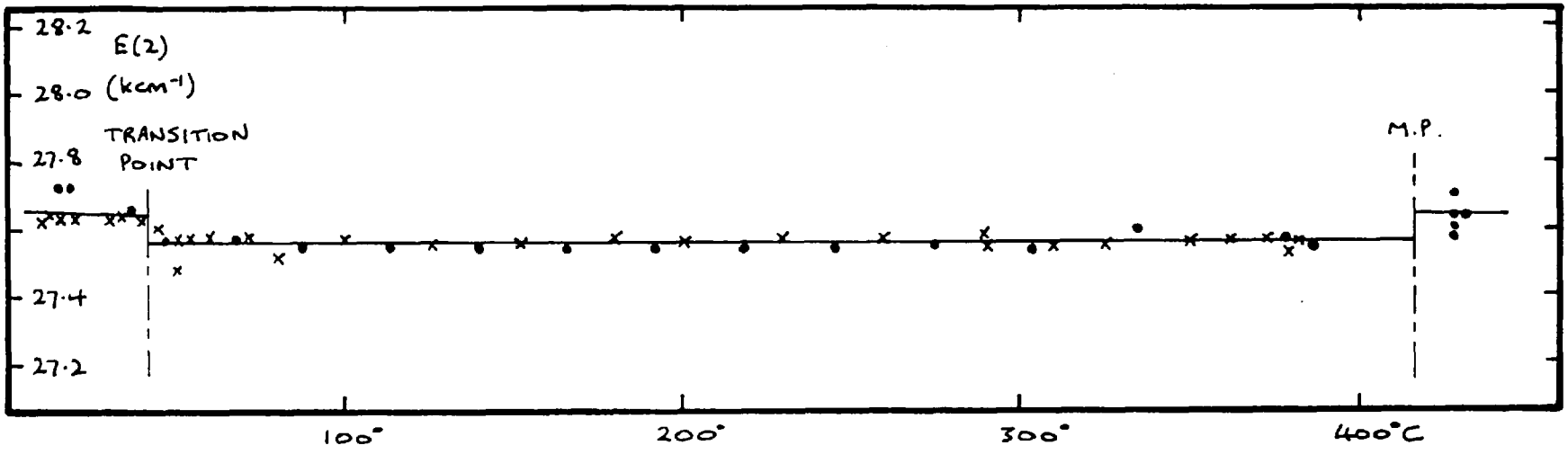
FIGURE 14.38 ABSORPTION SPECTRA OF POTASSIUM NITRITE.



A - 47.4°C (SOLID, ABOVE TRANSITION; RUN 1246)

B - 38.9°C (SOLID; RUN 1259).

FIGURE 14.39. ABSORPTION SPECTRA OF POTASSIUM NITRITE.



• - UNTREATED ANALAR SAMPLE (RUNS 1244 - 1273)

× - ZONE - REFINED SAMPLE (RUNS 1275 - 1336).

FIGURE 14.40. PLOT OF E(2) AGAINST TEMPERATURE FOR POTASSIUM NITRITE.

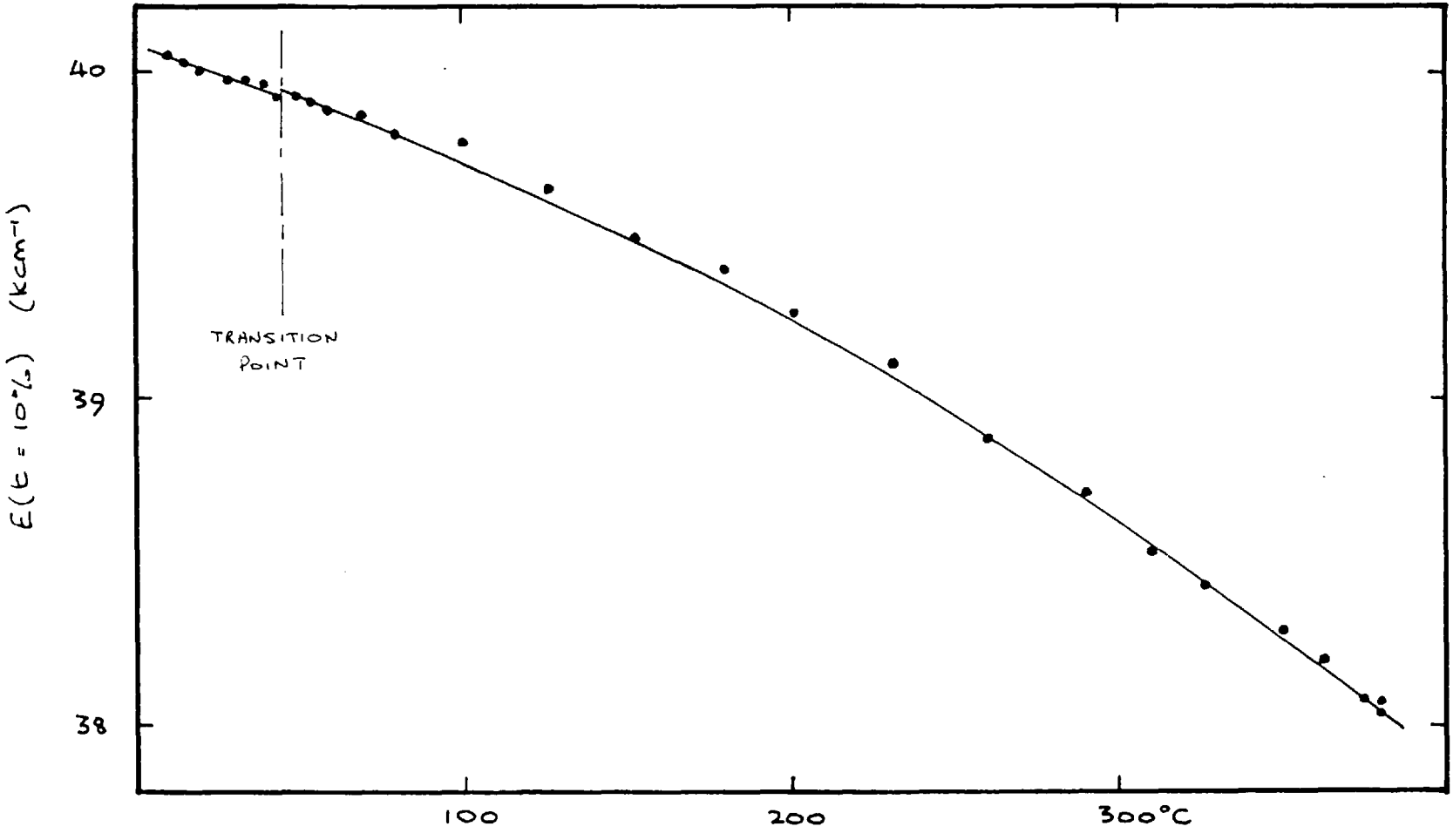


FIGURE 14.41. E(t = 10%) FOR ZONE-REFINED POTASSIUM NITRITE.

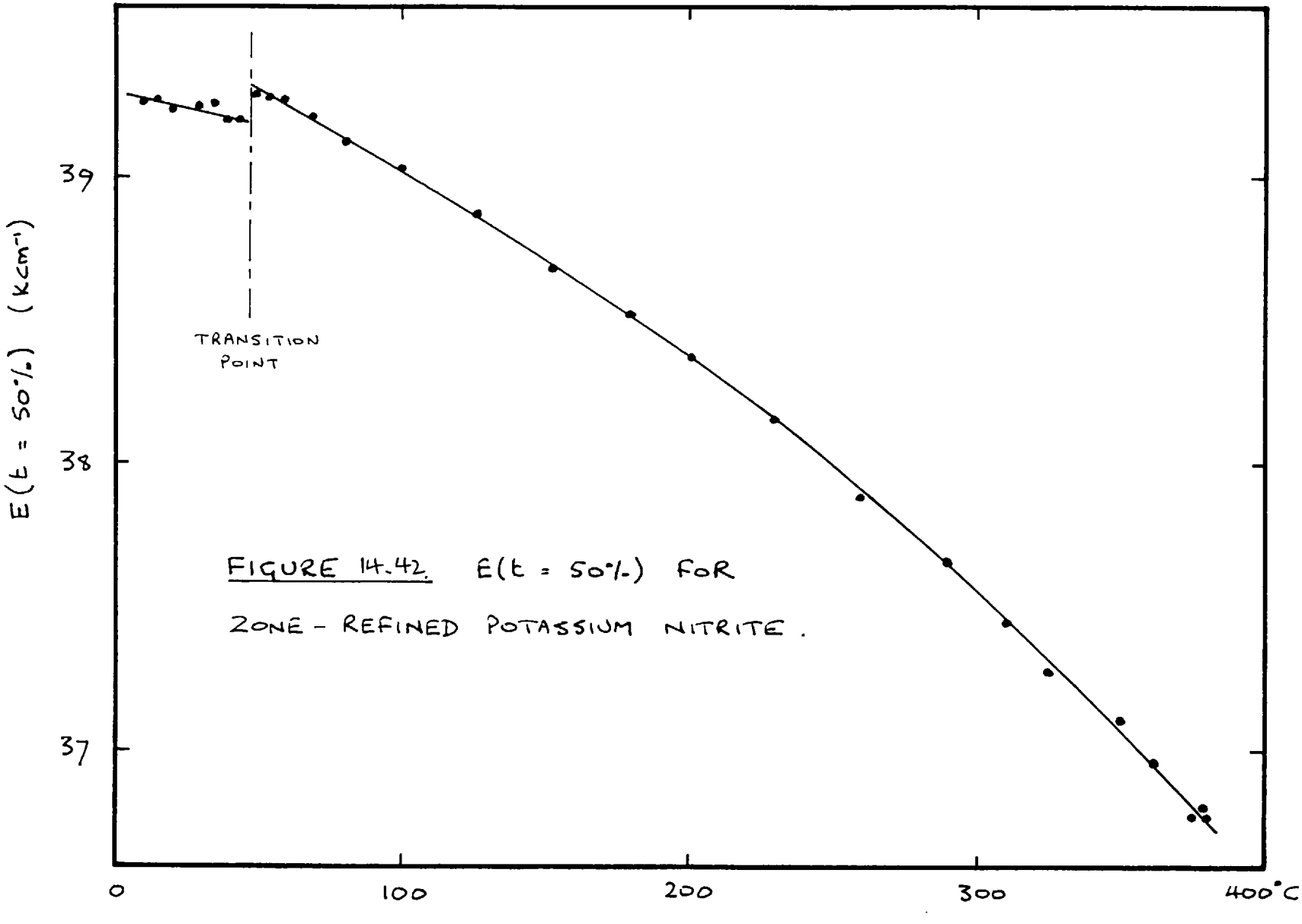


FIGURE 14.42. E(t = 50%) FOR ZONE-REFINED POTASSIUM NITRITE.

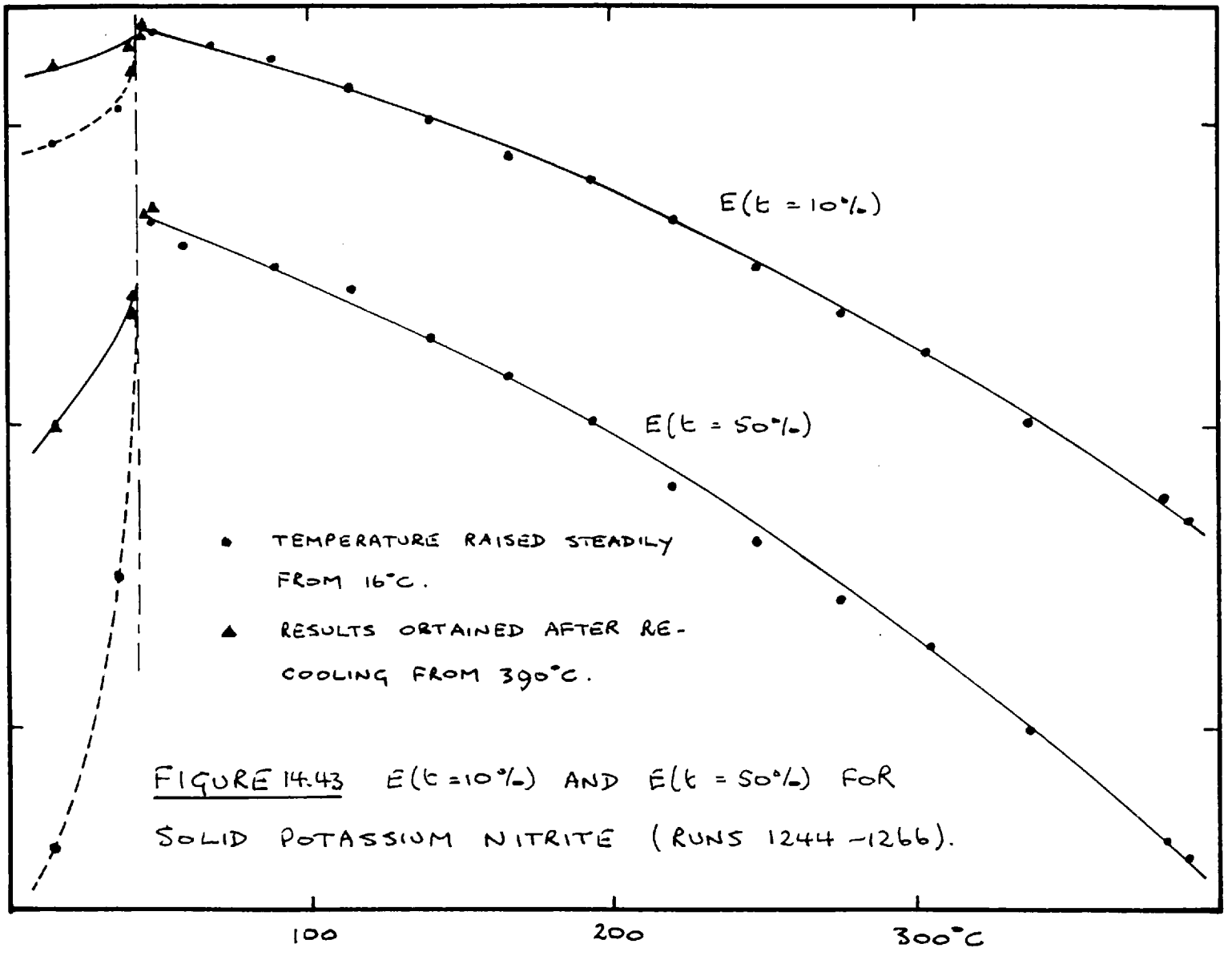


FIGURE 14.43 E(t = 10%) AND E(t = 50%) FOR SOLID POTASSIUM NITRITE (RUNS 1244 -1266).

erature, and remained practically constant between 50°C and the melting point. It increased abruptly by 70 cm^{-1} when the sample was fused.

The edge of the strong band was characterised by the frequencies at 10% and 50% transmission, E(t = 10%) and E(t = 50%). Figures 14.41 and 14.42 show these parameters plotted against temperature for the zone-refined sample, and Figure14.43 shows the same functions for the Analar sample. In both cases the plots show curvature between the transition temperature and the melting point; the movement of the band edge to lower frequencies accelerated as the temperature was raised. The non-reproducibility of the transmission below 40°C for the Analar sample (Figure 14.43) is probably due to changes in the degree of fragmentation of the sample, or to changes in its moisture content.

The significance of the results listed in this Chapter is discussed in Chapter 18.

REFERENCES TO CHAPTER 14.

1. F.C. Cracek, J. Amer. Chem. Soc., (1931), 53, 2609.

2. G.P. Smith and C.R. Boston, J. Chem. Phys., (1961), 34, 1396.

3. D. Meyerstein and A. Treinin, Trans. Farad. Soc., (1961), 57, 2104.

4. H. Schinke and F. Sauerwald, Z. anorg. Chem., (1960), 304, 25.

5. W.J. Davis, S.E. Rogers and A.R. Ubbelohde, Proc. Roy. Soc., (1953), A220, 14.

6. A.G. Keenan, "Kinetics and Mechanisms in Ionic Melts", final report, Sept. 1954 - Sept. 1957, Air Force Office Sci. Res., Project No. Chem 40-18, Contract No. AF18(600)-1148; Illinois Inst. Tech., Chicago, Ill.

7. G.P. Smith and C.R. Boston, Ann. N.Y. Acad. Sci., (1960), 79, 930.

8. A.B.F. Duncan, Phys. Revs., (1935), 47, 822.

9. A.K. Dutta, Proc. Roy. Soc., (1932), A138, 84.

10. W.G. Trawick and W.H. Eberhardt, J. Chem. Phys., (1954), 22, 1492.

CHAPTER 15.

THE STUDY OF PHASE-CHANGES BY MEASUREMENT OF % TRANSMISSION AT CONSTANT FREQUENCY.

15.1. Introduction.

The experimental technique is described in Section 11.13. The method depends upon the fact that the profile of the absorption spectrum of a thin film of a nitrate or nitrite underwent a small, abrupt shift when a transition occurred, and this caused a change in % transmission at a given frequency. In principle this change in transmission could be measured at any frequency at which absorption occurs, but for the nitrates the greatest change was obtained in the region of the steep edge of the strong absorption band ($\sim$40 kcm^{-1}). Under these conditions the transmission altered by up to 10% when the transition occurred, and this change could be made to cover the full scale of the recorder chart by using the 0 - 10% transmission scale of the spectrophotometer.

The change in transmission was due partly to a change in quantum absorption and partly to changes in the light-scattering properties of the sample. If a salt film was taken round a temperature cycle including a transition point the % transmission returned approximately to its original value, but correspondence was not always exact because of irreversible increases in scattering losses due to progressive fragmentation of the crystals. Figure 15.2 shows a typical example. Reproducibility was better for some transitions than for others, but in general the change in % transmission at a transition point was reproducible to within 10% (for a given sample).

To obtain a rough, preliminary estimate of the transition temperatures, each sample was heated from room temperature to its melting-point at 20°C per minute and then re-cooled at the same rate. The individual transitions were subsequently re-examined more carefully, using heating and cooling rates of 1° per minute. Superheating and -cooling were common, and for this reason it was sometimes difficult to reduce the transition range to below 10 - 15°C. This was particularly true for the transitions in ammonium nitrate at ~35°C and ~85°C (see also Section 14.6.3). When superheating and supercooling were less marked, the following technique was used.

A sample was heated at 1° per minute until the change began to take place. Before it was complete the sample was cooled slowly, whereupon the transformation was halted and then reversed. The temperature was noted at each stage. The information obtained in this way referred to a sample containing seeds of both phases, so the recrystallisation could not have been hindered by the slowness of nucleation processes. Transition ranges could be reduced to a fairly small size (~1°C) if this technique could be applied. When superheating and supercooling were more pronounced the transformation, when it eventually began, often occurred so rapidly that it was complete before the temperature could be altered. The sample then contained no seeds of the first phase, and reversal could be achieved only by overshooting the transition temperature in the opposite sense.

This survey of transition temperatures was undertaken as a preliminary to the measurement of the change in E(2) at the transition points. For this purpose it was sufficient to know the thermostat block temperatures

corresponding to the transitions, and a transition range of $5^{o}C$ was small enough. In this Chapter the aim has been to apply corrections to allow for the temperature gradients in the thermostat unit, and so to derive absolute upper and lower limits for the transition ranges. The information obtained in this way can then be compared directly with the literature.

The corrections have been made on the assumption that, when a sample was heated through a transition, transformation began at the edges (the hottest part) and then spread towards the centre as the temperature was raised further. On cooling the change was assumed to begin at the centre. The upper limit of the transition range was therefore found by calculating the temperature of the centre of the sample corresponding to the completion of change in % transmission in a heating half-cycle, and the lower limit is the temperature at the edge of the sample at the completion of change after cooling. These temperatures were calculated from the measured block temperatures by use of the data summarised in Section 11.8.

The results are given below. No transitions were found which had not previously been reported in the literature, although the transition in potassium nitrite at $40 - 50^{o}$ was 'discovered' before the author knew that it had already been reported. The transitions in potassium nitrate and potassium nitrite both showed features of particular interest, and were therefore studied in some detail.

15.2. Transitions in crystalline nitrates.

15.2.1. Potassium nitrate.

When a sample of the salt was heated from room temperature, a sudden change in % transmission (at 40 - 42 kcm^{-1}) was recorded at about 128°C. The lowest sample temperature at which the onset of the change was detected was 127.9°C, and if heating was carried out sufficiently slowly (at 2° per minute) the change was complete at 128.05°C.

In one experiment the sample was heated to 128.6°, when the change began to take place slowly. Before the transformation was complete, the temperature was lowered until the edge of the sample was at 126.7°. The change was reversed. This indicates that there is equilibrium between forms I and II at this transition-point, since the change can be made to occur in either sense by altering the temperature slightly. The equilibrium temperature must lie within the range 126.7 to 128.05°C.

If the salt was thermostatted at 130° for a few minutes, it was converted entirely into the high-temperature form. Its behaviour on cooling was then quite different from that recorded above. The % transmission returned to its original value in two stages. The first change was complete in about 20 seconds, and took place at sample temperatures within the range 120° - 122.9°C in different experiments. The second change was slower (occupying several minutes), and was observed at temperatures between 109 and 117°C. This shows that when the high-temperature modification (I) is cooled, it changes first into an intermediate form (III) which is later converted into the stable low-temperature form (II).

On one occasion a sample was cooled from 130° to 121°, when the transition from phase I to the metastable phase III took place to completion. The temperature of the sample was raised to 125.0°C (this being the temperature of the coolest part, i.e. the centre) and was held at this value for one hour. The % transmission at 42 kcm^{-1} returned to the value characteristic of phase I. This proves that there is equilibrium between forms I and III at some temperature between 121° and 125.0°C. Since in other experiments (described above) the change I → III was observed at sample temperatures between 120° and 122.9°, the I ⇌ III equilibrium must lie in the range 122.9 - 125.0°C.

In a final experiment a sample was cooled from 130 to 121°C, and allowed to transform to phase III. It was then heated at a rate of 1° per minute. The % transmission remained at the same level until the temperature of the warmest part of the sample reached 127.8°C, when the transmission increased abruptly to the value characteristic of phase I. This indicates that form III can be superheated above the I⇌III equilibrium temperature (123 - 125°C) until the II ⇌ I transition temperature is reached.

The findings described above are summarised in Figure 15.1, which represents the results of many experiments. A plot of % absorption against temperature for a single heating and cooling cycle is shown in Figure 15.2. In this experiment the heating was carried out at 0.5°C per minute and the cooling at 0.3° per minute (except in the ranges 122 - 120° and 115 - 112°, where the cooling rate was reduced to 0.15° per minute).

The results of this investigation are in entire qualitative agreement with those of Kracek (Ref 1), who studied

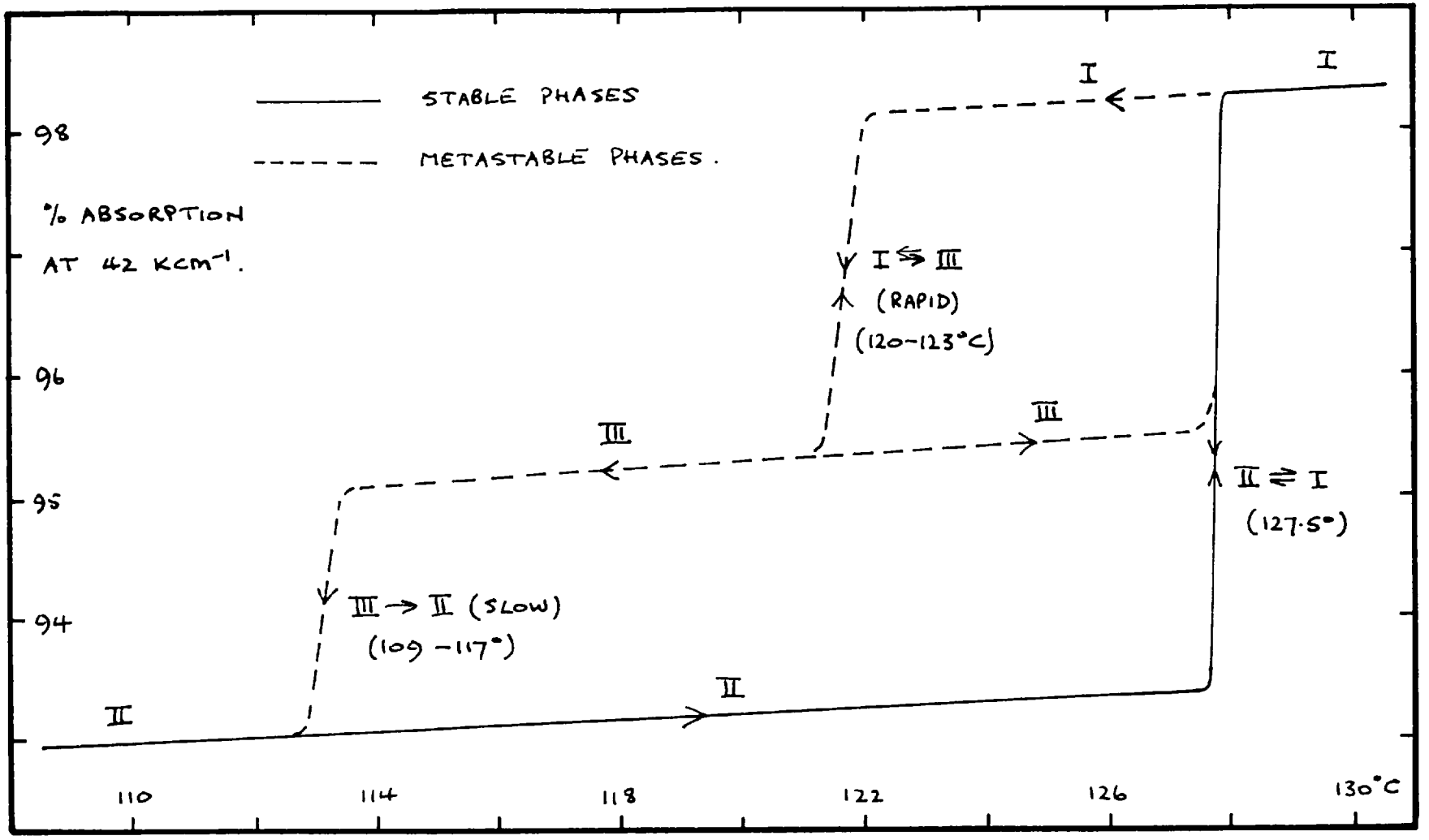


FIGURE 15.1. PHASE CHANGES IN POTASSIUM NITRATE AT 110 - 130°C.
(COMPOSITE DIAGRAM)

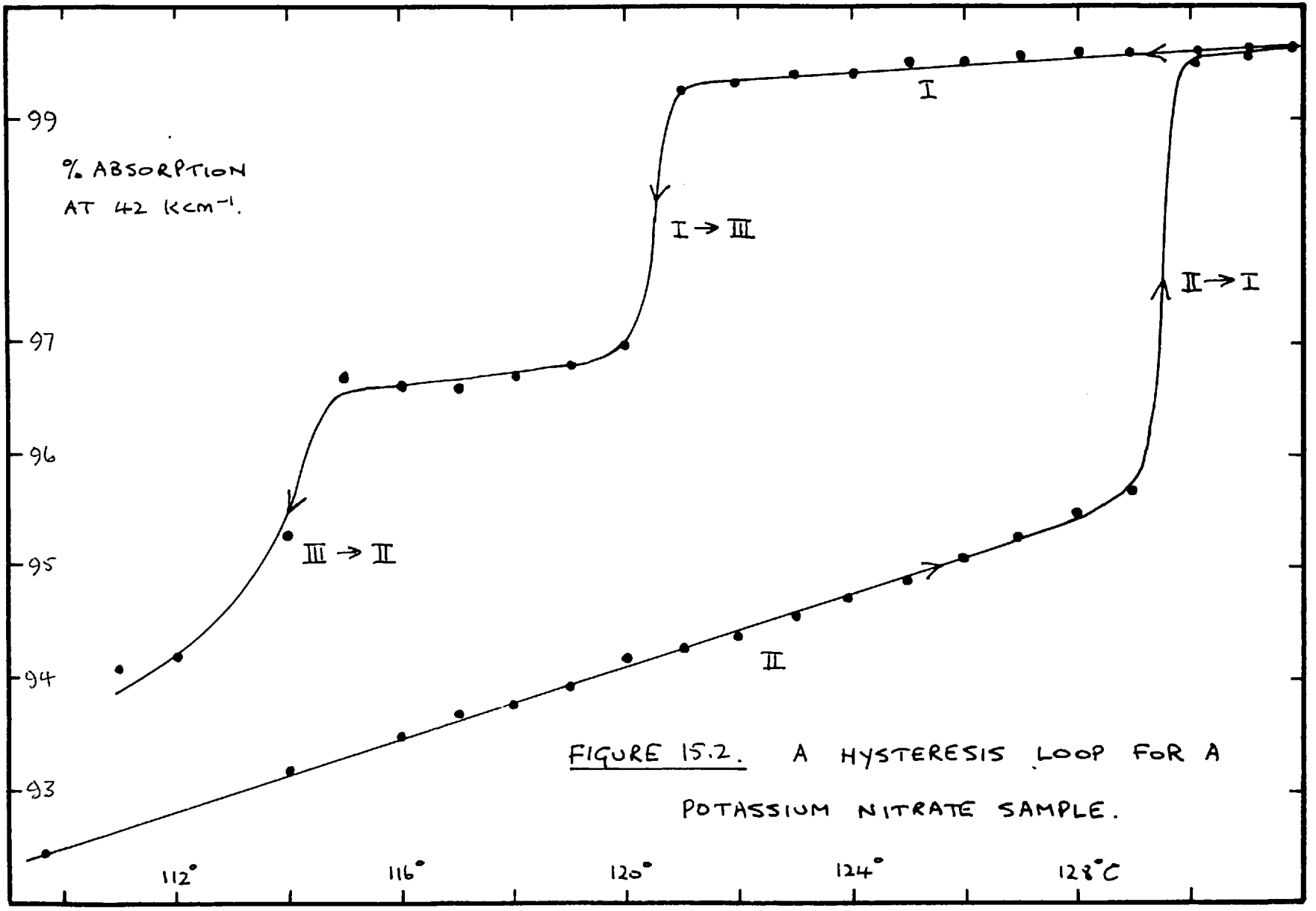


FIGURE 15.2. A HYSTERESIS LOOP FOR A POTASSIUM NITRATE SAMPLE.

the transitions by dilatometry and by thermal analysis. He found equilibrium between I and II at 127.7°C, and made the interesting observation that if a moist sample is cooled from 130° to just below 127° phase I changes into phase II without the intermediate appearance of phase III. The change presumably occurs by solution of I in the water, followed by crystallisation of II from the solution. Kracek also demonstrated the existence of a metastable equilibrium between I and III in the dry salt; he gives the equilibrium temperature as 126.1°C, which lies outside the range 122.9 - 125° obtained by the author. The present result is believed to be the more accurate. Agreement between the two sets of results is otherwise qualitatively complete.

The hysteresis associated with the transition in the dry salt is probably caused by the marked difference between the crystal structures of I and II. Both forms have pseudo-hexagonal symmetry when viewed along the c-axis; in form I the potassium ions and nitrate ions lie on two separate sets of straight lines parallel to the c-axis, but in form II the two sets become identical and each line passes through anions and cations stacked alternately (Ref 13). The transformation of I to II therefore requires considerable ionic rearrangement, so direct nucleation and growth of phase II within phase I would involve high inter-domain strain energies. The intermediate formation of phase III (whose structure has not been determined) presumably allows these strains to be avoided, at least in part.

15.2.2. Rubidium nitrate.

This salt has three transitions between room temperature

and its melting-point. As the temperature is raised, the crystal structure changes from hexagonal (form IV) to cubic (III), then to rhombohedral (II) and finally to cubic (I) again before the salt melts.

All three transitions were detected by the spectroscopic method. When a sample was heated from room temperature, the first transformation (IV → III) was complete when the centre of the salt film reached 163.9°C. On re-cooling, the reverse change was complete when the edge of the sample was at 158.4°C. These two temperatures therefore define the limits of the transition range.

When form III was further heated, the change to the rhombohedral form II began when the hottest part of the sample was at 222.3°C. The sample was cooled before this change was complete, and reversal was observed when the coolest part of the film reached 218.0°C.

When phase II was heated, the third transition began when the edge of the sample (the hottest part) reached 282.9°C, and was complete when the centre was at 283.4°C. On re-cooling, the change I → II occurred rapidly and completely at 282.0°C. The cycle of changes is therefore confined within the temperature range 282.0 - 283.4°C.

A sudden increase in % transmission corresponding to melting was observed when the edge of the sample reached 312.3°C.

15.2.3. Caesium nitrate.

This salt transforms from hexagonal (II) to cubic (I) at about 153°C. On heating a sample, the change II → I began

when the edge of the specimen reached 153.4°C, and was complete when the centre reached the same temperature. The sample was cooled until the reverse change had occurred. It was then re-heated until the change II → I began, and the thermostat was cooled before the change was complete. The transformation was reversed when the edge of the film reached 152.8°C. The transition range is therefore 152.8 - 153.4°C.

15.2.4. Ammonium nitrate.

Ammonium nitrate has three transitions between room temperature and its melting-point. Superheating and supercooling were very marked in the region of the lower two, and these transition temperatures could not be found accurately by the 'constant frequency' technique. By carrying out heating and cooling cycles, it was established that the first transition temperature lay in the range 29 - 44°C and the second between 78 and 88°C. It was possible to investigate the hysteresis associated with the transitions by measuring E(2) as a function of temperature (see Section 14.6.3).

The third transition, between the tetragonal form (II) and the cubic form I, took place more readily. On heating, the change II → I was complete at 125.0°C, and on cooling the reverse change was complete at 121.8°C.

15.2.5. Silver nitrate.

The experiments on this salt were carried out at a frequency of 35.2 kcm^{-1}, on the low-energy edge of the strong band. The sample was heated from 156°C at 1°C per

minute. A change began when the edge of the film reached 158.6°C. The salt was re-cooled before the transition was complete; the change was halted, and began to reverse when the centre of the film was at 157.6°C. The transition range can be given as 157.6 - 158.6°C.

On further heating the sample began to melt when its edges reached 207.9°C, and fusion was complete when the centre of the film was at 208.4°C.

15.2.6. Thallous nitrate.

Two transitions have been reported in the literature, at 75 and 145°C (see Table 15.1). The lower one could not be detected by the technique described here, although experiments were carried out both at 35.4 and 29.6 kcm^{-1} (on the low-energy edge of the strong band and the weak band respectively). A small change in % transmission was recorded at both these frequencies when the sample was heated through 146°C, (corresponding to the change II → I), but no reverse change was detected on cooling.

The sample was heated from 200°C at a rate of 1° per minute. A change in transmission showed that the film began to melt at the edges at 206.2°C and that fusion was complete at 206.3°C.

15.3. Summary of results for the nitrates.

The details in the foregoing paragraphs are summarised in Table 15.1, which also gives some values of transition

temperatures taken from the literature. The results from the present work are given in the form of a temperature range defining the limits of the transition (including any hysteresis). This range was of the order 1° - $5^{\circ}C$ (excepting the two lower transitions in ammonium nitrate), which is adequate for the purpose for which the measurements were made (see Section 15.1). It is not logical to try to derive single values of transition temperatures from this work. An equilibrium between two solid phases can be characterised by a single transition temperature only when the strain energy and inter-phase surface energy in the sample are negligible (Ref 11). This condition is unlikely to be satisfied in a dry, crystalline solid (unless the structures of the two phases are very simply related), so some hysteresis is normally to be expected if a dry sample is taken through a temperature cycle which includes a transition.

If the sample is in contact with a solvent it is possible for a phase-change to occur by solution of one phase followed by crystallisation of the other from solution, and under these conditions the two solid phases can be considered independent. The simple form of the phase rule then applies, and a sharp transition temperature may be expected. The temperature measured in this way would lie within the 'transition range' measured by the spectroscopic method.

TABLE 15.1. TRANSITION RANGES IN CRYSTALLINE NITRATES.

Salt	Transition range (°C)	
	Present work	Literature
KNO_3		
II ⇌ I	126.7 - 128.05	127.3 - 127.9 (Ref 1)
III ⇌ I	122.9 - 125.0	126.1 (Ref 1)
$RbNO_3$		
IV ⇌ III	158.4 - 163.9	163.5 ± 5 (Ref 3)
		164 (Ref 4)
		160 (Ref 5)
III ⇌ II	218.0 - 222.3	211 - 218 (Ref 5)
		219 (Ref 6)
II ⇌ I	282.0 - 283.4	291 (Ref 4)
		281 (Ref 5)
$CsNO_3$		
II ⇌ I	152.8 - 153.4	143 - 161 (Ref 7)
		163 (Ref 8)
		154 (Ref 4)

TABLE 15.1, continued.

Salt	Transition range (°C)	
	Present work	Literature
NH_4NO_3		
IV ⇌ III	29 - 44	41 (Ref 9) 35 (Ref 2) 32 (Ref 10)
III ⇌ II	78 - 88	86 (Ref 2) 86 (Ref 9) 82.7 (Ref 10)
II ⇌ I	121.8 - 125	127 (Ref 2) 125 (Ref 9) 125.5 (Ref 10)
$AgNO_3$		
II ⇌ I	157.6 - 158.6	159.6 (Ref 10) 160 (Ref 2)
$TlNO_3$		
III ⇌ II	-	75 ± 1.8 (Ref 10) 77.5 (Ref 2) 61 - 80 (Ref 7)
II ⇌ I	upper limit 146	145 ± 1.5 (Ref 10) 147 (Ref 2) 142.5 - 152.6 (Ref 7)

15.4. The transition in potassium nitrite at 40 - 50°C.

This transition was first detected during the zone-refining of the salt. When the potassium nitrite in the refining column was cooling after the passage of the molten zone, it was transparent until its temperature reached about 40°C. On further cooling the salt underwent a marked change; highly-reflecting crystal surfaces were formed, and these imparted a scintillating, brilliant appearance to the column and rendered it opaque. If the salt was re-heated above 50°C the clear appearance was restored. When the heater passed along the zone-refining column the 'clear' phase extended for some two or three cms on either side of it and was separated from the 'opaque' phase by fairly sharp boundaries.

Mother-of-pearl interference colours could be seen in a newly-formed sample of the 'opaque' phase, but if the salt was exposed to the atmosphere the colours faded and the scintillating appearance was lost within half an hour (although the material remained opaque). The fading spread from the exposed surfaces into the bulk of the sample and was almost certainly caused by moisture, as the following experiment shows. When some potassium nitrite was fused, cooled to room temperature and stored under vacuum, the interference colours in the opaque phase showed no reduction in intensity after 24 hours but immediately began to fade when air was admitted to the tube. One hour later the salt was visibly wet, and drops of concentrated solution could be poured off.

The transition was studied by the 'constant frequency' technique. In the range 40 - 50°C the temperature in the thermostat and sample was uniform to better than 0.1°C

(see Table 11.6), so the measured block temperatures required no correction. Frequencies were chosen either on the edge of the strong band ($\sim$ 40 kcm^{-1}) or in the region of relatively weak absorption between the two bands ($\sim$ 35 kcm^{-1}); in either case, the transformation from the 'opaque' to the 'clear' form was accompanied by large changes in % transmission (up to 60%).

Even when heating and cooling rates as low as 0.1°C per minute were used, the transition showed marked hysteresis. If the thermostat temperature was changed by increments of 1°C in the hysteresis region the % transmission reached a steady value at each stage, taking one or two minutes to do so.

The shape of the hysteresis loop in a plot of % transmission against temperature was reproducible for dry samples, but was influenced by the presence of moisture. Figure 15.3 shows the loop for a dry sample of the zone-refined salt, obtained in the following way. Two Spectrosil plates were heated to 430°C on the electric hotplate, the salt was taken from a desiccator (in which it had been stored over P_2O_5) and the sample was made up in the usual way (see Section 11.10). The salt film was allowed to freeze and was immediately transferred to the thermostat in the spectrophotometer. A heating and cooling cycle was carried out without delay, using a rate of temperature change of 0.5° per minute, and when this was finished the salt still had the scintillating appearance characteristic of the dry salt.

It can be seen from the diagram that the total length of the loop along the temperature axis is about 10°C, or more if the narrow end portions are taken into account. This length is difficult to measure precisely, but the width

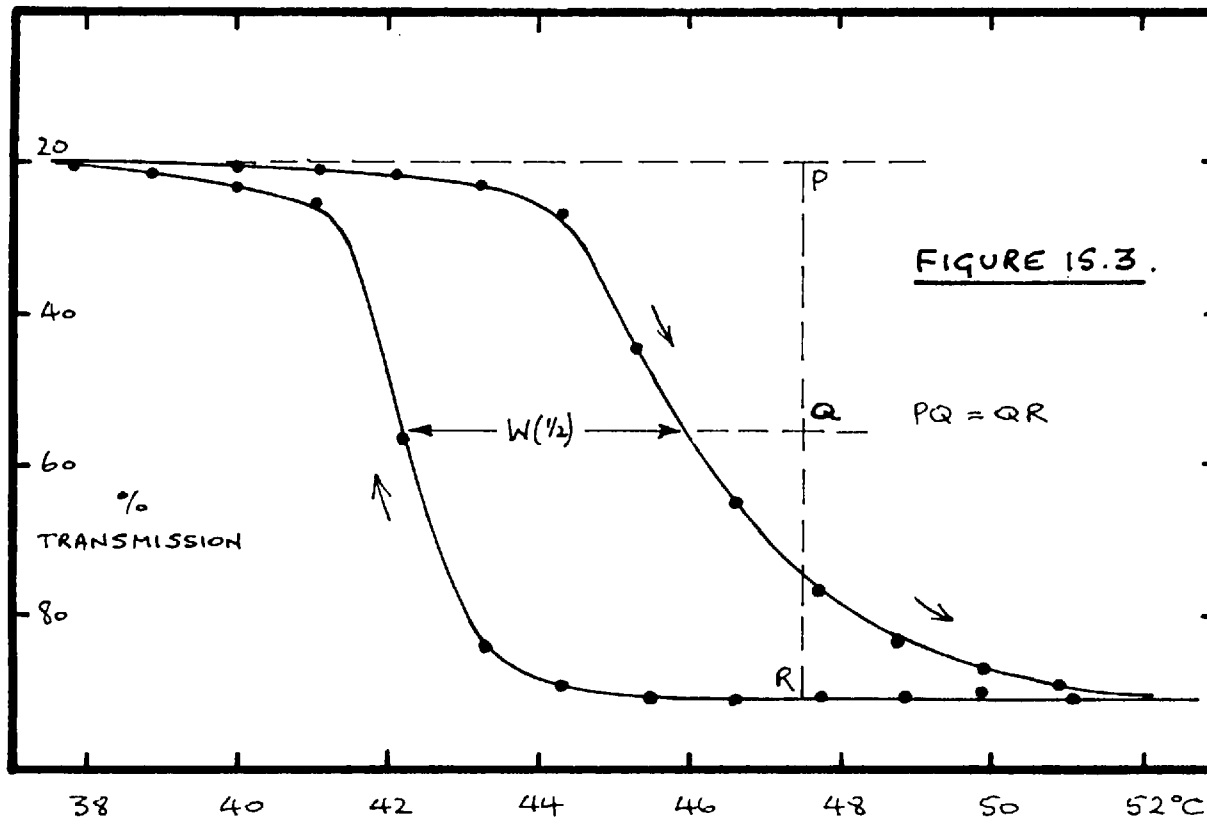


FIGURE 15.3.

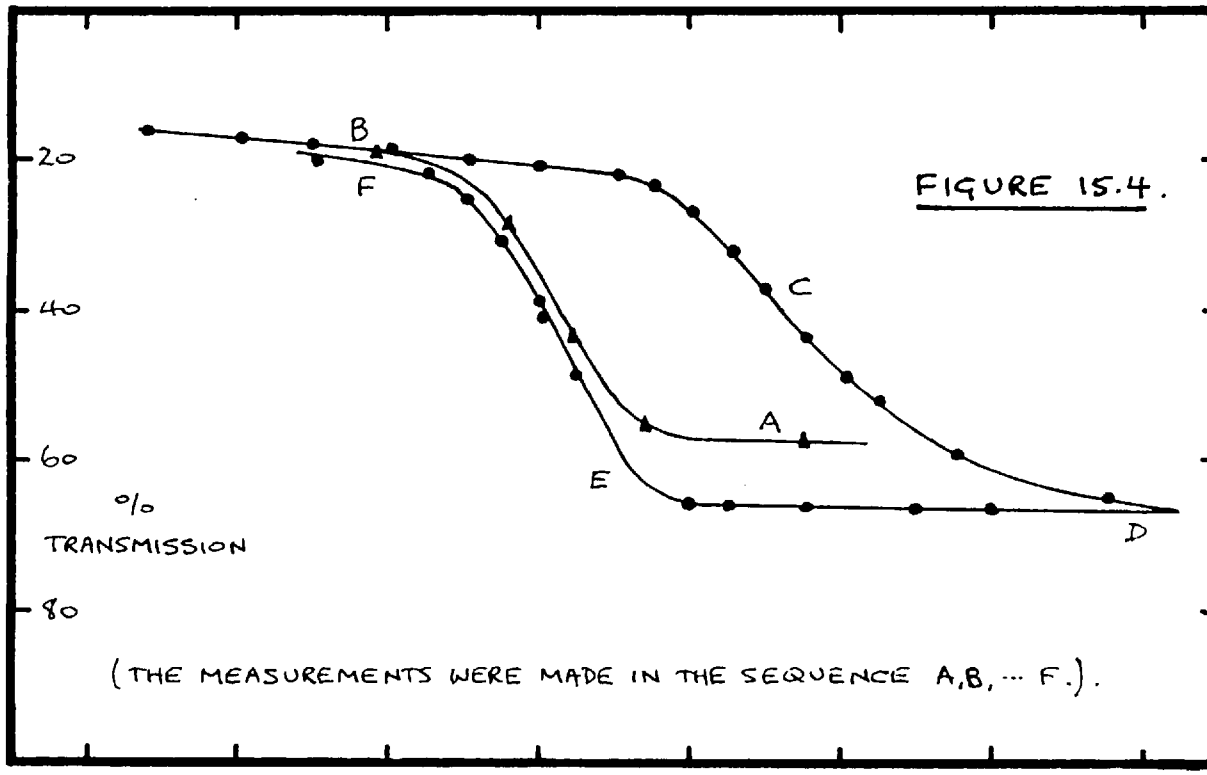


FIGURE 15.4.

(THE MEASUREMENTS WERE MADE IN THE SEQUENCE A, B, ··· F.).

HYSTERESIS CURVES FOR ZONE-REFINED POTASSIUM NITRITE.

FIG. 15.3 - DRY SAMPLE; FIG. 15.4 - MOIST SAMPLE.

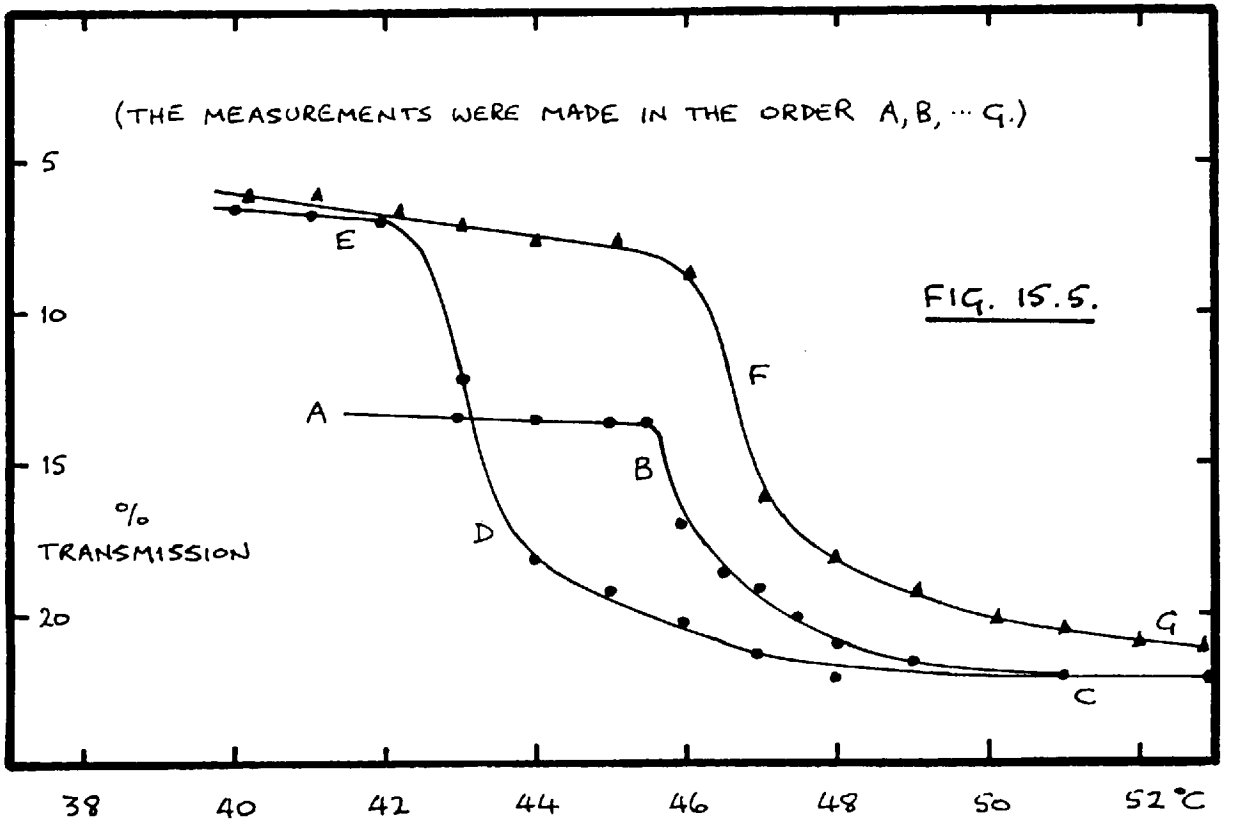


FIG. 15.5.

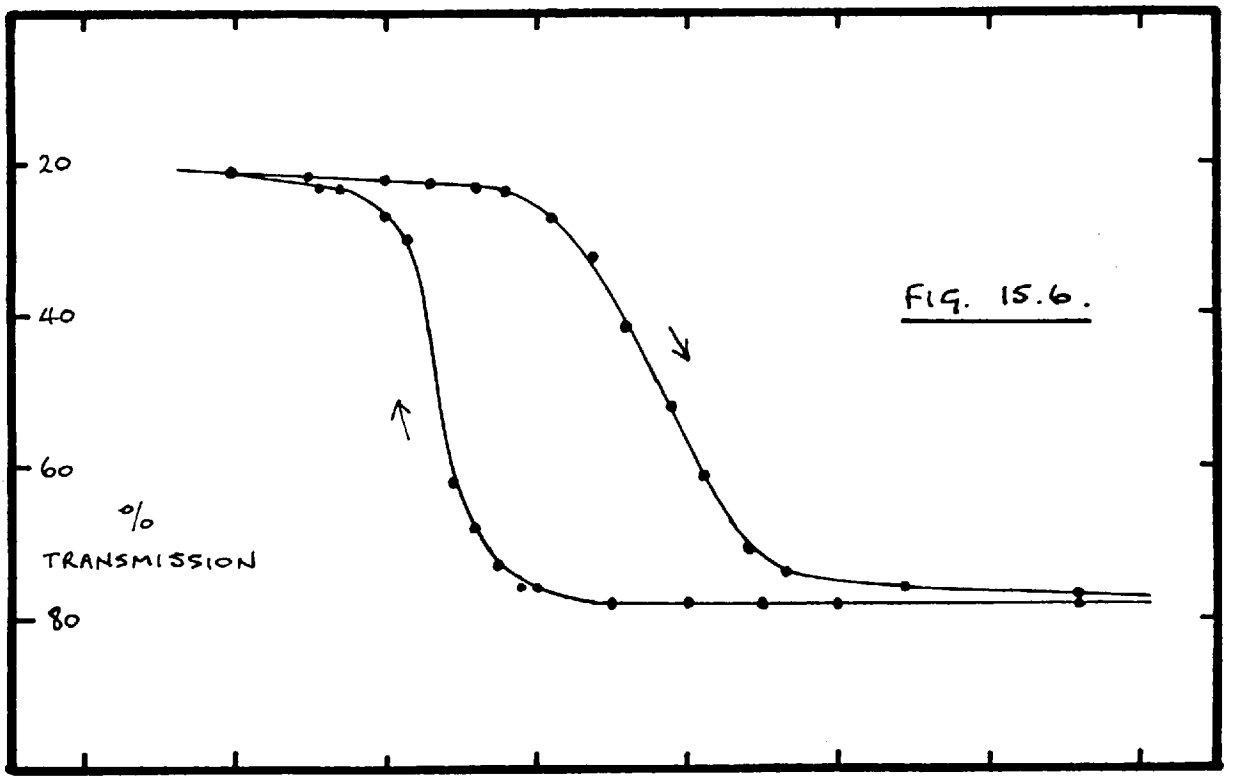


FIG. 15.6.

FIGURES 15.5 AND 15.6. HYSTERESIS CURVES FOR MOIST POTASSIUM NITRITE.

midway between the upper and lower transmission limits can be measured to ± 0.1°C because the sides of the loop are steep in this region. This width at half-height (marked on Figure 15.3 as W(½)) will be used to characterise the hysteresis; for the curve in Figure 15.3, W(½) is 3.7°C.

Attempts were made to study the effect of moisture on the width of the loop. It was difficult to obtain precise information because although the samples took up moisture from the atmosphere at room temperature some of this was lost again when the salt was heated to 50°C. If a temperature cycle 40° → 50° → 40° was carried out on a film which had been allowed to become moist at 20°, the water was driven off progressively and the % transmission failed to return to its original value at 40°C. Reproducible behaviour was found only when the water content of the sample had fallen below a certain level.

The salt film used to obtain the loop in Figure 15.3 was moistened at the edges with distilled water. After 24 hours the water had penetrated to the centre of the film, which had lost its scintillating appearance and was visibly wet. The sample was put back into the spectrophotometer and the temperature was changed in the sequence 50° → 40° → 50° → 40°C at a rate of 0.4°C per minute. Figure 15.4 shows a plot of % transmission against temperature. It is seen that a closed loop was obtained only during the last two half cycles; W(½) for this loop was 3.3°C.

In similar experiments carried out on two more moist samples made from zone-refined salt, W(½) had values 3.4° and 2.8°C. The curves are reproduced in Figures 15.5 and 15.6. The rates of temperature change in these two experiments were 0.2° and 0.1° per minute respectively.

These results show quite clearly that the hysteresis loop is narrowed by addition of moisture to a dry sample.

One experiment was carried out on a sample made up from Analar potassium nitrite taken straight from the reagent bottle. When heated at 0.2° per minute the film transformed to the high-temperature form at 43.0°C, the change being complete in about ten seconds. On immediate re-cooling, the reverse change took place equally rapidly at 40.7°C. W(½) for this cycle was therefore 2.3°C. The sample was then fused in the thermostat, and re-cooled to room temperature. A second heating and cooling cycle was performed. The transition now showed hysteresis; the change took place between 47° and 57° on heating and between 50° and 42° on cooling. This change from sharp and rapid transition to slow transformation with hysteresis was almost certainly caused by loss of moisture from the sample when it was fused between the two experiments. Since moisture had such a marked effect on the hysteresis loop it is not possible to say whether the ionic impurities present in the Analar salt (at least 0.3 mole %; Section 8.2.2) caused it to behave differently from the zone-refined samples.

The appearance of highly-reflecting crystal surfaces when the 'clear' phase is cooled below 40°C suggests that surface and strain energy are responsible for the hysteresis in dry samples. For an interval of some 5°C on either side of the transition temperature the sum of these two energies must be of the same order of magnitude as the free energy difference between the two (strain free) crystalline forms. In the previous sentence, 'transition temperature' is used to mean the temperature at which the two solid phases are in equilibrium in the presence of a solvent. In the experiments described above, the water would narrow the hysteresis loop

by allowing the transformation to take place by the alternative path

$$\text{I} \longrightarrow \text{solution} \longrightarrow \text{II}.$$

This does not involve the direct growth of one phase in a matrix of the other, so the production of strains and large areas of new inter-phase surfaces is avoided.

In the early stages of this work the transparent, glassy appearance of the 'clear' phase led to the suggestion that the substance actually was a glass, i.e. a non-crystalline, supercooled melt. This possiblity can now be dismissed, on the following grounds:

a) A few crystal interfaces could be seen in the solid phase above 50°C.

b) The boundaries between the 'clear' phase and the melt in the zone-refining apparatus were sharp and well-defined, particularly as the melt was lemon-yellow while the solid was almost colourless. If the 'clear' phase were a glass the transition from solid to liquid would be continuous.

c) The 'clear' phase could be re-formed from the 'opaque' phase by heating the latter above 50°C. For a true glass the process of crystallisation (vitrification) would be irreversible, and the glass could be re-formed only by melting the crystalline solid and re-cooling it.

It is more probable that the clear phase consisted of a relatively small number of crystals and that these broke up into domains of the low-temperature form when cooled below 40°C. If the crystal axes of the domains were related to

those of the original crystals the latter could be re-formed when the sample was heated. Behaviour of this kind has been observed in potassium dihydrogen phosphate (Ref 11) and in some of the transitions in crystalline nitrates (Ref 12).

15.5. Potentialities of the technique.

The relative convenience and economy of the spectroscopic technique for studying phase-transitions is demonstrated by the fact that the investigation of the complicated potassium nitrate transition occupied less than a week and required only a few milligrams of salt (which could be recovered if required). For the other nitrates, simple measurement of the transition ranges took only a few hours for each salt. The method has advantages over conventional dilatometry and thermal analysis if the substance to be investigated is difficult to prepare, since the latter techniques require samples of at least several grams.

The operation of the spectrophotometer and temperature control unit during an investigation involved only the turning of knobs, so 'remote control' of the whole apparatus would present no major difficulties. The technique therefore has obvious potential for the study of phase transitions in highly radio-active materials as well as in those whose lifetime is limited by chemical instability.

REFERENCES TO CHAPTER 15.

1. F.C. Kracek, J. Phys. Chem., (1930), 34, 188 and 255.

2. R. Cino, E. Ferroni and M. Cocchi, Ann. Chim. (Rome), (1957), 47, 841.

3. Bridgeman, Proc. Amer. Acad. Arts & Sci., (1916), 51, 581.

4. V.E. Plyushchev, I.B. Markina and L.P. Shklover, Doklady Akad. Nauk SSSR, (1956), 108, 645.

5. A. Mustajoki, Ann. Acad. Sci. Fenn., J Sarja A6, No 9, (1958).

6. Schwarz, Beiträge zur Kennt. Umwandl. Polym. Körper, Göttingen, (1894).

7. S. Sato, J. Sci. Res. Inst., (1954), 48, 59.

8. R. Cino, E. Ferroni and M. Cocchi, Ricerca Sci., (1957), 27, 2187.

9. K. Kamiyoshi and T. Yamakami, Sci. Reps. Res. Inst., Tokohu Univ., (1959), Ser. A, 11, 418.

10. International Critical Tables.

11. A.R. Ubbelohde, Quart. Revs. Chem. Soc., (1957), 11, 246. British Journ. Applied Phys., (1956), 7, 313.

12. R.N. Brown and A.C. Mclaren, Acta Cryst., (1962), 15, 974 and 977.

13. A.C. Mclaren, Reviews of Pure and Applied Chemistry, (1962), 12, 54.

D I S C U S S I O N

S E C T I O N

CHAPTER 16.

DISCUSSION: THE ELECTRICAL CONDUCTIVITY OF POTASSIUM NITRATE - BARIUM NITRATE MIXTURES.

There seems no doubt that the Wagner effect (see Section 3.7) occurs in crystalline nitrates as well as in the more widely studied alkali-metal and silver halides. The solid formed by freezing a solution of 0.1 mole % calcium nitrate in fused potassium nitrate has a conductivity three hundred times that of pure potassium nitrate at the same temperature (measurements made by Dr. E. Rhodes; Ref 1). The fact that the nitrate ion is polyatomic and non-spherical does not therefore prevent the appearance of cation vacancies when calcium ions are dissolved in solid potassium nitrate, these vacancies being large enough to accommodate a potassium ion and capable of movement away from their parent calcium ion under the influence of an electric field. It was thought necessary to establish this point; it might have been found that the vacancies were blocked by the adjacent nitrate ions. Blocking could occur, for example, by the onset of free three-dimensional rotation so that the nitrate ion became effectively spherical and occupied a greater volume than when stationary.

The results presented in Chapter 12 clearly show that there is no increase in conductivity when barium nitrate is dissolved in potassium nitrate melt; on the contrary, the conductivity falls progressively with rising barium ion concentration. The most obvious conclusion to be drawn from this is that the addition of barium ions does not cause an increase in the empty space available for the migration of cations in the melt; in fact they may actually

cause the ionic packing arrangement in the melt to contract slightly. The values of ΔH_σ and ΔH_Λ in Table 12.2 (the so-called "activation energies for conduction") increase steadily with barium-ion concentration, and although it is not strictly correct to identify either of these parameters with the height of the potential barrier which a cation must overcome to migrate through the melt (see page 31) we may conclude that the addition of divalent cations to fused potassium nitrate restricts the movement of the ions under an electrostatic potential gradient.

It is quite evident that the long-range order which is present in crystalline potassium nitrate must be absent in the melt, since it is the retention of this order (combined with the condition of electrical neutrality) which causes cation vacancies to be formed when divalent ions enter solid solution in the crystal lattice. This conclusion about the structure of the melt is consistent with the evidence from diffraction experiments mentioned in Chapter 7.

It is possible to make some more refined calculations of transport parameters in the mixed melts by using the equation developed by Bockris et al. and modified by Yaffe and van Artsdalen:

$$\Lambda_i = 5.18 \times 10^{18}(D + 2)zd_i^2.\exp(\Delta S^*/R).\exp(-\Delta H^*/RT)$$

(see Chapter 3).

In this equation, Λ_i is the equivalent conductivity due to a given ionic species of valency z, D is the microscopic dielectric constant, $2d_i$ is the distance moved by an ion when it jumps from one equilibrium position to the next and ΔS^* and ΔH^* are the entropy and enthalpy of activation

for the migration process.

For pure, fused potassium nitrate the transport number of the cation is known to be 0.60 (Ref 2), so Λ_i for the potassium ions is 0.60Λ (Λ being the measured equivalent conductivity). D is difficult to estimate, but the value 3 has been suggested by van Artsdalen and will be used here. A mean value

$$\bar{z} = \sum_i (n_i z_i) / \sum_i (n_i)$$

must be used for the valency of the cations in the mixtures, where n_i and z_i are respectively the equivalent fraction and valency of the i'th cationic species. d_i for pure potassium nitrate and pure barium nitrate melts has been estimated by assuming that the cations lie on a body-centred cubic lattice whose cell-constant a is related to the molar volume V_m by the equation

$$N.a^3 / 2 = V_m$$

(N = Avogadro's number); $2d_i$ is then equal to half the body diagonal of the unit cell, i.e. 0.866a. The molar volumes of the pure melts were taken from Chapter 13. Values of d_i for the mixtures were found by linear interpolation.

ΔS^* and ΔH^* have been calculated from these data, using the measured values of Λ and assuming that the sum of the cation transport numbers in the mixtures remains 0.60. The free energy of activation, ΔG^*, is given by

$$\Delta G^* = \Delta H^* - T\Delta S^*.$$

In the case of the mixtures, the activation parameters obtained in this way must be regarded as averages applying to the cation population as a whole.

TABLE 16.1. Transport parameters for KNO_3 - $Ba(NO_3)_2$ melts at 350°C.

Mole % $Ba(NO_3)_2$	$10^8.d_i$	z	ΔH^* (kcal / mole)	ΔS^* (e.u./ mole)	ΔG^* (kcal/ mole)
0.0	2.44	1.00	4.00	-6.59	8.11
2.5	2.45	1.025	4.05	-6.64	8.19
5.2	2.46	1.05	4.12	-6.71	8.30
12.4	2.49	1.125	4.24	-6.94	8.56

The Table shows that ΔH^* (which is identical with E_Λ of of Chapters 3 and 12) and ΔG^* both increase with rising barium ion concentration. ΔS^* is negative (showing that activation can be regarded as an ordering process), and becomes numerically larger as barium ions are added. All three parameters vary approximately linearly with barium concentration. These results are consistent with the general conclusions stated at the beginning of the Chapter; the addition of barium ions to fused potassium nitrate leads to some restriction in the migration of the ions in an electric field, which can be attributed to the electrostriction arising from the double charge on the barium ions. The phenomenon might be described as an 'anti-Wagner effect'.

The equivalent volumes of the mixtures provide confirmation for this interpretation of the conductivity results, and they are discussed in the next Chapter.

REFERENCES TO CHAPTER 16.

1. B. Cleaver, E. Rhodes and A.R. Ubbelohde, Discuss. Farad. Soc., (1961), 32, 210.

2. F.R. Duke, R.W. Laity and B. Owen, J. Electrochem. Soc., (1957), 104, 299.

3. E.R. van Artsdalen and I.S. Yaffe, J. Phys. Chem., (1955), 59, 118.

CHAPTER 17.

DISCUSSION: EQUIVALENT VOLUMES OF FUSED POTASSIUM NITRATE - BARIUM NITRATE MIXTURES.

17.1 Volume change on mixing fused potassium nitrate and barium nitrate.

If a pair of univalent cations are removed from the crystalline lattice of a 1:1 salt and are replaced by one divalent cation of the same or similar radius (the other cation site remaining empty), the overall volume of the crystal should remain unchanged. This has been shown to be so for solid solutions of calcium chloride in potassium chloride (Ref 1). If the same occurs when the potassium ions in fused potassium nitrate are replaced by barium ions, a plot of equivalent volume against composition for liquid mixtures should be a straight line parallel to the composition axis (i.e. the number of nitrate ions in a given volume of melt should be independent of the potassium/barium ratio).

Figure 13.1 shows at once that this is not the case; the equivalent volume of barium nitrate is estimated to be only 43.25 ml at 440°C, compared with 56.38 ml for potassium nitrate, so the total volume is reduced by some 23% when all the potassium ions are replaced by barium. Indeed, the fraction of the volume of the melt which is not attributable to the ions themselves actually decreases from 51% for potassium nitrate to 43% for barium nitrate. (These figures are based on the ionic volumes NO_3^- = 21.7 ml/mole and $K^+ = Ba^{++}$ = 5.9 ml/mole, found in the way described in

Chapter 7). The barium ions therefore cause the ions in a mixed melt to be even more closely packed than those in pure fused potassium nitrate, and thus bring about the 'anti-Wagner' conductivity effect described in the previous Chapter. Consistently with this picture, the coefficient of cubic expansion of the mixed melts decreases steadily with rising barium ion concentration (see column 4 of Table 13.4).

A second remarkable feature of the equivalent volume isotherms in Figure 13.1 is the fact that they are straight lines to a very high degree of approximation, the standard deviation of the experimental points from the lines of closest fit being less than 0.02% for the isotherms at 373°, 410° and 440°C.

It is interesting to compare the volume change on mixing (excess volume) in the system KNO_3 - $Ba(NO_3)_2$ with that in other binary salt mixtures and with that in mixtures of liquids made up of molecules rather than ions. Excess volumes for these two classes of mixtures are shown as a function of composition in Figures 17.1 and 17.2.

Parts VII and VIII of Figure 17.1 refer to the KNO_3 - $Ba(NO_3)_2$ system at 410° and 440°C respectively, and have been drawn on the assumption that the equivalent volume of barium nitrate is equal to its partial equivalent volume as given by equation 13.8. (Some assumption of this kind is necessary because it is impossible to make density measurements on mixtures containing more than 50 equiv.% barium, owing to decomposition). Parts VII and VIII of the Figure are therefore not strictly comparible with the others. The following method has been used to compensate for this difference.

Key to Figure 17.1.

The curves refer to the following pairs of ionic melts (the first-mentioned being the pure component at the left-hand side of the diagram).

I $MnCl_2$ + KCl, at 800°C (Ref 2)

II CdI_2 + KI, at 700°C (Ref 3)

III $CaCl_2$ + KCl, at 850°C (Ref 4)

IV $LiNO_3$ + KNO_3, at 350°C (Ref 5)

V KNO_3 + $NaNO_3$, at 400°C (Ref 2)

VI KNO_3 + KBr, at 730°C (Ref 3)

VII KNO_3 + $Ba(NO_3)_2$, at 410°C (present work)

VIII KNO_3 + $Ba(NO_3)_2$, at 440°C (present work).

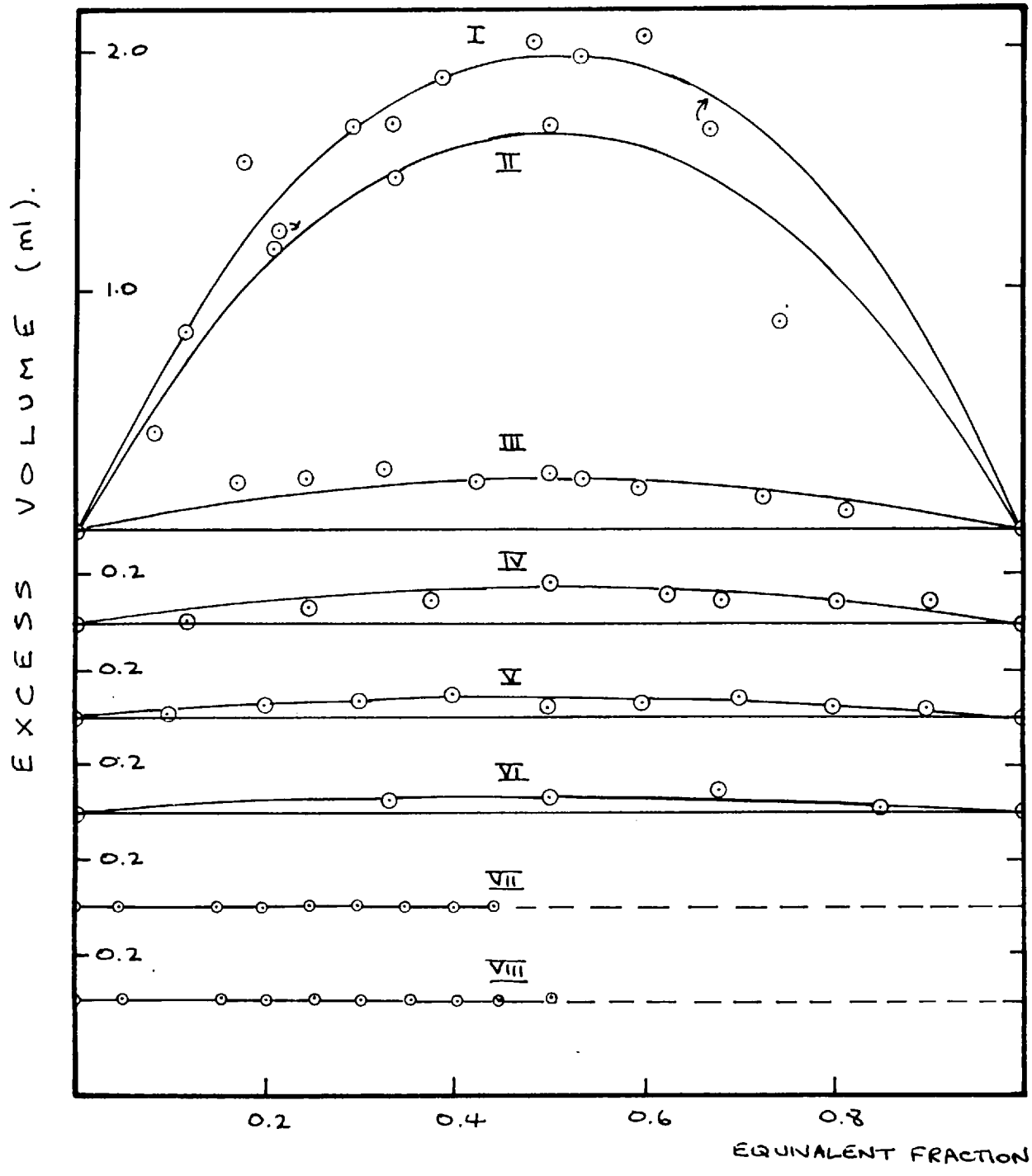


FIGURE 17.1. EXCESS VOLUMES OF SOME BINARY MIXTURES OF IONIC MELTS. (FOR KEY, SEE PREVIOUS PAGE).

Key to Figure 17.2.

The following mixtures are represented:

I benzene + cyclo-hexane, at 20°C (Ref 6)

II carbon tetrachloride + neo-pentane, at 0°C (Ref 7)

III neo-pentane + benzene, at 0°C (Ref 7)

IV argon + nitrogen, at 84°K (Ref 8)

V n-hexane + cyclo-hexane, at 20°C (Ref 9)

VI n-decane + n-hexadecane, at 20°C (Ref 10)

VII cyclo-hexane + iso-octane, at 30°C (Ref 11).

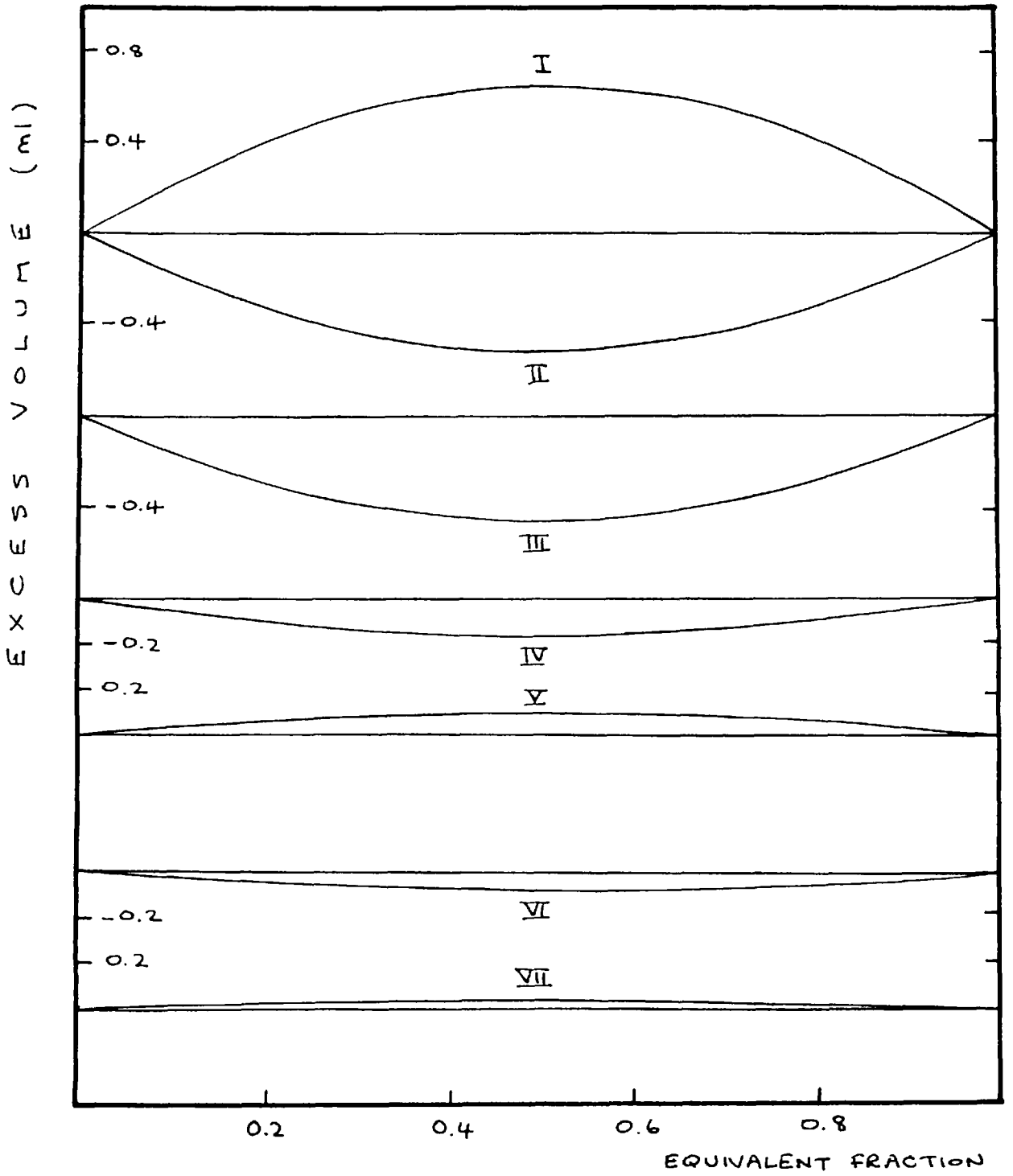


FIGURE 17.2. EXCESS VOLUMES OF SOME BINARY MIXTURES OF ORGANIC LIQUIDS. (FOR KEY, SEE PREVIOUS PAGE).

Suppose that a set of exact values of equivalent volumes were available for the system KNO_3 - $Ba(NO_3)_2$ over the entire composition range, and that a plot of excess volume against composition was in fact a parabola with a maximum (v^E_{max}) at 50 equiv. % barium. Suppose now that a straight line is fitted to the points in the composition range 0 - 50 equiv. % barium, by the method of least squares. (This line corresponds to the horizontal axis in parts VII and VIII of Figure 17.1). Clearly, the deviations (d) of the points from this straight line would be positive in the region 25% barium and negative near 0 and 50% (or vice versa). Mathematical analysis shows that the maximum deviation (d_{max}) occurs at 25 equiv. % barium, and that d_{max} is exactly one-tenth of v^E_{max} as defined above.

The deviations of the author's experimental equivalent volumes from the best straight lines through them were plotted against composition, at 410° and 440°C. The points were scattered randomly on both sides of the composition axis, and their distribution gave no grounds for supposing that the best line through them was a curve rather than a straight line. By trial and error, an estimate was made of the minimum value of d_{max} for which curvature in this plot could have been discerned above the random scatter due to measuring errors. This value of d_{max} was found to be 0.005 ml, and the corresponding value of v^E_{max} is 0.05 ml (from the relationship mentioned above). In other words, if the plot of equivalent volume against composition for the system KNO_3 - $Ba(NO_3)_2$ is really a parabola, v^E for a 50:50 mixture is less than 0.05 ml. Comparison with Figures 17.1 and 17.2 shows that this system approaches ideality at least as closely as any of the other mixtures illustrated (with the possible exception of the system cyclo-hexane + iso-octane, shown in part VII of Figure 17.2); i.e. it is as

nearly ideal as a mixture of the inert elements or of paraffin hydrocarbons.

Before these points are discussed, attention is drawn to the low standard deviation of the experimental results in parts VII and VIII of Figure 17.1 compared with parts I to VI. This demonstrates the superiority of Husband's method of density determination.

The following explanation can be put forward for the nearly ideal volume of mixing in the system KNO_3 - $Ba(NO_3)_2$. In pure melts of these salts, the cations have only nitrate ions as nearest neighbours, the probability of cation-cation contact being extremely small for energetic reasons (see Chapter 7, section 4). When the melts are mixed, the cations in the mixture still have only nitrate ions as nearest neighbours, so mixing does not enable contact to occur between any pairs of ions which were not already in contact in the pure components; the only new type of interaction in the mixture is that between potassium ions and barium ions occupying positions as second-nearest neighbours. Short-range effects between ions in contact, which usually play a dominant role in determining the volume change on mixing, can therefore undergo no change when potassium nitrate and barium nitrate are mixed; in this system, the deviations from ideality must arise mainly from interactions between second-nearest neighbours. Because of this circumstance, the excess functions v^E and h^E for binary salt mixtures having one ion in common sometimes show unusual relationships to eachother. For example, heat is evolved when fused nitrates of different alkali-metals are mixed (h^E negative), yet the volume of the mixture is greater than the sum of the volumes of the components at the same temperature (v^E positive)(Ref 12,13). Similar behaviour is unknown in the field of

molecular-liquid mixtures, in which the molecules of the two components invariably come into contact with each other.

17.2. Heat of mixing of fused potassium nitrate and barium nitrate.

It is interesting to consider whether the liquid system KNO_3 - $Ba(NO_3)_2$ also approaches ideality in respect of the heat of mixing. Direct thermochemical experiments would be complicated by the fact that pure barium nitrate cannot be fused without decomposition, so calorimetric techniques would be restricted to measurement of temperature changes on mixing solutions of different concentration, or measurement of the heat of solution of solid barium nitrate in an unsaturated solution. However, the order of magnitude of the excess heat h^E can be deduced from the freezing-point curve of the system. This curve has a eutectic point at 22.5 equiv. % barium nitrate (Ref 14), and the two branches otherwise show no discontinuous change of slope. The solid which separates when a liquid mixture is cooled must therefore be either pure barium nitrate or pure potassium nitrate. The activity (a) of potassium nitrate in the liquids on the potassium-rich branch of the freezing-point curve can be calculated from the equation

$$\ln a = (1/T_f - 1/T).L_f/R + \frac{C_L - C_S}{R}.(T_f/T - 1 - \ln T_f/T).$$

(cf. Ref 15). In this equation, T_f and T are the freezing-points (in ^oK) of pure potassium nitrate and of the solution respectively, L_f is the molar latent heat of fusion of pure potassium nitrate at temperature T_f, and C_L and C_S are the molar specific heats of liquid and solid potassium nitrate

at constant pressure (these specific heats being assumed independent of temperature in the range T to T_f). Using values of L_f, C_L and C_S obtained calorimetrically by Goodwin and Kalmus, (L_f = 2570 cal/mole, C_L = 33.7, C_S = 29.5 cal/mole/°C) and the freezing-points reported by Protsenko and Malakhova (Ref 14), the activities and activity coefficients (γ) of potassium nitrate in several mixtures have been calculated and are listed in Table 17.1. No similar calculation is possible for the barium-rich side of the diagram because L_f, C_L and C_S for this salt are not known (and cannot be measured directly because of decomposition).

It is easily shown that the free energy released when one mole of liquid potassium nitrate is added to a large volume of a KNO_3 - $Ba(NO_3)_2$ mixture is

$$(\bar{G} - \bar{G}_o) = (\bar{H} - \bar{H}_o) - T(\bar{S} - \bar{S}_o)$$
$$= RT \ln a,$$

where partial molar quantities are indicated by a bar and refer to potassium nitrate throughout. If the entropy of mixing, $(\bar{S} - \bar{S}_o)$, has the ideal value $-R \ln x$ (x = mole fraction KNO_3), then the heat of mixing, $(\bar{H} - \bar{H}_o)$, is equal to $RT \ln \gamma$ ($\gamma = a/x$). Table 17.1 shows that $RT \ln \gamma$ takes negative values, and reaches about -50 cal for a solution of the eutectic composition (12.7 mole % $Ba(NO_3)_2$). It seems likely, therefore, that heat would be evolved if pure, fused potassium and barium nitrates could be mixed, and extrapolation shows that the excess heat h^E for an equimolar mixture might be as high as 500 - 800 calories/mole. Calorimetric work by Kleppa (Ref 17) indicates that a heat of mixing of this order of magnitude is not unlikely; he has shown that the excess heats of equimolar mixtures of

TABLE 17.1.

Activities (a) and activity coefficients (γ) of potassium nitrate in KNO_3 - $Ba(NO_3)_2$ mixtures.

Temp. (°C)	Mole fraction KNO_3 (x)	a	γ (= a/x)	RT ln γ (cal/ mole)
336	1.000	1.000	1.000	-
327	0.974	0.969	0.995	-7.0
318	0.947	0.938	0.990	-12.0
307	0.919	0.901	0.981	-25.0
294	0.889	0.859	0.966	-44.7
288	0.873	0.840	0.961	-51.7

supercooled liquid calcium nitrate with fused sodium, potassium and rubidium nitrates are respectively 250, 650 and 900 calories/mole at 350°C.

This heat of mixing could arise in one of the following ways:

(a) Through unsymmetrical polarisation of the nitrate ions in the mixtures. In pure melts of either potassium nitrate or barium nitrate, each nitrate ion is surrounded by cations of one kind, so the electrostatic field which it experiences is relatively symmetrical. If in a mixture the nearest neighbours of a given nitrate ion include one barium ion, this divalent ion will exert a relatively large polarising effect because of the disymmetry of the total field. The heat evolved on mixing the pure salts is the energy of interaction between such induced dipoles and the divalent ions.

(b) Through a reduction in the repulsion energy between the divalent cations when a divalent nitrate is mixed with a univalent nitrate. In a pure melt the cations repel each other, the repulsion energy for any pair of ions being proportional to the product of their charges divided by the distance separating them. Consider a barium ion in pure barium nitrate melt, and suppose it to have n other barium ions at distance r as its nearest cation neighbours. The repulsive energy between the central ion and the others is $n.2^2/r$. Consider also a potassium ion in pure, fused potassium nitrate; suppose that it also has n potassium ions as nearest cation neighbours, also at distance r. The repulsion energy between the central ion and its neighbours in this case is $n.1^2/r$. Suppose now that the central barium ion in the first melt and the central potassium ion

in the second are exchanged. For the potassium ion surrounded by barium ions the repulsive energy is now n.1.2/r, and for the barium ion in the potassium nitrate it is n.2.1/r. The sum of these energies is 4n/r, which is less than the original sum of 5n/r. The difference represents the heat evolved when the transposition is made.

Generalisation of this argument leads to the conclusion that heat is evolved when potassium nitrate and barium nitrate melts are mixed. No account has been taken here of the fact that the molar volumes of the two salts are not equal, (i.e. the parameters n and r are probably not the same for the two pure melts), and interactions between more distant neighbours than the first have been ignored, but these refinements would not be expected to alter the general validity of the conclusion.

17.3. The structure of KNO_3 - $Ba(NO_3)_2$ melts.

If barium nitrate is made to enter solid solution in potassium nitrate, the overall structure of the potassium nitrate lattice is retained and there are regions of strain localised around each barium ion and its attendant cation vacancy. These strains could be relieved by clustering of the barium ions into groups, and, ultimately, by the formation of barium nitrate crystals as a separate phase (which actually occurs if the barium concentration exceeds about 0.1 mole %). It might be thought that the barium ions in a fused mixture of the two salts would show a similar tendency to form clusters. If this occurred the mixtures would show the 'positive deviations' characteristic of such a situation; the excess heat and excess volume would both be positive, and there might be a miscibility gap at

temperatures near the liquidus. The experimental evidence summarised above shows that no such behaviour is observed; the excess volume for the fused mixtures is near to zero and the excess heat is negative. The ultra-violet spectra of the melts provide further evidence against clustering of the barium ions. The frequency of the maximum of the weak absorption band of the nitrate ion is determined almost entirely by the first shell of cations surrounding each anion (see Chapter 18), so segregation of the cations into groups should cause the band to split into two maxima, corresponding respectively to nitrate ions having potassium ions as neighbours and those with barium ions as neighbours. The spectra reproduced in Figure 14.16 show no indication of splitting; the frequency of the maximum increases linearly with barium ion concentration (Figure 14.18). Lastly, the phase diagram for the system (Figure 10.4) shows no miscibility gap.

The conclusion to be drawn from this is that the barium ions in the liquid mixture are distributed evenly throughout the melt, showing, if anything, a tendency to avoid each other (because of the effects described under (a) and (b) above). It is clear that there can be no strains in the region of the barium ions in the fused mixtures; potassium nitrate melt accommodates barium ions by undergoing local changes in structure. This adjustment of structure appears to take place smoothly and continuously in the concentration range 0 - 50 equiv. % barium, so the amount of free space in any mixture can be calculated from the free space in the pure components by simple proportion. Since the free volume in fused barium nitrate is less than that in fused potassium nitrate (see page 326), this finding is in accord with the conclusions drawn in the previous Chapter and accounts for the 'anti-Wagner' conductivity effect therein described.

It is clearly a characteristic property of melts that they are incapable of sustaining local strains of the type which lead to vacancy formation in the corresponding crystals, and due note must be taken of this limitation when attempts are made to use a 'quasi-crystalline' model as a basis for the theoretical interpretation of the properties of ionic melts.

REFERENCES TO CHAPTER 17.

1. H. Pick and H. Weber, Z. Phys., (1950), 128, 409.

2. I.G. Murgulescu and St. Zuca, Rev. chim., Acad. rep. pop. Roumaine, (1959), 4, 227.

3. H. Bloom, I.W. Knaggs, J.J. Molloy and D. Welch, Trans. Farad. Soc., (1953), 49, 1458.

4. E.P. Vereshchetina and N.P. Luzhnaya, Izvest. Sekt. fiz-Khim. Anal., Inst. obshchei neorg Khim., (1954) 25, 188.

5. G.P. Smith, G.F. Petersen and W.M. Ewing, Oak Ridge National Report no. 2762 (1959).

6. A.R. Mathieson and J.C.J. Thynne, J. Chem Soc., (1956), p. 3708.

7. A. Desmyter and V. Mathot, J. Chem. Phys., (1953), 21, 782.

8. R.A.H. Pool and L.A.K. Staveley, Nature, (1957), 180, 1118.

9. H. Klapproth, Nova Acta Leop. Carol., (1940), 9, 309.

10. A. Desmyter and J.H. van der Waals, Rec. Trav. Chim. Pays-Bas, (1958), 77, 53.

11. F. Danusso, Mem. Accad. Lincei, (1952), 13, 131; (1954), 17, 109.

12. O.J. Kleppa and L.S. Hersh, J. Chem. Phys., (1961), 34, 351.

13. J.L. Katz, B.L. Powers and O.J. Kleppa, J. Chem. Phys., (1961), 35, 765.

14. P.I. Protsenko and A.Ya. Malakhova, Zh. neorg. Khim., (1957), 2, 2145.

15. I. Prigogine and R. Defay, "Chemical Thermodynamics", (trans. D.H. Everett), Longmans, London, 1954.

16. H.M. Goodwin and H.T. Kalmus, Phys. Revs. (1909), 28, 1.

17. O.J. Kleppa and L.S. Hersh, Discuss. Farad. Soc., (1961), 32, 99.

CHAPTER 18.

DISCUSSION: THE ULTRA-VIOLET ABSORPTION SPECTRA OF CRYSTALLINE AND FUSED NITRATES AND NITRITES.

18.1. The strong absorption bands of the nitrates and nitrites.

The results obtained for these bands are limited to data on the movements of their low-frequency edges with changing temperature. These movements can be summarised as follows:

a) For a given crystalline phase, the band edge always moved to lower frequency (or to higher extinction coefficient) with rising temperature. This movement was a linear function of temperature for the alkali nitrates and for silver nitrate below its transition at 158°C, and also for sodium nitrite. In the case of silver nitrate the increasingly rapid movement between 158° and the melting-point can be ascribed to overlap with the weak band. For potassium nitrite between 50° and 400°C the band-edge again accelerated towards lower frequencies when the sample temperature was raised. It is possible that this was caused by the presence in this region of two superimposed bands (having different rates of movement with temperature). The curvature could also be due to a ferroelectric - paraelectric transition in the solid, though supporting evidence on this point is not available.

b) The band-edge underwent abrupt shifts at crystal transitions and at melting-points, showing that the strong band is structure-sensitive. The directions of these shifts were not consistently either the same as or opposite to the corresponding movements of the weak band maximum,

which shows that the latter were not caused merely by changes in the degree of overlap of the strong band. The removal of this possible source of uncertainty is the main reason for presenting the band-edge results in such detail.

For the alkali nitrates, ammonium nitrate and the nitrites overlap between the two bands was so slight that it was not considered necessary to correct E(2) for this effect. In the case of silver and thallous nitrates overlap was more serious, but the difficulty was overcome by making measurements on the low-frequency edge of the weak band.

Since the maximum of the strong band was at 50 kcm^{-1} and 10,000 litres/mole.cm for the nitrates, and at 47 kcm^{-1} and 6,000 litres/mole.cm for the nitrites (see Chapter 6), it would clearly be wrong to assume that the movements of these maxima with temperature would be the same as, or even in the same sense as, the observed movements of the band-edge (which was followed only up to an extinction coefficient of 300). No quantitative significance can therefore be attached to the gradients $dE(t = x\%)/dT$. Indeed, for several of the salts examined this quantity was shown to vary with the value of x chosen (see, for example, Figures 14.8, 14.9, 14.11, 14.12), so it is not constant even for extinction coefficients up to 300. However, the fact that the strong and weak bands involve different electronic rearrangements suggests that the influence of the nitrate ion environment on the positions of the maxima may not be the same in the two cases. The direct measurement of E(1) and of its variation with temperature might therefore yield information on structural changes of a different kind to that provided by the present study of the weak band. The author's demonstration that the measurements made in air are subject to very large stray light errors at frequencies above 50 kcm^{-1} indicate that the work would best be undertaken with a vacuum spectrophotometer in order to

avoid this source of uncertainty.

18.2. The weak absorption band of the nitrates at 33 kcm^{-1}.

The results obtained for this band are sufficiently precise to justify a search for detailed correlations between spectral shifts and the structural and other changes accompanying them.

E(2), the frequency of the absorption maximum, is known to depend on the identity of the cation, on the temperature and in the case of solid phases on the crystal structure. These factors will be discussed separately.

18.2.1. Dependence of E(2) on the identity of the cation.

G.P. Smith has shown that, for nitrate melts containing cations of rare-gas electronic configuration, E(2) at 365°C is given (in units of cm^{-1}) by

$$E(2) = 30740 + 2740 \sum_i (X_i z_i / r_i) \qquad (18.1)$$

where X_i, z_i and r_i are the equivalent fraction, charge (in units of the electronic charge) and radius (A) of the i'th cationic species (see Chapter 6). The relationship was found to hold if z_i/r_i did not exceed about 3 A^{-1}.

This dependence of E(2) on cation charge/radius ratio is reasonably attributed to stabilisation of the lone-pair oxygen electrons by the cations, the effect increasing with the polarising power of the latter. The way in which this stabilisation causes the band maximum to be displaced to higher frequency (relative to its value for an isolated nitrate ion) is described on page 72 .

It is convenient to discuss the spectra of the nitric acid solutions at this point, because they provide convincing support for this idea that the displacement of the weak band to higher frequency is due to stabilisation by the cations of the electrons on the oxygen atoms of the nitrate ions.

In nitric acid - water mixtures the protons form bridges between the nitrate groups and the water molecules:

$$H_2O...H^+...ONO_2^- \ .$$

The form of the bond between the H atom and the nitrate group can change from ionic (corresponding to the formula $H_3O^+.NO_3^-$) to covalent (corresponding to $H_2O.\ H\text{-}ONO_2$) according to the position of the bridging proton, and a bond of intermediate type is possible. If the $H\text{-}ONO_2$ bond is covalent the oxygen electrons whose excitation gives rise to the weak absorption band become involved in the H-O bond, so their energy is lowered relative to their energy in a free nitrate ion. If some measure can now be found for the degree of covalency of this $H\text{-}ONO_2$ bond in mixtures containing different proportions of water, it will be possible to see whether the changes in E(2) with concentration are in the expected sense.

This information about bond type can be found by studying the bond lenths and angles in the nitrate group in different mixtures. These have been measured by X-ray diffraction in solid nitric acid and in the two crystalline hydrates $HNO_3.H_2O$ and $HNO_3.3H_2O$. The relevant facts are collected in Table 18.1; data for sodium nitrate and for methyl nitrate nitrate are also given, for comparison.

The nitrate ion in sodium nitrate has D_{3h} symmetry, i.e. the bonds are of equal length and the ONO angles are all 120°

TABLE 18.1. Structure of the nitrate group in sodium nitrate, nitric acid and its hydrates and in methyl nitrate (data from Refs. 1, 2 and 3).

Compound	N-OH bond (A)	N-O bonds (A)	$\widehat{ONO}$
$NaNO_3$ (s)	1.218	1.218	120°
$HNO_3.3H_2O$ (s)	1.26	1.22	122°
$HNO_3.H_2O$ (s)	1.29	1.20	127°
HNO_3 (s)	1.33	1.20	130 - 140°
CH_3ONO_2 (g)	1.36 ($N-OCH_3$)	-	-

In nitric acid and its hydrates, however, the symmetry of the nitrate group is lowered to C_{2v}; one N-O bond is longer than the other two, and the angle between the two short bonds is greater than 120°. It can be seen from Table 18.1 that this departure from D_{3h} symmetry increases in the sequence $HNO_3.3H_2O$, $HNO_3.H_2O$, HNO_3(s), the long N-O bond in crystalline HNO_3 being only slightly shorter than that in the covalent molecule of methyl nitrate. We may conclude that the extent to which the oxygen electrons are involved in the covalent H-O bonds increases in this same sequence.

If the shifts in the position of the weak absorption band are in fact due to stabilisation of the oxygen 'lone-pair' electrons, we would expect E(2) to increase as the water content of a nitric acid solution is decreased. Reference to Figure 14.31 shows that this is precisely what is observed, so the general correctness of the above interpretation of the shifts is confirmed.

It is noteworthy that E(2) for pure liquid nitric acid is the same as that for iso-propyl nitrate (38.5 kcm^{-1}), which is consistent with the views expressed above.

One further point can be made to conclude this discussion of the nitric acid solutions. Figure 14.32 shows that E(2) or E'(2) moves abruptly to higher values when a solid hydrate of nitric acid is fused. This corresponds to displacement of the H-O bond type towards the 'covalent' extreme; that is, the degree of stabilisation of the oxygen electrons increases on fusion. As will be seen later, this has its counterpart in the melting process of metallic nitrates.

The fact that the variation of E(2) with cation radius for fused alkali nitrates can be described by a relationship as simple as (18.1) is some evidence for supposing that only nearest-neighbour cations are active in influencing E(2) for a given nitrate ion. A more complicated expression would be required to describe the irregular variation of E_{max} with cation radius for the lowest-frequency absorption band of the alkali iodides (see Table 6.1).

Smith found that E(2) was lower than the value given by (18.1) if the nitrate melt contained cations of rare-gas configuration for which z/r exceeded 3 A^{-1} (e.g. Mg^{2+}, Y^{3+}). It is interesting to enquire whether the expression is valid for pure ammonium, silver and thallous nitrates. Table 18.2 shows values of E(2) for these salts calculated from Smith's expression, using ionic radii taken from Pauling (Ref 4). Since decomposition made it impossible to measure E(2) directly at 365°C for any of the three compounds, the available experimental results were extrapolated.

TABLE 18.2. Calculated and observed values of E(2) at 365°C.

Salt	Cation radius (A)	E(2) (kcm^{-1})	
		calc. from eqn. 18.1	observed
NH_4NO_3	1.48	32.6	32.9
$AgNO_3$	1.26	32.9	30.7
$TlNO_3$	1.44	32.6	32.4

For ammonium nitrate melt dE(2)/dT was assumed to be -1.2 cm^{-1} per °C (the value for $RbNO_3$ melt; Rb^+ and NH_4^+ have the same ionic radius), and E(2) at 365° was calculated from this gradient and the value of E(2) for the melt at 170°C. For silver nitrate the difference between E(2) and E'(2) was calculated at 0°C, and was assumed to have the same value just above the melting-point. E(2) was then found from the measured value of E'(2) for the melt, and dE(2)/dT was assumed to be -1 cm^{-1} per °C. For thallous nitrate the experimental value of E(2) just above the melting point was converted to 365° on the assumption that dE(2)/dT for the melt was the same as dE'(2)/dT (whose measured value was -0.5 cm^{-1} per °C).

The values of E(2) found in these various ways are listed in the last column of Table 18.2.

The 'observed' value of E(2) for ammonium nitrate is some 300 cm^{-1} higher than the 'calculated' value. This may be due to a tendency for protons to be shared between ammonia molecules and nitrate groups:

$$H_3N...H^+...ONO_2^- .$$

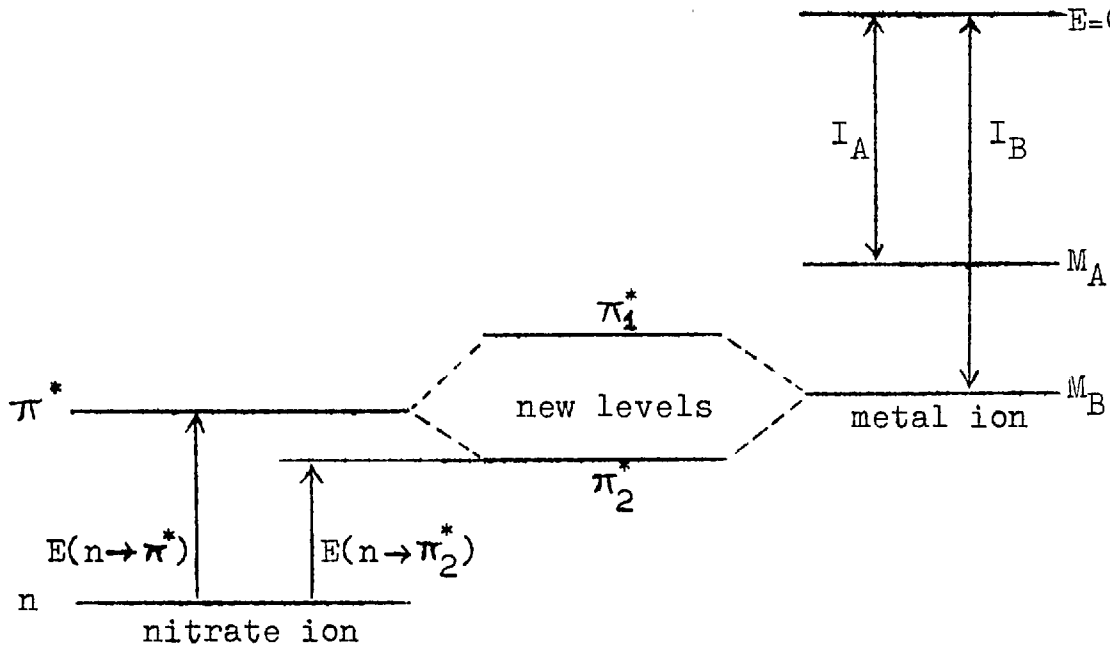
Such sharing would cause additional stabilisation of the oxygen electrons and would account for the displacement of the band to a higher frequency than that predicted by Smith's equation. There is direct evidence that free ammonia is present in ammonium nitrate melt (see page 265), which provides some support for this view. The fact that the displacement of the band maximum from the calculated value (compared with the corresponding displacement for the hydrate of nitric acid, $HNO_3.H_2O$) shows that proton sharing in ammonium nitrate is not very extensive; the melt can be regarded as made up of ions NH_4^+ and NO_3^- to a good first approximation.

For silver and thallous nitrates the observed values of E(2) are lower than the calculated ones (the differences being 2.2 and 0.2 kcm^{-1} respectively). Considered in the light of the foregoing paragraphs, this result is unexpected. Most of the differences between the general chemistry of Group A and Group B metals can be rationalised by supposing that the screening of the nuclear charge by the electrons is less efficient in the B-metals than in the A-metals; thus Ag^+ has greater polarising power than Na^+ in spite of the smaller radius of the sodium ion. On this basis we would expect E(2) for melts such as silver nitrate and thallous nitrate to be higher than the values calculated from equation 18.1, because the effective cationic charge of Ag^+ and Tl^+ should be greater than the formal values of one. To state this in another way, we would expect the interaction between cations and the oxygen of the nitrate group in its ground state to be stronger in B-metal nitrates than in the alkali nitrates, and the resulting stabilisation of the ground state should cause the weak band to be displaced to higher frequencies (as it is when H-O bond formation occurs in the more concentrated nitric acid solutions). That the observed

values of E(2) for silver and thallous nitrates are lower than the calculated ones is therefore surprising, and requires explanation in terms of some new hypothesis. A possible solution to the problem is put forward in the next paragraphs.

For nitrate melts containing the cations Ag^+, Tl^+, Mg^{2+}, Y^{3+} etc., the discrepancy between the observed E(2) and that predicted by Smith's expression may be due to stabilisation of the excited nitrate ion by the cations surrounding it. If the π^* orbital of the nitrate ion overlaps with the lowest empty orbital (M) of a neighbouring metal ion, these two could combine to give a pair of new orbitals (π_1^* and π_2^*) one of which has a lower energy than the original π^* nitrate orbital. The lower of these two new orbitals (π_2^*) would then receive the electron on excitation and the transition energy would thereby be reduced. The situation is illustrated by the energy-level diagram below, in which M_B and M_A represent the lowest unoccupied energy level in a B-group metal ion and an alkali metal ion respectively. I_B and I_A are the ionisation energies of the corresponding metal atoms.

It is a conclusion of wave-mechanical theory that the energy of π_2^* must be below that of π^*, the difference between them depending on the amount of mixing which the original orbitals π^* and M undergo. Mixing is maximal when π^* and M have equal energies, but is reduced if the energy of M is increased relative to that of π^* (Ref 5). This mechanism for the lowering of the energy of the upper state of the optical transition would therefore apply for group-B metal ions or for the smaller, polyvalent group-A ions such as Mg^{2+} and Y^{3+}, since the first empty orbital for these ions has relatively low energy. However, it



would not apply in alkali nitrate melts because the empty orbital M lies at higher energy in alkali ions than in B-metal ions (see diagram). Table 18.3 gives values of ionisation energies which confirm this point.

TABLE 18.3. First ionisation energies of metal atoms (Ref 6)

Metal	Li	Na	K	Rb	Cs	Ag	Tl
Ionisation energy (kcal/mole)	124	119	100	96	90	175	141

It is noteworthy that $E(2)_{calc.} - E(2)_{obs.}$ is greater for silver nitrate than for thallous nitrate. Since silver has a higher first ionisation potential than thallium, this is consistent with the above argument.

The results for the $Ba(NO_3)_2$ - KNO_3 mixtures (Figures 14.16, 14.17, and 14.18) provide strong support for the idea that E(2) is determined largely by the nearest neighbours of each nitrate ion. E(2) increases with barium concentration at constant temperature, but this might be due to the attendant decrease in the equivalent volume of the melt (see Chapter 13). However, the increase is still observed if a correction is applied to bring all the mixtures to the same equivalent volume (i.e. the mixtures with higher barium content were considered at higher temperatures such that the electrostriction brought about by the barium ions was offset by thermal expansion). Under these conditions the long-range forces in the melts must be identical, (i.e. the number of positive or negative charges per unit volume is the same in each mixture), so the residual dependence of E(2) on composition must be ascribed entirely to short-range effects.

An alternative way of demonstrating this would have been to equalise the equivalent volumes of the mixtures at constant temperature by application of pressure to the potassium-rich mixtures.

18.2.2. Variation of E(2) with temperature for individual crystalline phases and melts.

For a given crystalline form of a nitrate, the steady decrease in E(2) with rising temperature can arise from at least two causes, namely:

(a) Changes in the populations of the vibrational quantum levels of the crystal in its optical ground state (referring both to the internal vibrations of the

nitrate ion and to the vibrations of the ions about their mean lattice positions). The frequencies of the vibrational modes of the nitrate ion are 1390, 1050, 825 and 720 cm^{-1} (see Chapter 2); the fraction of the total number of ions which are in the first excited level of the lowest of these modes is of the order exp(- 720/kT), where k is Bolzmann's constant in cm^{-1} per ^{o}C. This fraction is equal to 0.023 at $0^{o}C$ and 0.22 at $400^{o}C$, so significant occupation of this first excited level occurs when a sample is heated from room temperature to $400^{o}C$. Lattice vibration frequencies are of the order 100 cm^{-1}, so the excited levels of these modes would be expected to be populated even at room temperature. The occupation of the vibrational energy levels causes the potential surface of the optical ground state of the nitrate ion to move nearer to that of the excited state, and so causes the band maximum to be displaced towards lower frequencies.

(b) Changes in the positions of the neighbours of the nitrate ions, which lead to changes in the electrostatic field experienced by the latter. Thermal expansion of a crystal or melt corresponds to a gradual increase in the average distance between a nitrate ion and its nearest-neighbour cations; this causes a reduction in the stabilisation of the optical ground state of the nitrate ion, and so contributes to the decrease in excitation energy with rising temperature.

The relative importance of factors (a) and (b) is unknown. In this connection it would be valuable to study the effect of pressure on E(2) for a given phase, at fixed temperature. The anion-cation distance could then be varied without altering the populations of the vibrational energy levels (i.e. without changing kT). A comparison of dE(2)/dV at

constant temperature with dE(2)/dV at constant pressure would allow the contributions of (a) and (b) to be evaluated separately.

If the movement of the cations away from the anions on thermal expansion were the predominant factor determining dE(2)/dT, we might expect there to be proportionality between this quantity and the coefficient of thermal expansion. Some relevant data are collected in Table 18.4, and show that no simple proportionality exists between dE(2)/dT and $1/V_o.dV/dT$ even for different crystalline modifications of the same salt. Presumably the relationship between these two also involves a factor which depends on the crystal structure of the phase concerned.

It is noteworthy that dE(2)/dT for fused nitrates is of the same order of magnitude as that for solid nitrates, despite the fact that the coefficients of expansion of the melts are generally about twice those for the solids. This can be interpreted in the following way. In the crystals, thermal expansion corresponds to an increase in the distances between the ions in the lattice; the formation of vacancies and other defects makes an insignificant contribution. In the melts, however, it appears that about one-half of the macroscopic thermal expansion is due to the appearance of voids; the remainder of the expansion is caused by increases in average anion-cation separation, and this alone leads to changes in E(2).

Sodium nitrate is the only salt for which any direct correlation can be discerned between thermal expansion and the corresponding changes in E(2). This substance has a continuous transition between 150° and 275°C, during which it undergoes only a very slight structural change; the crystals remain rhombohedral throughout, the unit cell parameters

TABLE 18.4. dE(2)/dT and coefficients of expansion for nitrates and nitrites. The values of dE(2)/dT were found by fitting straight lines to the experimental plots of E(2) against temperature, by least squares. In the formula for the coefficient of expansion V_o is the volume at 0°C (found by extrapolation when necessary).

Salt and phase		Temp. range (°C)	$\frac{dE(2)}{dT}$ ($cm^{-1}/°C$)	$\frac{1}{V_o}\frac{dV}{dT} \times 10^4$ (per °C)
$NaNO_3$	I	20 - 160	-2.5	1.7 (Ref 7)
	I	275 - 308	-2.4	
	melt	308 - 400	-1.8	4.3 (Ref 8)
KNO_3	II	20 - 127	-1.3	2.4 (Ref 9)
	I	127 - 334	-2.3	2.9 (Ref 9)
				3.3 (Ref 10)
	melt	335 - 441	-1.2	4.9 (Chap.13)
$RbNO_3$	IV	20 - 161	-1.4	2.4 (Ref 11)
	III	161 - 220	-1.0	4.1 (Ref 11)
	II	220 - 282	-3.1	-
	I	283 - 312	-0.6	-
	melt	312 - 422	-1.2	4.2 (Ref 8)
$CsNO_3$	II	20 - 153	-1.0	2.1 (Ref 11)
	I	153 - 408	-1.1	3.1 (Ref 11)
	melt	408 - 431	-2.1	4.9 (Ref 8)
NH_4NO_3	IV	16 - 35	-0.6	3.5 (Ref 12)
	III	35 - 85	-3.7	1.9 - 2.9 (Ref 12)
	II	85 - 124	-1.4	2.1 - 3.8 (Ref 12)

TABLE 18.4, continued.

Salt and phase		Temp. range (°C)	$\frac{dE(2)}{dT}$ ($cm^{-1}/°C$)	$\frac{1}{V_o}\cdot\frac{dV}{dT} \times 10^4$ (per °C)
NH_4NO_3	I	124 - 169	+0.6	4.1 - 4.2 (Ref 12)
	melt	169 - 174	-	-
$AgNO_3$	II	20 - 158	+0.7 0.0*	5.2 (Ref 13)
	I	158 - 208	0.0*	0.2 (Ref 13) 1.5 (Ref 10)
	melt	210 - 300	-	2.9 (Ref 14) 3.0 (Ref 13)
$TlNO_3$	III	20 - 75	-1.3 -0.4*	2.1 (Ref 11)
	II	75 - 145	+0.2 -1.6	2.2 (Ref 11)
	I	145 - 206	+0.8 -0.7*	3.8 (Ref 11)
	melt	214 - 290	-0.5*	4.0 (Ref 11)
$NaNO_2$	I	20 - 281	-1.7	2.6 (Ref 15)
	melt	281 - 380	-0.9	4.4 (Ref 16)
KNO_2	II	10 - 45	-0.8	-
	I	45 - 420	0.0	-
	melt	430	-	-

numbers marked * are dE'(2)/dT rather than dE(2)/dT.

being a = 6.32A, α = 47°14' at 20°C and a = 6.56A, α = 45°35' at 280°C (Ref 17). Plots of E(2) and of specific volume (v) (Figure 14.7) show a similarity of form throughout the transition region, the increase in v being associated with a decrease in E(2). However, the relationship between the two quantities breaks down at the melting-point; E(2) and v both <u>increase</u> on fusion. This suggests that E(2) is really determined by the anion-cation separation, and that this happens to be a monotonic function of v throughout the transition region (but not through the melting point).

It is not profitable to try to derive the exact form of the relationship between E(2) and v for solid sodium nitrate, for the following reason. If the relationship is of the form $E(2) = a + b.v^n$, (a,b and n being constants), trial values of n might be chosen and E(2) plotted against v^n for each of them. The plot would be a straight line when the correct value of n was used, otherwise it would be a curve.

Unfortunately this procedure is inapplicable in the present case. The change in E(2) between 0°C and 300°C is only 3%, and that in v is only 7%. Under these circumstances a plot of E(2) against v^n would be a straight line for <u>any</u> value of n, because the relative change in the two variables is so small. This point becomes clear if the above expression for E(2) is written

$$E(2)_{t^oC} = a + b(v_o + \delta v)^n,$$

(v_o being the value of v at 0°C). Expansion of the second term as a power series gives

$$E(2)_{t^oC} = a + bv_o^n\left(1 + \frac{n\,\delta v}{v_o} + \frac{n.(n-1)}{2}.\left(\frac{\delta v}{v_o}\right)^2 \ldots\right)$$

If $\delta v/v_o$ is only 0.07, the sum inside the bracket can be

approximated with good accuracy by its first two terms. The expression then becomes

$$E(2)_{t^oC} = a + b.v_o^n \left(1 + \frac{n.\delta v}{v_o}\right)$$

$$= A + B.n.\delta v$$

$$= A + B.n(v - v_o),$$

where A and B are constants. This is an equation to a straight line, irrespective of the value of n, and it is not possible to find n from the slope of this line because B is also unknown.

The full line in Figure 18.1 shows the function $(a + bv^n)$ plotted against temperature for $n = -2/3$ (which corresponds to equation 6.3, page 74). The values of the constants a and b were derived from the E(2) values in the temperature range 20 - 150°C. The black circles are the experimental points; it is seen that they lie on the calculated line with good accuracy throughout the transition region and up to the melting-point, but not beyond. The argument given above shows that equally good fit could be expected for any other value of n, so this agreement obtained with $n = -2/3$ must not be taken as implying support for equation 6.3. It does show, however, that the relationship between E(2) and v keeps the same form from room temperature right up to the melting point. This confirms that the structural change in the transition region is relatively slight, involving only the onset of a measure of orientational randomisation in the nitrate ions. The reasons for the breakdown of the E(2) - v relationship at the melting point are discussed in the next section.

To conclude this section, a suggestion is made which bears

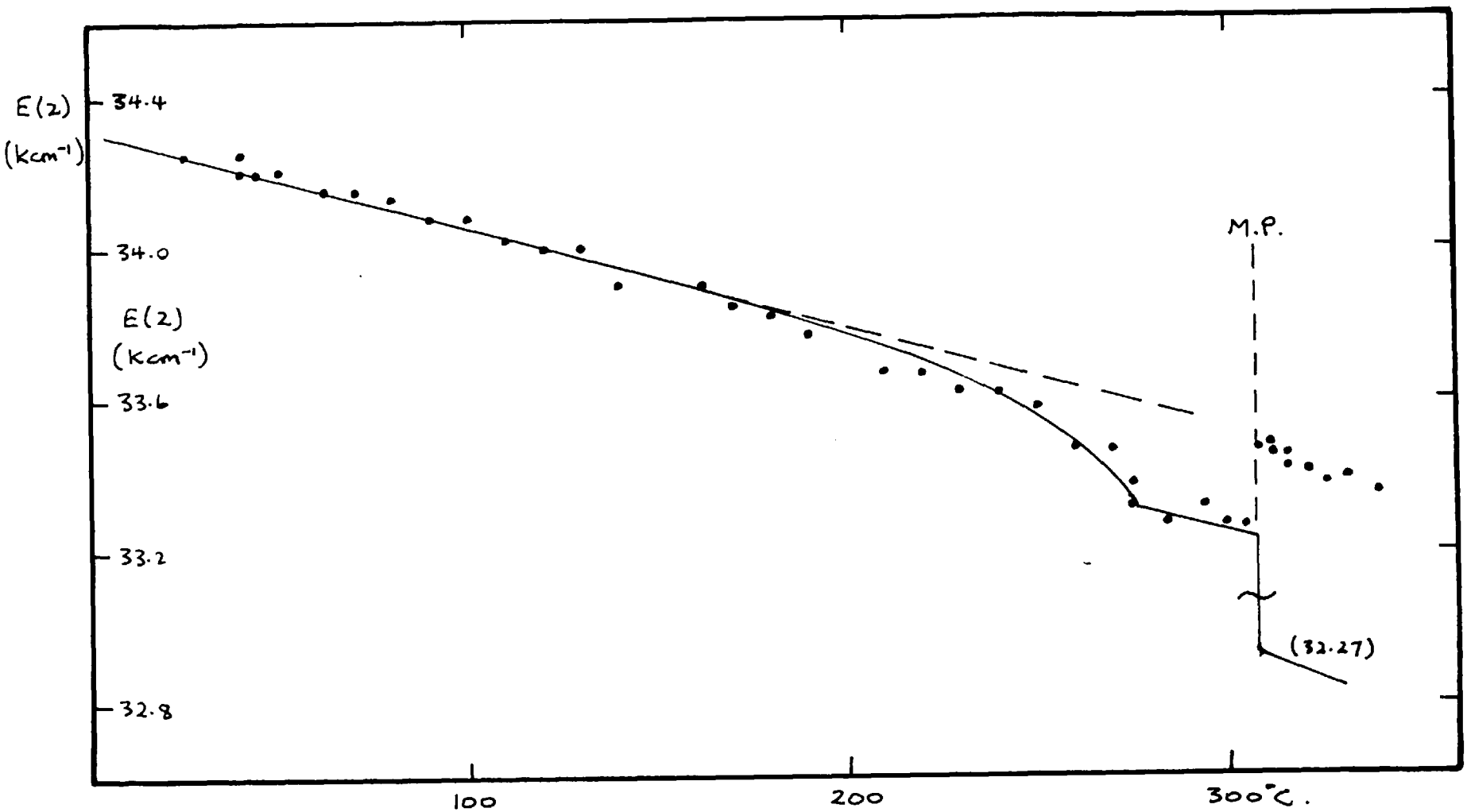


FIGURE 18.1. E(2) FOR SODIUM NITRATE. THE FULL LINE WAS OBTAINED IN THE WAY DESCRIBED ON PAGE 358.

on the question of nitrate ion rotation in other crystals. Examination of Table 18.4 shows that dE(2)/dT and dE'(2)/dT are relatively low for NH_4NO_3(I), $RbNO_3$(I), $AgNO_3$(I) and $TlNO_3$(I), although the coefficients of expansion of these phases have normal values.

In the cubic form (I) of NH_4NO_3, the nitrate ion occupies a site at the body centre of a CsCl-type unit cell (Ref 12). Since the effective symmetry of a group must be at least as high as that of the site which it occupies, the nitrate ion must be free to rotate so that its time-averaged 'shape' is spherical (save that orientations in which an N-O bond points directly towards an NH_4^+ ion may be excluded because of the high repulsion involved). This random movement of the nitrate ion would tend to reduce the stabilising effect of the cations on the oxygen lone-pair electrons, because this stabilisation is conditional on the positioning of the cations in the regions of high (negative) potential immediately around each oxygen atom. If the nitrate ion is rotating freely this influence of the cations on E(2) is generally less marked than is normally the case, and this explains why E(2) changes relatively little during thermal expansion of NH_4NO_3(I).

Pending complete X-ray structure determinations, the low values of dE(2)/dT (or dE'(2)/dT) for $RbNO_3$(I), $AgNO_3$(I) and $TlNO_3$(I) may be taken as tentative evidence for spherical rotation of the nitrate ions in these crystals also.

18.2.3. Abrupt changes in E(2) at transition points and melting points.

Table 18.5 gives the values of $\Delta E(2)$ for each nitrate studied. These values were found by fitting straight lines

to the experimental plots of E(2) against temperature (by least squares); the interval between the ends of two such lines at a transition temperature gave $\Delta E(2)$ directly. For silver and thallous nitrates values of $\Delta E'(2)$ are also listed, and were obtained in the same way.

It is instructive to try to relate these abrupt shifts with the structural changes accompanying them.

It might be expected that an increase in the molar volume at a transition point would be associated with a decrease in the stabilisation of the nitrate ion ground state by the neighbouring cations, and so would cause a reduction in E(2). Some volume changes at transition points and melting points are included in Table 18.5. Comparison of these with the $\Delta E(2)$ values shows that the above hypothesis is not always bourne out; an increase in molar volume is often accompanied by a decrease in E(2), but the reverse is sometimes true at transition points. The non-correlation is particularly striking at the melting-points; $\Delta E(2)$ and V both increase on fusion for all nitrates except $RbNO_3$.

A much more satisfactory correlation is obtained if $\Delta E(2)$ is compared with the change in the distance between the oxygen atoms of the nitrate group and their nearest-neighbour cations ($\delta r(M\text{-}O)$. In cases for which the crystal structures are known precisely enough for this distance to be calculated, a reduction in the M-O distance at a transition is always associated with an increase in E(2). The data collected in Table 18.6 show that this is true for the transition in potassium nitrate at 127°C and for that in rubidium nitrate at 220°C. The correlation is demonstrated particularly well by the results for ammonium nitrate, for which fairly complete structural information is available. $\Delta E(2)$ and $\delta r(M\text{-}O)$ have opposite signs for the transitions

TABLE 18.5. Abrupt changes in E(2) and in molar volume (V) at transition points and melting points. In the Table, V is the molar volume immediately below the transition point, and ΔE and ΔV are considered as positive if E or V increase when the substance is heated through the transition.

Salt	Transition	Temp. (°C)	$\Delta E(2)$ (cm^{-1})	100. $\Delta V/V$
$NaNO_3$	I - melt	308	+180	+10.7 (Ref 18)
KNO_3	II - I	127.5	+70	+1.0 (Ref 9)
	I - melt	334	+170	+3.3 (Ref 18)
$RbNO_3$	IV - III	161	0	+5 (Ref 19)
	III - II	220	+80	+1.3 (Ref 19)
	II - I	282.5	-70	+17 (Ref 19)
	I - melt	312	+270	-0.2 (Ref 18)
$CsNO_3$	II - I	153	-50	-
	I - melt	408	+160	+12.1 (Ref 18)
NH_4NO_3	IV - III	35	+290	+3.8 (Ref 12)
	III - II	85	-660	-1.3 (Ref 12)
	II - I	124	-110	+2.1 (Ref 12)
	I - melt	169	+300	+12 (Ref 20)
$AgNO_3$	II - I	158	-150 -290*	0.0 (Ref 13)
	I - melt	208	+280*	+0.7 (Ref 13)

Figures marked * are $\Delta E'(2)$.

TABLE 18.5, continued.

Salt	Transition	Temp. (°C)	$\Delta E(2)$ (cm^{-1})	100. $\Delta V/V$
$TlNO_3$	III - II	75	-10 0*	-0.2 (Refs 21 & 22)
	II - I	145	+20 +10*	+2 (Ref 21)
	I - melt	206	+620 +350*	+5.6 (Ref 11)
$NaNO_2$	I - melt	281	+280	+9.0 (V_s: Ref 15, V_L: Ref 16)
KNO_2	II - I	45	-80	-
	I - melt	423	+70	-

Figures marked * are $\Delta E'(2)$.

at 35° and 85°C, in agreement with the above rule, but the situation at the third transition at 124° requires more detailed explanation. In II the nitrate ions can occupy either one of two equivalent orientations, and remain in one orientation for a long time compared with the period of a lattice vibration (Ref 28). In I, on the other hand, the nitrate ion rotates freely (Ref 12) so the NH_4-O distance cannot be calculated. However, the onset of rotation would be expected to correspond to a reduction in the cation-oxygen interaction, and this is in accord with the negative value of $\Delta E(2)$ recorded for the II - I transition.

Structure determinations for the remaining nitrates are disappointingly lacking, but we may predict that, when

TABLE 18.6. Cation-oxygen distances in crystalline nitrates. The values given here are the result of a complete survey of the crystallographic literature up to mid-1963.

Salt and transition	$\Delta E(2)$ (cm^{-1})	r(M-O) (A) below transition	r(M-O) (A) above transition	δr(M-O) (A)
KNO_3 II - I	+70	2.82 (Ref 23)	2.69 (Ref 10)	-0.13
$RbNO_3$ III - II	+80	2.98 (Ref 24)	2.82 (Ref 10)	-0.16
$CsNO_3$ II - I	-50	-	2.96 (Ref 25)	-
NH_4NO_3 IV - III	+290	2.96 (Ref 26)	2.7 (Ref 27)	-0.26
III - II	-660	2.7 (Ref 27)	3.13 (Ref 28)	+0.43
II - I	-105	3.13 (Ref 28)	-	-
$TlNO_3$ III - II	0*	2.4 (Ref 22)	-	-
$NaNO_2$ I - melt	+280	2.48 at 185°C (Ref 29)	-	-
KNO_2 II - I	-80	2.71 (Ref 30) 2.74 (Ref 31)	-	-

The figure marked * is $\Delta E'(2)$.

complete X-ray investigations of these salts are carried out, the M-O distance will be found to increase (with rising temperature) at those transition points for which $\Delta E(2)$ is negative, and vice versa.

We may now use this result that the sign of $\Delta E(2)$ reflects the sense of the change in nearest-neighbour cation-oxygen distance to interpret the changes in E(2) on fusion of the nitrates. The fact that E(2) always increases at the melting-point means that the nearest cation-oxygen distance always decreases when a nitrate is fused. The macroscopic increase in volume which often accompanies melting must be ascribed to regions of mis-fit between adjacent ionic aggregates. This evidence for the reduction in cation-oxygen separation on fusion of nitrates is one of the most important results in this thesis. Although there is a body of indirect support for this hypothesis (see Chapters 3 and 7) the work reported here is probably the clearest and most comprehensive demonstration of the effect which has yet been made. Earlier workers have been able to use diffraction techniques to show that a reduction in nearest-neighbour anion-cation separation occurs when alkali halides are fused (see Section 7.1). However, these techniques give much less conclusive results when applied to nitrate melts; the presence of non-spherical , polyatomic anions complicates the radial distribution curve, and the superposition of several peaks in the region r = 1.5 - 2.5A limits the accuracy with which r(M-O) can be found to one or two tenths of an Angstrom. It is shown in the next paragraphs that the change in r(M-O) on fusion is of this order of magnitude, so values of δ r(M-O) based on diffraction evidence would be totally unreliable.

It is possible to estimate the order of magnitude of the reduction in the cation-oxygen distance on fusion of nitrates by using Smith's empirical equation (18.1). For a given monovalent cation this can be written

$$E(2) = 30740 + 2740/r_+ \quad (cm^{-1}). \qquad (18.2)$$

If this equation is differentiated, the small change in E(2) at the melting point can be expressed in terms of an apparent change δr_+ in the cation radius:

$$\Delta E(2) = -2740.\ \delta r_+/r_+^2 . \qquad (18.3)$$

Values of δr_+ have been calculated from the observed shifts $\Delta E(2)$, and are listed in Table 18.7. It is noteworthy that these are of the same order of magnitude as the shrinkage in anion-cation distance on fusion of alkali halides (as measured by diffraction techniques; see Section 7.1).

Table 18.7 also includes values of δr_+ at transition points, calculated from eqn. 18.3. These compare moderately well with the values of $\delta r(M-O)$ in Table 18.6, derived from crystallographic data.

At this point we may conveniently discuss the reasons for the sluggishness of the transitions involving phase III of ammonium nitrate. In the absence of a solvent, transformations between forms IV, II and I occur relatively easily because the structures of these three phases are very simply related. When form I is cooled, the face diagonals of the cubic unit cell become the a axes of the tetragonal cell of II (i.e. $a_{II} \sim \sqrt{2}.\ a_I$), and c_{II} (=4.95A) is formed by slight expansion of a_I (=4.40A). If cooled rapidly, II can be made to transform directly into IV; c_{II} becomes c_{IV}, and the two

TABLE 18.7. Apparent change in cation radius (δr_+) at nitrate transition points and melting points (Calculated from equation 18.3).

Salt and transition		Temp. (°C)	$\Delta E(2)$ (cm^{-1})	δr_+ (A)
$NaNO_3$	I - melt	308	+180	-0.06
KNO_3	II - I	127	+70	-0.05
	I - melt	334	+170	-0.11
$RbNO_3$	IV - III	161	0	0.00
	III - II	220	+80	-0.06
	II - I	282.5	-70	+0.06
	I - melt	312	+270	-0.22
$CsNO_3$	II - I	153	-50	+0.05
	I - melt	408	+160	-0.17
NH_4NO_3	IV - III	35	+290	-0.23
	III - II	85	-660	+0.53
	II - I	124	-110	+0.09
	I - melt	169	+300	-0.24
$AgNO_3$	II - I	158	-290*	+0.17
		208	+280*	-0.16
$TlNO_3$	III - II	75	0*	0.00
	II - I	145	+10*	-0.01
	I - melt	206	+350*	-0.27

Figures marked * are $\Delta E'(2)$.

a axes of II become a_{IV} and b_{IV}. Again, only a slight ionic rearrangement is involved (c_{II} = 4.95, c_{IV} = 4.96A; a_{II} = 5.74, a_{IV} = 5.75, b_{IV} = 5.45A). Thus transformations between I, II and IV involve the production of very little strain energy, and single crystals remain single if cycled through these transitions. On the other hand the structure of the orthorhombic form III is not simply related to any of the others, and if the changes II → III or IV → III are carried out on a single crystal it is broken up into randomly oriented domains of III (Ref 32). The strain energy and surface energy required for these transformations are responsible for the hysteresis described in Section 15.2.4.

18.3. The weak absorption band of the nitrites at 27 kcm^{-1}.

From the results obtained for sodium and potassium nitrites we may conclude tentatively that this absorption band of the nitrites responds to environmental changes in a similar way to the weak band of the nitrates. Thus, the band maximum for sodium nitrite moves to lower frequency as a linear function of temperature when the solid is heated, and shifts abruptly to higher frequency at the melting-point. For potassium nitrite E(2) decreases by some 70 cm^{-1} at the transition point and increases by about the same amount at the melting point, but shows practically no change between 50°C and 390°C. It seems that the influence of the cations on the nitrite ion energy levels which are involved in the optical transition undergoes little change between these temperatures. This is consistent with the idea that the nitrite ions have a measure of orientational freedom above 50°C. The electrons involved in the transition are the nitrogen 'lone pair', and these would be expected to be less influenced by the cations if the nitrite ions are free to

assume any orientation than if the lone pair is always directed towards one particular cation. In support of the hypothesis of orientational freedom, it has been shown that crystalline potassium nitrite has an abnormally high standard entropy even at 20°C; the values for lithium, sodium and potassium nitrites are 22.8, 24.7 and 35.0 e.u./mole, respectively (Ref 33).

Frame et al (Ref 16) measured the electrical conductivity of solid potassium nitrite as a function of temperature. They observed a sharp increase in conductivity at 365°C, which they ascribed to a crystal transition. The present work does not confirm the existence of a polymorphic transition point in this region; the plots of E(2) and of E(t = x%) against temperature show no discontinuity (see Figures 14.4o and following), and no abrupt change in % transmission was recorded when a sample was heated from 300° to 400°C at constant frequency.

18.3.1. Relationship between E(2) and cation radius for nitrites.

At room temperature, E(2) for sodium nitrite is 28.7 kcm^{-1} and E(2) for potassium nitrite is 27.6 kcm^{-1}. It is noteworthy that the difference between these figures, 1.1 kcm^{-1}, is the same as the difference between E(2) for sodium and potassium nitrates at room temperature (34.3 and 33.2 kcm^{-1}, respectively). It appears that an equation analogous to (18.1) may apply to the series of alkali nitrites, i.e. E(2) decreases with increasing cation radius. Using the two points at present available, the equation at 20°C is

$$E(2)_{20°C} = 25190 + 3270/r_+ \quad (cm^{-1}), \qquad (18.4)$$

and for the melts at 420°C it is

$$E(2)_{420^{\circ}C} = 28260 + 2106/r_{+} \quad (cm^{-1}). \quad (18.5)$$

It will be interesting to see whether these equations are satisfied when E(2) is measured for the remaining alkali nitrites and for mixtures containing alkaline earth ions. (For the mixtures the term $1/r_{+}$ in (18.4) and (18.5) must be replaced by $\sum(X_i z_i/r_i)$, cf. page 72). From the spectroscopic point of view such a study would present no difficulty which has not already been solved by the author and his predecessors; the major obstacle to be overcome will be the preparation of lithium, rubidium and caesium nitrites and alkaline-earth nitrites (none of which is available commercially) in purity better than 99 mole %. This will not be a straightforward task because these nitrites are probably miscible with the corresponding nitrates in the solid state. Successful purification may be achieved by zone-refining or by the use of ion exchange resins.

18.4. Possibilities for future work.

Further advances may be made by studying the spectra of other salts for which the anion can undergo internal transitions of the $n \rightarrow \pi^*$ type, over temperature ranges which include the melting-points. All salts containing polyatomic oxy-anions have absorption bands of this kind and should in principle be susceptible to investigation. In practice, two factors limit the choice of suitable materials:

(a) The weak $n \rightarrow \pi^*$ band often overlaps with the stronger $\pi \rightarrow \pi^*$ and charge-transfer bands which are found at

higher frequency. This occurs, for example, in the carbonates and sulphates, for which the $n \rightarrow \pi^*$ band is observed only as a shoulder. It would be impossible in these cases to measure E_{max} with the necessary precision ($\pm$ 50 cm^{-1}).

(b) Chemical decomposition often occurs when salts are fused. This eliminates interesting substances such as chlorites, hypochlorites, thiosulphates, sulphites and many others.

The dichromates have two well-defined absorption bands in the visible and near ultra-violet regions. Although the extinction coefficients are rather high for convenience (about 6000 litre/mole.cm; Ref 34), it may be possible to overcome this difficulty.

Lastly, it would be particularly interesting to study the charge-transfer absorption spectra of the alkali halides and nitrates over temperature ranges including the melting points. These spectra lie in the vacuum ultra-violet, and will be difficult to measure because of the very high extinction coefficients involved (10^3 - 10^4 litres/mole.cm). This work is important because the charge-transfer spectra in the two groups of compounds should show the same dependence on structure, so a comparison of the spectral changes on fusion should allow the melting process in nitrates to be compared directly with that in the halides. (It is not possible to use the author's work as the basis for such a comparison because the $n \rightarrow \pi^*$ absorption band of the nitrates has no counterpart in the halide spectra). The results of such an investigation may help to explain why the nitrates have such low melting points compared with the alkali halides. Although this problem is partly understood, more insight is needed for its complete elucidation. Spectroscopic methods

of investigation are particularly valuable because they relate to processes on an atomic scale, and so may give information about changes in the immediate environment of an ion during fusion (in suitable cases). As the author's work has shown, these changes may be completely different from those which might be inferred from parameters such as molar volume or heat of fusion, which reflect the overall, macroscopic properties of the system.

Progress along these lines will require the solution of formidable practical problems. These stand as a challenge to the patience and ingenuity of future workers.

REFERENCES TO CHAPTER 18.

1. Sass, Vidale and Donohue, Acta Cryst, (1957), 10, 567.

2. Luzatti, Acta Cryst., (1953), 6, 152 and 157.

3. L.E. Sutton (Ed.), "Interatomic distances", Chemical Society Special Publication No. 11, 1958.

4. L. Pauling, "The Nature of the Chemical Bond", Cornell University Press, Ithaca, N.Y. (3rd Edition).

5. C.A. Coulson, "Valence", Oxford (1952), pp 71 - 73 and 79.

6. J.A.A. Ketelaar, "Chemical Constitution", Elsevier, Amsterdam, (1958), (2nd. edition), page 41.

7. J.C. Kracek, J. Amer. Chem. Soc., (1931), 53, 2609.

8. G.P. Smith and C.R. Boston, J. Phys. Chem., (1961), 34, 1396.

9. E. Cohen and H.L. Bredée, Z. phys. Chem., (1929), A140, 391.

10. H.F. Fischmeister, J. Inorg. Nucl. Chem., (1956), 3, 182.

11. "International Critical Tables", McGraw Hill, N.Y.

12. Hendricks, Posnjak and Kracek, J. Amer. Chem. Soc., (1932), 54, 2766.

13. Davis, Rogers and Ubbelohde, Proc. Roy. Soc., (1953), A220, 14.

14. Boardman, Dorman and Heymann, J. Phys. Chem., (1949), 53, 375.

15. Izmailzade, Annagiev and Abdullaeva, Kristallografiya, (1961), 6, 773.

16. Frame, Rhodes and Ubbelohde, Trans. Farad. Soc., (1959), 55, 2039.

17. Kracek, Posnjak and Hendricks, J. Amer. Chem. Soc., (1931), 53, 1183, 2609, 3339.

18. Schinke and Sauerwald, Z. anorg. Chem., (1960), 304, 25.

19. R.N. Brown and A.C. McLaren, Acta Cryst., (1962), 15, 974.

20. Hendricks, Deming and Jefferson, Z. Krist., (1933), 85, 143.

21. Brown and McLaren, Acta Cryst., (1962), 15, 977.

22. Kennedy and Patterson, Z. Krist., (1961), 116, 143.

23. D.A. Edwards, Z. Krist., (1931), A80, 154.

24. U. Korhonen, Ann. Acad. Sci. Fenn., Ser A, (1951), Nr. 102.

25. U. Korhonen, Ibid., (1953), Nr. 150.

26. C.D. West, J. Amer. Chem. Soc., 54, 2256.

27. T.H. Goodwin and J. Whetstone, J. Chem. Soc., (1947), 1455.

28. Y. Shinnaka, J. Phys. Soc. Japan, (1956), 11, 393.

29. Kay, Frazer and Ueda, Acta Cryst., (1962), 15, 506.

30. Ziegler, Z. Krist., (1936), 94, 491.

31. "Strukturbericht", 4, 39 (1936).

32. R.N. Brown and A.C. McLaren, Proc. Roy. Soc., (1962), A266, 329.

33. J.D. Ray and R.A. Ogg, J. Phys. Chem., (1957), 60, 1599.

34. G.P. Smith and C.R. Boston, Ann. N. Y. Acad. Sci., (1960), 79, 930.

* * * * * * * * * *

APPENDIX A.

DETAILS OF EXPERIMENTAL PROCEDURE USED FOR CALIBRATING A "PALLADOR" THERMOCOUPLE AT THE STEAM-, NAPHTHALENE- AND SULPHUR-POINTS. (SEE PAGE 184)

The steam point.

The apparatus used is illustrated in Figure A.1

The flask was filled with distilled water, and a few pieces of porcelain added.

The thermocouple, in its protective Pyrex sheath, was lowered into the central tube of the steam jacket. The sheath contained a little silicone oil to improve thermal contact. A hood of aluminium foil prevented condensed water from running down the sheath and onto the tip of the couple.

The apparatus was protected by draught shields, and the water was boiled until the reflux line reached a steady level inside the water condenser.

The tip of the couple was moved by increments of one inch from top to bottom of the steam jacket, and the E.M.F. was measured when equilibrium had been reached at each position. The experiment was repeated for different positions of the reflux line in the condenser, i.e., for different heating rates.

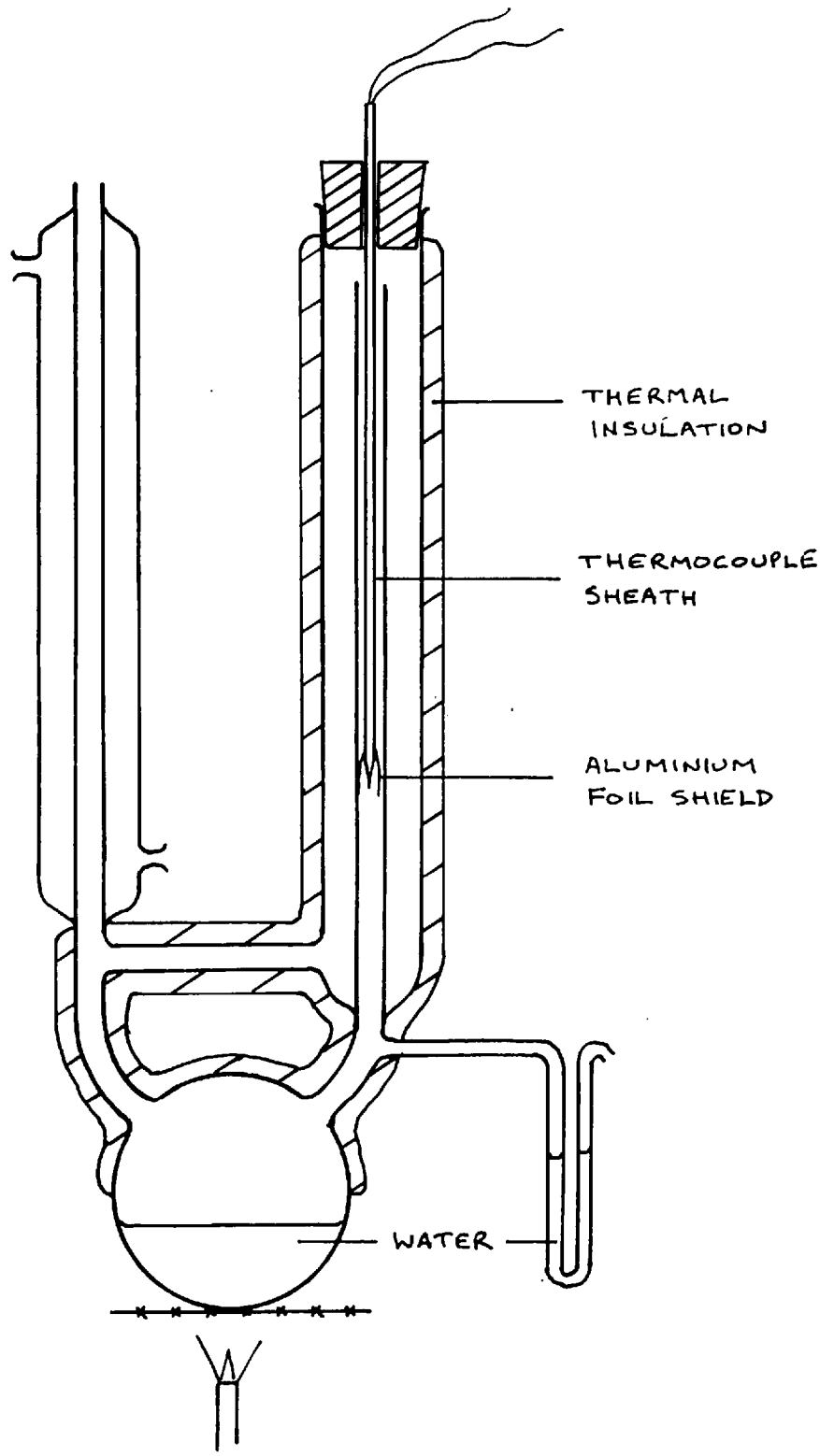


FIGURE A1. STEAM-POINT APPARATUS.

The atmospheric temperature and pressure were read, and the pressure above the boiling water found by applying a small correction, calculated from the difference in levels in the water manometer attached to the boiler. The pressure was corrected to $0^{\circ}C$, and the boiling-point of water at this pressure found from standard tables (Ref.1).

The results are presented in Table A.1..

TABLE A.1.

Distance of tip from top of jacket (inches)	E. M. F. (mv) Distance of reflux line from bottom of condenser (inches)			
	1"	3"	5"	8"
1	4.572	4.572	4.574	4.573
2	4.572	4.576	4.578	4.579
3	4.571	4.573	4.577	4.578
4	4.571	4.571	4.572	4.577
5	4.575	4.578	4.579	4.581
6	4.580	4.581	4.582	4.583
7	4.580	4.582	4.581	4.582
8	4.580	4.580	4.582	4.583
9	4.580	4.580	4.582	4.585
10	4.580	4.582	4.585	4.585

The values underlined are within 0.003 of 4.580 mv., and this figure was adopted.

The atmospheric pressure was 768.5 mm. at $21^{\circ}C$, and the corrected pressure 765.9 mm. at $0^{\circ}C$. The boiling-point of water at this pressure is $100.2_1{}^{\circ}C$.

The corresponding points are therefore:

$$E = 4.580 \text{ mv}; \qquad t = 100.2^{\circ}C.$$

The naphthalene point.

The apparatus and technique used were similar to those described for the steam point. The naphthalene (Hopkin & Williams, Ltd., "for molecular weight determination") was redistilled before use. The manometer attached to the boiler was filled with "Apiezon" vacuum oil of density 1.2. When the naphthalene was refluxing steadily, the difference between the oil levels in the two limbs was 0.7 mm.

Because naphthalene has a lower latent heat of vaporisation than water, it was more difficult in this case to keep the liquid refluxing at a steady level. The experiment was therefore carried out at one rate of heating only. Two sets of readings were taken; the tip of the thermocouple was moved from the top to the bottom of the vapour-jacket during the first set, and from the bottom to the top in the second.

The results are presented in Table A.2.

The value 10.838 mv. was taken as correct; the underlined figures lie within 0.001 mv. of this.

The atmospheric pressure was 764.6 mm. at 22.3°C, and the corrected pressure at 0°C was 761.8 mm. The boiling-point of naphthalene at this pressure was found to be $218.0_6^{\circ}C$.

The corresponding points were therefore:

$$E = 10.838 \text{ mv}; \qquad t = 218.1^{\circ}C.$$

TABLE A.2.

Distance of tip from top of jacket (inches)	E. M. F. (mv)	
	First set	Second set
1	10.838	-
2	10.837	10.837
3	10.832	10.832
4	10.838	10.838
5	10.837	10.837
6	10.834	10.834
7	10.833	10.834
8	10.833	10.832
9	10.825	10.828
10	10.822	10.820

The sulphur point.

The apparatus used has already been referred to on page 109, and is illustrated on page 110.

Two aluminium hoods were fixed over the tip of the Pyrex sheath containing the couple; these acted as radiation shields, and also prevented condensed liquid sulphur from running down the sheath and onto the thermocouple tip.

The readings were taken with the sulphur refluxing at a level just above the top of the thermal insulation. The first set of readings were taken as the tip of the couple was moved down the tube, the second as it was moved up.

The E.M.F.s recorded at the different depths of immersion are presented in Table A.3.

TABLE A.3.

Distance of tip from top of tube (inches)	E. M. F. (mv)	
	First set	Second set
3	24.442	-
4	24.448	24.442
5	24.448	24.448
6	24.448	24.448
7	24.442	24.448
8	24.439	24.442
9	24.430	24.438
10	24.426	24.430
11	24.411	-
12	24,416	-

The value 24.448 mv. (underlined in the table) was taken as correct. The atmospheric pressure was 762.4 mm. at 23.0°C, or 759.6 mm. at 0°C. The boiling-point of sulphur at this pressure is given in the literature as 444.5_6°C (Ref.2).

The corresponding values at the sulphur point were therefore:

$$E = 24.448 \text{ mv.}; \qquad t = 444.6^{\circ}\text{C.}$$

REFERENCES TO APPENDIX A.

1. Perry, "Chemical Engineering Handbook", page 365.

2. E. Griffiths, "Methods of Measuring Temperature".

APPENDIX B.

The following tables give the results of the preliminary conductivity measurements made on pure potassium nitrate (runs 1 - 4 and 6 - 8) and on one mixture (run 5; potassium nitrate + 5 equiv.% barium nitrate). The serial numbers indicate the order in which the results were obtained.

Run 1 (pure potassium nitrate).

Serial number	Temperature (°C)	Cell conductivity (mmho)	Specific conductivity ($ohm^{-1}cm^{-1}$)
2	337.2	1.700	0.6264
3	339.9	1.732	0.6382
5	346.5	1.794	0.6610
4	358.4	1.902	0.7008
15	358.4	1.894	0.6979
1	374.2	2.039	0.7514
6	388.6	2.163	0.7970
7	402.5	2.280	0.8397
8	418.2	2.427	0.8938
14	418.2	2.427	0.8938
9	434.2	2.560	0.9428
10	449.9	2.699	0.9940
11	467.2	2.879	1.0603
12	487.1	3.100	1.1417
13	504.7	3.290	1.2117

APPENDIX B. (continued)

Run 2 (pure potassium nitrate)

Serial number	Temperature	Cell conductivity (mmho)	Specific conductivity ($ohm^{-1}cm^{-1}$)
1	337.2	1.687	0.6214
2	339.9	1.708	0.6292
11	340.0	1.714	0.6314
3	346.5	1.766	0.6505
4	358.4	1.862	0.6859
5	374.2	1.997	0.7356
6	388.6	2.132	0.7854
7	402.5	2.259	0.8319
8	418.2	2.397	0.8828
9	434.2	2.542	0.9362
10	449.9	2.682	0.9877

Run 3 (pure potassium nitrate)

Serial number	Temperature (^{o}C)	Cell conductivity (mmho)	Specific conductivity ($ohm^{-1}cm^{-1}$)
1	340.0	1.714	0.6314
2	346.5	1.782	0.6564
3	358.4	1.886	0.6948
4	374.2	2.028	0.7471
5	388.6	2.152	0.7927
6	402.5	2.274	0.8377
7	418.2	2.410	0.8876
8	434.2	2.554	0.9406
9	449.9	2.697	0.9933

APPENDIX B. (continued)

Run 4 (pure potassium nitrate)

Serial number	Temperature (^{o}C)	Cell conductivity (mmho)	Specific conductivity ($ohm^{-1}cm^{-1}$)
9	340.0	1.720	0.6336
10	340.0	1.719	0.6332
8	346.5	1.785	0.6575
11	346.5	1.783	0.6568
7	358.4	1.890	0.6962
12	358.4	1.888	0.6955
6	374.2	2.026	0.7463
5	388.6	2.152	0.7927
13	402.5	2.268	0.8353
4	402.5	2.273	0.8371
3	418.2	2.409	0.8872
2	434.2	2.553	0.9402
1	449.9	2.696	0.9929

APPENDIX B. (continued)

Run 5 (potassium nitrate + 5 equiv.% barium nitrate)

Serial number	Temperature (°C)	Cell conductivity (mmho)	Specific conductivity ($ohm^{-1}cm^{-1}$)
11	332.0	1.607	0.5920
10	337.2	1.654	0.6093
9	339.9	1.678	0.6181
8	346.5	1.733	0.6384
12	346.5	1.733	0.6384
7	358.4	1.832	0.6749
6	374.2	1.969	0.7253
5	388.6	2.091	0.7703
4	402.5	2.207	0.8128
3	418.2	2.342	0.8625
2	434.2	2.481	0.9137
1	449.9	2.621	0.9653

Run 6 (pure potassium nitrate)

Serial number	Temperature (°C)	Cell conductivity (mmho)	Specific conductivity ($ohm^{-1}cm^{-1}$)
1	337.2	1.699	0.6259
2	339.9	1.723	0.6347
3	346.5	1.782	0.6564
4	358.4	1.884	0.6940
5	374.2	2.018	0.7434
6	388.6	2.139	0.7880
7	402.5	2.255	0.8305
8	418.2	2.387	0.8791
9	434.2	2.522	0.9288
10	449.9	2.658	0.9789

APPENDIX B. (continued)

Run 7 (pure potassium nitrate)

Serial number	Temperature (°C)	Cell conductivity (mmho)	Specific conductivity ($ohm^{-1}cm^{-1}$)
9	337.2	1.700	0.6262
8	339.9	1.728	0.6365
7	346.5	1.787	0.6583
6	358.4	1.892	0.6970
5	374.2	2.027	0.7467
4	388.6	2.150	0.7920
3	402.5	2.263	0.8334
2	418.2	2.395	0.8820
1	434.2	2.527	0.9306

Run 8 (pure potassium nitrate)

Serial number	Temperature (°C)	Cell conductivity (mmho)	Specific conductivity ($ohm^{-1}cm^{-1}$)
1	339.9	1.727	0.6362
2	346.5	1.787	0.6583
3	358.4	1.892	0.6970
4	374.2	2.031	0.7482
5	388.6	2.154	0.7935
6	402.5	2.271	0.8364
7	418.2	2.403	0.8850
8	434.2	2.540	0.9354

APPENDIX C.

DETAILS OF SPECTROSCOPIC EXAMINATIONS MADE ON THIN FILMS OF NITRATES AND NITRITES.

The results obtained from different samples of the same salt are listed separately. The mass of salt per unit area of the sample, when known, and the settings of the spectrophotometer controls, are given at the head of each table. The measured frequencies are in units of 1,000 cm^{-1} (1 kcm^{-1}).

All the values of E(2) and E'(2) listed below have been corrected for the effect of mis-shaping of the spectrophotometer cam (see pages 157 to 160). The size of the correction varied with frequency, and is given at the beginning of each group of results. It always took the form of a small addition to the value obtained from the frequency scale of the instrument. No correction has been applied to the frequencies measured on the low-energy edge of the strong band (E(t = 10%), etc.), because these figures have no absolute significance. Importance is attached to the changes in each parameter for a particular sample as the temperature was raised; these changes are not influenced by the correction. The absolute significance of the band-edge measurements is limited by the fact that sample thicknesses were known only approximately.

SODIUM NITRATE (Sample 1) Runs 248 - 306.

Resolution 4; scan-speed 3; damping 2; chart speed 40"/hour; transmission scale 0 - 100%.

The sample was solid for the whole of this series, and contained 0.011 grm salt per cm^2 (thickness 49 μ at 20°C). The absorption at the maximum of the weak band rose steadily from 91% to 94% as the temperature was raised.

The correction for cam mis-shaping was +0.04 kcm^{-1}.

Run number	Block temp. (°C)	E(2) (kcm^{-1})		Run number	Block temp.	E(2) (kcm^{-1})
248	15	34.3		282	265	33.6
249	15	34.2		284	271	33.5
253	50	34.2		286	272	33.5
255	100	34.1		288	274	33.5
257	152	34.0		290	275	33.4
259	200	33.8		292	276	33.5
261	211	33.8		294	277	33.4
266	220	33.8		298	278	33.4
270	230	33.7		300	279	33.4
273	240	33.8		302	280	33.4
275	250	33.7		304	291	33.4
278	255	33.6		306	302	33.3
280	260	33.6				

SODIUM NITRATE. (Sample 2). Runs 332 - 343

Resolution 5; scan-speed 3; damping 3; chart speed 40"/hour; transmission scale 0 - 100%.

For runs 332 - 342 the sample was solid and contained 0.0048 grm salt/cm^2 (thickness 21μ at 20°C). The sample was melted for run 343, and after cooling to room temperature it was found to contain 0.0035 grm salt per cm^2 (thickness 15μ at 20°C). The % absorption at the maximum of the weak band rose steadily from 67% to 72% as the solid was heated (runs 332 - 342), and dropped to 59% for run 343.

The correction for cam mis-shaping was +0.04 kcm^{-1}.

Run number	Block temp. (°C)	E(2) (kcm^{-1})
332	16	34.3
333	100	34.1
334	150	33.9
335	200	33.8
336	241	33.7
337	250	33.6
338	260	33.6
339	271	33.5
340	281	33.4
341	290	33.4
342	300	33.4
343	316	33.4

SODIUM NITRATE. (Sample 3) Runs 344 - 367

Resolution 5; scan-speed 3; damping 3; chart speed 40"/hour; transmission scale 0 -100%.

For runs 344 - 351 the sample contained 0.013 grm salt per cm^2 (thickness 57 μ at 20°C). The salt was melted for runs 353 - 356, after which it contained 0.0057 grm salt/cm^2. This sample was used again as a solid in runs 357 - 365, was melted for 366 and frozen again for 367. It finally contained 0.0021 grm salt/cm^2.

The % absorption at the maximum of the weak band was 93 - 94% for runs 344 - 351, and fell from 87% to 78% in runs 353 - 356. The transmission rose from 68% to 73% in runs 357 - 365, and fell to 47% for 366 and 29% for 367. The correction for cam mis-shaping was +0.04 kcm^{-1}.

Run number	Block temp. (°C)	E(2) (kcm^{-1})	Run number	Block temp. (°C)	E(2) (kcm^{-1})
344	31	34.2	358	53	34.2
345	31	34.2	359	100	34.2
347	151	33.9	360	150	34.0
349	151	34.0	361	199	33.9
351	241	33.7	362	200	33.8
353	320	33.4	363	251	33.6
354	333	33.5	364	269	33.5
355	347	33.4	365	301	33.4
356	371	33.3	366	321	33.5
357	18	34.2	367	292	33.3

SODIUM NITRATE. (Sample 5) Runs 369 - 380

Resolution 5; scan-speed 3; damping 3; chart speed 40"/hour; transmission scale 0 -100%.

The sample was fused for run 369, solid for 370 - 373, liquid for 374 and again solid for 377 and 380. At the end of the series, the film contained 0.0064 grm salt per cm^2 (thickness 28 μ at 20°C).

The % absorption varied irregularly, and is included in the table.

The correction for cam mis-shaping was +0.04 kcm^{-1}.

Run number	Block temp. (°C)	E(2) (kcm^{-1})	% absorption.
369	314	33.5	68
370	301	33.3	47
372	301	33.5	72
373	301	33.3	72
374	315	33.4	67
377	302	33.3	47
380	302	33.4	53

SODIUM NITRATE. (Sample 6) Runs 383 - 425

Resolution 5; scan-speed 3; damping 3; chart speed 40"/hour; transmission scale 0 - 100%.

The sample contained 0.0090 grm salt/cm^2 when prepared (thickness 40μ at 20°C). It was used as a solid film for runs 383 - 412, and was molten during runs 412 - 425. After re-freezing and cooling, the film was found to contain 0.0027 grm salt/cm^2.

The % absorption rose from 70 to 76% as the solid was heated from 40° to 305°C. It dropped to 52% when the sample was melted (run 412), and was further reduced to 48% as the temperature was raised to 399°C.

The correction for cam mis-shaping was +0.04 kcm^{-1}.

Run number	Block temp. (°C)	E(2) (kcm^{-1})	Run number	Block temp. (°C)	E(2) (kcm^{-1})
383	40	34.29	395	140	33.94
384	40	34.2	396	161	33.94
385	42	34.2	397	171	33.89
386	50	34.2	398	180	33.86
387	61	34.19	399	190	33.81
388	70	34.19	400	210	33.71
389	80	34.17	401	220	33.71
390	90	34.12	402	231	33.66
391	100	34.12	403	241	33.66
392	110	34.06	404	250	33.62
393	120	34.04	405	260	33.55
394	131	34.04	406	270	33.51

SODIUM NITRATE. (Sample 6) (continued)

Run number	Block temp. (°C)	E(2) (kcm^{-1})
407	275	33.42
407A	275	33.36
408	285	33.31
409	295	33.36
410	300	33.31
411*	305	33.31
412**	308	33.51
412A	308	33.52
412B	308	33.50
413	312	33.50
414	317	33.46
415	321	33.45
416	321	33.42
417	327	33.42
418	332	33.44
419	341	33.39
420	352	33.37
421	362	33.36
422	372	33.36
423	382	33.34
424	397	33.38
425	399	33.32

* solid

** liquid

SODIUM NITRATE. (Sample 4) Runs 428 - 476

Resolution 5; scan-speed 3; damping 3; chart speed 40"/hour; transmission scale 0 -100%.

The sample was melted and re-frozen three times in the spectrophotometer thermostat before the series was begun. It was liquid for runs 428 - 430, and solid for the remainder.

After run 476, the sample contained 0.0007_7 grm salt per cm^2 (thickness 3.4μ at 20°C).

In the table, E(t = x%) is the frequency on the low-energy edge of the strong band for which the transmission is x%. The basis on which the values of x were chosen is explained on page 242.

Liquid sample:

Run number	Block temp. (°C)	E(t=50%) (kcm^{-1})	E(t= 53.5%) (kcm^{-1})	E(t=10%) (kcm^{-1})	E(t= 12.5%) (kcm^{-1})
428	311	40.13	40.00	41.28	41.17
429	309	40.16	40.09	41.30	41.20
430	309	40.16	40.05	41.34	41.22

SODIUM NITRATE. (Sample 4) (continued)

Solid sample:

Run number	Block temp. (°C)	E(t=50%) (kcm^{-1})	E(t=10%) (kcm^{-1})
431	302	39.65	40.73
433	292	39.65	40.78
434	294	39.67	40.72
435	297	39.60	40.70
436	300	39.60	40.67
437	304	39.60	40.72
440	288	39.64	40.69
441	278	39.75	40.78
442	283	39.74	40.75
443	276	-	40.76
444	275	-	40.85
445	274	-	40.80
446	272	39.77	-
447	272	39.76	40.80
448	268	39.80	40.82
449	263	39.83	40.86
450	257	39.84	40.86
451	251	39.91	40.95
452	244	40.00	41.00
453	236	40.09	41.02
454	226	40.13	41.08
455	220	40.17	41.13
456	212	40.25	41.20
457	203	40.29	41.21
458	194	40.36	41.25
459	186	40.44	41.30

SODIUM NITRATE. (Sample 4) (continued)

Solid sample (continued):

Run number	Block temp. (°C)	E(t=50%) (kcm^{-1})	E(t=10%) (kcm^{-1})
460	176	-	41.35
461	168	-	41.40
462	159	-	41.46
463	149	40.60	41.49
464	138	40.68	41.51
465	128	40.73	41.60
466	118	40.83	41.68
467	108	40.87	41.70
468	98	40.95	41.76
469	88	-	41.78
470	79	-	41.82
471	69	41.07	41.86
472	59	-	41.90
473	49	41.20	42.00
474	40	-	41.98
475	30	41.22	42.00
476	21	-	42.00

POTASSIUM NITRATE. (Sample 1) Runs 709 - 748

Resolution 3; scan-speed 3; damping 2; chart speed 40"/hour; transmission scale 0 - 100%.

The sample was solid for runs 709 - 744, and liquid for 745 - 748. The film contained 0.026 grm salt per cm^2 at the beginning of the series (thickness 122 μ at 20°C).

The % absorption at the maximum of the weak band increased from 55% to 60% over the temperature interval 20.8° to 127.3°. It increased abruptly to 70% as the transition temperature (127.8°) was traversed, and increased steadily from this value to 79% as the salt was heated to its melting-point. The absorption fell to 62% when the sample melted. The correction for cam mis-shaping was +0.04 kcm^{-1}.

Run number	Block temp. (°C)	E(2) (kcm^{-1})	Run number	Block temp. (°C)	E(2) (kcm^{-1})
709	21	32.92	721	127	32.82
710	21	32.92	722	127	32.82
711	30	32.91	723	128	32.92
712	40	32.93	724	130	32.92
713	60	32.91	725	129	32.91
714	80	32.90	726	130	32.86
715	100	32.85	727	133	32.86
716	113	32.88	728	137	32.91
717	113	32.75	729	145	32.83
718	122	32.79	730	162	32.84
719	124	32.79	731	181	32.81
720	126	32.80	732	199	32.75

POTASSIUM NITRATE. (Sample 1) (continued)

Run number	Block temp. (°C)	E(2) (kcm^{-1})
733	218	32.71
734	237	32.66
735	257	32.64
736	277	32.63
737	298	32.56
738	314	32.60
739	322	32.55
740	329	32.56
741	331	32.56
742	332	32.54
743	333	32.54
744 *	334	32.55
745 **	335	32.60
746	337	32.62
747	339	32.57
748	341	32.59

* solid

** liquid

POTASSIUM NITRATE. (Sample 2) Runs 749 - 760

Resolution 3; scan-speed 3; damping 2; chart speed 40"/hour; transmission scale 0 - 100%.

The sample was solid for run 749, and liquid for the remainder of the series. The % absorption dropped from 82% in run 749 to 62% in run 751, and fell gradually to 54% as the temperature of the melt was raised. These changes were probably due to a gradual fall in the thickness of the sample. The correction for cam mis-shaping was +0.04 kcm^{-1}.

Run number	Block temp. (^{o}C)	E(2) (kcm^{-1})
749	331	32.54
751	336	32.58
752	338	32.60
753	343	32.61
754	351	32.60
755	360	32.57
756	376	32.55
757	397	32.56
758	419	32.51
759	441	32.46
760	441	32.47

POTASSIUM NITRATE (Sample 3) Runs 1593 - 1629.

Resolution 3; scan-speed 3; damping 3; chart speed 80"/hour; transmission scale 0 - 100%.

During this series the chassis of the spectrophotometer was fan-cooled to minimise the thermal drift in the frequency calibration. The Balmer line of the hydrogen spectrum was scanned after runs 1593, 1609 and 1629; it appeared within 20 cm^{-1} of the correct position (15,237 cm^{-1}) on each occasion.

The % absorption at the maximum of the weak band rose steadily from 60% to 64% as the sample was heated from 40°C to 126°C. It increased abruptly to 74.5% at the transition point (128°), and continued to increase to 90% as the solid was heated to the melting-point. The absorption fell to 82% when the sample was fused, and dropped to 67% as the melt was heated (probably because melt was extruded from between the Spectrosil plates). After re-freezing and cooling to room temperature, the sample contained 0.0096 grm salt per cm^2 (thickness 46μ at 20°C).

The correction for cam mis-shaping was +0.04 kcm^{-1}.

POTASSIUM NITRATE (Sample 3) (continued)

Run number	Block temp. (°C)	E(2) (kcm^{-1})	Run number	Block temp. (°C)	E(2) (kcm^{-1})
1593	42	33.16	1612	160	32.91
1594	39	33.12	1613	213	32.85
1595	40	33.13	1614	268	32.68
1596	42	33.10	1615	297	32.64
1597	62	33.13	1616	320	32.60
1598	61	33.08	1617	320	32.59
1599	57	33.15	1618	327	32.62
1600	87	33.06	1619	327	32.62
1601	112	32.96	1620	327	32.64
1602	119	33.04	1621	330	32.61
1603	126	33.03	1622	330	32.64
1604	127	33.03	1623	336	32.63
1605	127	33.04	1624	336	-
1606	130	32.99	1625	336	32.76
1607	130	33.04	1626	336	32.74
1608	134	33.03	1627	339	32.70
1609	143	33.00	1628.	339	32.69
1610	141	32.98	1629	339	32.72
1611	141	33.00			

POTASSIUM NITRATE (Sample 3) (continued) Runs 1594 - 1622.

Resolution 3; scan-speed 3; damping 3; chart speed 80"/hour; transmission scale 0 - 100%.

In the table, E(t = 10%) and E(t = 30%) are the frequencies on the low-energy edge of the strong band for which the transmission of the sample is 10% and 30%, respectively. All results in this table refer to the solid salt.

Run number	Block temp. (°C)	E(t=10%) (kcm^{-1})	E(t=30%) (kcm^{-1})
1594	39	40.66	39.71
1595	40	40.67	39.66
1596	42	40.67	39.67
1597	62	40.50	39.53
1598	61	40.55	39.58
1599	57	40.58	39.60
1600	87	40.37	39.45
1601	112	40.20	39.20
1602	119	40.15	39.15
1603	126	40.13	39.14
1604	127	40.12	39.10

POTASSIUM NITRATE (Sample 3) (continued).

Run number	Block temp. (^{o}C)	E(t=10%) (kcm^{-1})	E(t=30%) (kcm^{-1})
1605	127	39.88	39.00
1606	130	39.65	38.87
1607	130	39.65	38.86
1608	134	39.60	38.84
1609	143	39.60	38.83
1610	141	39.55	38.76
1611	141	39.54	38.73
1612	160	39.35	38.58
1613	213	38.80	38.07
1615	297	37.72	36.95
1616	320	37.47	36.68
1617	320	37.35	36.35
1618	327	37.27	36.30
1619	327	37.23	36.30
1621	330	37.24	36.18
1622	330	37.19	36.19

POTASSIUM NITRATE (Sample 4) Runs 1639 - 1652.

Resolution 2; scan-speed 3; damping 2; chart speed 120"/hour; transmission scale 0 - 100%.

This series of scans was made in order to follow the movement of the strong-band edge through the melting-point.

The salt film was melted and re-frozen twice in the thermostat unit, and then melted a third time. The sample was liquid during runs 1639 to 1643, solid for 1644 to 1648 and again liquid for 1649 to 1652. There was no significant difference between the two sets of results for the liquid, which indicates that the melt film had the same thickness on the two occasions.

After re-freezing and cooling to room temperature at the end of the series, the sample contained 0.0006 grm salt per cm^2 (thickness 2.8μ at 20°C).

In the table, E(t = x%) is the frequency on the band-edge for which the transmission is x%.

Run number	Block temp. (°C)	E(t= 10.8%) (kcm^{-1})	E(t= 31.2%) (kcm^{-1})	E(t= 51.1%) (kcm^{-1})
1639	335	41.15	40.42	39.78
1640	335	41.15	40.42	39.78
1641	335	41.15	40.43	39.80
1642	335	41.14	40.43	39.82
1643	335	41.16	40.44	39.80
1649	335	41.16	40.43	39.82
1650	335	41.19	40.47	39.85
1651	335	41.17	40.47	39.82
1652	335	41.18	40.45	39.82

POTASSIUM NITRATE (Sample 4) (continued).

Run number	Block temp. (^{o}C)	E(t=10%) (kcm^{-1})	E(t=30%) (kcm^{-1})	E(t=50%) (kcm^{-1})
1639*	335	41.21	40.45	39.83
1640*	335	41.20	40.46	39.82
1641*	335	41.20	40.49	39.84
1642*	335	41.20	40.46	39.87
1643*	335	41.22	40.48	39.86
1644**	332	40.95	40.24	39.59
1645**	332	40.95	40.23	39.60
1646**	332	40.94	40.23	39.58
1647**	331	40.93	40.22	39.61
1648**	331	40.93	40.23	39.61
1649*	335	41.23	40.47	39.86
1650*	335	41.25	40.52	39.90
1651*	335	41.23	40.51	39.88
1652*	335	41.24	40.50	39.87

* liquid sample

** solid sample

RUBIDIUM NITRATE (Sample 3) Runs 636 - 695.

Resolution 4; scan-speed 3; damping 2; chart speed 40"/hour; transmission scale 0 - 100%.

The sample was solid for runs 636 to 681, and liquid for 683 to 695. The % absorption at the maximum of the weak band changed abruptly at the transition temperatures, but increased steadily with rising temperature for each of the solid modifications. The changes are detailed in the table.

Temperature range (^{o}C)	% absorption
26 → 162	71 → 77
163 → 219	79 → 82
221 → 281	76 → 79
285 → 310	77
(M.P. 312°)	
314 → 422	77 → 74

The correction for cam mis-shaping was +0.04 kcm^{-1}.

RUBIDIUM NITRATE (Sample 3)

Run number	Block temp. (°C)	E(2) (kcm^{-1})	Run number	Block temp. (°C)	E(2) (kcm^{-1})
636	26	32.63	666	242	32.45
637	34	32.66	667	261	32.39
638	44	32.66	668	271	32.43
639	60	32.65	669	278	32.33
640	77	32.65	670	279	32.31
641	99	32.62	671	280	32.36
642	120	32.61	672	281	32.38
643	140	32.53	673	285	32.26
644	151	32.52	674	286	32.26
645	157	32.48	675	286	32.28
646	157	32.50	676	291	32.29
647	160	32.46	677	297	32.28
648	161	32.51	678	301	32.26
649	162	32.48	679	307	32.26
650	163	32.47	680	308	32.25
651	164	32.53	681	310	32.26
652	165	32.50	683	314	32.52
654	180	32.51	684	315	32.54
655	200	32.46	685	318	32.50
656	210	32.51	686	324	32.55
657	216	32.45	687	324	32.54
658	218	32.48	688	335	32.46
659	219	32.46	689	346	32.45
660	219	32.44	690	357	32.46
661	221	32.55	691	367	32.50
662	223	32.53	692	378	32.44
663	225	32.53	693	400	32.45
664	231	32.50	694	411	32.39
665	231	32.48	695	422	32.40

RUBIDIUM NITRATE (Sample 1) Runs 586 - 634.

Resolution 5; scan-speed 3; damping 3; chart speed 40"/hour; transmission scale 0 - 100%.

The sample was melted and re-frozen four times in the thermostat before the series was begun. It was liquid during runs 586 to 590, and solid for the remainder.

In the table, E(t = x%) is the frequency on the low-energy edge of the strong band for which the transmission is x%.

Run number	Block temp. (°C)	E(t=50%) (kcm^{-1})	E(t=10%) (kcm^{-1})
586	317	38.59	39.89
587	316	38.63	39.90
588	315	38.63	39.93
589	314	38.58	39.94
590	313	38.64	39.96
591	310	38.60	39.92
592	311	38.62	39.94
593	312	38.64	39.95
594	305	38.67	39.97
595	300	38.72	40.00
596	291	38.82	40.05
597	286	38.86	40.09
598	285	38.82	40.10
599	284	38.86	40.11
600	283	38.83	40.10
601	282	38.77	40.10
602	281	-	40.15
603	278	38.78	40.20

RUBIDIUM NITRATE (Sample 1) (continued).

Run number	Block temp. (^{o}C)	E(t=50%) (kcm^{-1})	E(t=10%) (kcm^{-1})
604	269	38.89	40.23
605	259	38.95	40.28
606	241	39.12	40.38
607	230	39.15	40.45
608	225	39.27	40.50
609	223	39.23	40.55
610	222	39.24	40.53
611	220	39.26	40.56
612	220	39.41	40.55
613	218	39.43	40.58
614	216	39.50	40.58
615	210	39.48	40.65
616	200	39.52	40.70
617	190	39.61	40.78
618	179	39.74	40.81
619	179	39.68	40.82
620	170	39.78	40.90
621	166	39.83	40.92
622	164	39.88	40.95
623	163	39.90	40.94

RUBIDIUM NITRATE (Sample 1) (continued).

Run number	Block temp. (^{o}C)	E(t=50%) (kcm^{-1})	E(t=10%) (kcm^{-1})
624	162	40.00	41.08
625	161	40.00	41.13
626	160	40.09	41.13
627	151	40.13	41.18
628	134	40.23	41.27
629	115	40.38	41.37
630	97	40.49	41.43
631	80	40.58	41.52
632	61	40.67	41.59
633	43	40.74	41.65
634	28	41.00	41.69

CAESIUM NITRATE. (Sample 4). Runs 532 - 572.

Resolution 4; scan-speed 3; damping 2; chart-speed 40"/hour; transmission scale 0 - 100%.

The sample contained 0.051 grm salt per cm^2 at the beginning of the series (thickness 182μ at 20°C). The film was solid for runs 532 to 566, and liquid for 568 to 572.

The % absorption at the maximum of the weak band rose steadily from 77% at 19°C (run 532) to 91% at 404°C (run 566). There was no abrupt change in % absorption at the transition temperature (152°C). The absorption fell to 81% when the sample was fused, and remained at this value for runs 568 to 572. The correction for cam mis-shaping was +0.04 kcm^{-1}.

Run number	Block temp. (°C)	E(2) (kcm^{-1})	Run number	Block temp. (°C)	E(2) (kcm^{-1})
532	19	32.52	545	151	32.41
533	30	32.56	547	153	32.36
534	48	32.52	548	154	32.33
535	68	32.53	549	155	32.35
536	90	32.44	550	158	32.35
537	110	32.46	551	167	32.36
538	120	32.43	552	184	32.33
539	130	32.41	553	201	32.30
540	141	32.46	554	227	32.29
541	146	32.41	555	253	32.28
542	148	32.44	556	280	32.21
543	149	32.42	557	307	32.19
544	150	32.41	558	334	32.16

CAESIUM NITRATE. (Sample 4) (continued)

Run number	Block temp. (^{o}C)	E(2) (kcm^{-1})
559	362	32.16
560	362	32.11
561	381	32.08
562	390	32.11
563	399	32.04
564	400	32.09
565	402	32.11
566*	404	32.10
568**	408	32.23
569	411	32.24
570	415	32.24
571	421	32.21
572	431	32.19

* solid sample

** liquid sample

CAESIUM NITRATE (Sample 1) Runs 480 - 526

Resolution 5; scan speed 3; damping 3; chart speed 40"/hour; transmission scale 0 - 100%.

The sample was melted and re-frozen three times in the thermostat before the series was begun. It was liquid for runs 480 - 483, and solid for 484 - 526. At the end of the series the sample contained 0.0013 grm salt per cm^2 (thickness 3.7μ at 20°C).

In the table, E(t=x%) is the frequency on the low-energy edge of the strong band for which the transmission is x%. The choice of values for x is discussed on page 242.

Liquid sample:

Run number	Block temp. (°C)	E(t= 50%) (kcm^{-1})	E(t= 53.9%) (kcm^{-1})	E(t= 10%) (kcm^{-1})	E(t= 12.8%) (kcm^{-1})
480	410	38.14	37.91	39.64	39.52
481	409	38.17	38.00	39.68	39.55
482	409	38.20	38.00	39.70	39.55
483	416	38.13	37.95	39.68	39.53

CAESIUM NITRATE (Sample 1) (continued)

Solid sample:

Run number	Block temp. (°C)	E(t=50%) (kcm^{-1})	E(t=10%) (kcm^{-1})
485	401	38.12	39.67
486	403	38.10	39.65
487	399	38.18	39.66
488	393	38.31	39.78
489	387	38.30	39.75
490	378	38.35	39.78
491	367	38.40	39.88
492	356	38.50	39.90
493	346	-	39.98
495	328	38.80	40.10
496	311	38.84	40.23
497	293	39.10	40.37
498	275	39.20	40.47
499	258	39.28	40.54
500	240	39.41	40.67
501	223	39.54	40.78
502	206	39.68	40.88
503	189	39.85	41.00
504	173	39.95	41.10
505	164	40.00	41.13

CAESIUM NITRATE (Sample 1) (continued)

Run number	Block temp. (°C)	E(t=50%) (kcm^{-1})	E(t=10%) (kcm^{-1})
506	157	40.10	41.16
507	156	40.10	41.17
508	155	40.10	41.17
509	154	40.10	41.18
510	153	40.13	41.19
511	153	40.10	41.19
512	152	40.10	41.20
514	152	40.23	41.28
515	152	40.22	41.23
516	151	40.22	41.25
517	149	40.23	41.27
518	144	40.23	41.28
519	134	40.27	41.36
520	118	40.38	41.42
521	101	40.48	41.51
522	84	40.59	41.58
523	68	40.68	41.67
524	52	40.72	41.71
525	36	40.80	41.75
526	26	40.83	41.79

CAESIUM NITRATE. (Sample 5) Runs 1580 - 1591

Resolution 3; scan-speed 3; damping 2; chart speed 80"/hour; transmission scale 0 - 100%.

The sample was melted and re-frozen four times in the sample thermostat of the spectrophotometer; melting occurred at a block temperature of 409°C. It was finally melted a fifth time, and left for ten minutes, during which the % transmission at 39 kcm^{-1} remained constant (to ± 0.5%). Runs 1580 to 1586 were made on the liquid sample, and runs 1587 to 1591 on the solid.

After cooling to room temperature at the end of the series, the sample contained 0.0015 grm salt per cm^2 (thickness 4.0μ at 20°C).

In the table, E(t = x%) is the frequency for which the transmission on the low-energy edge of the weak band is x%.

Run number	Block temp. (°C)	E(t=50%) (kcm^{-1})	E(t=53.9%) (kcm^{-1})	E(t=10%) (kcm^{-1})	E(t=12.8%) (kcm^{-1})
1580	420	38.27	38.15	39.57	39.45
1581	420	38.26	38.12	39.58	39.45
1582	416	38.32	38.18	39.68	39.57
1583	416	38.33	38.21	39.68	39.56
1584	411	38.44	38.27	39.71	39.61
1585	411	38.40	38.28	39.71	39.60
1586	409	38.42	38.32	39.73	39.61
1587	405	38.33	-	39.61	-
1588	405	38.32	-	39.61	-
1589	402	38.32	-	39.62	-
1590	400	38.36	-	39.65	-
1591	397	38.36	-	39.65	-

ACCURATE RESULTS FOR ALKALI NITRATE MELTS. RUNS 1411 - 1436 AND 1550 - 1559.

Resolution 3; scan-speed 3; damping 2; chart speed 120"/hour; transmission scale 0 - 100%.

The results listed here refer to the fused salts just above their melting-points. The frequency calibration of the spectrophotometer was checked before and after each salt spectrum by recording the Balmer line from the hydrogen lamp (15,237 cm^{-1}). The results were accepted only if this line appeared within 10 cm^{-1} of the correct position on each occasion.

Throughout these measurements the main chassis of the spectrophotometer was fan-cooled. This precaution was taken in order to minimise thermal drift in the calibration (see page 157).

The correction for cam mis-shaping was +0.04 kcm^{-1}, in all cases.

The frequencies in the Table refer to air as the standard medium.

ACCURATE RESULTS FOR ALKALI NITRATE MELTS (continued)

Salt	Run number	Block temp. (^{o}C)	E(2) (cm^{-1})
$NaNO_3$ (M.P. 308°C)	1411	312	33,530
	1412	312	33,510
KNO_3 (M.P. 334°C)	1432	338	32,700
	1435	339	32,700
	1436	341	32,700
$RbNO_3$ (M.P. 310°C)	1421	318	32,510
	1424	318	32,480
$CsNO_3$ (M.P. 409°C)	1550	418	32,150
	1553	419	32,150
	1555	419	32,155
	1557	419	32,165
	1559	419	32,160

POTASSIUM NITRATE + 10 EQUIV. % BARIUM NITRATE

Runs 761 - 769.

Resolution 3; scan-speed 3; damping 2; chart speed 40"/hour; transmission scale 0 - 100%.

A single sample was used, and it was liquid throughout (the liquidus temperature for this mixture is 318°C; see Figure 10.4 on page 140). After re-freezing at the end of the series, the sample contained 0.012 grm salt per cm^2 (thickness 56 μ at 20°C).

The % absorption at the maximum of the weak band remained steady at 92 - 93%.

The correction for cam mis-shaping was +0.04 kcm^{-1}.

Run number	Block temp. (°C)	E(2) (kcm^{-1})
761	321	32.80
762	321	32.80
763	330	32.76
764	340	32.77
765	374	32.73
766	401	32.65
767	420	32.65
768	441	32.66
769	441	32.64

POTASSIUM NITRATE + 20 EQUIV. % BARIUM NITRATE.

Runs 701 - 708.

Resolution 3; scan-speed 3; damping 2; chart speed 40"/hour; transmission scale 0 - 100%.

The sample was liquid throughout the series; the liquidus temperature for this mixture is 294°C (see diagram on page 140).

The % absorption at the maximum of the weak band remained steady at 63 - 65% as the temperature was raised.

The correction for cam mis-shaping was +0.04 kcm^{-1}.

Run number	Block temp. (°C)	E(2) (kcm^{-1})
701	306	33.00
702	306	32.99
703	320	32.98
704	330	32.93
705	341	32.91
706	373	32.91
707	411	32.81
708	440	32.81

POTASSIUM NITRATE + 35 EQUIV.% BARIUM NITRATE.

Runs 770 - 776.

Resolution 5; scan-speed 3; damping 2; chart speed 40"/hour; transmission scale 0 - 100%.

The sample was liquid throughout; the liquidus temperature for this mixture is 364°C (see diagram on page 140). After re-freezing at the end of the series, the sample was found to contain 0.0052 grm salt per cm^2 (thickness 21μ at 20°C).

The % absorption at the maximum of the weak band fell from 54% to 49% as the temperature was lowered from 440°C to 371°C.

The correction for cam mis-shaping was +0.04 kcm^{-1}.

Run number	Block temp. (°C)	E(2) (kcm^{-1})
770	440	33.25
771	440	33.21
772	420	33.19
773	400	33.24
774	380	33.26
775	371	33.30
776	371	33.29

POTASSIUM NITRATE + 50 EQUIV.% BARIUM NITRATE.

Runs 696 - 698.

Resolution 5; scan-speed 3; damping 3; chart speed 40"/hour; transmission scale 0-100%.

The sample was liquid throughout; the liquidus temperature for this mixture is 437°C (see diagram on page 140).

The % absorption at the maximum of the weak band remained steady at 87 - 88%.

The correction for cam mis-shaping was +0.04 kcm^{-1}.

Run number	Block temp. (°C)	E(2) (kcm^{-1})
696	460	33.54
697	451	33.55
698	440	33.52

AMMONIUM NITRATE. (Sample 5). Runs 993 - 1008.

Resolution 3; scan-speed 3; damping 2; chart speed 80"/hour; transmission scale 0 - 100%.

The sample was prepared (see page 184), and transferred from the hotplate to the thermostatted cell at 134°C before the transition at 35°C had occurred. This prevented excessive scattering losses from the 'sample' beam.

The salt was solid for runs 993 to 1002, liquid for 1003 to 1005 and again solid from 1006 to 1008.

The % absorption at the maximum of the weak band increased from 62% to 68% as the solid was heated, and dropped to 61% on fusion. It remained at this level when the sample was re-frozen.

The correction for cam mis-shaping was +0.04 kcm^{-1}.

Run number	Block temp. (°C)	E(2) (kcm^{-1})	Run number	Block temp. (°C)	E(2) (kcm^{-1})
993	126	32.81	1001	161	32.79
994	131	32.85	1002	164	32.86
995	136	32.82	1003	169	33.18
996	141	32.79	1004	172	33.13
997	146	32.79	1005	174	33.14
998	151	32.76	1006	156	32.85
999	156	32.82	1007	159	32.86
1000	156	32.82	1008	161	32.86

AMMONIUM NITRATE (Sample 6) Runs 1009 - 1030.

Resolution 3; scan-speed 3; damping 2; chart speed 80"/hour; transmission scale 0 - 100%.

The sample was prepared on the hotplate (see page 184) and transferred directly to the thermostat at 140°C, so that it did not undergo the transition at 35°C. The sample was solid during all the scans, although it was melted and re-frozen between 1010 and 1011. This was done in order to obtain a salt film which had undergone no solid - solid transitions, and from which scattering and reflection losses were therefore relatively slight.

The % absorption was 88% for runs 1009 and 1010, and 91 - 92% for 1011 to 1017. It fell to 87% when the transition at 126°C was traversed, and remained within the range 84 - 87% for 1018 to 1029. The correction for cam mis-shaping was +0.04 kcm^{-1}.

Run number	Block temp. (°C)	E(2) (kcm^{-1})	Run number	Block temp. (°C)	E(2) (kcm^{-1})
1009	134	32.79	1020	109	32.92
1010	158	32.81	1021	99	32.95
1011	158	32.80	1022	94	32.97
1012	153	32.82	1023	89	32.97
1013	148	32.83	1024	84	32.96
1014	142	32.84	1025	79	32.97
1015	137	32.77	1026	74	33.01
1016	132	32.81	1027	69	33.01
1017	127	32.82	1028	58	32.99
1018	120	32.97	1029	48	33.04
1019	115	32.92	1030	38	33.44

AMMONIUM NITRATE (Sample 6) (continued) Runs 1031 - 1043.

Resolution 3; scan-speed 3; damping 2; chart speed 80"/hour; transmission scale 0 - 10%.

The sample was left overnight at 15°C after run 1030 of the previous series. Scattering and reflection losses were now extremely high (about 86%), and it was necessary to use the 0 - 10% transmission scale in order to define the maximum of the weak band with sufficient accuracy.

The correction for cam mis-shaping was +0.04 kcm^{-1}.

Run number	Block temp. (°C)	E(2) (kcm^{-1})
1031	15	33.54
1032	15	33.54
1033	18	33.54
1034	23	33.54
1035	28	33.55
1036	33	33.53
1037	38	33.53
1038	43	33.52
1039	48	33.51
1040	53	33.78
1041	53	33.76
1042	53	33.81
1043	53	33.67

AMMONIUM NITRATE (Sample 6) (continued). Runs 1045 - 1066

Resolution 3; scan-speed 3; damping 2; chart speed 80"/hour; both transmission scales.

The sample was fused after run 1044. It was liquid in 1045, and solid for the remainder of this series. Between 1057 and 1058 the sample was cooled below 35°C and re-heated to 84°C, to convert it to the orthorhombic modification (III). Both transmission scales were used; the runs marked * were carried out on the 0 - 10% scale, the remainder on the 0 - 100% scale.

The % absorption at the maximum of the weak band (after correction for scattering losses) was 96% in run 1046 (160°C), and fell to 87% as the sample was cooled to 84°C.

The correction for cam mis-shaping was +0.04 kcm^{-1}.

Run number	Block temp. (°C)	E(2) (kcm^{-1})	Run number	Block temp. (°C)	E(2) (kcm^{-1})
1045	171	33.07	1056	85	32.89
1046	160	32.81	1057*	85	32.97
1047*	160	32.84	1058	84	33.65
1048	131	32.83	1059*	84	33.68
1049*	131	32.87	1060*	89	32.99
1050	120	32.95	1061*	79	33.00
1051*	120	32.98	1062*	68	33.13
1052	131	32.84	1063*	58	33.34
1053*	131	32.87	1064*	48	33.46
1054	90	32.92	1065*	38	33.82
1055*	90	32.94	1066*	33	33.84

AMMONIUM NITRATE (Sample 7) Runs 1067 - 1086.

Resolution 3; scan-speed 3; damping 2; chart speed 80"/hour; transmission scale 0 - 100%.

In this series the temperature was raised gradually from room temperature to 100°C. Transitions occurred between runs 1071 and 1072 (orthorhombic IV to orthorhombic III) and between runs 1083 and 1084 (orthorhombic III to tetragonal II).

The % absorption at the maximum of the weak band was 61 - 62% for runs 1067 - 1071, 58 - 60% for runs 1072 - 1083 and the same for runs 1084 to 1086.

The correction for cam mis-shaping was +0.04 kcm^{-1}.

Run number	Block temp. (°C)	E(2) (kcm^{-1})	Run number	Block temp. (°C)	E(2) (kcm^{-1})
1067	19	33.52	1077	50	33.70
1068	18	33.51	1078	55	33.71
1069	25	33.51	1079	60	33.68
1070	30	33.45	1080	65	33.69
1071	35	33.24	1081	70	33.65
1072	35	33.83	1082	75	33.65
1073	35	33.82	1083	80	33.66
1074	40	33.82	1084	86	32.94
1075	45	33.77	1085	91	32.92
1076	48	33.74	1086	101	32.93

SILVER NITRATE. (Sample 2) Runs 887 - 929

Resolution 3; scan-speed 3; damping 2; chart speed 80"/hour; transmission scale 0 - 100%.

The sample was solid for runs 887 to 917, liquid for 918 to 921, solid for 922 and again liquid for 923 to 929. At the end of the series the sample contained 0.0012 grm salt per cm^2 (thickness 2.8μ at 20°C).

The % absorption at the maximum of the weak band remained practically constant at 85 - 86% between room temperature and the transition temperature (158°C) (runs 887 - 911). It increased abruptly to 90% when the transition occurred, and rose gradually to 93% as the melting-point was approached. The absorption fell to 87% when the sample was fused. At this stage, the sample was re-frozen and cooled to room temperature, when its absorption was found to be only 72% (cf. the initial value of 85%). The sample was re-fused, and the absorption returned to 87%. These results suggest that the thickness of the sample decreased when it was fused for the first time (after run 917).

In the table, E(2) is the frequency at the maximum of the weak band. E'(2) is the frequency on the low-energy edge of this band for which the transmission (I/I_o) is given by $\log (I/I_o) = 0.3 \log (I/I_o)_{max}$, where $(I/I_o)_{max}$ refers to the maximum of the weak band. E(t = 4%) is the frequency on the low-energy edge of the strong band for which the transmission of the sample is 4%. The significance of these parameters is discussed on page 242.

The correction for cam mis-shaping was +0.06 kcm^{-1} for E(2), and +0.07 kcm^{-1} for E'(2).

SILVER NITRATE. (Sample 2) (continued)

Run number	Block temp. (°C)	E(2) (kcm^{-1})	E'(2) (kcm^{-1})	E(t=4%) (kcm^{-1})
887	20	30.84	28.65	35.51
888	20	30.82	28.65	35.50
889	20	30.85	28.67	35.50
893	20	30.86	28.60	35.48
894	19	30.88	28.63	35.44
895	31	30.86	28.64	35.43
896	40	30.88	28.67	35.36
897	50	30.89	28.67	35.35
898	60	30.86	28.65	35.27
899	60	30.89	28.65	35.30
900	70	30.91	28.69	35.24
901	70	30.86	28.64	35.22
902	78	30.89	28.64	35.17
903	88	30.87	28.63	35.11
904	97	30.86	28.64	35.04
905	107	30.91	28.65	35.00
906	117	30.93	28.62	34.98
907	128	30.93	28.65	34.91
908	138	30.96	28.67	34.85
909	148	30.97	28.67	34.78
910	153	30.96	28.63	34.76

SILVER NITRATE (Sample 2) (continued).

Run number	Block temp. (^{o}C)	E(2) (kcm^{-1})	E'(2) (kcm^{-1})	E(t=4%) (kcm^{-1})
911	158	30.96	28.64	34.71
912	159	30.78	28.41	34.18
913	162	30.81	28.37	34.12
913A	162	30.80	28.33	34.12
914	175	30.78	28.33	34.00
915	185	30.76	28.34	33.93
916	195	30.80	28.36	33.63
917	200	30.89	28.35	33.65
918	206	30.96	28.38	33.34
919	207	-	28.37	33.24
921	210	-	28.67	33.18
922	20	-	28.65	35.77
923	210	-	28.67	33.15
924	210	-	28.59	33.10
925	216	-	28.57	33.20
926	216	-	28.52	-
927	227	-	28.47	-
929	238	-	28.53	-

THALLOUS NITRATE. (Sample 2) Runs 781 - 844

Resolution 3; scan-speed 3; damping 2; chart speed 40"/hour; transmission scale 0 - 100%.

The sample was fused and re-frozen in the thermostat before run 781. It was solid for runs 781 to 829, and liquid for 830 to 842. Runs 843 and 844 were carried out after the sample had been re-cooled to room temperature. Some decomposition of the sample probably occurred during the runs after 835; the % transmission in the region of the strong band was zero in runs 781 to 835, 1% in 837, 3% in 840 and 10% in 842. This transmission was due to gas bubbles, which displaced the melt as decomposition proceded.

At the end of the series the sample contained 0.0023 grm salt per cm^2 (thickness 4.0 μ at 20°C).

The % absorption at the maximum of the weak band rose steadily from 85% to 91% as the solid was heated, and increased abruptly to 96% when the salt was fused. After re-freezing the sample and cooling it to room temperature, the absorption was 73%.

In the table E(2) is the frequency at the maximum of the weak band, and E'(2) is the frequency at a point on the low-energy edge of the weak band for which the transmission (I/I_o) is given by $\log (I/I_o) = 0.3 \log (I/I_o)_{max}$, $(I/I_o)_{max}$ being the transmission at the maximum of the band.

The correction for cam mis-shaping was +0.04 kcm^{-1} for E(2) and +0.08 kcm^{-1} for E'(2).

THALLOUS NITRATE. (Sample 2) (continued).

Run number	Block temp. (°C)	E(2) (kcm^{-1})	E'(2) (kcm^{-1})
781	26	31.92	29.85
782	26	31.91	29.88
783	26	31.89	29.86
784	31	31.93	29.91
785	36	31.92	29.86
786	46	31.92	29.85
787	55	31.89	29.92
788	65	31.86	29.85
789	70	-	29.88
790	73	31.83	29.86
791	75	31.84	29.91
792	77	31.85	29.86
793	78	31.89	29.88
794	78	31.80	29.84
795	78	31.82	29.88
796	79	31.81	29.86
797	80	31.89	29.88
798	83	31.76	29.84
799	85	31.83	29.83
800	91	31.80	29.88
801	101	31.82	29.84
802	111	31.82	29.80
803	121	31.82	29.80
804	131	31.81	29.78
805	136	31.80	29.76
806	139	31.72	29.72
807	142	31.78	29.76
808	143	31.80	29.72
810	144	31.82	29.79
811	146	31.88	29.79

THALLOUS NITRATE. (Sample 2) (continued).

Run number	Block temp. (°C)	E(2) (kcm^{-1})	E'(2) (kcm^{-1})
812	147	31.85	29.74
813	148	31.91	29.80
814	150	31.85	29.73
815	152	31.86	29.71
816	158	31.89	29.75
817	168	31.91	29.70
818	178	31.84	29.75
819	189	31.96	29.81
820	189	31.85	29.70
821	189	31.84	29.68
822	194	31.85	29.70
823	197	31.88	29.66
824	199	31.87	29.69
825	202	31.93	29.70
826	202	31.92	-
827	203	31.92	29.71
828	205	31.91	29.73
829	206	31.91	29.68
830	207	32.54	30.08
831	208	32.47	30.08
832	210	32.54	30.08
833	213	32.51	30.08
834	219	32.47	30.08
835	229	-	30.03
836	239	-	30.03
837	250	-	30.08
838	260	-	30.08
839	271	-	30.03
840	294	-	30.03

THALLOUS NITRATE (Sample 3) Runs 846 - 881.

Resolution 5; scan-speed 3; damping 3; chart speed 40"/hour; transmission scale 0 - 100%.

The sample was solid for run 846, after which it was melted and re-frozen four times. The % transmission of the liquid was measured at 30,400 cm^{-1} after each fusion; the values obtained were 32%, 31.8%, 32% and 32%.

Runs 847 to 849 were carried out on the melt. The sample was then frozen, and runs 850 to 881 carried out on the solid. At the end of the series, the sample contained 0.0026 grm salt per cm^2 (thickness 4.8μ at 20°C).

The % absorption at the maximum of the weak band was 82% in run 846. The absorption rose to 94 - 95% for the melt (runs 847 to 849), fell to 88% on re-freezing (run 850) and then decreased gradually to 81% as the solid was cooled (runs 850 to 881).

In the table, E(2) is the frequency corresponding to the maximum of the weak band. E'(2) is the frequency at a point on the low-energy edge of the weak band at which the transmission (I/I_o) is given by $\log (I/I_o) = 0.3 \log (I/I_o)_m$, where $(I/I_o)_m$ is the transmission at the maximum of the weak band.

THALLOUS NITRATE (Sample 3) (continued).

The correction for cam mis-shaping was +0.04 kcm^{-1} for E(2) and +0.08 kcm^{-1} for E'(2).

$E(t_S = 4\%)$ is the frequency on the low-energy edge of the strong band for which the solid sample transmits 4% of the radiation. $E(t_L = 4\%)$ and $E(t_L = 4.7\%)$ are the frequencies on the same band-edge at which the liquid sample transmits 4% and 4.7%, respectively. The choice of these parameters is explained on page 242.

The results for the liquid sample are tabulated first.

Run number	Block temp. (°C)	E(2) (kcm^{-1})	E'(2) (kcm^{-1})
847	209	32.35	29.97
848	209	32.56	30.03
849	208	32.54	30.11
Run number	Block temp. (°C)	$E(t_L=4\%)$ (kcm^{-1})	$E(t_L=4.7\%)$ (kcm^{-1})
847	209	34.60	34.48
848	209	34.50	34.38
849	208	34.45	34.37

THALLOUS NITRATE. (Sample 3) (continued)

Run number	Block temp. (°C)	E(2) (kcm^{-1})	E'(2) (kcm^{-1})	E(t_S=4%) (kcm^{-1})
846	20	31.90	29.97	36.0
850	204	31.84	29.72	35.50
851	202	31.84	29.74	35.47
852	196	31.86	29.73	35.57
856	175	31.82	29.62	35.59
857	164	31.77	29.70	35.65
858	153	31.80	29.72	35.72
859	151	31.79	29.78	35.74
860	148	31.80	29.77	35.75
861	145	31.85	29.77	35.80
862	143	31.84	29.73	35.80
863	140	31.84	29.75	35.80
864	137	31.82	29.75	35.78
865	132	31.80	29.78	35.83
866	122	31.82	29.78	35.80
867	111	31.77	29.77	35.93
868	111	31.76	29.77	35.93
869	101	31.72	29.80	35.95
870	90	31.73	29.81	36.00
871	82	31.76	29.82	36.00
872	77	31.72	29.84	36.03
873	80	31.81	29.84	36.08
874	75	31.81	29.84	36.08
875	72	31.78	29.85	36.09
876	69	31.79	29.84	36.10
877	67	31.79	29.84	36.13
878	62	31.80	29.87	36.13
879	51	31.82	29.87	36.13
880	41	31.73	29.86	36.25
881	31	31.79	29.88	36.28

0.24N NITRIC ACID. Runs 1135 - 1136

Resolution 3; scan-speed 3; damping 2; chart speed 80"/hour; transmission scale 0 - 100%.

The spectra were obtained with the solution in a silica cell of path-length 1 mm; a similar cell filled with distilled water was placed in the reference compartment.

The % absorption at the maximum of the weak band was 32% for both runs.

The molar extinction coefficient, ϵ, at the maximum of the band is calculated to be 7.0 litres/mole.cm.

The correction for cam mis-shaping was +0.04 kcm^{-1}.

Run number	Block temp. (^{o}C)	E(2) (kcm^{-1})
1135	15	33.14
1136	15	33.14

NITRIC ACID TRIHYDRATE. runs 1140 - 1150

Resolution 3; scan-speed 2; damping 2; chart speed 160"/hour; transmission scale 0 - 100%.

The % absorption at the maximum of the weak band was in the range 39 - 45%. The acid was examined as a thin film between Spectrosil plates. This hydrate freezes at -18.5°C (see page 146).

The correction for cam mis-shaping was +0.04 kcm^{-1}.

Run number	Block temp. (°C)	E(2) (kcm^{-1})
1140	-6	34.91
1141	-10	35.10
1142	-16	34.99
1143	-28	34.55
1145	-30	34.54
1146	-23	34.57
1148	-14	35.14
1149	-11	35.14
1150	+13	35.14

NITRIC ACID MONOHYDRATE. Runs 1134A - 1142A

For runs 1134A - 1136A, the factors were:
resolution 3; scan-speed 3; damping 2; chart speed 80"/hour; transmission scale 0 - 100%.

For runs 1137A - 1142A, the factors were:
resolution 3; scan-speed 2; damping 2; chart speed 160"/hour; transmission scale 0 - 10%.

In the table, E'(2) is the frequency on the low-energy side of the weak band for which the extinction coefficient is 0.7 times the extinction coefficient at the band maximum. The % absorption at the maximum was in the region of 25%. This hydrate freezes at -37°C (see page 146).

The correction for cam mis-shaping was +0.04 kcm^{-1}.

Run number	Block temp. (°C)	E'(2) (kcm^{-1})
1134A	+13	34.69
1135A	-4	34.54
1136A	-12	34.64
1137A	-42	33.94
1138A	-40	34.24
1140A	-42	33.45
1142A	-8	34.36

SODIUM NITRITE. (Sample 1) Runs 1177 - 1180 and 1213 - 1224

Resolution 3; scan-speed 3; damping 2; chart speed 80"/hour; both transmission scales.

The sample was made up from Analar salt taken straight from the reagent bottle. It was solid for runs 1177 to 1180 and 1213 to 1219, and liquid for 1220 to 1224. After re-freezing and cooling to room temperature, the salt film contained 0.0009 grm salt per cm^2 (thickness 4.1μ at 20°C).

The % absorption at the maximum of the weak band rose steadily from 81% to 97.5% as the solid was heated. It dropped to 74% when the sample was fused, and fell further to 36% by the end of the series. It seems likely from these figures that the thickness of the film fell substantially when the salt was fused, and fell further when the melt was heated. The correction for cam mis-shaping was +0.07 kcm^{-1}.

In the table, the results obtained with the 0 - 10% transmission scale are marked *; those obtained with the 0 -100% scale are unmarked.

Run number	Block temp. (°C)	E(2) (kcm^{-1})	Run number	Block temp. (°C)	E(2) (kcm^{-1})
1177	10	28.71	1218*	273	28.23
1178	20	28.69	1219	273	28.21
1180	45	28.66	1220	282	28.44
1213	265	28.19	1221	288	28.46
1214	265	28.19	1222	300	28.47
1215*	265	28.20	1223	331	28.53
1216*	265	28.24	1224	379	28.37
1217*	273	28.25			

SODIUM NITRITE. (Sample 2) Runs 1173 - 1176 and 1181 - 1212

Resolution 3; scan-speed 3; damping 2; chart speed 80"/hour; both transmission scales.

The sample was made up from zone-refined material (see page 104). It was solid for runs 1173 to 1176 and 1181 to 1200, and liquid for 1201 to 1212. After re-freezing and cooling to room temperature, the salt film contained 0.0047 grm salt per cm^2 (thickness 22μ at 20°C).

The % absorption at the maximum of the weak band increased steadily from 92% to 99% as the solid was heated, and fell to 98% when the solid was fused.

In the table, the results obtained by the use of the 0 - 10% transmission scale are marked *; those with the 0 - 100% scale are unmarked.

The correction for cam mis-shaping was +0.07 kcm^{-1}.

Run number	Block temp. (°C)	E(2) (kcm^{-1})	Run number	Block temp. (°C)	E(2) (kcm^{-1})
1173	10	28.67	1187	109	28.52
1175	10	28.65	1188	135	28.43
1176	10	28.76	1189	162	28.35
1181	10	28.65	1190	189	28.28
1182	13	28.57	1191	215	28.27
1183	23	28.61	1192	243	28.28
1184	32	28.64	1193*	243	28.22
1185	57	28.59	1194	254	28.25
1186	83	28.55	1195*	254	28.26

SODIUM NITRITE. (Sample 2) (continued)

Run number	Block temp. (^{o}C)	E(2) (kcm^{-1})
1196	265	28.30
1198*	265	28.20
1199	273	28.34
1200*	273	28.27
1202*	279	28.50
1204*	282	28.51
1205	282	28.57
1207*	282	28.47
1208	288	28.54
1209*	288	28.45
1210*	288	28.39
1211*	299	28.48
1212*	299	28.48

SODIUM NITRITE. (Sample 3) Runs 1233 - 1243

Resolution 3; scan-speed 3; damping 2; chart speed 80"/hour; transmission scale 0 - 100%.

The sample was made up of zone-refined salt (see page 104). It was solid for runs 1233 to 1239, and liquid for 1240 to 1243. After re-freezing and cooling to room temperature, the sample contained 0.0008 grm salt per cm^2 (thickness 3.9μ at 20°C).

The % absorption at the maximum of the weak band rose steadily from 63 to 66% as the solid was heated, and remained at 66% when the sample was fused. The correction for cam mis-shaping was +0.07 kcm^{-1}.

In the table, E(t = 10%) and E(t = 50%) are the frequencies on the low-energy edge of the strong band for which the transmission is 10% and 50%, respectively.

Run number	Block temp. (°C)	E(2) (kcm^{-1})	E(t=10%) (kcm^{-1})	E(t=50%) (kcm^{-1})
1233	50	28.45	42.48	40.62
1234	101	28.44	42.11	40.07
1235	153	28.37	41.65	39.57
1236	206	28.29	41.14	39.15
1237	261	28.20	40.48	38.64
1238	260	28.23	40.53	38.70
1239	271	28.24	40.17	38.61
1240	277	28.44	39.70	38.50
1241	289	28.44	39.62	38.42
1242	301	28.46	39.59	38.39
1243	333	28.39	39.42	38.12

POTASSIUM NITRITE. (Sample 1)) Runs 1244 - 1273

Resolution 3; scan-speed 3; damping 2; chart speed 80"/hour; transmission scale 0 - 100%.

The sample was made up from Analar material taken straight from the reagent bottle. It was solid for runs 1244 to 1267, and liquid for 1268 to 1273. After re-freezing and cooling to room temperature, the salt film contained 0.0006 grm salt per cm^2 (thickness 3.2μ at 20°C).

The % absorption at the maximum of the weak band fell gradually from 88% to 81% as the sample was heated from 15° to 389°C (runs 1244 to 1259), and returned to 88-89% when the sample was re-cooled to its initial temperature (runs 1260 to 1266). The % absorption fell to 43% when the sample was fused; this was probably due to a reduction in the thickness of the film.

The correction for cam mis-shaping was +0.06 kcm^{-1}.

Run number	Block temp. (°C)	E(2) (kcm^{-1})
1244	15	27.73
1245	37	27.65
1246	47	27.56
1247	68	27.57
1248	88	27.54
1249	114	27.54
1250	140	27.54
1251	166	27.54

POTASSIUM NITRITE (Sample 1) (continued).

Run number	Block temp. (°C)	E(2) (kcm^{-1})
1252	193	27.54
1253	220	27.54
1254	247	27.54
1255	275	27.55
1256	304	27.53
1257	337	27.59
1258	382	27.57
1259	389	27.54
1260	16	27.73
1262	41	27.64
1263	41	27.65
1264	44	27.58
1265	44	27.56
1266	44	27.54
1268	430	27.70
1270	430	27.59
1271	430	27.63
1272	430	27.63
1273	430	27.57

POTASSIUM NITRITE (Sample 1) (continued) Runs 1244 - 1266.

Resolution 3; scan-speed 3; damping 2; chart-speed 80"/hour; transmission scale 0 - 100%.

Run number	Block temp. (^{o}C)	E(t=10%) (kcm^{-1})	E(t=50%) (kcm^{-1})
1244	15	39.94	37.60
1245	37	40.05	38.52
1246	47	40.30	39.68
1247	68	40.27	39.60
1248	88	40.22	39.53
1249	114	40.13	39.46
1250	140	40.02	39.30
1251	166	39.90	39.17
1252	193	39.82	39.02
1253	220	39.69	38.80
1254	247	39.53	38.62
1255	275	39.38	38.43
1256	304	39.25	38.28
1257	337	39.02	38.00
1258	382	38.77	37.63
1259	389	38.69	37.58
1260	16	40.20	39.0
1262	41	40.18	39.37
1263	41	40.27	39.44
1265	44	40.34	39.70
1266	44	40.30	39.72

POTASSIUM NITRITE. (Sample 2) Runs 1281 - 1336.

Resolution 3; scan-speed 3; damping 2; chart speed 80"/hour; transmission scale 0 - 10%.

The sample was made up from zone-refined material (see page 104). The correction for cam mis-shaping was +0.06 kcm^{-1}.

Run number	Block temp. (°C)	E(2) (kcm^{-1})	Run number	Block temp. (°C)	E(2) (kcm^{-1})
1281	10	27.62	1308	126	27.55
1282	10	27.63	1310	152	27.56
1284	15	27.63	1312	180	27.57
1286	20	27.63	1314	201	27.56
1288	29	27.62	1316	230	27.57
1290	35	27.63	1318	260	27.57
1292	40	27.63	1320	290	27.58
1294	44	27.63	1321	290	27.54
1296	49	27.57	1323	310	27.54
1298	54	27.57	1326	325	27.55
1300	59	27.57	1328	351	27.56
1302	70	27.58	1330	362	27.56
1304	79	27.51	1332	375	27.56
1306	100	27.57	1334	380	27.56
			1336	380	27.52

POTASSIUM NITRITE (Sample 2) continued)

Runs 1280 - 1335.

Resolution 3; scan speed 3; damping 2; chart speed 80"/hour; transmission scale 0 - 100%.

In the table, E(t = 10%) and E(T = 50%) are the frequencies on the low-energy edge of the strong band for which the transmission of the sample is 10% and 50% respectively.

Run number	Block temp. (°C)	E(t=10%) (kcm^{-1})	E(t=50%) (kcm^{-1})
1280	10	40.05	39.26
1283	15	40.03	39.27
1285	20	40.00	39.23
1287	29	39.98	39.25
1289	35	39.98	39.26
1291	40	39.96	39.20
1293	44	39.92	39.20
1295	49	39.93	39.29
1297	54	39.91	39.28

POTASSIUM NITRITE (Sample 2) (continued).

Run number	Block temp. (^{o}C)	E(t=10%) (kcm^{-1})	E(t=50%) (kcm^{-1})
1299	59	39.89	39.27
1301	69	39.86	39.21
1303	80	39.81	39.12
1305	100	39.73	39.03
1307	126	39.65	38.87
1309	152	39.50	38.68
1311	180	39.40	38.52
1313	201	39.26	38.37
1315	230	39.10	38.15
1317	260	38.88	37.88
1319	290	38.71	37.66
1322	310	38.53	37.45
1324	325	38.43	37.28
1327	351	38.29	37.10
1329	362	38.20	36.96
1331	375	38.08	36.77
1333	380	38.08	36.77
1335	380	38.04	36.79

Offprinted from the *Discussions of The Faraday Society*, 1962, No. 32

STRUCTURAL INFLUENCES ON ION MIGRATION IN CRYSTALS AND MELTS

By B. Cleaver, Elizabeth Rhodes and A. R. Ubbelohde
Dept. of Chemical Engineering and Chemical Technology, Imperial College of Science and Technology, London, S.W.7.

Received 19*th June*, 1961

Divalent cations incorporated in crystals of uni-univalent halides increase the electrical conductivity by creating additional cation vacancies (the Wagner effect). A similar effect has now been observed experimentally in crystalline nitrates.

In contrast with the Wagner effect, similar additions to ionic melts decrease the electrical conductivity. Published evidence for halides and fresh experimental evidence for nitrates permits estimates of changes in the activation parameters for ion migration, when divalent cations are added to uni-univalent molten salts. Such melts are normally much more compressible than the corresponding crystals; the greater electrostatic forces associated with the higher charges appear to cause a shrinkage which hinders ion migration.

Processes of easy migration in ionic crystals are generally thought to be associated with various kinds of crystal defects, at which the conditions controlling a hop from one crystal site to the next are more favourable than at ideal lattice sites. Various kinds of crystal defects may help ion migration, such as single lattice vacancies (Schottky defects), paired anion+cation vacancies, or ions located at interstitial lattice sites (Frenkel defects). Cooperative crystal defects such as dislocations may also provide favourable migration paths.

The Wagner effect provides a means of studying the dependence of migration processes on the number of vacant lattice sites. Incorporation of small concentrations of divalent cations in solid solutions in uni-univalent crystal halides, in favourable cases, merely creates an equivalent number of cation vacancies in the lattice, so that the whole assembly remains electrically neutral. Apparently the structure is kept rigid by the repulsion forces between ions; at the dilutions studied, any shrinkage of the crystal is restricted to values predicted by ion contact radii and Vegard's law.

In the Wagner effect, the increase in number of cation vacancies greatly outweighs any change of migration parameters due to lattice shrinkage, and large increases are observed in ion conductance, for example, in lithium halides [2] and sodium chloride.[3]

Two possible extensions of the Wagner effect are investigated in the present paper.

(i) With crystals containing non-spherical polyatomic ions the different local interactions might impede the production of vacancies; Wagner effects might, in fact, only appear in crystals with ions of inert-gas type. This has been tested for the system $KNO_3+Ca(NO_3)_2$. A marked increase in conductivity is found on introducing calcium ions in solid solution in crystalline KNO_3, as is detailed below. Because the ionic radii of K^+(1·33 Å) and Ba^{2+}(1·35 Å) are closely matched, it would have been preferable to make these experiments with solid solutions of barium ions in KNO_3 but other work indicated that the solubility of $Ba(NO_3)_2$ in KNO_3 is inconveniently low.[4,5] Ca^{2+} ions have adequate solubility and were used in the present research.

(ii) According to the quasi-crystalline model for the structure of ionic melts, these can be regarded as formed by expanding the lattice of the crystal somewhat on melting and then introducing various types of positional disorder.[6-8] A

question of interest is whether melts show Wagner effects similar to those of the crystals from which they are formed. This has been tested by measuring ion conductances for mixtures of melts of KNO_3 with $Ba(NO_3)_2$. These were chosen to give a closer match of cation radii than with the systems $KNO_3+Ca(NO_3)_2$ used for the solids. Nitrate melts containing Ba^{2+} ions are also chemically stable over wider ranges of composition and temperature than melts containing Ca^{2+} ions. This allows determinations of other parameters of importance in elucidating the structure of ionic melts, such as equivalent volumes and gas solubilities in mixtures.[9,10] Existing data have also been used to calculate conductances of mixtures of melts of NaCl and $CaCl_2$.[11]

Both halide and nitrate melts show a diminution of ionic conductance when divalent cations replace monovalent cations. The bearing of this and other information about uni/divalent mixtures, on theories of structures of melts, is discussed.

EXPERIMENTAL

WAGNER EFFECT IN CRYSTALLINE POTASSIUM NITRATE

Using polycrystalline solids, and methods of measurement previously described [12] the d.c. electrical conductivity of pure KNO_3 was compared, over a range of temperatures, with that of KNO_3 containing up to 0·01 mole fraction of $Ca(NO_3)_2$.

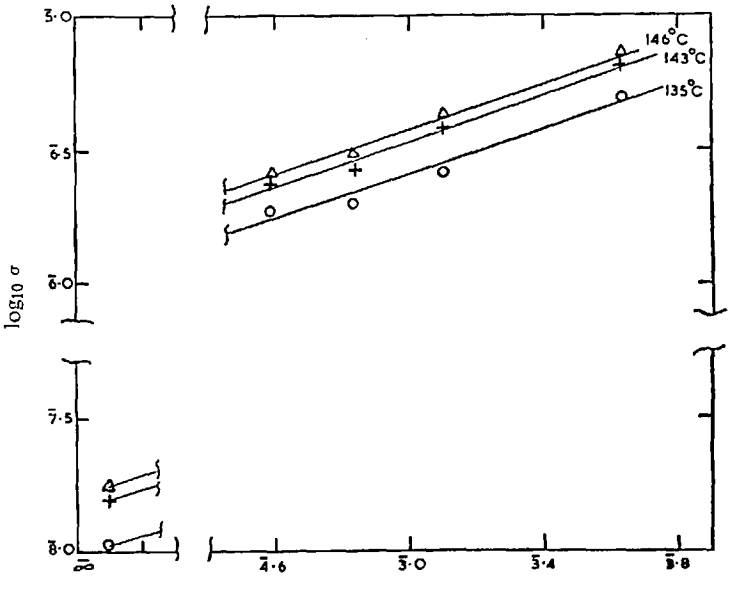


FIG. 1.—Increase in conductivity of solid KNO_3 on adding $Ca(NO_3)_2$.
Curves drawn for constant temperatures: △, 146°C; +, 143°C; ○, 135°C.

A.c. conductances at 1592 c/sec were determined using a Wayne-Kerr Universal bridge. For pure KNO_3 values obtained were found to be the same as by d.c. methods. For the solid solutions, very much higher conductances were obtained using a.c.; the origin of this has not yet been elucidated.

KNO_3 (Judex A.R. grade) containing less than 0·001 % of cation or anion impurities was carefully dried by the thermal shock technique.[13] $Ca(NO_3)_2$ (anhydrous, Judex lab. reagent) was dried at 250°C for ten days; care was taken to ensure that it remained dry in making up the mixtures. These were prepared in the molten state under an atmosphere of dry nitrogen and were allowed to solidify slowly in the conductivity cell.

Measurements were made with the cell in a molten-salt thermostat (±0·10°C) above 160°C and either an oil bath (±0·10°C) or a solid aluminium block furnace (±1°C) below 160°C. Results for the electrical conductance of the solids are plotted in fig. 1 for various temperatures below the eutectic, in order to make any Wagner effects evident where there can be no possible interference from traces of melt. Fig. 2 shows the results for the polycrystalline solids over a much wider range of temperatures, and in fact does not

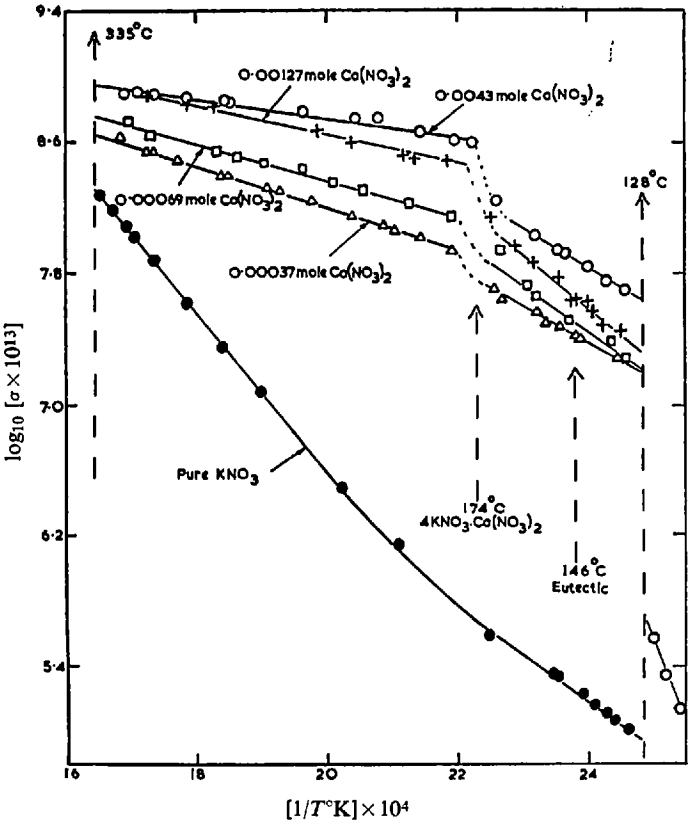


FIG. 2.—Conductivities of pure KNO_3 and solid solutions of $Ca(NO_3)_2$ in KNO_3.

Pure KNO_3, ●. △, 0·00037; □, 0,00069; +, 0·00127; ○, 0·0043, mole fractions of $Ca(NO_3)_2$.

335°C freezing point of pure KNO_3; 174°C incongruent melting point of compound $4\,KNO_3\,.\,Ca(NO_3)_2$; 146°C eutectic temperature; 128°C transition temperature of pure KNO_3.

indicate any break at the eutectic temperature (146°C) showing that at these low concentrations of $Ca(NO_3)_2$, melt formation can be neglected. Fig. 2 also shows breaks in the conductance of the polycrystalline solids at the transition temperature of pure KNO_3 (128°C) and at the non-congruent melting point of the crystal compound $4\,KNO_3\,.\,Ca(NO_3)_2$ (174°C), beyond which a new crystal structure with its own conductance parameters appears in the solid.

Determinations of the freezing-point depression of KNO_3 by $Ca(NO_3)_2$ show the incongruently melting compound $Ca(NO_3)_2\,.\,4\,KNO_3$ at 174° and a eutectic temperature at 146°C (fig. 3).[14] Conductivity measurements suggest that the compound may also exist in the melt.[15] We have made cryoscopic measurements of high precision near the freezing point of pure KNO_3,[16] in order to evaluate the extent of solid solution of calcium nitrate. This appears to be small, since the ratio i of theoretical to observed freezing-point

depressions is fractionally greater than unity only for mixtures containing less than 0·003 mole fraction of $Ca(NO_3)_2$. In table 1, i is calculated [9] using a value of 2·57 kcal/mole for the latent heat of fusion of KNO_3.[17]

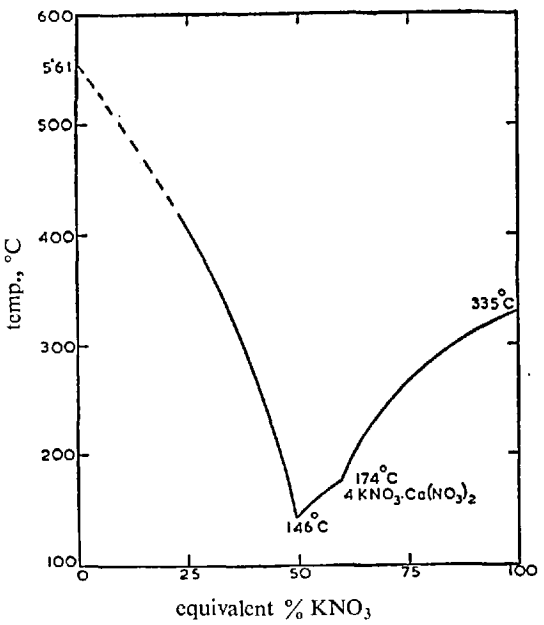


FIG. 3.—Phase diagram of KNO_3+$Ca(NO_3)_2$ mixtures (after Protsenko and Belova).

TABLE 1.—FREEZING POINTS (°K) OF KNO_3 WITH ADDED $Ca(NO_3)_2$

mole fraction $Ca(NO_3)_2$	f.p. °K	i
0·00000	608·25	—
0·00086	608·08	1·00021
0·00246	607·55	1·00006
0·00479	606·78	0·99969
0·00692	606·18	0·99973
0·00893	605·45	0·99914
0·01122	604·65	0·99948
0·01330	603·95	0·99836
0·01627	602·90	0·99770
0·01879	602·00	0·99693

CONDUCTANCES OF MIXTURES OF MOLTEN NITRATES

Mixtures of KNO_3 with $Ba(NO_3)_2$ were studied at 1592 c/sec using the a.c. Wayne-Kerr bridge. Our own investigations [18] and other work [19] show that polarization effects can be neglected (less than 0·5 %) and that any variation of conductance of the melt is likewise negligible over large frequency ranges. The results can conveniently be illustrated by plotting the difference function log (Λ_x/Λ) against $1/T$°K, where Λ_x is the equivalent conductance of the melt for an equivalent fraction x of barium nitrate and Λ is the equivalent conductance of KNO_3 at the same temperature (fig. 4). To determine these ratios, values of Λx and Λ were based on the lines of closest fit calculated from the data obtained for pure KNO_3 and the mixtures, using the equation

$$\Lambda_x = (\Lambda_0)_x \exp\left[-(E_\Lambda)_x/RT\right]. \qquad (1)$$

The equivalent conductances were obtained from the measured specific conductances using previously determined equivalent volumes of the mixtures.[9] Table 2 records the parameters $(\Lambda_0)_x$ and $(E_\Lambda)_x$ corresponding to the lines of closest fit for eqn. (1); also

included are the parameters $(\sigma_0)_x$ and $(E_\sigma)_x$ for specific conductance. When two ranges of temperature are given, this indicates a slight curvature in the experimental plot. Lines of closest fit were calculated separately for the temperature ranges quoted. Fig. 5 illustrates the match between eqn. (1) and the experimental points.

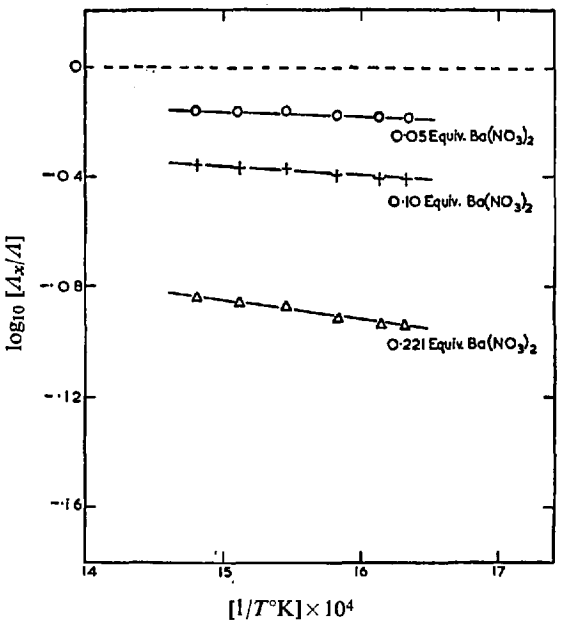


FIG. 4.—Equivalent conductance ratios for molten mixtures of $KNO_3+Ba(NO_3)_2$. O, 0·05; +, 0·10; and △, 0·221 equivalent fractions of $Ba(NO_3)_2$.

TABLE 2.—PARAMETERS FOR THE CONDUCTANCE OF $KNO_3+Ba(NO_3)_2$ MELTS

x (equivalent fraction of $Ba(NO_3)_2$	temp. range °C	$(E_\sigma)_x$ kcal/mole	$(\sigma_0)_x$ ohm^{-1} cm^{-1}	$(E_\Lambda)_x$ kcal/mole	$(\Lambda_0)_x$ ohm^{-1} cm^2
	340-389	3·61±0·03	12·5±0·3	4·00	924
	374-434	3·38±0·03	10·4±0·3	3·75	762
0·05	332-389	3·72±0·03	13·1±0·3	4·05	927
	374-434	3·49±0·02	10·9±0·3	3·85	801
0·01	332-389	3·80±0·03	13·4±0·3	4·12	927
	374-434	3·64±0·01	11·7±0·3	4·00	844
0·221	340-403	3·92±0·03	13·4±0·3	4·24	904

CONDUCTANCES OF MIXTURES OF MOLTEN CHLORIDES

Published results for melts of mixed chlorides suitable for comparison with the Wagner effects in the solids are not abundantly available. Fig. 6 shows a plot of the function $\log(\Lambda_x/\Lambda)$ against $1/T$°K for mixtures of $CaCl_2$ with NaCl.[11]

DISCUSSION

THE WAGNER EFFECT

The Wagner effect, the occurrence of which is well known for halides, has now been demonstrated for solid nitrates. Fig. 1 illustrates the large increases in conductance observed when Ca^{2+} is incorporated into KNO_3, at three different temperatures. The trends in the slopes of the plots in fig. 2 and the breaks at the transition to a non-congruent crystal compound, complicate the interpretation of the Wagner effect with solid nitrates. Some of the features illustrated may be due

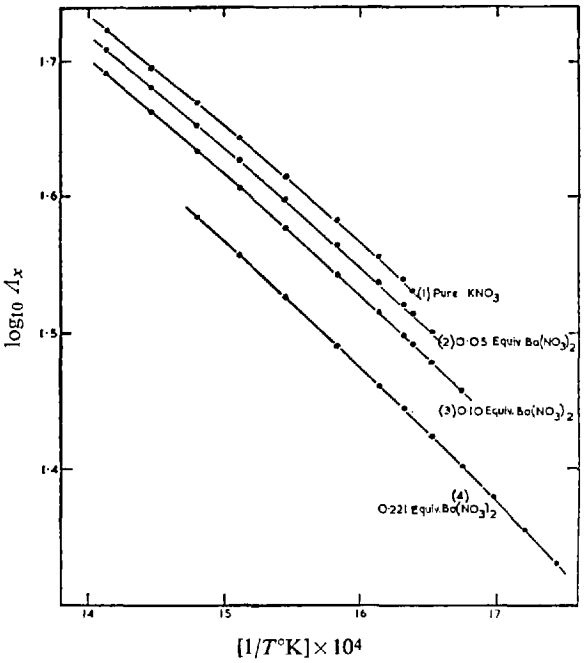


FIG. 5.—Equivalent conductances of $KNO_3+Ba(NO_3)_2$ melts.

(1) Pure KNO_3; (2) 0·5; (3) 0·10; (4) 0·221 equivalent fractions of $Ba(NO_3)_2$. Experimental error is equal to radius of small circles.

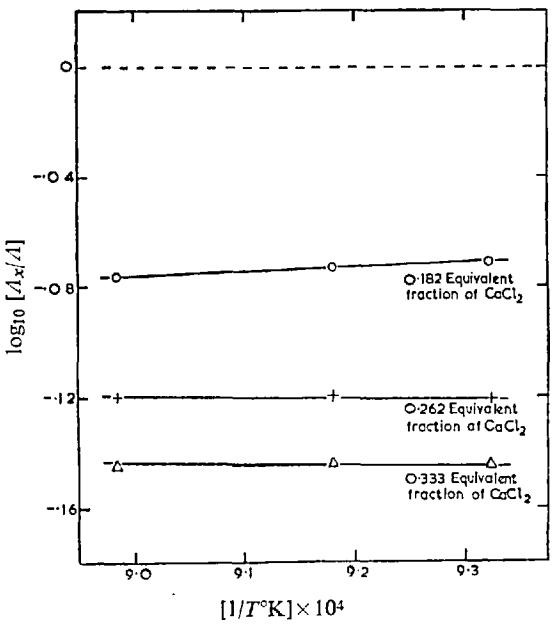


FIG. 6.—Equivalent conductance ratios for molten mixtures of $NaCl+CaCl_2$.

O, 0·182; +, 0·262; △, 0·333 equivalent fractions of $CaCl_2$.

to special modes of interaction between the non-spherical nitrate anion and an adjacent cation hole. Further research on Wagner effects with other non-spherical ions is necessary to test this possibility.

Because the extent of solid solution is small, it is not possible to estimate the concentration of Ca^{2+} ions actually incorporated in the crystal lattice of KNO_3. This will obviously increase as the proportion of $Ca(NO_3)_2$ added increases, and accounts for the rise in conductance near the origin in fig. 1. No independent calculation of the number of holes created seems feasible at present.

CONDUCTANCES OF MIXED MELTS

Both NaCl and KNO_3 show decreases in conductance when divalent cations are incorporated in the melts. This can probably be attributed to the electrostrictive shrinkage of free volume of the uni-univalent melts as the concentration of divalent cations increases. It is noteworthy that the proportional decreases in Λ_x are about the same for NaCl as for KNO_3, whilst expansions in volume on melting [20] are considerably greater for the salt with spherical ions ($\Delta V_f/V_s = 25$ % for NaCl and 1 % for KNO_3).

The electrostrictive effect of divalent cations on a uni-univalent melt should be comparable with the effect of external pressure. Direct measurements of changes of conductance of pure melts under external pressure would provide useful confirmation of this model for comparison with the present findings, but are not yet available. An estimate of the magnitude of this effect can be obtained by comparing the compressibilities of the crystal and the melt. Values of the isothermal compressibilities of sodium and potassium chlorides and nitrates in the crystal [21,22] and the melt,[23] extrapolated to the freezing point, are given in table 3.

TABLE 3.—ISOTHERMAL COMPRESSIBILITIES ($\beta_T \times 10^{12}$)

salt	NaCl	KCl	$NaNO_3$	KNO_3
freezing point (°C)	800	770	308	335
compressibility of solid (cm^2 $dynes^{-1}$)	5·0	6·3	4·2	—
compressibility of liquid (cm^2 $dynes^{-1}$)	28·7	36·2	18	20
β_T (liquid)/β_T (solid)	5·75	5·75	4·3	—

Some refinements to the above model are feasible with melts of $KNO_3 + Ba(NO_3)_2$ since our results are available in detail for this system. The absolute rate equation for equivalent conductances can be written as

$$\Lambda = 5{\cdot}18 \times 10^{18}(D+2)zd_i^2 \exp(\Delta S^{\ddagger}/R) \exp(-\Delta H^{\ddagger}/RT) \qquad (2)$$

Methods of calculating $D(\sim 3)$ and d_i are as discussed by Yaffe and Van Artsdalen.[24] The mean charge z was taken as

$$z = \sum n_i z_i / \sum n_i.$$

Table 4 shows trends in the parameters Λ_0, $\Delta H^{\ddagger}$, $\Delta S^{\ddagger}$ and $\Delta G^{\ddagger}$ when $Ba(NO_3)_2$ is added to liquid KNO_3.

TABLE 4.—CONDUCTANCE PARAMETERS FOR $KNO_3 + Ba(NO_3)_2$ MELTS AT 350°C

equivalent fraction $Ba(NO_3)_2$, x	0	0·05	0·1	0·221
molar volume (ml) [9]	54·310	53·711	53·105	51·656
d_i (Å)	3·459	3·427	3·400	3·337
Λ_0 (ohm^{-1} cm^2)	924	927	927	904
$\Delta H^{\ddagger}$ (kcal/mole)	+4·00	+4·05	+4·12	+4·24
$\Delta S^{\ddagger}$ (cal/mole deg.)	−6·91	−6·99	−7·01	−7·11
$\Delta G^{\ddagger}$ (kcal/mole)	+8·31	+8·40	+8·48	+8·78

Plots (not shown) of the activation parameters $\Delta G^{\ddagger}$, $\Delta S^{\ddagger}$ and $\Delta H^{\ddagger}$ indicate approximately linear increases of all three as the electrostriction increases.

The conclusion is that no vestiges of any creation of holes are perceptible in these melts, when divalent cations are added. In uni-univalent ionic melts, effects of incorporating divalent cations thus appear to be much less localized than in the corresponding crystals. A similar conclusion can be reached from measurements of the solubility of water vapour in molten nitrates,[10] and from changes in volume of mixed nitrate melts.[9] It points to an obvious limitation in the usefulness of incorporating strictly local effects into any quasi-crystalline model for ionic melts.

1 Koch and Wagner, *Z. physik. Chem. B*, 1937, **38**, 295.
2 Haven, *Rec. trav. chim.*, 1950, **69**, 1259, 1471, 1505.
3 Van Bueren, *Imperfections in Crystals* (North-Holland, Amsterdam, 1960), p. 542.
4 Protsenko and Bergman, *Zhur. Obshchei Khim.*, 1951, **21**, 1580.
5 Protsenko and Malakhova, *Zhur. Neorg. Khim.*, 1957, **2**, 2145.
6 Frenkel, *Kinetic Theory of Liquids* (Clarendon Press, Oxford, 1946, 2nd ed.).
7 Ubbelohde, *Quart. Rev.*, 1950, **4**, 380.
8 Blander, *J. Physic. Chem.*, 1959, **63**, 1262.
9 Cleaver, Rhodes and Ubbelohde, *Proc. Roy. Soc. A*, 1961, ~~in press.~~
10 Frame, Rhodes and Ubbelohde, *Trans. Faraday Soc.*, 1961, ~~in press.~~
11 Vereshchetina and Luzhnaya, *Akad. Nauk S.S.S.R., Izvest. Sekt. Fiz. Khim. Anal.*, 1954, **25**, 188.
12 Frame, Rhodes and Ubbelohde, *Trans. Faraday Soc.*, 1959, **55**, 2039.
13 Rhodes and Ubbelohde, *Proc. Roy. Soc. A*, 1959, **251**, 156.
14 Protsenko and Belova, *Zhur. Neorg. Khim.*, 1957, **2**, 2617.
15 Luzhnaya, Evseeva, Vereschchetina, *Zhur. Neorg. Khim.*, 1956, **1**, 1490.
16 Rhodes and Ubbelohde, *Trans. Faraday Soc.*, 1959, **55**, 1705.
17 Goodwin and Kalmus, *Physic. Rev.*, 1909, **28**, 1.
18 Plester, Rogers and Ubbelohde, *Proc. Roy. Soc. A*, 1956, **235**, 469.
19 Murphy and Wetmore, *Can. J. Chem.*, 1959, **37**, 1397.
20 Ubbelohde, *Proc. Chem. Soc.*, 1960, 332.
21 Born and Huang, *Dynamical Theory of Crystal Lattices* (Clarendon Press, Oxford, 1954), p. 52.
22 *Int. Crit. Tables* (McGraw-Hill, New York), 1928, **3**, 50.
23 Bockris and Richards, *Proc. Roy. Soc. A*, 1957, **241**, 44.
24 Van Artsdalen and Yaffe, *J. Physic. Chem.*, 1955, **59**, 118.

PRINTED IN GREAT BRITAIN AT
THE UNIVERSITY PRESS
ABERDEEN

Offprinted from the *Discussions of The Faraday Society*, 1962, No. 32

CHANGES OF ULTRA-VIOLET ABSORPTION SPECTRA ON MELTING IONIC CRYSTALS

CHANGES OF ULTRA-VIOLET ABSORPTION SPECTRA ON MELTING IONIC CRYSTALS

By B. Cleaver, Elizabeth Rhodes and A. R. Ubbelohde

Dept. of Chemical Engineering and Chemical Technology, Imperial College of Science and Technology, London, S.W.7.

Received 4th July, 1961

The ultra-violet spectra of crystalline and molten nitrates of Na, K, Rb and Cs and of molten mixtures of KNO_3 with $Ba(NO_3)_2$ have been recorded at temperatures between 20°C and 450°C, over the frequency range 54,000 cm^{-1} to 27,000 cm^{-1}. The frequency of maximum absorption decreases with increasing temperature in temperature ranges well away from phase-changes; this shift is found to match the thermal expansion of the crystals quite closely in cases where this is known. Abrupt shifts in the absorption maxima are found at transition temperatures. The results are interpreted in terms of a model for the excited state. It is concluded that, despite any increase in volume which occurs when nitrates melt, the closest anion-cation distances decrease when melting occurs. This distance also decreases when monovalent cations in a melt are replaced by divalent ions of the same repulsion radius.

Ultra-violet spectra of solid and molten nitrates of the alkali metals are essentially similar in the range 54,000 cm^{-1} to 27,000 cm^{-1}. A strong, broad peak is found with a maximum at 48,000-47,000 cm^{-1}, whose absorption coefficient in units of 10^3 cm^{-1} is about 0·7 for $LiNO_3$, 6·0 for $NaNO_3$ and 2·3 for KNO_3.[1] A second, weaker peak is found in the range 34,000-32,000 cm^{-1}. Both peaks are likewise observed in aqueous solutions of nitrates [2] and are generally attributed to excitation of the nitrate ion.[3-5]

The major absorption peak appears to correspond with that observed for crystalline alkali halides [6] in the range 64,000-46,000 cm^{-1} and for molten LiI at about 43,000 cm^{-1}.[1] With nitrates, the weaker peak seems plausibly attributed to a transition forbidden by selection rules, becoming permitted due to perturbation of the nitrate ion by the field of the cations. Thus, the peak is strongest for $LiNO_3$ (absorption coefficient $0{\cdot}9 \times 10^3$ cm^{-1}) [1] and becomes weaker as the cation radius increases. The first absorption band corresponds to the excitation of an electron from a π orbital to a strongly antibonding orbital and the second to excitation from a weakly antibonding to a strongly antibonding orbital.[5] In both excited states, the orbital of the excited electron is at the periphery of the nitrate ion and overlaps to some extent the first co-ordination shell of cations.

Since the excited electron is remote from the nitrate ion from which it originated, it may be regarded as located in a spherical well approximately characterized by the surrounding shell of nearest cations.[7] On the basis of various simplifying assumptions, the energy E for excitation at peak absorption is given by

$$E = E_0 + h^2/8mr_0^2, \qquad (1)$$

where E_0 is the ionization potential of the anion, h is Planck's constant and m the mass of the electron. r_0 is the radius of the potential well retaining the excited electron, and is a parameter of particular interest in correlations between absorption bands and changes of structure of condensed ionic systems as their temperature changes.

Eqn. (1) leads to the derivative

$$dE/dT = -(h^2/4mr_0^3)dr_0/dT. \quad (2)$$

If $(3/r_0)(dr_0/dT)$ may be equated with the cubic coefficient of expansion γ of the ionic assembly, then

$$dE/dT = -(h^2/12mr_0^2)\gamma. \quad (3)$$

The following experimental results for various nitrates in the range 20-450°C show that changes in the optical spectra frequently give quite good correlations with thermal expansions, provided these are observed well away from transitions or melting points. However, at both types of transition, abrupt shifts in E are found which do not correspond with volume changes. These findings can be used to throw light on the nearest neighbour structures of ionic melts. Absorption spectra of mixed melts of KNO_3 with $Ba(NO_3)_2$ have also been recorded and have been correlated with a diversity of thermodynamic data now available for such systems.

EXPERIMENTAL

MATERIALS

Sodium and potassium nitrates (Judactan A.R. containing less than 0·003 % of anion and 0·002 % of cation impurities) and barium nitrate (Judex A.R.) were used without further purification apart from drying. Rubidium nitrate (Johnson, Matthey & Co. 99·9 %) and caesium nitrate (Judex Laboratory Reagent 99·8 %) were each recrystallized once from distilled water. All salts were dried by the thermal shock technique [1] and were stored over P_2O_5 in a desiccator prior to use.

Absorption spectra of the salts, as polycrystalline films and as melts, were recorded at intervals of about 15 deg. from room temperature to 450°C. In the neighbourhood of thermodynamic transitions, spectra were recorded at intervals of between 1 and 2 deg. For this purpose, a Unicam S.P. 700 recording spectrophotometer was used in the frequency range quoted above. Films of salt varying in thickness between 4 μ and 140 μ were held between two flat plates of Spectrosil quartz. For the thicker films, two spacers of Pt/Ir foil helped to keep these plates apart. This assembly was supported in a stainless steel holder, maintained at the desired temperature by means of a thermostat illustrated in fig. 1. A similar compensating unit was maintained at the same temperature in the reference compartment of the spectrophotometer, without any salt between the two quartz plates. Each unit was surrounded by a water-cooled jacket which, even with the thermostats at 450°C, did not permit a rise of more than 2°C in the surrounding framework of the spectrophotometer. Electronic control of each of the two thermostats maintained the block temperatures to within ±0·01°C. However, there was always a temperature gradient between the edge and the centre of the sample, where a clear optical path had to be provided for passage of the ultra-violet beam. This difference was measured for various temperatures and was about 2°C at 200°C, and 5°C at 450°C (the centre being cooler). Temperatures were measured by means of a Johnson Matthey Pallador thermocouple calibrated by conventional means.

To make up a specimen, the two Spectrosil plates were heated on a small electric hotplate, above the melting point of the salt to be used. A few crystals of salt were scattered on one plate, melted, and covered with the second plate. The assembly was allowed to cool, and after removing salt extruded at the edges the thickness of salt film was determined by weighing.

Three different scanning procedures were used to obtain all the information required about the spectra.

(i) Using a thin sample (about 5 μ), the operating frequency of the spectrophotometer was set at a value about the middle of the steeply rising edge of the strong absorption peak between 38,000 to 40,000 cm^{-1}. The recording chart was set in motion, and the temperature of the thermostat was slowly raised from 20°C to above the melting point. It was found that the percentage absorption rose steadily, due to a shift of the absorption edge towards longer wave lengths. An abrupt change was generally apparent on traversing a solid-solid or solid-liquid transformation; this occurred in the reverse direction on cooling the assembly gradually. By reducing the rate of temperature change to about 1 deg./5 min, transformation temperatures could be located to within 2 deg., from the abrupt changes observed.

(ii) Thicker specimens were required to obtain adequate absorption spectra in the region 38-27,000 cm^{-1}. Thickness was adjusted by trial and error, until the maximum absorption was between 50 and 80 %. Tests with films of $NaNO_3$ ranging in thickness from 24 μ to 65 μ verified that the position estimated for the maximum absorption, $E(2)$, did not depend on the thickness. This made it unnecessary to take special precautions against possible changes in film thickness at the melting point. Normally, $E(2)$ was evaluated from experiments with a rising sequence of temperatures.

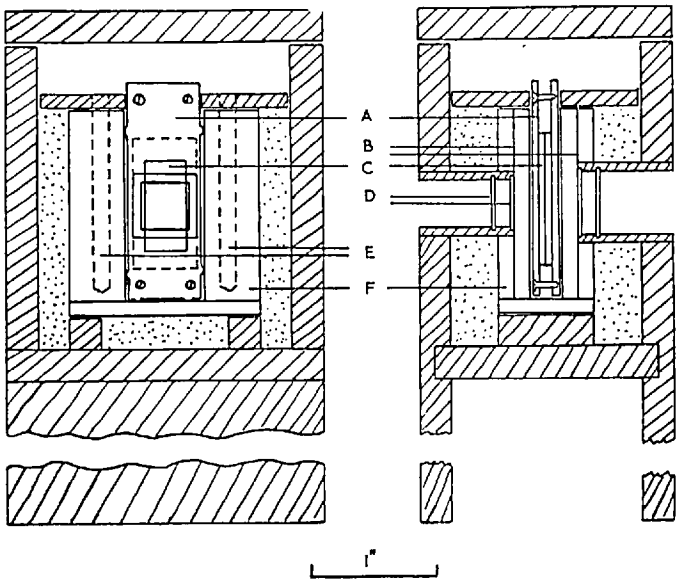


FIG. 1.—U.-v. absorption cell and thermostat.

A, stainless-steel cell holder; B, heaters; C, quartz cell; D, quartz windows; E, resistance thermometers and thermocouple; F, copper block. Shaded areas represent thermal insulation of Brelite and Sindanyo sheet.

(iii) Even with samples as little as 5 μ thick, it was not possible to define directly the maximum of the strong absorption peak at about 47,000 cm^{-1}, as practically all the radiation was absorbed in the range 51,000-40,000 cm^{-1}. Chords were therefore drawn for percentages of transmission between 10 and 20 %, and the mean energy for 100 % absorption was evaluated by extrapolating a line joining the midpoints of these chords to 100 % absorption. Tests showed that the values of $E(1)$ obtained in this way were dependent on the thickness of the film used. Thus, with $NaNO_3$, $E(1)$ was 47,180 cm^{-1} for a film 24 μ thick and 46,830 cm^{-1} for a film 65 μ thick.

Because of this effect, the following technique was adopted to ensure that $E(1)$ was measured for solid and melt films of the same thickness. The sample was placed in the spectrophotometer cell, and heated a few degrees above its melting point. The frequency was set to a value on the steep edge of the first band (38,000-40,000 cm^{-1}), and the sample was frozen and re-melted several times until the % absorption of the melt reached a constant value. Three or four spectra were then recorded for the melt. The sample was immediately cooled below the melting point, and spectra were obtained for the solid.

RESULTS

Fig. 2-4 illustrate some characteristic absorption spectra. Detailed plots of the positions of absorption maxima as a function of temperature are illustrated in fig. 5-8, for nitrates of the alkali metals sodium, potassium, rubidium and caesium.

Fig. 9 illustrates changes in $E(2)$ for various molten mixtures of KNO_3 with $Ba(NO_3)_2$. Table 1 gives the values of $E(2)$ at a number of temperatures for the alkali nitrates; also included are the volume changes on fusion.[8]

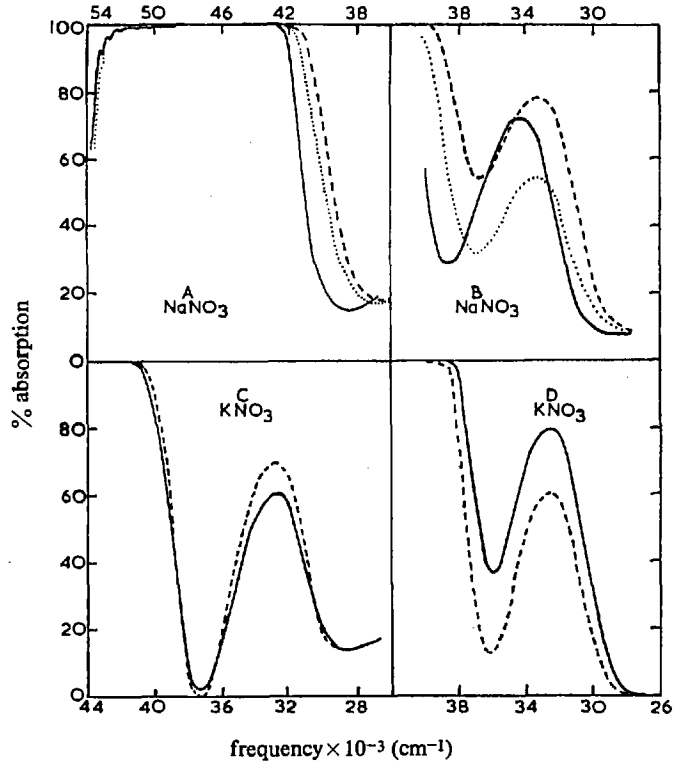


FIG. 2.—Absorption spectra of $NaNO_3$ and KNO_3.

(A) $NaNO_3$ 1st peak, — 40°C, - - - 305°C, ... 308°C (melt).
(B) $NaNO_3$ 2nd peak, — 40°C, - - - 304°C, ... 308°C (melt).
(C) KNO_3 2nd peak, — 127°C (orthorhombic), - - - 130°C (rhombohedral).
(D) KNO_3 2nd peak, — 333°C (solid), - - - 338°C (melt).

TABLE 1.—FREQUENCIES $\times 10^{-3}$ (cm^{-1}) OF ABSORPTION MAXIMA $E(2)$ FOR ALKALI NITRATES

cation	m.p. (°C)	$E(2) \times 10^{-3}$ (cm^{-1}) solid, at 20°C	solid, at 5° below m.p.	melt, 5° above m.p.	$\Delta V_f/V_s$ %
Na^+	308	34·25	33·28	33·46	11
K^+	334	32·88	32·50	32·56	3
Rb^+	310	32·79	32·16	32·48	0
Cs^+	406	32·70	31·97	32·15	12

DISCUSSION

CORRELATIONS BETWEEN SHIFTS OF ABSORPTION MAXIMA AND THE THERMAL EXPANSION OF CRYSTALS AND MELTS

According to eqn. (2) and (3) derived from the approximate theory, a close correlation may be expected between the shift of maximum absorption with temperature and the thermal expansion of the crystals. One way of testing this is

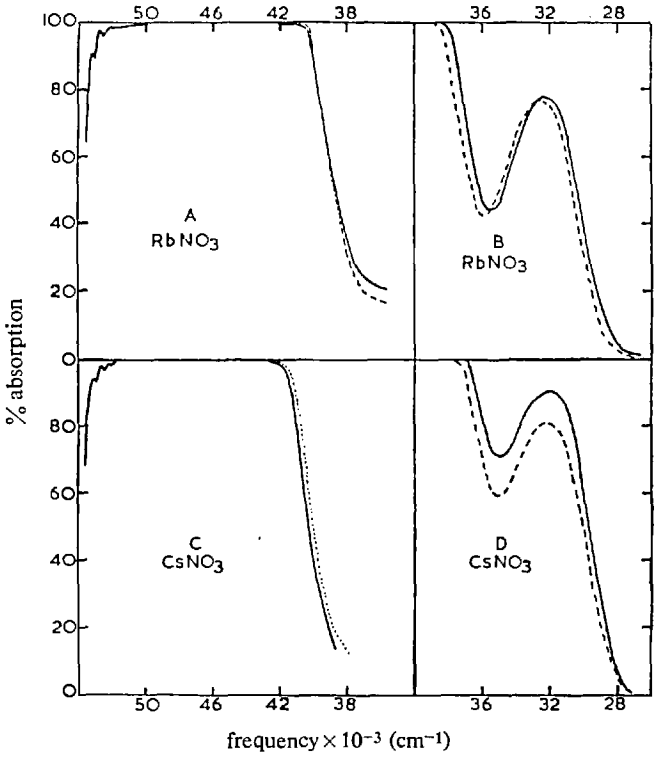


FIG. 3.—Absorption spectra of $RbNO_3$ and $CsNO_3$.
(A) $RbNO_3$ 1st peak, — 281°C, - - - 284°C (unknown crystal transition).
(B) $RbNO_3$ 2nd peak, — 308°C, - - - 313°C (melt).
(C) $CsNO_3$ 1st peak, — 404°C, - - - 408°C (melt).
(D) $CsNO_3$ 2nd peak, — 152°C (hexagonal), - - - 154°C (cubic).

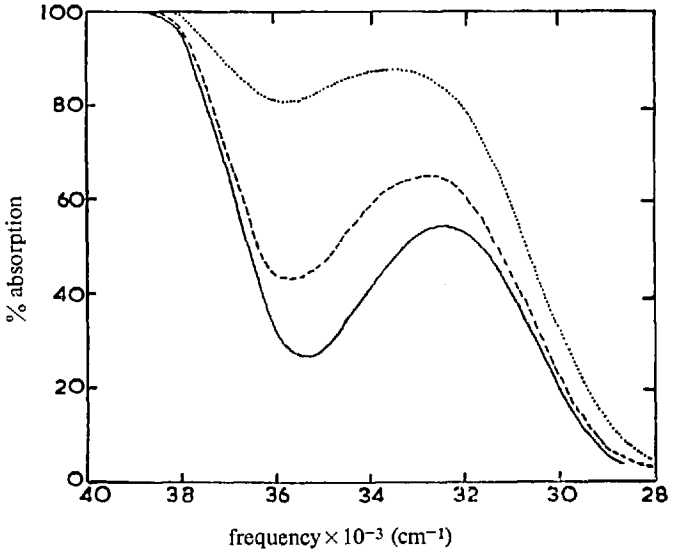


FIG. 4.—Absorption spectra of $KNO_3+Ba(NO_3)_2$ melts at 440°C.
— pure KNO_3; - - - 20 equiv. % $Ba(NO_3)_2$; . . . . 50 equiv. % $Ba(NO_3)_2$.

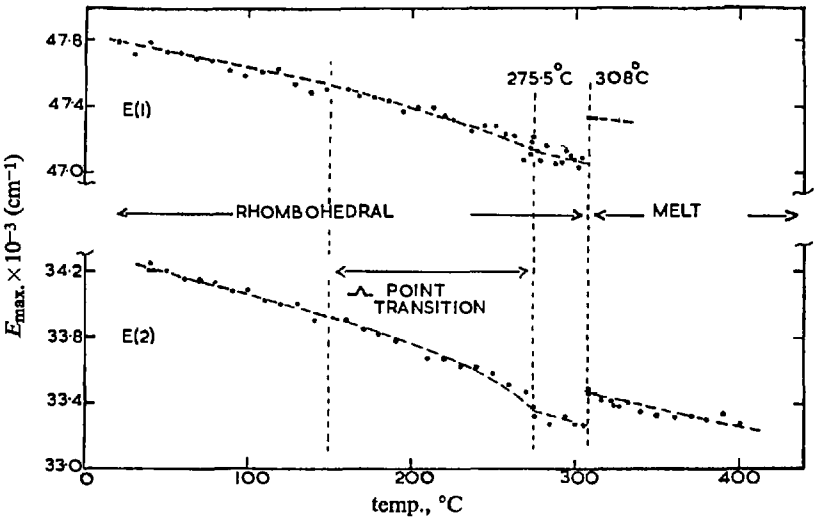


FIG. 5.—Temperature dependence of the first and second absorption band maxima of sodium nitrate.

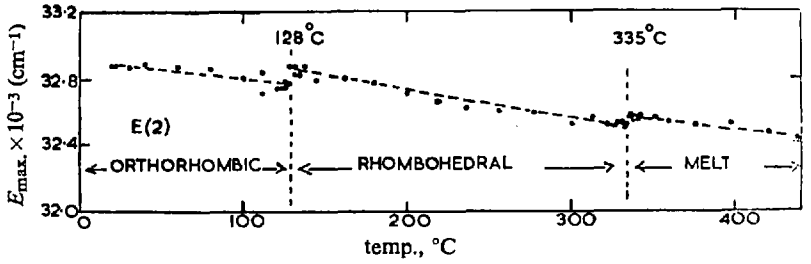


FIG. 6.—Temperature dependence of the second absorption band maximum of potassium nitrate.

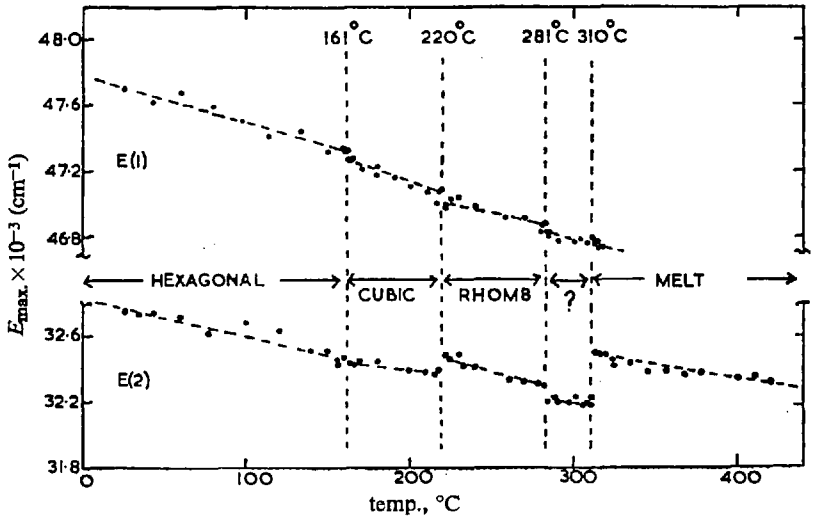


FIG. 7.—Temperature dependence of the first and second absorption band maxima of rubidium nitrate.

to calculate the nominal radius r_0 of the excited orbital, using dE/dT from the present data and inserting published coefficients of thermal expansion in eqn. (3). The constant $h/12\,mc$ was taken as $2{\cdot}02\times10^{-11}$ to give the results recorded in table 2.

It will be seen that for the solids, values of r_0 are approximately the same as the sum of the cation radius r_+ and the anion-cation distance r_{+-} calculated from the

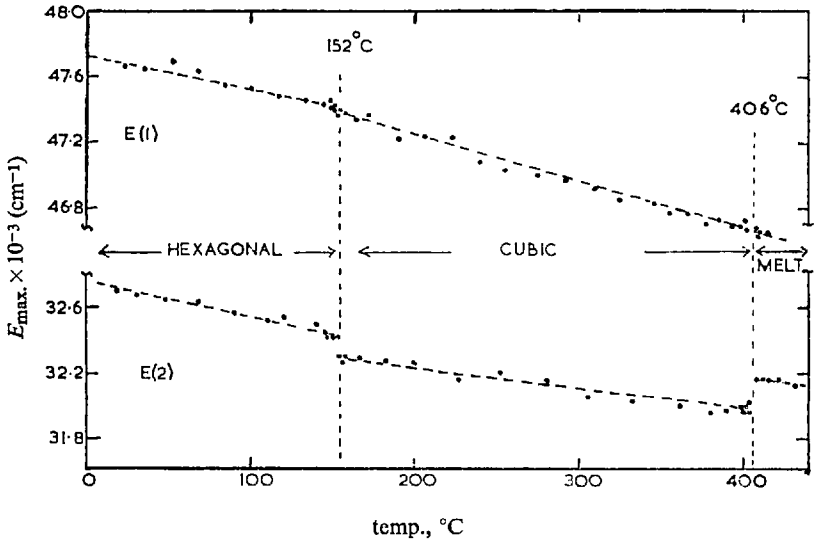


FIG. 8.—Temperature dependence of the first and second absorption band maxima of caesium nitrate.

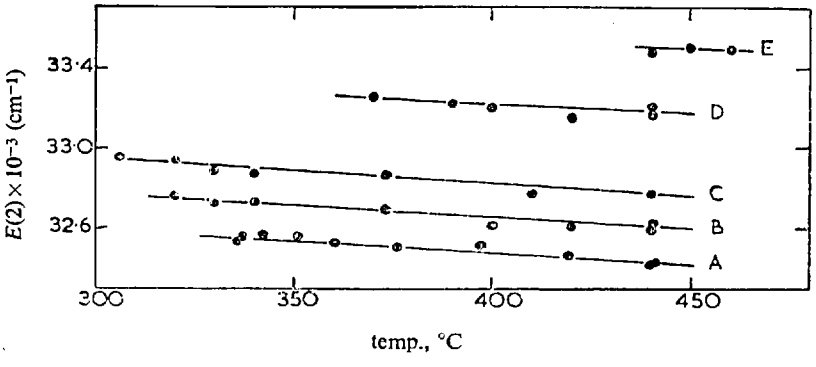


FIG. 9.—Temperature dependence of the second absorption band maximum of $KNO_3+Ba(NO_3)_2$ melts.

A, pure KNO_3; B, 10 equiv. % $Ba(NO_3)_2$; C, 20 equiv. % $Ba(NO_3)_2$; D, 35 equiv. % $Ba(NO_3)_2$; E, 50 equiv. % $Ba(NO_3)_2$.

crystal structure. This lends support to the assumption used for the approximate theory that the excited orbital does not extend beyond the shell of nearest neighbour cations.

For the melts, values of r_0 (calculated from the known thermal expansions and present data) are higher, in some cases considerably higher than $[(r_+)+(r_{+-})]$. This appears to be due to the fact that a substantial fraction of the thermal expansion of such melts arises from the creation of holes and free space in the liquid, rather than

an increase of the average distance between anions and cations, so that the assumption on which eqn. (3) was based is no longer valid.

Table 1 shows that, in spite of the increases in volume which occur at the melting points, both peaks shift to higher energies or show no change when melting occurs.

TABLE 2.—CALCULATED VALUES OF r_0 FOR ALKALI NITRATES

cation	r_+ [10] (Å)	r_{+-} (Å)	temp. range (°C)	dE_1/dT (cm^{-1} $deg.^{-1}$)	dE_2/dT (cm^{-1} $deg.^{-1}$)	γ [9] (10^{-4} $deg.^{-1}$)	$r_0(1)$ (Å)	$r_0(2)$ (Å)	$[r_+ + r_{+-}]$ (Å)
Na^+	0·95	3·24	0-150	−1·93	−2·60	1·65	4·16	3·59	4·19
			melt	—	−2·30	3·7	—	5·7	—
K^+	1·33	3·52 *a*	0-127	—	−1·0	2·2	—	6·65	4·85
			127-334	—	−1·75	2·8	—	5·69	—
			melt	—	−1·4	4·9	—	8·4	—
Rb^+			0-162	−2·83	−2·30	2·05	3·81	4·24	—
	1·48	3·77 *b*	162-220	−3·6	−1·0	3·41	4·37	8·3	5·25
			220-283	−2·3	−2·6	—	—	—	—
			283-310	−1·5	—	—	—	—	—
			melt	—	−1·8	4·05	—	6·74	—
Cs^+			0-152	−1·8	−2·0	2·05	4·8	4·55	—
	1·69	3·88 *b*	152-406	−2·9	−1·38	2·92	4·51	6·55	5·57
			melt	—	—	4·11	—	—	—

(*a*) The value $r_{+-} = 3{\cdot}52$ Å for KNO_3 is a mean value; each nitrogen atom has six nearest-neighbour potassium ions at 3·25, 3·74, 3·29(2) and 3·78 Å(2).[11]

(*b*) The values of r_{+-} for $RbNO_3$ and $CsNO_3$ refer to the cubic modifications; again the figures given are mean values.[12]

So far as the simple theory can be applied, this would indicate the formation of ionic complexes in which the anions and cations are closer in the melt than in the crystal. The loss of symmetry in local force fields on melting would help to explain this effect, which may be fairly general.[13, 14]

THE LAMBDA-POINT TRANSITION IN SODIUM NITRATE

Measurements of the specific heat and molar volume of sodium nitrate [15] reveal a well-defined lambda-point transition with a peak at 275·5°C. X-ray observations show no abrupt change of structure; this remains rhombohedral throughout but there are small changes in the parameters of the unit cell:

$$\text{at } 20°\text{C}, \quad a = 6{\cdot}32\,\text{A}°, \quad \alpha = 47°\ 14',$$

$$\text{at } 280°\text{C}, \quad a = 6{\cdot}56\,\text{A}°, \quad \alpha = 45°\ 35'.$$

This makes it of special interest to compare our present detailed observations of absorption spectra with published volume changes. If the cube of the average distance between anion and cation neighbours can be taken as directly proportional to the specific volume v of the crystal, $r_0^3 = bv$, where b is a constant and eqn. (1) transforms to

$$E = E_0 + b'v^{-2/3}, \tag{4}$$

where E_0 and b' are independent of temperature. From the numerous results in the linear portion of the expansion curve between 20°C and 150°C (cf. fig. 10), values of these constants can be computed by a least-squares method. They are found to be:

$$E_0(1) = 28{,}520\ \text{cm}^{-1}, \quad b'(1) = 11{,}180\ \text{cm g}^{-2/3};$$

$$E_0(2) = \ 9{,}790\ \text{cm}^{-1}, \quad b'(2) = 14{,}210\ \text{cm g}^{-2/3}.$$

These values which refer to the two absorption maxima, used separately to test the assumptions made, can then be inserted into (4) to calculate the expected changes in E in the region where the volume of the salt is changing steeply. It will be seen that (fig. 10) these calculated values (full line) and the experimental points for E show good agreement in the solid-solid transition region. This finding indicates that the premonitory expansion in $NaNO_3$ is accompanied by a proportionate separation of the ions. Very near the lambda peak, temperature gradients in the specimens preclude any correlation of data closer than 2°C to the peak temperature.

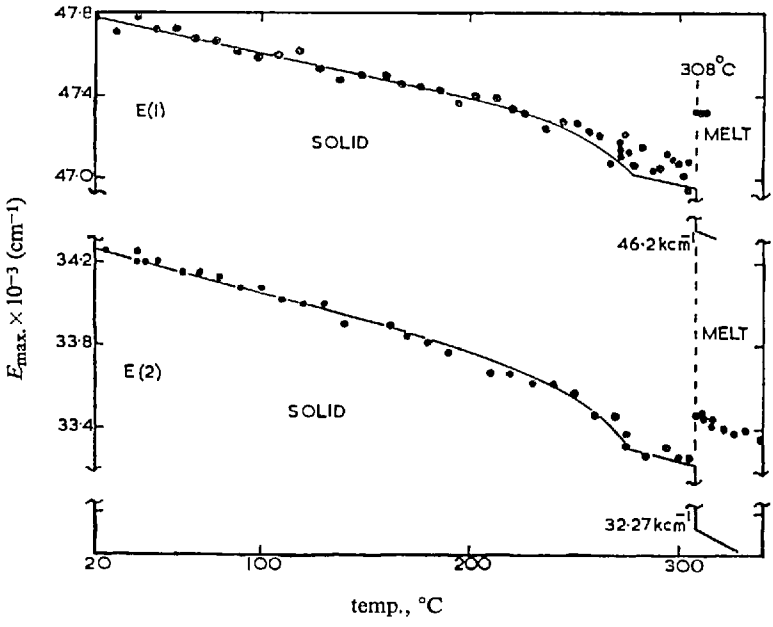


FIG. 10.—Calculated line for change of $E_{max.}$ with temperature (see eqn. (4)) compared with expt. points for $NaNO_3$.

The agreement between optical and thermodynamic data for the lambda transition makes it all the more striking that at the melting point of sodium nitrate the expansion in volume on fusion of about 11 % is not matched by a corresponding shift in $E(1)$ or $E(2)$ to smaller values; in fact, the observed shifts point to a contraction of r_0. Though it must be remembered that this is a nominal radius calculated from a simplified theory, this result supports previous conclusions that nitrate melts contain ionic complexes in which the anion-cation distance is similar to and even shorter than, that in the crystal.

MIXED MELTS OF KNO_3 WITH $Ba(NO_3)_2$

These are of some interest, since the partial molal volumes [16] indicate practically zero volume change on mixing the pure melts. Absorption spectra point to a pronounced shift of the $E(2)$ peak to higher energies as more $Ba(NO_3)_2$ is added. For this series of mixtures, coefficients of thermal expansion are known in considerable detail. Plots (not shown) indicate that the shifts in $E(2)$ are about twice as large as could be accounted for from volume changes, if these are taken to give the average anion-cation distance. Localized interactions between the doubly charged Ba^{2+} and the ionic complexes appear to make significant contributions to the overall structure of these melts; further work is needed for their elucidation.

[1] Rhodes and Ubbelohde, *Proc. Roy. Soc. A*, 1959, **251**, 156.
[2] Buck, Singhadeja and Rogers, *Anal. Chem.*, 1954, **26**, 1240.
[3] Schaumann, *Z. Physik*, 1932, **76**, 106.
[4] Sayre, *J. Chem. Physics*, 1959, **31**, 73.
[5] McEwen, *J. Chem. Physics*, 1961, **34**, 547.
[6] Fesefeldt, *Z. Physik*, 1930, **64**, 623.
[7] Smith and Symons, *Disc. Faraday Soc.*, 1957, **24**, 206.
[8] Sauerwald and Schinke, *Z. anorg. Chem.*, 1960, **304**, 25.
[9] *Int. Crit. Tables* (McGraw Hill, New York, 1928).
[10] Pauling, *The Nature of the Chemical Bond*, 2nd ed. (Oxford, 1940).
[11] Wyckoff, *The Structure of Crystals* (Interscience, New York, 1930).
[12] *Strukturberichte*, II, 381.
[13] Ubbelohde, *Proc. Chem. Soc.*, 1960, 332.
[14] Levy, Agron, Bredig and Danford, *Ann. N.Y. Acad. Sci.*, 1960, **79**, 762.
[15] Cracek, Posnjak and Hendricks, *J. Amer. Chem. Soc.*, 1931, **53**, 1183, 2609, 3339.
[16] Cleaver, Rhodes and Ubbelohde, *Proc. Roy. Soc. A*, 1961, in press.

PRINTED IN GREAT BRITAIN AT
THE UNIVERSITY PRESS
ABERDEEN

Reprinted without change of pagination from the
Proceedings of the Royal Society, A, *volume* 262, pp. 435–442, 1961

Melting and crystal structure : volume changes on mixing nitrate melts

By B. Cleaver, Elizabeth Rhodes and A. R. Ubbelohde, F.R.S.
Department of Chemical Engineering and Chemical Technology, Imperial College of Science and Technology, London, S.W.7

Measurements have been made of the densities of liquid potassium nitrate containing up to 50 equivalents per cent of barium nitrate. Within the temperature range from the liquidus to 440 °C, isotherms of equivalent volume as a function of equivalent composition were found to be straight lines. The excess volume of mixing for any pair of melts in this composition range is thus zero. Partial equivalent volumes of both components are independent of composition at a given temperature, and are given by

$$\bar{V}_m(\mathrm{KNO_3}) = 53{\cdot}17 + 0{\cdot}0229(t-300),$$
$$\bar{V}_m(\mathrm{Ba(NO_3)_2}) = 41{\cdot}75 + 0{\cdot}0107(t-300),$$

where t is the temperature in degrees centigrade.

This somewhat unusual mixing behaviour is discussed in relation to possible structures for nitrate melts, and in relation to available information about excess volumes of mixing for other ionic melts and liquids generally.

Introduction

Attention has previously been drawn to the small increase in volume on melting crystalline nitrates, and other low-melting salts (Ubbelohde 1960) compared with larger increases on melting salts with ions of the inert gas type (Ubbelohde 1959). This difference, together with much other evidence about salts with low melting points, has been interpreted on the basis of differing structures of the two types of ionic melts. A 'quasi-crystalline' structure seems appropriate to describe melts with 'inert gas' ions. One version of this model starts with a somewhat expanded crystal lattice as a reference structure for the melt. Various types of positional disorder, such as lattice holes, interstitial occupancies, and co-operative positional defects are then superimposed on this reference structure to give the structure actually found.

On the other hand, some ionic melts may in addition contain types of packing which cannot be represented with reference even to a defective crystal lattice. Thus there is evidence for the presence of association complexes in such melts (Davis, Rogers & Ubbelohde 1953; Rhodes & Ubbelohde 1959). The formation of complexes is helped by the loss of symmetry of the crystal field when melting occurs (Ubbelohde 1960). In molten nitrates, possible complexes include

$$M\mathrm{NO_3}, \quad [M(\mathrm{NO_3})_2]^- \quad \text{and} \quad [M_2(\mathrm{NO_3})]^+;$$

considerably larger clusters may be formed by association as the temperature falls to the melting point or even lower. Such considerations make it particularly interesting to investigate volume changes resulting from the mixing of ionic melts. Probably one of the simplest cases for which studies of specific volumes can lead

to tests of different models is presented by mixtures of a uni-univalent salt, with a di-univalent salt with a common ion. Since the crystal lattice can be regarded as rigid to a first approximation, a solid solution of a di : uni salt in a uni : uni salt would be expected to contain one cation vacancy for each divalent cation introduced. Examples for which such a production of vacancies has been verified include Cd^{2+} in NaCl (Etzel & Maurer 1950); Ba^{2+} in KCl (Kelting & Witt 1949) and Cd^{2+} in AgBr (Tetlow 1950). This phenomenon does not appear to have been previously reported for salts with polyatomic ions, but has recently also been verified for Ca^{2+} dissolved in crystals of KNO_3 (Rhodes & Ubbelohde 1960, unpublished observations). If a quasi-crystalline melt behaves in a similar way to the crystals, addition of a 2 : 1 to a 1 : 1 salt should likewise give rise to an equivalent number of vacancies in the melt. This might be detected from its effect on specific volumes, on gas solubilities and on ionic conductance.

The present paper refers to density measurements carried out on molten mixtures of KNO_3 and $Ba(NO_3)_2$. These salts crystallize without water of hydration, and the two cations have practically the same repulsion radii in simple ionic crystals (K^+ = 1·33 Å, Ba^{2+} = 1·35 Å, Pauling 1950). Specific volumes of the melts have been measured with an accuracy of approximately 0·05 %. To about the same accuracy, the partial equivalent volumes of the two species are found to be independent of composition at a given temperature. Such behaviour has been established for few other pairs of liquids, whether ionic or molecular. Its significance in relation to the structure of the melts is discussed below.

Experimental and results

Densities of pure potassium nitrate and of ten mixtures containing between 5 and 50 equiv. % of barium nitrate were measured with an accuracy of ± 0·001 g/ml. between the liquidus temperature and 440 °C. Unfortunately, accurate measurements could not be made on mixtures richer in barium nitrate, because such melts evolved gases at perceptible rates at all temperatures above the liquidus.

The potassium and barium nitrates were Judactan A.R. grade salts. Batch analyses showed less than 0·0003 % of cation or 0·002 % of anion impurities for KNO_3, and less than 0·001 % of cation or 0·001 % of anion impurities for $Ba(NO_3)_2$. These salts were not further purified but were very carefully dried by the thermal shock technique (Rhodes & Ubbelohde 1959). The freezing point of pure dry KNO_3 was found to be 334·7 ± 0·3 °C. The freezing point of pure $Ba(NO_3)_2$ could not be determined accurately since it decomposed on melting. Measurements were made with a Pyrex manometric densitometer, by the technique of Husband (1958). Temperatures were maintained by immersing the densitometer in a thermostatically controlled bath containing the molten ternary eutectic

$$KNO_3 : NaNO_3 : NaNO_2$$

(m.p. 156 °C), the temperature of which was controlled electronically to within ± 0·1 °C. Temperatures were measured to ± 0·1 °C with a calibrated Johnson, Matthey and Co. Pallador thermocouple in a Pyrex sheath the tip of which was in contact with the densitometer.

The density of the melt ρ at any temperature is given by the formula

$$\rho = \frac{M}{V_0}\left(1 \pm \frac{A\rho_0 h}{M}\right), \tag{1}$$

which is identical with the series formula given by Husband (1958). The positive or negative sign is used according as the pressure is applied to the long or short capillary of the densitometer. M is the mass of salt in the densitometer, V_0 the volume of the densitometer up to the fiducial mark, A the area of cross-section of the capillary, ρ_0 the density of the manometric fluid and h the manometric height.

TABLE 1. VOLUME PARAMETERS OF MELTS OF POTASSIUM NITRATE AND BARIUM NITRATE

$Ba(NO_3)_2$ (equiv. %)	a (ml.)	$10^2 b$ (ml./°C)	$10^4 b/a$ (per °C)	temperature range (°C)	σ (ml.)
0	53·18	2·275	4·28	340 to 440	0·01
4·954	52·57	2·248	4·28	330 to 440	0·002
9·867	52·00	2·170	4·17	320 to 440	0·002
14·963	51·47	2·103	4·09	320 to 440	0·005
19·730	50·91	2·057	4·04	320 to 440	0·01
24·704	50·35	1·980	3·93	320 to 440	0·01
29·953	49·74	1·932	3·88	340 to 440	0·005
34·957	49·15	1·883	3·83	373 to 440	0·005
39·741	48·60	1·833	3·77	410 to 440	—
44·566	48·05	1·769	3·68	410 to 440	—
50·022	$V_m = 49·79$ at 440 °C				

V_m, the volume of melt containing 1 gram-ion of nitrate, has been calculated from the observed density ρ by means of the expression

$$2\rho V_m = 2M_1(1-x) + M_2 x, \tag{2}$$

where M_1 and M_2 are the molecular weights of potassium nitrate and barium nitrate respectively and x is the equivalent fraction of barium nitrate in the mixture. For each mixture, V_m was found to be a linear function of temperature (t °C). Values of the parameters a and b in the equation

$$V_m = a + b(t - 300) \tag{3}$$

were evaluated for each mixture, by the method of least squares. Table 1 records the values obtained, and the standard deviations σ of the points from the straight lines. Also tabulated is b/a, the mean coefficient of cubic expansion of the melt $(1/V)\,\mathrm{d}V/\mathrm{d}t$ referred to the volume at 300 °C. Values of the molar volume of pure potassium nitrate derived from the parameters given in table 1 are intermediate between those recorded by earlier workers (Jaeger 1917; Bloom, Knaggs, Molloy & Welch 1953). It is estimated that a systematic error of $\pm 0·005$ is to be added to the standard error 2σ to give the total probable error in the above figures.

The isotherms of V_m against composition (in equivalents per cent) were also found to be straight lines. Standard deviations of individual experimental values were less than 0·015 ml. at 440, 410, 373 and 340 °C. The intercepts of these lines at $x = 0$

and $x = 1$ gave the partial equivalent volumes $\overline{V}_m$ of potassium nitrate and barium nitrate at each of these temperatures. These values were found to conform (with a standard deviation of 0·02 ml.) to the linear equations

$$\overline{V}_m[Ba(NO_3)_2] = 41{\cdot}75 + 0{\cdot}0107(t - 300), \tag{4}$$

$$\overline{V}_m(KNO_3) = 53{\cdot}17 + 0{\cdot}0229(t - 300), \tag{5}$$

t being the temperature in degrees centigrade.

TABLE 2. VOLUME PARAMETERS FOR MELTING OF NITRATES

	potassium nitrate			
t (°C)	V_S (ml.)*	V_L (ml.)†	ΔV_f (ml.)	$\Delta V_f/V_S$ (%)
334·6	52·48	53·96	1·48	2·81
340·0	52·55	54·09	1·53	2·91
373·0	53·06	54·84	1·78	3·35
410·0	53·63	55·68	2·05	3·82
440·0	54·09	56·38	2·29	4·22
	barium nitrate			
t (°C)	V_S (ml.)‡	V_L (ml.)	ΔV_f (ml.)	$\Delta V_f/V_S$ (%)
288·0§	40·82	41·62	0·80	1·96
340·0	40·93	42·18	1·25	3·06
373·0	41·00	42·53	1·54	3·75
410 0	41·07	42·93	1·86	4·53
440·0	41·13	43·25	2·12	5·16
592·0§	41·44	44·88	3·45	8·31

* Calculated from the density at 335 °C and the coefficient of cubic expansion, both measured by X-ray diffraction (Fischmeister 1956). Slightly higher values of V_S for potassium nitrate are obtained if dilatometric measurements due to Bredée & Cohen (1929) are used; thus V_S at 334·6 °C is calculated to be 52·57 ml.

† Present work.

‡ Calculated from the density at 23 °C (3·244 g/ml., *International Critical Tables*) and the mean coefficient of cubic expansion between 10 and 250 °C, measured by X-ray diffraction (Vegard & Roer 1941).

§ 592·0 °C is the melting point of barium nitrate, and 288 °C is the eutectic temperature of the system potassium nitrate+barium nitrate (Protsenko & Malakhova 1957).

On the assumption that the equivalent volume isotherms remain linear over the entire composition range, the partial equivalent volumes in (3) and (4) may be equated to the equivalent volumes, V_L, of the pure melts (extrapolated into the supercooled region for barium nitrate). The equivalent volumes of the corresponding pure solids, V_S (extrapolated above the melting point in the case of potassium nitrate) have been calculated from their densities and coefficients of expansion as reported by other workers. From these results may be deduced the volume change ΔV_f which occurs when one equivalent of the solid melts or when it dissolves in the other component to form a solution of any concentration. Values of V_L, V_S and $\Delta V_f/V_S$ are listed in table 2.

Discussion

When a divalent cation occupies the site of a monovalent cation in a crystalline salt, a neighbouring cation site is left vacant to maintain electrostatic neutrality. Because of the holes formed in the crystal lattice, the equivalent volume of such a solid solution is likely to show positive deviations from the ideal mixture law. For example, this appears to be the case for small amounts of calcium chloride in solid solution in potassium chloride (Pick & Weber 1950). Deviations of the same kind might be expected if barium ions could be made to enter solid solution in potassium nitrate. Solid solutions usually maintain the crystal structure of either pure component, with considerable strain, until there is an abrupt change to the structure of the other component. One example is presented by the system

$$\mathrm{KI(f.c.c.)} + \mathrm{CsI(b.c.c.)}$$

(Martienssen 1957) which undergoes a fairly abrupt change-over at about 60 % CsI. But even if a substitution mechanism applies for the crystals, volumes of the mixed melts have now been found to obey the ideal mixture law with high accuracy, subject to the reasonable assumption that the equivalent volume isotherms remain linear over the experimentally inaccessible part of the composition range. Equations (4) and (5) show that in the mixed melts there is a shrinkage of about 25 % when potassium is completely replaced by barium.

Apparently addition of barium ions does not create an additional vacancy for each divalent ion added to the fluid, even in quite dilute solutions. Observations on the solubilities of polar gases in mixed nitrate melts (Frame, Rhodes & Ubbelohde 1961) and on their electrical conductivities (Cleaver, Rhodes & Ubbelohde, unpublished observations) likewise lead to the conclusion that the addition of divalent cations to a uni-univalent nitrate melt does not greatly alter the number of holes in the fluid. This must in part be attributed to the absence of rigidity in the quasi-crystalline fluid. In fact, the non-spherical anions appear to screen the electrostatic fields due to the different cations, so that the mixture behaves as might be expected for closely similar neutral molecules. Comparison of the system potassium nitrate + barium nitrate with results for other systems shows that the small deviations from linearity of the equivalent volume isotherms are an unusual feature. To illustrate this, the excess volumes of some binary ionic melts and of some mixtures of molecular liquids are plotted in figures 1 and 2. The excess volumes of potassium nitrate + barium nitrate mixtures at 410 and 440 °C were calculated on the assumption that the equivalent volume of liquid barium nitrate is equal to its partial equivalent volume, at the same temperature, in the mixtures on which density measurements were carried out.

In figure 1, large excess volumes observed in the systems $CdI_2 + KI$ and $MnCl_2 + KCl$ may be attributed to the formation of complex ions such as $[CdI_3]^-$, $[CdI_4]^{2-}$, $[MnCl_3]^-$ and $[MnCl_4]^{2-}$ in the mixed melts; but smaller excess volumes are also observed in systems in which complex formation is not thought to occur.

In view of the interest of the present findings for theories about the structure of

liquids it would be useful to know if any other thermodynamic properties of the system potassium nitrate + barium nitrate show ideal behaviour. Heats of mixing of solutions of different concentration do not appear to have been measured directly, but some information can be derived from the freezing-point curve of the system.

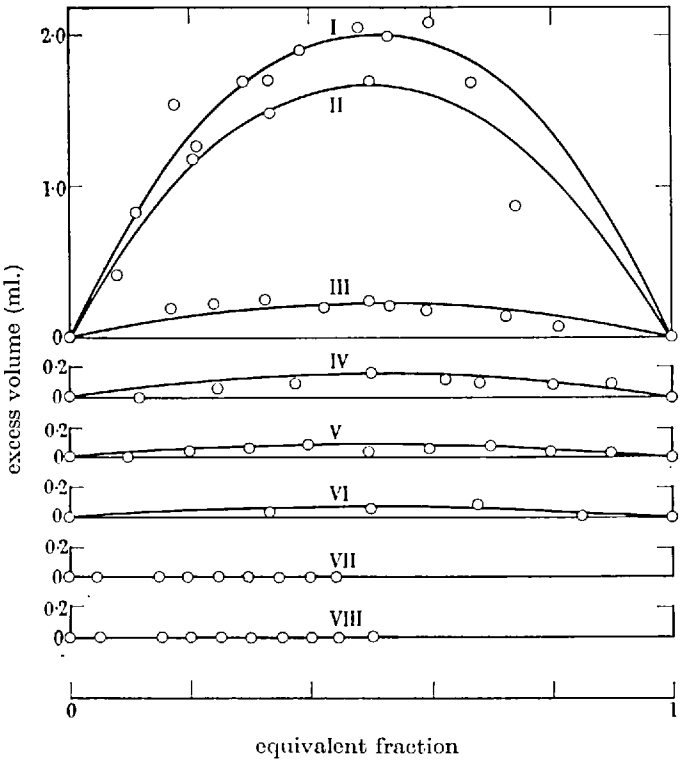


FIGURE 1. Excess volumes (per equivalent) of some binary mixtures of ionic melts. I, $MnCl_2 + KCl$ at 800 °C (Murgulescu & Zuca 1959); II, $CdI_2 + KI$ at 700 °C (Bloom, Knaggs, Molloy & Welch 1953); III, $CaCl_2 + KCl$ at 850 °C (Vereshchetina & Luzhnaya 1954); IV, $LiNO_3 + KNO_3$ at 350 °C (Smith, Petersen & Ewing 1959); V, $KNO_3 + NaNO_3$ at 400 °C (Murgulescu & Zuca 1959); VI, $KNO_3 + KBr$ at 730 °C (Bloom *et al.* 1953); VII, $KNO_3 + Ba(NO_3)_2$ at 410 °C (present work); VIII, $KNO_3 + Ba(NO_3)_2$ at 440 °C (present work).

Cryoscopic data in the range between the pure liquid and the eutectic (Protsenko & Malakhova 1957) may be used to calculate the activity a of potassium nitrate in solutions, by means of the expression

$$\ln a = \frac{L_f}{R}\left[\frac{1}{T_f} - \frac{1}{T}\right] + \frac{C_L - C_S}{R}\left[\frac{T_f}{T} - 1 - \ln\frac{T_f}{T}\right] \qquad (6)$$

(cf. Prigogine & Defay 1954). T_f and T are the freezing points in °K of pure potassium nitrate and of the solution, respectively; L_f is the molar latent heat of fusion of potassium nitrate at T_f; C_L and C_S are the molar specific heats at constant pressure of liquid and solid potassium nitrate (assumed to be independent of

temperature). Values of L_f, C_L and C_S determined calorimetrically (Goodwin & Kalmus 1909) are:

$$L_f = 2570 \text{ cal mole}^{-1},$$
$$C_L = 33{\cdot}7 \text{ cal mole}^{-1}\,^{\circ}\text{C}^{-1},$$
$$C_S = 29{\cdot}5 \text{ cal mole}^{-1}\,^{\circ}\text{C}^{-1}.$$

Activities and activity coefficients calculated on this basis are recorded in table 3.

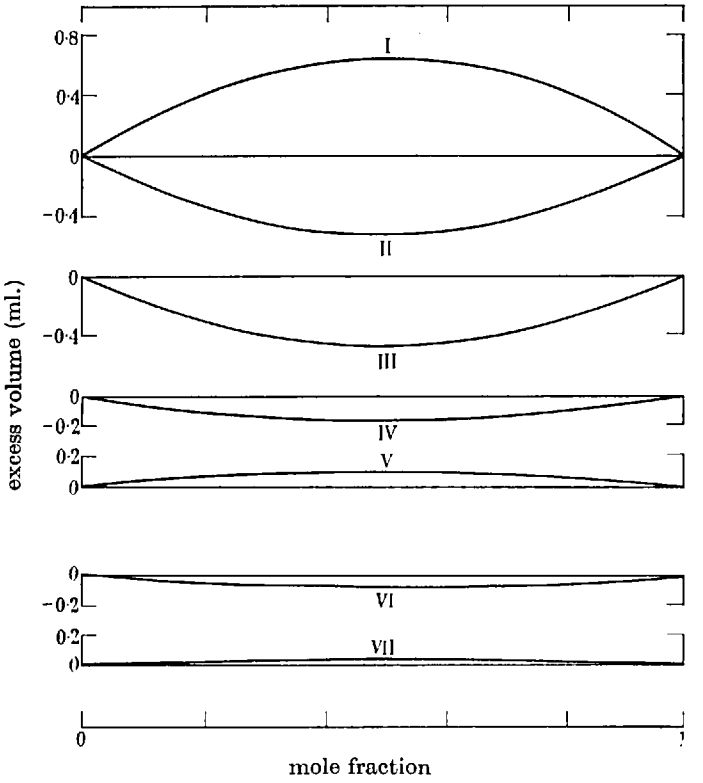


FIGURE 2. Excess volumes of some binary mixtures of molecular liquids. I, Benzene + *cyclo*hexane at 20 °C (Mathieson & Thynne 1956); II, carbon tetrachloride + *neo*-pentane at 0 °C (Desmyter & Mathot 1953); III, *neo*-pentane + benzene at 0 °C (Desmyter & Mathor 1953); IV, argon + nitrogen at 84 °K (Pool & Staveley 1957); V, *N*-hexane *cyclo*hexane at 20 °C (Klapproth 1940); VI, *N*-decane + *n*-hexadecane at 20 °C (Desmyter & van der Waals 1958); VII, *cyclo*hexane + *iso*-octane at 30 °C (Danusso 1952, 1954).

Some information about the order of magnitude of heats of solution of KNO_3 in the melt may be derived from these activities. The increase of free energy on adding one mole of liquid KNO_3 to a large volume of the mixed melts is

$$\mu - \mu_0 = \bar{H} - \bar{H}_0 - T(\bar{S} - \bar{S}_0)$$
$$= RT \ln a, \qquad (7)$$

where partial molar quantities refer to potassium nitrate throughout. If the entropy of mixing has the ideal value $\bar{S} - \bar{S}_0 = -R \ln x$, then the heat of mixing, $\bar{H} - \bar{H}_0$, is equal to $RT \ln \gamma$.

Table 3 shows that $RT \ln \gamma$ takes negative values, and reaches about -50 cal for a solution of the eutectic composition (22·5 equiv. % barium nitrate). This

suggests that heat may be evolved when a solution is diluted with pure liquid potassium nitrate, but it is also possible that the deviations of γ from unity are due partly to non-ideal entropy of mixing.

It seems probable that the excess heat contents of the mixtures, unlike the excess volumes, differ appreciably from zero. However, since the value of the entropy of mixing is uncertain, this conclusion must remain tentative until it can be confirmed by direct calorimetric measurements.

TABLE 3. ACTIVITIES AND ACTIVITY COEFFICIENTS OF KNO_3 IN MIXED MELTS WITH $Ba(NO_3)_2$

T (°C)	mole fraction KNO_3, x	a	$\gamma = \frac{a}{x}$	$RT \ln \gamma$ (cal/g equiv.)
336 (m.p.)	1·000	1·000	1·000	—
327	0·974	0·969	0·995	− 7·0
318	0·947	0·938	0·990	−12·0
307	0·919	0·901	0·981	−25·0
294	0·889	0·859	0·966	−44·7
288	0·873	0·840	0·961	−51·7

REFERENCES

Bloom, H., Knaggs, I. W., Molloy, J. J. & Welch, D. 1953 *Trans. Faraday Soc.* p. 1458.
Bredée, H. L. & Cohen, E. 1929 *Z. phys. Chem.* **140**A, 391.
Danusso, F. 1952 *Mem. Accad. Lincei*, **13**, 131.
Danusso, F. 1954 *Mem. Accad. Lincei*, **17**, 109.
Davis, W. J., Rogers, S. E. & Ubbelohde, A. R. 1953 *Proc. Roy. Soc.* A, **220**, 14.
Desmyter, A. & Mathot, V. 1953 *J. Chem. Phys.* **21**, 782.
Desmyter, A. & van der Waals, J. H. 1958 *Rec. Trav. chim. Pays-Bas*, **77**, 53.
Etzel, H. W. & Maurer, J. 1950 *J. Chem. Phys.* **18**, 1003.
Fischmeister, H. F. 1956 *J. Inorg. Nucl. Chem.* **3**, 182.
Frame, J. P., Rhodes, E. & Ubbelohde, A. R. 1961 *Trans. Faraday Soc.* (In publication.)
Goodwin, H. M. & Kalmus, H. T. 1909 *Phys. Rev.* **28**, 1.
Husband, L. J. B. 1958 *J. Sci. Instrum.* **35**, 300.
Jaeger, F. M. 1917 *Z. anorg. Chem.* **101**, 1.
Kelting, H. & Witt, H. W. 1949 *Z. Phys.* **126**, 697.
Klapproth, H. 1940 *Nova Acta Leop. Carol.* **9**, 309.
Martienssen, N. 1957 *Phys. and Chem. Solids*, **2**, 257.
Mathieson, A. R. & Thynne, J. C. J. 1956 *J. Chem. Soc.* p. 3708.
Murgulescu, I. G. & Zuca, St. 1959 *Rev. chim., Acad. rep. pop. Roumaine*, **4**, 227.
Pauling, L. 1950 *The nature of the chemical bond* (2nd ed.), p. 346. London: Oxford University Press.
Pick, H. & Weber, H. 1950 *Z. Phys.* **128**, 409.
Pool, R. A. H. & Staveley, L. A. K. 1957 *Nature, Lond.* **180**, 1118.
Prigogine, I. & Defay, R. 1954 *Chemical thermodynamics* (translated by Everett, D. H.). London: Longmans.
Protsenko, P. I. & Malakhova, A. Ya. 1957 *Zh. neorg. Khim.* **2**, 2145.
Rhodes, E. & Ubbelohde, A. R. 1959 *Proc. Roy. Soc.* A, **251**, 156.
Smith, G. P., Petersen, G. F. & Ewing, W. M. 1959 *Oak Ridge Nat. Rep.* no. 2762.
Tetlow, S. 1950 *Z. phys. Chem.* **195**, 197, 213.
Ubbelohde, A. R. 1959 *The structure of electrolytic solutions* (edited by W. J. Hamer), p. 401. New York: Wiley.
Ubbelohde, A. R. 1960 Liversidge Lecture, *Proc. Chem. Soc.*, p. 332.
Vegard, L. & Roer, K. I. 1941 *Avh. norske Vidensk-Akad.* **1**, no. 17.
Vereshchetina, E. P. & Luzhnaya, N. P. 1954 *Izvest. Sekt. fiz.-Khim. Anal., Inst. obshchei neorg. Khim.*, **25**, 188.

PRINTED IN GREAT BRITAIN AT THE UNIVERSITY PRESS, CAMBRIDGE
(BROOKE CRUTCHLEY, UNIVERSITY PRINTER)